Université de Strasbourg

Mémoire présenté pour l'obtention de l'

Habilitation à Diriger des Recherches

Laurence Choulier

Chargée de Recherche CR1-CNRS
UMR 7021
Laboratoire de Bioimagerie et Pathologies

Aptamères ciblant des cellules de glioblastome exprimant l'intégrine α5β1

Soutenance le 21 juin 2018

Composition du jury :

Pr. Muriel Barberi-Heyob	Rapporteur
Pr. Sylvie Fournel	Rapporteur
Pr. Stéphane Dedieu	Rapporteur
Dr. Rodolphe Jaffiol	Examinateur
Dr. Monique Dontenwill	Garant

SOMMAIRE

ABREVIATIONS

2'F	2'-fluororiboside pyrimidique (ou 2'-fluoro)
AM	adrénomédulline
AMM	autorisation de mise sur le marché
BHE	barrière hémato-encéphalique
BSA	'bovine serum albumin'
DMLA	dégénérescence maculaire liée à l'âge
EGFR	'epidermal growth factor receptor'
ELISA	'enzyme linked immunosorbent assay'
EMA	'European medecines agency'
EPO	'European patent office'
Fab	fragment d'anticorps
FDA	'food and drug administration'
GBM	glioblastoma multiforme
HIV	virus de l'immunodéficience humaine
HPV	'human papillomavirus'
HTS	'high throughput screening'
IM	'interaction map'
IMD	'integrin-mediated death'
INPI	institut national de la propriété intellectuelle
K_A	affinité à l'équilibre (M)
K_D	affinité à l'équilibre (M^{-1}). $K_D = 1 / K_A$
k_{off}	paramètre cinétique de dissociation (s^{-1})
k_{on}	paramètre cinétique d'association ($M^{-1}.s^{-1}$)
MAGI-1	'membrane-associated guanylate kinase (MAGUK) inverted protein 1'
MEC	matrice extra-cellulaire
NGS	'next generation sequencing'
OMS	organisation mondiale de la santé
PBS	phosphate-buffered saline
PCR	'polymerase chain reaction'
PDZ	trois premières protéines identifiées contenant ce domaine : PSD-95, Dlg, and ZO-1
PEG	polyéthylène glycol
PM	poids moléculaire
PMSA	'prostate specific membrane antigen'
PPR	'pentatricopeptide repeat proteins'
PTP-1b	'tyrosine phosphatase-1b'
QSAR	'quantitative structure-activity relationship'
RGD	arginine-glycine-acide aspartique
RT	transcription inverse
RU	'resonance unit'
SAR	'structure-activity relationship'
scFv	'single-chain variable fragment'
SELEX	'selective evolution of ligand by exponential enrichment'
SOMAmer	'slow off-rate modified aptamer'
SPR	'surface plasmon resonance'
TAR	'trans-activation response'
TB4	'transforming growth factor β-binding protein'
TMZ	témozolomide
VEGF	'vascular endothelial growth factor'
VMTP	protéine de coque du virus de la mosaïque du tabac
XNA	'xeno nucleic acid'

CURRICULUM VITAE

Etat civil
Née le 21 septembre 1973
à Belfort (90)
Nationalité française
Mariée, 3 enfants

Adresse professionnelle
CNRS/UMR 7021
Laboratoire de Bioimagerie et Pathologies
Université de Strasbourg, Faculté de Pharmacie
74, route du Rhin, 67401 Illkirch Cedex
Tel. 03 68 85 41 97 Fax. 03 68 85 43 13
e-mail : laurence.choulier@unistra.fr

Cursus scientifique

1997-2001 **Doctorat** en Biologie moléculaire/Immunochimie
IBMC (Institut de Biologie Moléculaire et Cellulaire, Strasbourg)
Direction : Dr. Danièle Altschuh
'Cinétiques d'interaction antigène-anticorps : identification des facteurs qui influencent l'activité de liaison et ingénierie prédictive'

2001-2003 **Post-doctorat**-Université d'Oxford (GB), NDOG (Nuffield Depart of Obstetrics and Gynaecology)
Direction : Pr. Helen Mardon
'Investigations fonctionnelles des interactions entre intégrines et protéines de la matrice extra-cellulaire'

2003 **Post-doctorat**-Université Victor Ségalen
IECB (Institut Européen de Chimie-Biologie, Bordeaux)
Direction : Dr. J-Jacques Toulmé
'Criblage par SELEX d'aptamères anti-glutène impliqués dans la maladie coeliaque'

2004-2011 **Chargée de Recherche-UMR7242** (directeurs : Pr. Claude Kédinger, puis Dr. Jean-Luc Galzi), ESBS-IREBS (Institut de Recherche de l'Ecole Supérieure de Biotecnologie de Strasbourg, Illkirch), équipe 'Biocapteurs', Dr. Danièle Altschuh
Développement de deux axes de recherche principaux
'Biocapteurs moléculaires'
'Stratégies de sélection et d'optimisation de molécules à potentiel diagnostic et/ou thérapeutique'

depuis 2012 **Chargée de Recherche-UMR7021, anciennement UMR7213** (directeur : Pr. Yves Mély), Faculté de Pharmacie (Illkirch),
équipe 'Intégrine et cancer', Dr. Monique Dontenwill
Développement d'un axe de recherche
'*Aptamères ARN ciblant des cellules de glioblastome exprimant l'intégrine α5β1'*

Encadrement

Synthèse :

Etudiants	Avant 2012	Depuis 2012
Doctorants	- Encadrement durant 11 mois d'une étudiante sud-africaine	- Coencadrement en cours d'une doctorante - Encadrement de la thèse de pharmacie d'une étudiante interne (DES IPR)
M2	1	2 (1 en cours)
M1 et équivalents	4	9
L3 et équivalents	1	5
BTS 2ème année	/	1
BTS 1ère année	/	1

Détails :

Participation à l'encadrement de deux étudiantes en thèse :

oct 2007-sept 2008	Aletia NAIDOO, durant ses 11 mois de stage à Strasbourg lors de son doctorat (doctorante de l'Université Kwazulu Natal, Pietermaritzburg, Afrique du Sud)
depuis octobre 2017	Elisabete CRUZ DA SILVA

Encadrement d'une thèse de pharmacie-D.E.S d'innovation pharmaceutique et recherche (IPR) :

depuis septembre 2017	Marie-Cécile MERCIER

Encadrement d'une post-doctorante :

janv-sept 2005	Karin ENANDER

Encadrement d'étudiants en Master 2 :

oct-déc 2002	M. ROONA, Université d'Oxford
janvier-juin 2016	Beatriz IZQUIERDO (ERASMUS, Polytechnic University of Valencia, Espagne)
depuis janvier 2018	Lisa BUHR (M2 BioIngénierie et Médicaments, Université de Lorraine, Nancy)

Encadrement d'étudiants en Master 1 et équivalents :

juin-juill 1999	Etudiant de 2ème année de l'ESBS (Ecole Supérieure de Biotechnologie de Strasbourg)
juill 2005	Kathrin HEINZMANN & Charline SANTAMARIA, 3ème année de l'ESBS, ULP
jan-août 2008	Marie BESSE, 2ème année de l'ESBS, ULP
avril-juin 2012	Guillaume RENNER, M1 Physiopathologie-de la molécule à l'homme, Unistra
avril-juin 2012	Olivier IMBS, M1 Physiopathologie-de la molécule à l'homme, Unistra
janv-mars 2013	Célia JACOBERGER-FOISSAC, M1 Immunologie et Inflammation, Unistra
sept 2013-mars 2014	Cécile CHAZEAU, 5ème année de Pharmacie, Unistra
janv-fév 2014	Samuel NICAISE, M1 Physiopathologie-de la molécule à l'homme, Unistra
janv-fév 2015	Marta UCEDA, M1 Pharmacologie, Unistra
mai-juin 2016	Nathan CHABOCHE, M1 Concept & prod de molécules d'intérêt thérapeutique,Unistra
janv-mars 2017	Amandine BADIE, M1 BMCI, parcours Immunologie et Inflammation, Unistra
janv-fév 2017	Lisa BUHR, M1 BioIngénierie et Médicaments, Université de Lorraine, Nancy

Encadrement d'étudiants en Licence 3 et équivalents :

fév-avr 1998	Etudiant en 1ère année de magistère de Chimie-Biologie, ULP
juin 2012 (2 sem)	Anne-Sophie LEGROS & Eric HURST, 3ème année de médecine, Unistra
juin 2012 (3 sem)	Julie KESSLER, 3ème année de médecine, Unistra
fév-juill 2015	Marine FENAT, Stage de licence profess. de Biotechnologie, Université de Reims
sept-déc 2015	Marine FENAT, employée sous contrat SATT Conectus

Encadrement d'étudiants BTS 2ème année :

janv-fév 2014	Alessandro DE LEO, BTS Biotechnologie, Lycée Jean Rostand, Strasbourg

Encadrement d'étudiants en BTS 1ère année :

mai-juill 2013	Alessandro DE LEO, BTS Biotechnologie, Lycée Jean Rostand, Strasbourg

Encadrement d'élèves de 3ème et 2nde (stages d'observation en milieu professionnel) :

avril 2013	Elève de 2nde
déc 2013	Louise MARECHAL, élève de 3ème, Collège Sébastien Brant, Eschau
fév-mars 2016	Camille GILBERT & Léa MEYER, élèves de 3ème, Collège d'Illkirch

Formation à la SPR ('surface plasmon resonance') :

sept 2007	Sebastien LALEVEE, doctorant de l'IGBMC, Strasbourg
oct 2007	Sonsoles MARTIN-SANTAMARIA, chercheure de l'Université San Pablo, Madrid
mars 2008	Julien BEYRATH, doctorant de l'IBMC, Strasbourg
avril 2008	Utilisateurs d'une société privée (Transgène)
juill 2008-juin 2009	Pierre FECHTER, chercheur de l'IBMC, Strasbourg
juill-oct 2008	Anthony GOBERT & Philippe GIEGE, chercheurs de l'IBMP, Strasbourg
oct-nov 2010	Marta BRUCZKO & Kamila FILIPIAK, étudiantes l'Université San Pablo, Madrid
mars 2015	Marta UCEDA-MARTIN, Orianne MESSNER & Charlotte ROMANET Formation SPR, UE Recherche & Plateformes, M1 Pharmacologie, Unistra

Expertises et activités scientifiques

Révision d'articles scientifiques - Derniers journaux concernés :
Analytical Biochemistry, Journal of Molecular Recognition, Process Biochemistry, Cancers, Aptamers, Cells
Evaluation de plusieurs projets pour le Cancéropôle Grand-Est - Soutien à l'émergence de projet
Editrice académique pour Cancers-Edition spéciale 'FAK signaling pathway in cancers' (sortie prévue en mai 2018)
Membre élue du conseil de laboratoire de l'UMR 7021 (mandat 2018-2023)

Enseignement

mars-mai 1996	Tutorat de biochimie sur MacIntosh (étudiants en DEUG 2ème année)
janv-mai 1998	Microbiologie fondamentale et physiologie (BTS, Lycée Jean Rostand, Strasbourg)
oct 1999	Formation en mesures cinétiques par SPR (formation INSERM, Strasbourg)
mars 2007	TP d'instrumentation biophysique (étudiants de l'ESBS, Illkirch)
déc 2007	Cours fondamentaux de SPR (M1, Strasbourg)
janv 2008	TP, TD d'instrumentation biophysique (étudiants de l'ESBS, Illkirch)
mars 2010	Cours fondamentaux de SPR (M1, Strasbourg)
avr 2012	Cours fondamentaux de SPR (M1, Strasbourg)
mars 2015	Cours, TP, TD de SPR (M1 Pharmacologie, UE Recherche et Plateformes)
février 2016	Cours, TP, TD de SPR (M1 Pharmacologie, UE Recherche et Plateformes)
mars 2017	Cours, TP, TD de SPR (M1 Pharmacologie, UE Recherche et Plateformes)
fév-mars 2017	TP, TD d'instrumentation biophysique (étudiants de l'ESBS, Illkirch)
2017-2018	Chercheure associée à la Maison pour la Science en Alsace (accompagnement scientifique du collège pilote Mandela d'Illkirch et de la résidence scientifique du collège de Wingen/Moder)

Membre de jurys au sein de l'Université de Strasbourg

16-17/05/2013 **Jury de M1 Biologie moléculaire et cellulaire intégrée,**
parcours Biologie et génétique moléculaire
UE Initiation à la Communication Scientifique (ICS)
7/03/2014 **Jury de M1**, 5ème année de Pharmacie
UE Initiation à la recherche
27/05/2014 **Jury de M1**, 5ème année de Pharmacie
UE Initiation à la recherche
11-12/05/2015 **Jury de M1 Biologie moléculaire et cellulaire intégrée,**
parcours Biologie et génétique moléculaire
UE Initiation à la Communication Scientifique (ICS)
23/07/2015 **Jury de M1**, 5ème année de Pharmacie
UE Projet professionnel
18/05/2017 **Jury de M1 Biologie moléculaire et cellulaire intégrée,**
parcours Biologie et génétique moléculaire
UE Initiation à la Communication Scientifique (ICS)
17/05/2018 **Jury de M1 Biologie moléculaire et cellulaire intégrée,**
parcours Biologie et génétique moléculaire
UE Initiation à la Communication Scientifique (ICS)

Participation à des congrès, séminaires, réunion de travail

avec présentations orales

22-25/06/1998	XXVth Young scientists forum, Québec *Analyse de la relation entre structure et fonction de reconnaissance* *antigène-anticorps par mutagenèse dirigée et analyse cinétique à l'aide d'un biocapteur*
14/09/1998	**Conférence invitée** - Institut National de la Recherche en Agroalimentaire, Colmar *Presentation of the BIACORE technology*
4-8/07/1999	13th International Symposium on Affinity Technology and Bio-Recognition, Compiègne *Kinetic analysis of the effect on Fab binding of identical substitutions* *in a peptide and its parent protein*
30/05/2000	Secondes rencontres françaises Biacore, Paris *Kinetics in buffer space*
9/98-08/2000	Présentation de mes résultats 2 fois / an lors des réunions du consortium européen 'Reversible Antibodies'
4/04/2006	Vendredis de l'ESBS, Illkirch *Sélection d'aptamères sur Biacore*
8-9/04/2010	Probes for peptide science: design and methodological development, Paris *Peptide-based fluorescent ratiometric sensors for direct detection of proteins*
2/07/2010	**Conférence invitée** - Institut de Biologie Moléculaire des Plantes, Strasbourg *Surface Plasmon Resonance Biosensors: Principle of the technology & Applications*
14/09/2010	**Conférence invitée** - University San Pablo-CEU, Madrid *Surface Plasmon Resonance Biosensors: Principle of the technology & Applications*
14/10/2010	Séminaire Biacore, GE Healthcare Life Sciences seminar, Illkirch *Développement de biocapteurs peptidiques fluorescents* *pour la détection directe d'une cible protéique*
5/04/2018	**Conférence invitée** - Maison pour la Science en Alsace, Colmar *Jusqu'où peut-on voir les choses ? Une plongée vers l'infiniment petit*
19/07/2018	**Conférence invitée** - EuroSciCon Clinical Research Biomarkers 2018, Prague *Aptamers targeting cell-surface biomarkers as probes for cyto- and histo-chemistry*

avec présentations par posters

2-4/09/1998	BIAsymposium 1998, Edinburgh (GB) Choulier L., Rauffer-Bruyère N., Ben Khalifa M. & Altschuh D. *Are peptides good mimics for the functional properties of a protein ligand?*
4-8/07/1999	13th International Symposium on Affinity Technology and Bio-Recognition, Compiègne Andersson K., Gülich S. & Choulier L. *Kinetics in buffer space*
21-26/11/1999	Doctoriales® d'Alsace, Mittelwihr Choulier L. *Analyse des relations entre structure et cinétiques d'interaction* *antigène-anticorps à l'aide d'un biocapteur et traitements informatiques de données*
8-13/02/2002	Keystone symposia "Biological response to extracellular matrix", Banff (Canada) Choulier L, Altroff H, Handford P, Campbell ID, Stuart DI, Jones Y & Mardon HJ *Dissecting integrin-ligand interactions using biosensor technology*
5-6/07/2002	2nd joint UK/German Meeting "Cellular interactions in the Immune System", Berlin Choulier L, Altroff H, Handford P, Knott V, Campbell ID, Abrescia N, Stuart DI, Jones Y, Van der Merwe A & Mardon HJ *Surface plasmon resonance studies on interactions between integrins and* *extracellular matrix ligands*
30/04-4/05/2005	VIth European Symposium of the Protein Society, Barcelona Choulier L, Altroff H, Jovanovic J Stuart DI, Van der Merwe A, Handford P, & Mardon HJ

Surface plasmon resonance: a powerful approach to dissect interactions between integrins and extracellular matrix ligands

5-8/07/2008 20th Meeting of the European Association for Cancer Research, Lyon
Choulier L, Martin-Santamaria S, Roldós V, Ramos A, Altschuh D & de Pascual-Teresa B
SPR label-free ranking of small molecule negative modulators of adrenomedullin

16-17/04/2009 Journées Campus d'Illkirch 2009, Illkirch
Choulier L, Shvadchak VV, Enander K, Klymchenko AS, Naidoo A, Demchenko AP, Mely Y & Altschuh D
Peptide-based fluorescent ratiometric sensors for direct detection of proteins

16-17/04/2009 Journées Campus d'Illkirch 2009, Illkirch
Choulier L, Martin-Santamaria S, Roldós V, Ramos A, Altschuh D & de Pascual-Teresa B
SPR label-free ranking of small molecule negative modulators of adrenomedullin

20-21/11/2014 Canceropôle Grand-Est, Strasbourg
Choulier L, Fechter P, Ray A-M, Bandin A-F, Renner G, Noulet F, Etienne-Selloum N, Lelong-Rebel I, Martin S, Lehmann M & Dontenwill M
Selection of RNA aptamers against integrin α5β1

24-25/06/2016 Aptamers in Bordeaux, Bordeaux
Fenat M, Fechter P, Etienne-SelloumN, Lelong-Rebel I, Martin S, Lehmann M, Dontenwill1 M & Choulier L
RNA aptamers as ligands of integrinα5β1 in glioblastoma

sans présentations

23/01/1999 Biacore meeting day, Paris
3-5/05/2000 JOBIM 'Journées Ouvertes Biologie Informatique Mathématiques', Montpellier
10-11/06/2002 Conference "From gene to functional protein", Amersham, Paris
27-29/09/2004 Ecole thématique CNRS-CEA de Biologie/Chimie/Informatique, Aussois
'Criblage à haut débit : vers un criblage à haut contenu'
29-30/11/2007 Biacore symposium, Munich
30/10-3/11/2008 XXIème Congrès de Biophysique, Figeac
3-4/05/2010 Journées Campus d'Illkirch, Illkirch
20-21/09/2011 2011 ACCITH Forum (GDR 'Anticorps et ciblage thérapeutique'), Illkirch
22-23/09/2011 10ème Colloque de la Section 30 du CoNRS, Illkirch
2-3/11/2011 5ème Forum du Cancéropôle du Grand-Est, Strasbourg
12-13/11/2012 6ème Forum du Cancéropôle du Grand-Est, Strasbourg
25-26/11/2013 7ème Forum du Cancéropôle du Grand-Est, Strasbourg
2/07/2015 Biacore user meeting, Lyon
19/05/2017 5 ans de la Maison pour la Science en Alsace, Strasbourg

Financements

Contrats en tant que coordinatrice ou partenaire :

2010-2011 Projet Hubert Curien - PICASSO 2010
Design, synthesis and 3D-QSAR study of small molecules targeting adrenomedullin and PAMP in several diseases
Coordinateur français : Dr Laurence CHOULIER, ESBS, FRE 3211, Illkirch
Coordinateur espagnol : Dr Sonsoles MARTIN-SANTAMARIA, University San Pablo-CEU, Madrid
1 800 euros

2015-2016 Pré-maturation SATT Conectus
Anti-α5β1 aptamers characterisation
Coordinateur : Dr Laurence CHOULIER, Faculté de pharmacie, UMR 7213, Illkirch
43 380 euros

2015-2016 **Projets de Recherches exploratoires - PEPS IDEX 2015**

Caractérisation fonctionnelle d'aptamères ARN ciblant l'intégrine α5β1

Coordinateur : Dr Laurence CHOULIER, Faculté de pharmacie, UMR 7213, Illkirch

20 000 euros

2018-2020 **Projet IDEX Interdisciplinaire 'Emergence' 2017 - Unistra/CNRS**

Identification de la pharmacopée minérale médiévale arabe et extraction de fractions actives pour de nouvelles combinaisons anti-infectieuses

Coordinateur : Dr Pierre FECHTER, IREBS, UMR 7242, Illkirch

Partenaires : Dr Laurence CHOULIER, Faculté de pharmacie, UMR 7021, Illkirch
Dr Véronique PITCHON, UMR 7044, Strasbourg
Dr Catherine VONTHRON, Faculté de pharmacie, UMR 7200, Illkirch

44 000 euros

Et participation à plusieurs contrats :

1998-2001 **European Community Contract BIO4-CT98-0502**

Reversible antibodies

Coordinateur : Dr. Magnus Malmqvist, Biacore AB, Uppsala, Suède

2002-2005 **European Community Contract QLK1-CT-2002-02077**

Quantification of coeliac disease toxic gluten in foodstuffs using a chip system with integrated extraction, fluidics and biosensoric detection

Coordinateur : Dr. Ciara O'Sullivan, Universitat Rovira i Virgili, Espagne

2005-2006 **Contrat DGA n° 05 34 013**

Evaluation de biocapteurs peptidiques basés sur de nouvelles sondes fluorescentes

Coordinateur : Dr. Danièle Altschuh, UMR 7175, ESBS

Montant : 40 K€

2006 **Subvention du Ministère de la recherche espagnol**

Optimisation de ligands de l'adrénomédulline à action anti-tumorale, par une approche QSAR

Coordinateur : Dr. Beatriz de Pascual-Teresa Fernandez, University San Pablo-CEU, Espagne

Montant : 5 K€

2006-2008 **Contrat ANR06-2_139030**

Étude RMN des bases structurales de l'interférence de l'oncoprotéine E6 avec les interactions cellulaires médiées par les domaines PDZ

Coordinateur : Pr. Bruno Kieffer, UMR 7104, IGBMC

Montant : 30 K€

2007-2011 **Subvention ANR 07-BLAN-0287**

Développement de biocapteurs synthétiques fluorescents basé sur des sondes de la famille des 3HC

Coordinateur : Pr. Yves Mély, Faculté de Pharmacie, Strasbourg

Montant : 50 K€

2008-2011 **ARC n°3171**

Bases moléculaires du cancer du col de l'utérus: structure, fonction et inhibition de l'oncoprotéine virale E6

Coordinateur : Dr. Gilles Travé, Equipe Oncoprotéines, ESBS

Montant : 50 K€

2016-2017 **ARC 16/417/S07**

Cavéoline-1, intégrine α5β1 et miR-30 : marqueurs prédictifs, facteurs pronostics et nouvelles options thérapeutiques pour les tumeurs des voies aérodigestives à haut potentiel métastatique*

Coordinateur : Dr. Sophie Martin, Faculté de Pharmacie, Strasbourg

Organisation de conférences et de congrès

16/06/2000	**Forum ADDAL** (Association des Docteurs et Doctorants d'Alsace), Strasbourg
27/09/2007	**Journée des utilisateurs SPR** d'Alsace et de Lorraine, ESBS, Illkirch
14-17/09/2010	**Forum des Jeunes Chercheurs 2010** (SFBBM), Strasbourg
4-5/04/2013	**Journées Campus d'Illkirch 2013**
7-8/04/2014	**Journées Campus d'Illkirch 2014**
13-14/04/2015	**Journées Campus d'Illkirch 2015**
7-8/06/2018	**Forum BioChem**, Strasbourg
19-20/07/2018	**EuroSciCon Clinical Research & Biomarkers**, Prague

Animation scientifique

16-17/10/2005	**Fête de la science**, Strasbourg
27/09/2007	**Relais pour la vie**, Ligue nationale contre le cancer, Nordheim
29/01/2011	**Table ronde des métiers**, Lycée Louis Pasteur, Strasbourg
4/02/2012	**Table ronde des métiers**, Lycée Louis Pasteur, Strasbourg
13/02/2013	**Ose la Recherche**, Vaisseau, Strasbourg
19/02/2014	**Ose la Recherche**, Vaisseau, Strasbourg
18/02/2015	**Ose la Recherche**, Vaisseau, Strasbourg
13/11/2015	**Kids universities**, Strasbourg
9/03/2016	**Ose la Recherche**, Vaisseau, Strasbourg
8/02/2017	**Ose la Recherche**, atelier parents, Vaisseau, Strasbourg
7/04/2017	**Forum des métiers** au collège d'Illkirch
4/10/2017	**Les étoiles du savoir**, cercle Gutenberg, MSA et jardin des sciences, Strasbourg
22/11/2017	**DECLICS**, Lycée Jean Monnet, Strasbourg

Formations suivies

3-5/06/1997	Biacore kinetic data analysis software (SPRevolution), Grenoble
7-13/09/1997	AIDS research, La Londe les Maures
27/10-7/11/1997	Expression de protéines recombinantes, Grenoble
16-20/11/1998	Immunodétection de peptides, technologie Spot, Montpellier
8-18/03/1999	New software for Biacore kinetic data processing, Uppasala (Suède)
4-7/05/1999	Sequence analysis and homology modeling, Strasbourg
4-17/01/2000	Technique du Phage display, Strasbourg
24/01-4/02/2000	New software for Biacore kinetic data processing, Uppasala (Suède)
12/12/2001	BBSCR meeting day "Membrane protein production", Oxford (GB)
22-24/11/2004	Formation CNRS 'Conduite d'exposés scientifiques', Strasbourg
depuis déc 2005	Formation Sauveteurs secouristes du travail, Strasbourg et recyclage d'une ½ journée/an ou 1 journée/2 ans
1/04/2010	Formation Excel-Représentation graphique-Office 2007, Strasbourg
26-27/04/2010	Formation Excel-Perfectionnement Fonctions-Office 2007, Strasbourg
31/05-1/06/2010	Formation Excel-Bases de données-Office 2007, Strasbourg
10-11/06/2010	Stage Bioinformatique, Illkirch
14-15/04/2014	Formation Word-Perfectionnement Fonctions-Office 2010, Strasbourg
21-22/09/2015	Animation de réunion (CNRS Alsace), Strasbourg
22/09/2016	Monter un projet ANR (CNRS Alsace), Strasbourg
28/09/2016	Les gestes qui sauvent, Illkirch
27-28/03,4-5/05 8-9/06, 19/09/2018	Management des Hommes et des équipes, Strasbourg

Publications

1999

1. Choulier, L., Rauffer-Bruyère, N., Ben Khalifa, M., Martin, F., Vernet, T. & Altschuh D. (1999). Kinetic analysis of the effect on Fab binding of identical substitutions in a peptide and its parent protein. *Biochemistry* **38**, 3530-3537.

2000

2. Choulier, L., Lafont, V., Hugo, N. & Altschuh, D. (2000). Covariance analysis of protein families: the case of the variable domains of antibodies. *Proteins* **41**, 475-484.
3. Khalifa, M., Weidenhaupt, M., Choulier, L., Chatellier, J., Rauffer-Bruyère, N., Altschuh, D. & Vernet, T. (2000). Effects on interaction kinetics of mutations at the VH-VL interface of Fabs depend on the structural context. *J. Mol. Recognit.* **13**, 127-139.
4. Schwalbach, G., Sibler, A.-P., Choulier, L., Deryckère, F. & Weiss, E. (2000). Production of fluorescent single-chain antibody fragments in *Escherichia coli*. *Protein Expr. Purif.* **18**, 121-132.

2001

5. Andersson, K., Choulier, L., Hämäläinen, M., Van Regenmortel, M.H.V., Altschuh, D. & Malmqvist, M. (2001). Predicting the kinetics of peptide-antibody interactions using a multivariate experimental "design" of sequence and chemical space. *J. Mol. Recognit.* **14**, 62-71.
6. Choulier, L., Laune, D., Orfanoudakis, G., Wlad, H., Janson, J.-C., Granier, C. & Altschuh, D. (2001). Delineation of a linear epitope by multiple peptide synthesis and phage display. *J. Immunol. Methods* **249**, 253-264.
7. Khalifa, M., Choulier, L., Hortat-Jacob, H., Altschuh, D. & Vernet, T. (2001). BIACORE® data processing: an evaluation of the global fitting procedure. *Anal. Biochem.* **293**, 194-203.
8. Van Regenmortel, M.H.V. & Choulier, L. (2001). Recognition of peptides by antibodies and investigations of affinity measurements using biosensor technology. *Combinatorial Chemistry & High Throughput Screening* **4**, 385-395.

2002

9. Choulier, L., Orfanoudakis, G., Robinson, P, Laune, D., Ben Khalifa, M., Granier, C., Weiss, E. & Altschuh, D. (2002). Comparative properties of two peptide-antibody interactions, as deduced from epitope delineation. *J. Immunol. Methods* **259**, 77-86.
10. Choulier, L., Andersson, K., Hämäläinen, M., Van Regenmortel, M.H.V., Malmqvist, M. & Altschuh, D. (2002). QSAR studies applied to the prediction of antigen-antibody interaction kinetics as measured by BIACORE. *Protein Eng.* **15**, 373-382.
11. Weidenhaupt, M., Khalifa, M.B., Hugo, N., Choulier, L., Altschuh, D. & Vernet, T. (2002). Functional mapping of conserved, surface-exposed charges of antibody variable domains. *J. Mol. Recognit.* **15**, 94-103.

2003

12. Altroff, H., Choulier, L. & Mardon, H.J. (2003). Synergistic activity of the ninth FIII domain of fibronectin depends on its structural stability. *J. Biol. Chem*. **278**, 491-497.

2004

13. Lee, S.S., Knott, V., Jovanovic, J., Harlos, K., Grimes, J.M., Choulier, L., Mardon, H.J., Stuart, D.I., Handford, P.A. (2004). Structure of the integrin binding fragment from fibrillin-1 gives new insights into microfibril organization. *Structure*. **12**, 717-729.

2005

14. Choulier, L., Altschuh, D., Zeder-Lutz, G. & Van Regenmortel, M.H.V. (2005). Biosensor characterization of structure-function relationships in viral proteins. *Methods in Microbiology*. **34**, 213-238.
15. Dejaegere, A., Choulier, L., Lafont, V., De Genst, E. & Altschuh, D. (2005). Variations in antigen-antibody association kinetics as a function of pH and salt concentration: a QSAR and molecular modeling study. *Biochemistry* **44**, 14409-14418.

2007

16. Jovanovic, J., Takagi, J., Choulier, L., Abrescia, N.G.A., Stuart, D.I., Van der Merwe, P.A., Mardon, H.J. & Handford, P.A. (2007). Avb6 is a novel receptor for human fibrillin-1: comparative studies of molecular determinants underlying integrin-RGD affinity and specificity. *J. Biol. Chem.* **282**, 6743-6751.

2008

17. Enander, K., Choulier, L., Linnéa-Olsson, A., Yushchenko, D.A., Kanmert, D., Klymchenko, A.S., Demchenko, A.P., Mély, Y. & Altschuh, D. (2008). A peptide-based, ratiometric biosensor construct for direct fluorescence detection of a protein analyte. *Bioconjug. Chem.* **19**, 1864-70
18. Greschik, H., Althage, M., Flaig, R., Sato, Y., Peluso-Iltis, C., Chavant, V., Choulier, L., Cronet, P., Rochel, N., Schüle, R., Strömstedt, P.E., Moras, D. (2008). Communication between the ERR alpha homodimer interface and the PGC-1alpha binding surface via the helix 8-9 loop. *J. Biol. Chem*. **283**, 20220-20230.
19. Roldós, V., Martín-Santamaría, S., Julián, M., Martínez, A., Choulier, L., Altschuh, D., de Pascual-Teresa, B. & Ramos, A. (2008). Small Molecule Negative Modulators of Adrenomedullin: Design, Synthesis, and 3D-QSAR Study. *Chem. Med. Chem.* **3**, 1345-55.

20. Sibler, A.P., Baltzinger, M., Choulier, L., Desplancq, D. & Altschuh, D. (2008). SPR identification of mild elution conditions for affinity purification of E6 oncoprotein, using a multivariate experimental design. *J. Mol. Recognit.* **21**, 46-54.

2010

21. Choulier, L.*, Schvadchak, VV., Naidoo, A., Klymchenko, AS., Mély, Y & Altschuh, D. (2010). A peptide-based fluorescent ratiometric sensor for quantitative detection of proteins. *Anal. Biochem.* **401**, 188-195. (*corresponding author)
22. Choulier, L.* & Enander, K. (2010). Environmentally Sensitive Fluorescent Sensors Based on Synthetic Peptides. *Sensors* **10**, 3126-3144. (*corresponding author)

2011

23. Hammani, K., Gobert, A., Hleibieh, K., Choulier, L., Small, I.& Giegé, P. (2011) An Arabidopsis dual-localized pentatricopeptide repeat protein interacts with nuclear proteins involved in gene expression regulation. *Plant Cell*. **23**, 730-40.
24. Löfas, S., Choulier, L., Zeder-Lutz, G., Baltzinger, M., Altschuh, D. (2011) Surface plasmon resonance. *RSC Biomolecular Sciences.* **22**, 136-55.

2012

25. Zeder-Lutz, G., Choulier, L., Besse, M., Cousido-Siah, A., Figueras, FXR., Didier, B., Jung, ML., Podjarny, A. & Altschuh, D. (2012). Validation of SPR screening of a diverse chemical library for the discovery of protein tyrosine phosphatase 1b binders. *Anal. Biochem*. **421**, 417-427.
26. Altschuh, D., Björkelund., H., Strandgård, J., Choulier, L., Malmqvist, M. & Andersson, K. (2012). Deciphering complex protein interaction kinetics using Interaction Map. *Biochem Biophys Res Commun*. **428**, 74-9.

2013

27. Janouskova, H., Ray, A.M., Noulet, F., Lelong-Rebel, I., Choulier, L., Schaffner, F., Lehmann, M., Martin, S., Teisinger, J. & Dontenwill, M. (2013). Activation of p53 pathway by Nutlin-3a inhibits the expression of the therapeutic target α5 integrin in colon cancer cells. *Cancer Lett*. **336**, 307-18.
28. Choulier, L.*, Nomine, Y., Zeder-Lutz, G., Charbonnier, S., Didier, B., Jung, M.L. & Altschuh, D.* (2013). Chemical library screening using a SPR-based inhibition in solution assay: simulations and experimental validation. *Anal. Chem*. **85**, 8787-95. (*corresponding authors).
29. Duval, M., Korepanov, A., Fuchsbauer, O., Fechter, P., Haller, A., Fabbretti, A., Choulier, L., Micura, R., Klaholz, B., Romby, P., Springer, M. & Marzi, S. (2013). Escherichia coli ribosomal protein S1 unfolds structured mRNAs onto the ribosome for active translation initiation. *Plos. Biol.* 11, e1001731.

2014

30. Ray, A.M., Schaffner, F., Janouskova, H., Noulet, F., Rognan, D., Lelong-Rebel, I., Choulier, L., Blandin, A.-F., Lehmann, M., Martin, S., Neubauer, S., Rechenmacher, F., Kessler, H. & Dontenwill, M. (2014). Single cell tracking assay reveals an opposite effect of selective small non-peptidic α5β1 or αvβ3/β5 integrin antagonists in U87MG glioma cells. *Biochim Biophys Acta*. **1840**, 2978-87.

2015

31. Nominé, Y., Choulier, L., Travé, G., Vernet, T. & Altschuh, D. (2015). Antibody binding selectivity: alternative sets of antigen residues entail high-affinity recognition. *PLoS One.* **10**(12), e0143374.
32. Jung, A.C., Ray, A.M., Ramolu, L., Macabre, C., Simon, F., Noulet, F., Blandin, A-F., Renner, G., Lehmann, M., Choulier, L., Kessler, H., Abecassis, J., Dontenwill, M. & Martin, S. (2015). Caveolin-1-negative head and neck squamous cell carcinoma primary tumors display increased epithelial to mesenchymal transition and prometastatic properties. *Oncotarget.* **6**(39), 41884-901.
33. Vernet, T., Choulier, L., Nominé, Y., Bellard, L., Baltzinger, M., Travé, G. & Altschuh, D. (2015). Spot peptide arrays and SPR measurements: throughput and quantification in antibody selectivity studies *J. Mol. Recognit*. **28**(10), 635-44.

2016

34. Renner, G., Noulet, F., Mercier, M-C., Choulier, L., Etienne-Selloum, N., Gies, J-P., Lehmann, M, Lelong-Rebel, I., Martin, S. & Dontenwill, M. (2016). Expression/activation of α5β1 integrin is linked to the β-catenin signaling pathway to drive migration in glioma cells. *Oncotarget* **7**(38), 62194-207.
35. Blandin, A-F., Noulet, F., Renner, G., Mercier, M-C., Choulier, L., Vauchelles, R., Ronde, P., Carreiras, F., Etienne-Selloum, N., Vereb, G., Lelong-Rebel, I., Martin, S., Dontenwill, M. & Lehmann, M. (2016). Glioma cell dispersion is driven by α5 integrin-mediated cell-matrix and cell-cell interactions. *Cancer Lett.* **376**(2), 328-38.
36. Renner, G., Janouskova, H., Noulet, F., Koenig, V., Guerin, E., Bär, S., Nuesch, J., Rechenmacher, F., Neubauer, S., Kessler, H., Blandin, A-F, Choulier, L., Etienne-Selloum, N., Lehmann, M., Lelong-Rebel, I., Martin, S. & Dontenwill, M. (2016). Integrin α5β1 and p53 convergent pathways in the control of anti-apoptotic proteins PEA-15 and survivin in high-grade glioma. *Cell Death Differ.* **23**(4), 640-53.

2017

37. Mercier, M.-C., Dontenwill, M. & Choulier, L.* (2017). Selection of nucleic acid aptamers targeting tumor cell-surface protein biomarkers. *Cancers*. **9**(6), pii: E69. (*corresponding author).

Actes de congrès:

38. Choulier, L., Martin-Santamaria, S., Roldos, V., Ramos, A., Altschuh, D., & de Pascual-Teresa, B. (2008). SPR label-free ranking of small molecule negative modulators of adrenomedullin. *European Journal of Cancer Supplements*, **6**, 152. [Meeting abstract, EACR, Lyon]
39. Duval, M., Korepanov, A., Fuchsbauer, O., Fechter, P., Haller, A., Fabbretti, A., Choulier, L., Micura, R., Klaholz, B., Romby, P., Springer, M. & Marzi, S. (2014). Ribosomal protein S1 unfolds structured mRNAs on the ribosome for translation initiation in Escherichia coli. *FEBS J.* **281**. Special Issue: SI Supplement: 1, 290 [Meeting Abstract FEBS EMBO 2014, Paris, France]
40. Dontenwill, M., Janouskova, H., Renner, G., Ray, A.-M., Noulet, F., Choulier, L., Etienne-Selloum, N., Lehmann, M., Lelong-Rebel, I. & Martin, S. (2014). Improved cytotoxic therapy by dual targeting of α5β1 integrin and p53 pathway in glioblastoma. Eur. J. Cancer. 50(5), Supplement: 5, S199-S200 [Meeting Abstract: 825 Published: JUL 2014]
41. Burgy, M., Jung, A., Ray, A.-M., Ramolu, L., Macabre, C., Simon, F., Noulet, F., Blandin, A.-F., Renner, G., Lehmann, M., Choulier, L., Kessler, H., Abecassis, J., Dontenwill, M. & Martin, S. (2016). Caveoline-1: potential prognostic and therapeutic interest in VADS tumors. *Bulletin du Cancer*. **103**(6), Supplement: 1, S114-5 [Meeting Abstract: PC-04]
42. Choulier, L., Fenat, M., Fechter, P., Blandin, A.-F., Renner, G., Etienne-Seloum, N., Lelong-Rebel, I., Martin, S., Lehmann, M. & Dontenwill, M. (2016). Characterization of RNA aptamers as specific ligands of integrin alpha5 beta1. *European Journal of Cancer* 61(1), Supplement 1, S126 [Meeting Abstract EACR24, Poster Session: Experimental/Molecular Therapeutics, Pharmacogenesis I: 576]

SYNOPSIS

L'objet de mon doctorat au sein de l'UMR 9021 à l'IBMC (Institut de Biologie Moléculaire et Cellulaire, Université Louis Pasteur, Strasbourg) a été d'acquérir une meilleure compréhension des paramètres capables d'influencer les cinétiques des interactions antigène-anticorps, afin de moduler ces paramètres de manière prédictive, en utilisant une description quantitative des relations structure-activité. Un criblage par présentation de peptides à la surface de phages ('phage display') suivi de détection de peptides synthétisés sur membrane de cellulose, a également permis d'identifier les épitopes de deux fragments d'anticorps.

Mon 1er stage post-doctoral au NDOG (Nuffield Department of Obstetrics and Gyneacology) dans l'équipe de Helen Mardon à l'Université d'Oxford (Grande-Bretagne) m'a permis d'étendre mon expérience des relations structure-activité de reconnaissance à des systèmes d'interaction plus complexes, entre intégrines (dont α5β1) et protéines de la matrice extracellulaire et de me familiariser à la biologie de ces récepteurs, dans un environnement médical.

Lors de mon 2ème stage post-doctoral, au sein de l'U386-INSERM à l'Institut Européen de Chimie et Biologie (IECB, Bordeaux), dirigée par Jean-Jacques Toulmé, j'ai acquis une deuxième expérience concernant la conception et le criblage moléculaire de banques, en utilisant une méthode bien établie dans le laboratoire de Jean-Jacques Toulmé, et de mieux appréhender les problèmes liés à cette approche : le SELEX ('systematic evolution of ligands by exponential enrichment', Ellington & Szostak, 1990 ; Robertson & Joyce, 1990 ; Tuerk & Gold, 1990).

En 2004, j'ai été recrutée au CNRS à l'IREBS (Institut de Recherche de l'Ecole Supérieure de Biotechnologie de Strasbourg) dans l'équipe 'Biocapteurs' dirigée par Danièle Altschuh. J'y ai développé plusieurs axes de recherche. Les deux axes particulièrement décrits dans ce manuscrit concernent les biocapteurs moléculaires peptidiques et les stratégies de sélection et d'optimisation de molécules à potentiel diagnostic et/ou thérapeutique.

En mars 2012, j'ai intégré l'UMR 7213, renommée UMR 7021 en janvier 2018, Laboratoire de Bioimagerie et Pathologies, dirigée par Yves Mély, au sein de la faculté de pharmacie de Strasbourg. Mes recherches actuelles sont développées dans l'équipe 'Signalisation tumorale et cibles thérapeutiques' dirigée par Monique Dontenwill. L'axe 'Intégrines et cancer' de cette équipe s'intéresse particulièrement à une protéine membranaire, l'intégrine α5β1, comme marqueur diagnostique, pronostique et cible thérapeutique pour les tumeurs cérébrales.

Ce manuscrit ne retrace pas l'ensemble mais uniquement les principales étapes des dix dernières années de mon parcours scientifique. Il concerne à la fois mes derniers projets de recherche au sein de l'IREBS (UMR 7242) et mon activité de recherche au sein de l'UMR 7021. Ce manuscrit est divisé en deux parties principales. Mes travaux de recherches des années antérieures à 2008 (1997-2008) sont brièvement abordés en Annexe.

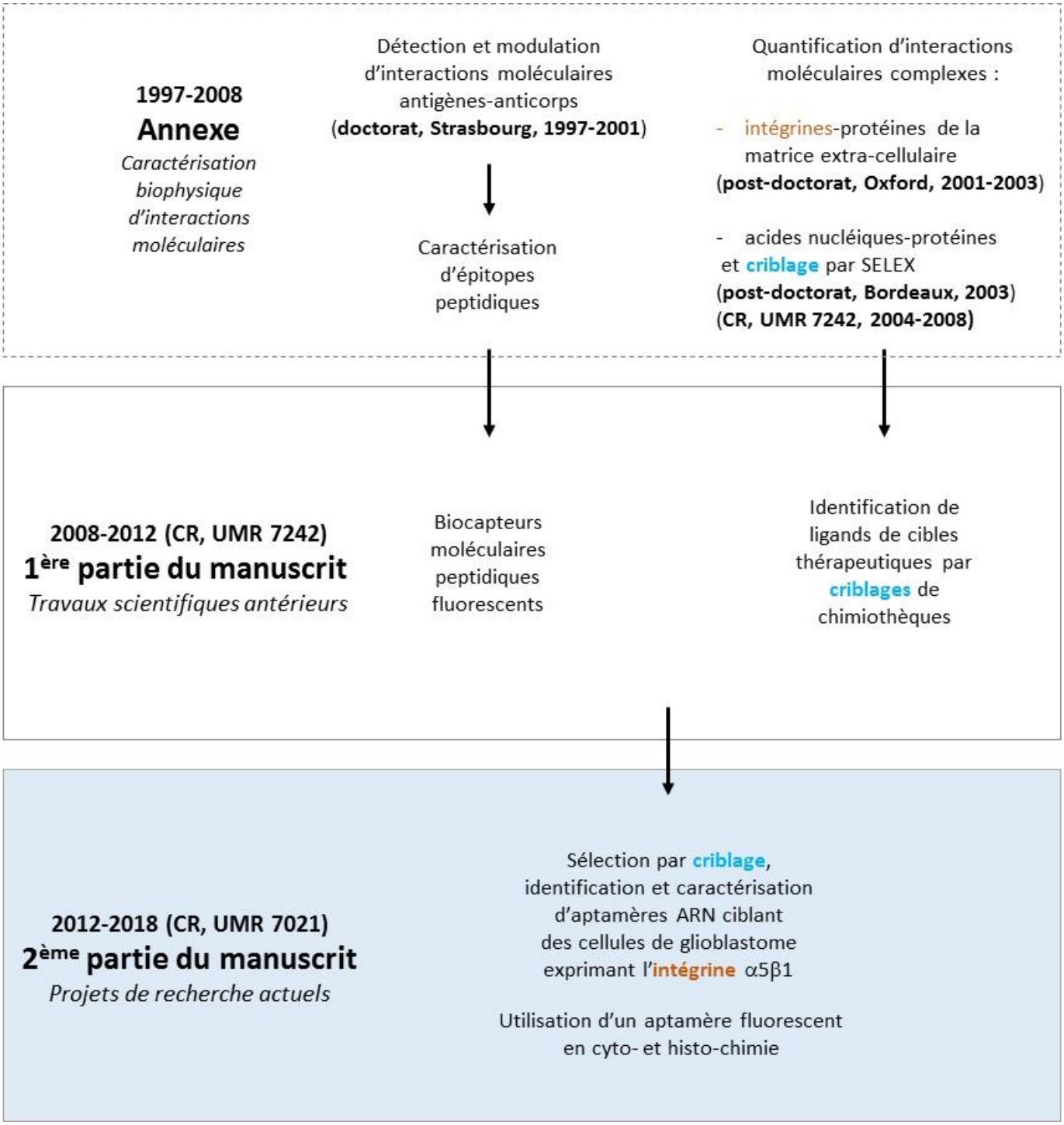

Dans la première partie de ce manuscrit, intitulée ‘Projets scientifiques antérieurs’ (2008-2012), sont décrits le développement de biocapteurs moléculaires et l’identification de ligands de cibles thérapeutiques par criblage de chimiothèques. C’est grâce à la caractérisation préalable (décrite en Annexe) de deux épitopes peptidiques (par synthèse multiple de peptides sur membrane SPOT, ‘phage display’ et QSAR ‘quantitative structure-activity relationship’) que nous avons pu entreprendre le développement de biocapteurs peptidiques fluorescents. C’est également grâce à une bonne connaissance des interactions moléculaires complexes par SPR (‘surface plasmon resonance’), que les criblages de chiomiothèques ont pu être réalisés.

Dans une deuxième partie, intitulée ‘Projets de recherche actuels’, sont décrites de manière plus approfondie, mes recherches concernant la sélection et la caractérisation d’aptamères ARN ciblant les cellules de glioblastome exprimant l’intégrine α5β1. Une sélection d’aptamères a été réalisée par criblage, nommé SELEX ; une technique que j’ai apprise lors de mon deuxième post-doctorat, à Bordeaux. L’intégrine α5β1, la cible de ce criblage, est l’une des intégrines dont j’avais appréhendé la complexité et étudié son interaction avec la fibronectine, lors de mon premier post-doctorat, à Oxford. A l’issue du SELEX, nous avons identifié un aptamère nommé H02. Cet aptamère directement couplé à un fluorophore a notamment été utilisé pour détecter l’intégrine α5β1 en cyto- et histo-chimie. Les perspectives de ce projet sont intégrées à la fin de cette deuxième partie.

Les articles et revues cités dans ces deux parties principales sont insérés en fin de chapître les concernant.

Travaux scientifiques antérieurs

(années 2008-2011)

A. Développement de biocapteurs moléculaires fluorescents

Revue 1 et Article 1

Résumé :

Un biocapteur moléculaire combine au sein d'une même molécule :
- un récepteur : élément de reconnaissance capable de reconnaître la molécule d'intérêt (analyte) à détecter
- un transducteur : détecteur capable de convertir l'évènement de reconnaissance biologique en un signal mesurable. Le transducteur d'un biocapteur moléculaire fluorescent est un fluorophore.

Avant même mon intégration au sein de l'UMR 7213, une collaboration avait été établie avec l'équipe d'Yves Mély pour développer des peptides en tant que biocapteurs moléculaires fluorescents sensibles à l'environnement : le fluorophore sensible à l'environnement est couplé dans une région du récepteur proche du site de liaison à l'analyte, mais non-essentiel pour l'interaction. L'interaction récepteur-analyte provoque alors un changement de l'environnement physico-chimique du fluorophore, traduit par une variation de ses propriétés de fluorescence. Deux systèmes d'interaction peptide-anticorps bien caractérisés précedemment au laboratoire, nous ont servi de modèles d'étude. Nous avons défini les positions optimales des deux peptides sur lesquelles coupler le fluorophore pour que les peptides fonctionnent en tant que biocapteurs moléculaires sensibles à l'environnement, pour détecter des protéines.

Dans cette partie sont inclus une revue sur les biocapteurs peptidiques fluorescents sensibles à l'environnement (Revue 1) et un article décrivant l'un des deux systèmes d'interaction et les propriétés d'un biocapteur peptidique (Article 1).

D’après la définition de l’IUPAC (International Union of Pure and Applied Chemistry), un biocapteur est un dispositif intégré, capable de fournir des informations spécifiques quantitatives ou semi-quantitatives. Il est composé d’un élément de reconnaissance d’origine biologique et d’un transducteur. L’élément de reconnaissance biologique (le récepteur) réagit spécifiquement avec la molécule d’intérêt (l’analyte). Le transducteur agit en tant que détecteur, convertissant l’évènement de reconnaissance moléculaire en un signal mesurable. En oncologie, notamment, alors que la détection d'un cancer à une phase précoce augmente considérablement les chances de réussite du traitement, des biocapteurs sont testés pour détecter des biomarqueurs moléculaires, notamment des protéines et des acides nucléiques (Jayanthi et al., 2017). Les biocapteurs ont de faibles limites de détection, permettant ainsi la détection de biomarqueurs dans les échantillons physiologiques de l’ordre du fg/ml au ng/ml. Ils permettent également de gagner du temps, de ré-utiliser le récepteur, mais aussi de détecter plusieurs biomarqueurs simultanément. Ces biocapteurs, qui utilisent principalement des transducteurs électrochimiques ou optiques et permettent une détection en temps réel, sont toutefois restreints aux laboratoires qui disposent d’instruments sophistiqués, extrêmement fiables, mais couteux.

Lorsque le récepteur et le transducteur sont intégrés au sein d’une même molécule, on parle de biocapetur moléculaire. Un biocapteur moléculaire (Hellinga et Marvin., 1998) est donc une molécule composée d’un récepteur, covalemment associé à un transducteur, généralement un fluorophore. Le récepteur reconnaît l’analyte, alors que le fluorophore répond à l’évènement de reconnaissance et le transforme en un signal facilement mesurable. Les biocapteurs fluorescents sont utilisés pour la détection et la quantification d’analytes. Ils ont des applications potentielles dans les domaines de la médecine, de l’industrie agroalimentaire, de la défense ou protection de l’environnement, mais aussi en biologie fondamentale pour appréhender des évenements biologiques. L’application de ce principe prometteur aux anticorps se heurte à de nombreuses difficultés. Pour coupler covalemment un fluorophore à une protéine recombinante, la méthode la plus couramment utilisée consiste à remplacer un acide aminé donné par une cystéine et de coupler le fluorophore à son groupement thiol. Cette approche nécessite la production et purification de grandes quantités de protéines recombinantes, est difficilement implémentable à du ‘microarray’ dans lequel l’immobilisation de la protéine biocapteur risque de la dénaturer. En outre, cette méthode est relativement compliquée. En effet, mutations et/ou couplages peuvent (i) diminuer le taux d’expression protéique, (ii) dimininuer ou inhiber la liaison de l’analyte, (iii) provoquer une perte de stabilité, ou l’agrégation ou la dénaturation de la protéine ou (iv) induire une absence de signal de fluorescence…. Le fluorophore peut même parfois être

couplé sur les chaînes latérales de lysines. Il s'agit alors d'une réaction 'parasite'. Ces problèmes peuvent être résolus par l'utilisation d'autres récepteurs synthétisés chimiquement, en grande quantité, et plus stables, tels que des peptides, de petits composés chimiques et même des aptamères (Musumeci et al., 2017 ; Hori et al., 2018).

Le principe d'un biocapteur moléculaire sensible à l'environnement repose sur le fait qu'un fluorophore sensible à l'environnement est couplé dans une région du récepteur proche du site de liaison à l'analyte, mais non-essentiel pour l'interaction. La liaison récepteur-analyte provoque alors un changement de l'environnement physico-chimique du fluorophore, traduit par une variation de ses propriétés de fluorescence, telle qu'une extinction ou une intensification de fluorescence ou un shift du spectre d'émission. En 2010, j'ai été invitée à écrire une revue pour le journal Sensors, au sujet de biocapteurs peptidiques fluorescents sensibles à l'environnement (Choulier & Enander, 2010). Cette revue est inclue à la fin de ce paragraphe (Revue 1). Karin Enander, que j'ai encadrée lors de son post-doctorat au sein de l'IREBS, a participé à son écriture.

La position peptidique optimale pour le couplage du fluorophore est difficile à prédire, particulièrement en absence de données structurales. Cette position doit être telle que le mircoenvironnement du fluorophore soit modifié lors de la liaison de l'analyte. Bien que plus facile à implémenter pour un peptide que pour une protéine, le choix de la position optimale de couplage du fluorophore est difficilement prédictible. Notamment, la distance entre le résidu marqué et l'épitope peptidique n'est pas un paramètre généralisable à tout système d'interaction peptide-protéine pour développer un biocapteur peptidique. En collaboration avec Yves Mély et Andrey Klymchenko (UMR 7213, Illkirch), notamment autour de deux projets (DGA 'Evaluation de biocapteurs peptidiques basés sur de nouvelles sondes fluorescente ' et ANR 'Développement de biocapteurs synthétiques fluorescents basé sur des sondes de la famille des 3HC (3-hydroxychromone)', nous avons montré qu'une construction synthétique, formée d'un peptide couplé à un fluorophore ratiométrique, fonctionne comme biocapteur moléculaire sensible à l'environnement, dans deux systèmes d'interaction anticorps-peptide (Enander et al., 2008 ; Choulier et al., 2010), déjà bien identifiés au sein du laboratoire (Andersson et al., 2001 ; Choulier et al., 1999, 2001, 2002a & 2002b ; voir aussi la partie 'Annexe'). Par diverses expériences, telles que 'phage display' et analyses mutationnelles, nous savions déjà quels résidus des peptides étaient importants pour la liaison des fragments d'anticorps.

Le premier modèle (Enander et al., 2008) concerne l'interaction entre le Fab 57P et un peptide correspondant à la séquence 134-151 de la VMTP (protéine de coque du virus de la mosaïque du tabac). Un fluorophore ratiométrique de la famille des 3HC a été couplé indépendamment sur des cystéines remplaçant les acides aminés d'origine, en 2 positions de la séquence peptidique, à 2 et 7 résidus de l'épitope fonctionnel (acides aminés 146 et 151 de la VMTP, respectivement). Nous avons montré que le fluorophore n'influence pas les cinétiques d'interaction Fab-peptide et que le peptide marqué à 7 résidus de l'épitope (position 151 de la VMTP) agit comme biocapteur. Une variation de 40% de l'intensité de fluorescence est enregistrée lors de la liaison du Fab 57P. Le peptide couplé en position 146 n'a, quant à lui, pas les propritées d'un biocapteur. Le couplage du fluorophore à proximité de l'épitope n'est pas une condition suffisante à l'obtention d'un biocapteur peptidique.

Le deuxième modèle (Choulier et al., 2010) a confirmé la possibilité de fabriquer des biocapteurs peptidiques sensibles à l'environnement pour la détection de protéines. Il s'agit de l'interaction entre le scFv $1F4_{Q34S}$ et des peptides mimant la partie N-terminale de l'oncoprotéine E6 du papillomavirus humain (HPV_{16}). Trois peptides de taille variable, ont été utilisés. Ils miment les séquences 4-17, 7-17 et 9-17 de l'oncoprotéine E6. L'épitope fonctionnel correspond aux résidus 9-14 de la séquence peptidique. Nous avons choisi trois positions à substituer, respectivement à zéro, deux et cinq résidus distants de la première position identifiée comme importante pour la liaison du fragment d'anticorps (position 9). Ces peptides ont été marqués par le fluorophore à leur extrémité N-terminale. Nous avons montré que sur les trois peptides marqués avec un fluorophore ratiométrique, seul le peptide 3HC-7-17, marqué à une distance de deux résidus de l'épitope présente les propriétés d'un biocapteur. Lors de l'interaction avec le scFv, une variation d'intensité de fluorescence de 47% est observée. Nous avons également montré qu'une telle construction permet (i) d'avoir accès aux K_Ds de l'interaction scFv-peptides non-marqués, (ii) de réaliser une courbe de calibration, et (iii) de détecter le scFv jusqu'à 15 nM dans un milieu simple (tampon) et avec une limite de 50-100 nM en milieu plus complexe (BSA 'bovine serum albumin' à 100 μg/ml). Cette publication est inclue ci-dessous (Article 1).

Revue 1

Choulier, L.* & Enander, K. (2010). Environmentally Sensitive Fluorescent Sensors Based on Synthetic Peptides. *Sensors* **10**, 3126-3144. (*corresponding author)

Sensors **2010**, *10*, 3126-3144; doi:10.3390/s100403126

OPEN ACCESS

sensors

ISSN 1424-8220

www.mdpi.com/journal/sensors

Review

Environmentally Sensitive Fluorescent Sensors Based on Synthetic Peptides

Laurence Choulier [1,*] and Karin Enander [2]

[1] Biosensor group, CNRS / Université de Strasbourg, IREBS, Parc d'Innovation, Boulevard Sébastien Brandt, BP 10413, 67412 Illkirch cedex, France

[2] Division of Molecular Physics, Department of Physics, Chemistry and Biology, Linköping University, 581 83 Linköping, Sweden; E-Mail: karen@ifm.liu.se

* Author to whom correspondence should be addressed; E-Mail: laurence.choulier@unistra.fr; Tel.: +33-3-68854846; Fax: +33-3-68854683.

Received: 6 January 2010; in revised form: 27 February 2010 / Accepted: 24 March 2010 / Published: 31 March 2010

Abstract: Biosensors allow the direct detection of molecular analytes, by associating a biological receptor with a transducer able to convert the analyte-receptor recognition event into a measurable signal. We review recent work aimed at developing synthetic fluorescent molecular sensors for a variety of analytes, based on peptidic receptors labeled with environmentally sensitive fluorophores. Fluorescent indicators based on synthetic peptides are highly interesting alternatives to protein-based sensors, since they can be synthesized chemically, are stable, and can be easily modified in a site-specific manner for fluorophore coupling and for immobilization on solid supports.

Keywords: peptide biosensors; environmentally-sensitive fluorophore

1. Introduction

A molecular biosensor [1] is a molecule composed of a biological recognition element (receptor) covalently associated with a transducer, generally a fluorophore, for signaling. The receptor is selected to

specifically recognize a molecule of interest (analyte), while the fluorophore responds to the recognition event and transforms it into a measurable signal. The molecular biosensor can be distinguished from a chemosensor by the nature of the receptor, which is typically a biomacromolecule such as a nucleic acid (DNA or RNA), or a protein (often an enzyme or an antibody). Fluorescent molecular biosensors are mainly designed for the detection and quantification of analyte, with potential applications in the fields of medicine, agro-industry, defense or protection of the environment, but are also exploited to understand biomolecular events.

Compared to an immunoassay, which requires indirect labeling and multistep reactions, the detection of an analyte by a fluorescent biosensor is simple, direct and can be appreciated in real-time. The principle of sensing is illustrated in Figure 1. When an environmentally sensitive fluorophore is coupled near the binding site of a receptor, it will respond to changes in the physico-chemical environment induced by complex formation, by altering its fluorescence properties. Typically, polarity variations in the immediate vicinity of the fluorophore result in quenching or enhancement of the fluorescence and/or a wavelength shift in the emission spectrum. Recent reviews describe the structures, key physical parameters (extinction coefficients, excitation and emission wavelengths, quantum yields, size, hydrophobicity, stability) and advantages of some of the most common environmentally-sensitive fluorophores [2], or the design of biosensor molecules based on proteins [3]. While implemented with many different types of protein receptors, analytes and fluorophores, site-specific incorporation of fluorophores in proteins remains a challenge. The most widely used approach to covalently couple an extrinsic fluorophore to a recombinant protein involves the replacement of a less reactive amino acid residue with cysteine, followed by dye coupling to the free thiol group of the purified protein in buffer. This approach is straightforward, but difficult to implement on a general basis because mutations and coupling can lead to poor expression levels, deleterious effects on analyte binding, poor stability, aggregation or unfolding. Moreover, side reactions between thiol-reactive fluorophores and lysine side chains have been observed [4,5]. Other approaches to coupling a fluorophore at a specific site of proteins involve nonsense suppression [6], active-site-selective labeling [7-9], post-photoaffinity labeling modification [10-12], and, for chemically solid-phase synthesized proteins, the Suzuki-coupling reaction [13] and native-chemical ligation of peptides [14].

Protein-based environmentally-sensitive fluorescent biosensors have been successfully used for analyte detection and quantification with affinities varying from 0.2 nM to 150 mM, sometimes even in immobilized formats [14-17]. Still, synthetic peptides are interesting alternatives as receptors, because they provide obvious advantages over proteins in terms of production and stability. Peptide synthesis is straightforward and cost-effective and peptide-dye constructs can be manufactured at large scale. Moreover, synthetic peptides are robust, offer an even larger chemical versatility than recombinant proteins and are easily modified in a site-specific manner by means of orthogonal protection group strategies. Thus, peptides should have a great potential as components in molecular biosensors.

This review will specifically focus on biosensor constructs based on synthetic peptides and designed for the detection of biomolecular analytes by transduction *via* environmentally sensitive fluorescent dyes. Detection based on energy transfer (FRET) or changes in anisotropy will not be considered. The peptide

may either serve as the recognition unit to provide 'intrinsic recognition' (Section 2) or as a scaffold onto which other recognition elements can be grafted ('extrinsic recognition', Section 3).

Figure 1. Principle of a fluorescent peptide biosensor. **A)** Schematic drawing showing the effect of analyte binding. The fluorophore attached close to the binding site responds to a microenvironmental change. **B)** Binding of analyte is detected by changes in the fluorescence emission spectrum. Adapted from [18], with permission from the American Chemical Society.

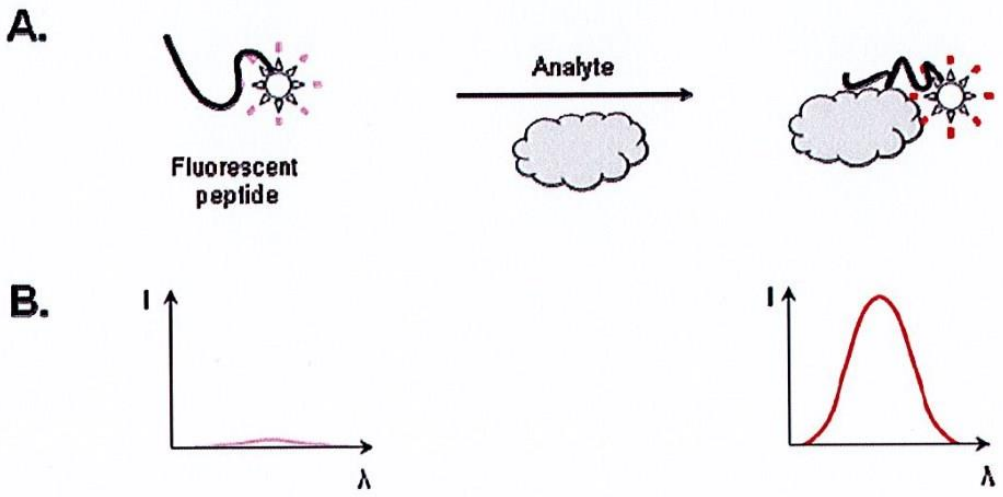

2. Synthetic Peptide Sensors: Peptides as Recognition Elements

Half of the reported protein biosensors are based on bacterial periplasmic binding proteins and target sugars, the reason being that these proteins are well described and that sugar binding induces a pronounced conformational change that may result in local changes in the chemical environment in many parts of the protein. In contrast, most of the singly-labeled fluorescent peptide biosensors target proteic or peptidic analytes. Binding-related peptide sensors constructed by labeling of an amino acid residue and by incorporation of a fluorescent amino acid are listed in Tables 1 and 2, respectively, together with targeted analytes, sensor affinities and performances. Sensors for enzymes, where the fluorescence signal is changed in response to the enzymatic activity (discussed in Section 2.1.), are not included.

This section will describe how and for what purpose peptide biosensors are constructed.

Table 1. Environmentally sensitive fluorescent peptide biosensors constructed by labeling of an amino acid.

System characteristics			Sensor affinity and performance		References
Analytes	**Receptors**	**Fluorophores**	**Maximum fluorescent signal change upon analyte-receptor interaction**	**K_D of the corresponding analyte-receptor complex**	
DNaK chaperone	Targeting sequence of the precursor of mitochondrial aspartate aminotransferase	Acrylodan	4-fold	1.4 μM	[19]
SecB chaperone	Bovine pancreatic trypsin inhibitor	Acrylodan	3.4 -fold	5.4 nM	[20]
Cholecystokinin (CCK) receptor	Peptides agonist and antagonist of the CCK receptor	Alexa, NBD[a], Acrylodan	NR	ND[d]	[21]
Cholecystokinin (CCK) receptor	Peptides agonist of the CCK receptor	Alexa^{488}	NR	ND[d]	[22]
Secretin receptor	Analogues of the hormone secretin	Alexa^{488}	NR	ND[d]	[23]
α-amylase[#]	Library of designed loop peptides	Fluorescein	> 4-fold	1.1 μM	[24]
β-lactoglobulin[#]	Mini-library of designed β-strand peptides	Fluorescein	2.5-fold	ND	[25]
PKA, α-amylase, β-galactosidase, lysozyme, hexokinase, S-100	Peptides derived from substrates of 4 kinases (PKA, c-Src kinase, c-Abl tyrosine kinase & PKC)	Spiropyran	NR	ND	[26]
Calmodulin[#]	Mini-library of designed α-helical peptides	TAMRA[b]	4-fold	1.5 μM	[27]
GRP94	VSV8, the immonudominant peptide epitope of the vesicular stomatitis virus	Acrylodan, Nile-red	NR	ND[d]	[28]
Fab 57P	Sequence 134-151 of the tobacco mosaic virus coat protein	3-hydroxychromone[c]*	1.4-fold[e]	2.4 nM	[29]
scFv 1F4	N-terminus sequence of the E6 protein of human papillomavirus 16	3-hydroxychromone[c]*	1.5 -fold[e]	1nM	[30]
Double-stranded DNA	Polypeptide derived from the Hin recombinase of *Salmonella typhimurium*	Oxazole yellow	>1.1-fold	10 nM	[31]

NR. Not reported; ND. Not determined; [a]4-nitrobenzoxadiazole; [b]5-(and-6)-carboxytetramethylrhodamine; [c]2-(2-furanyl)-3-hydroxychromone
[d]K_i or EC50 values were reported; [e]This number refers to changes in the ratio of the intensities of the twoemission bands characteristic of this dye; [#]Main protein used as analyte; *Ratiometric fluorophores are inherently quantitative as the ratiometric signal is independent of probe concentrations.

Table 2. Environmentally sensitive peptide biosensors constructed by incorporating a fluorescent amino acid in the peptide sequence.

System characteristics			Sensor affinity and performance		References
Analytes	**Receptors**	**Fluorescent amino acids**	**Maximum fluorescent signal change upon analyte-receptor interaction**	**K_D of the corresponding analyte-receptor complex**	
δ-opioid receptor	δ-opioid antagonists	DANA[a] (Aladan)	NR	ND[d]	[32]
14-3-3 protein	Caged phosphopeptides	DANA[a] (Aladan)	4-fold	700 nM	[33]
Cholecystokinin (CCK) receptor	Peptides agonist of the CCK receptor	DANA[a] (Aladan)	NR	ND[d]	[34]
14-3-3 protein	Phosphopeptides	4-DAPA[b]	6-fold	4.6 μM	[35]
PDZ domains	C-terminal sequence of stargazin, CRIPT, NR2a and GluR1	4-DAPA[b]	265-fold	0.2 μM	[36]
SH2 phosphotyrosine-binding domains	SH2 domains	6-DMNA[c*]	11-fold	2.4 μM	[37]
Class II MHC proteins	HLA-DR-binding peptides	4-DAPA[b] and 6-DMNA[c*]	1100-fold	ND[d]	[38]

NR. Not reported; ND. Not determined; [a]6-(2-dimethylaminonaphthoyl)alanine; [b]4-N,N-dimethylaminophtalimidoalanine; [c]6-N,N-dimethylamino-2,3-naphtalimidoalanine; [d]K_i or EC50 values were reported; *Can be used as ratiometric fluorophore

2.1. Applications of Peptide Biosensors

Protein chips are expected to become important tools for direct analyses of biomolecular function and interaction in a high-throughput fashion. Hisakazu Mihara and his team contribute to this development by designing protein-detection systems, where peptide-based biosensor molecules with defined secondary structures are used as capture agents. Interactions are reported by environmentally sensitive fluorophores attached to the peptides. Libraries of peptides with β-strand (16 peptides, [25]), β-loop (126 peptides, [24]) and α-helix (20 peptides, [27]) structures were synthesized. In proteins, the solvent accessible part of these secondary structure elements is often implicated in the recognition of protein partners. Peptides were introduced into separate wells of a microplate, either involving covalent immobilization *via* an N-terminal cysteine [24,25] or adsorbed [27]. The resulting peptide arrays were used to produce characteristic protein fingerprints (PFP), allowing discrimination between a range of proteins. The proteins could be detected down to 1.2 fmol [27]. Tomizaki and Mihara [26] developed a fluorescence sensing system for the detection of proteins using a photochromism-based assay (P-CHROBA) technique. Spiropyran derivatives were attached to the N-termini of eight peptides. When irradiated by UV or visible light, spiropyran undergoes a reversible transition to a highly fluorescent merocyanine form with rate constants that depend on the microenvironment of the dye. Changes in these constants were used to detect complex formation between the spiropyran-containing peptides and six different proteins. Even this small number of peptides gave rise to unique PFPs and allowed for successful discrimination between the proteins.

Many peptide-based biosensors were constructed to gain insights into peptide-protein interaction systems. Fluorophore-peptide conjugates were used as probes to resolve the interaction kinetics of peptide-chaperone (*E. coli* DnaK and SecB) interactions and to gain insights into the relative polarity of the peptide binding site [19,20]. Similarly, Wearsch *et al.* [28] investigated complex formation between the chaperone GRP94 and a peptide derived from the vesicular stomatitis virus labeled with an environmentally sensitive fluorophore. By using peptides derived from cholecystokinin (CCK) and modified with the fluorophore Alexa, Laurence J Miller's group demonstrated that the environment of the fluorophore is different when the peptide is bound to type A [21] and type B [22] CCK receptors. By incorporating the fluorescent amino acid DANA (6-(2-dimethylaminonaphthoyl)alanine) in the N-terminus, the mid-region, or the C-terminus of the peptide, pronounced differences in the mechanism of CCK binding and activation of these structurally related receptors were shown [34]. Further, Harikumar *et al.* [23] examined the binding environment of a peptide agonist to family B of G protein-coupled secretin receptors by attaching Alexa Fluor 488 at four different positions throughout the pharmacophore. Peptide-based biosensors were also used to probe the phosphorylation-dependent binding of an octapeptide to the 14-3-3 protein (see Section 2.2.1) and to study intramolecular interactions [32].

Several peptide biosensors equipped with environmentally-sensitive fluorophores were designed for the detection of enzymes and for monitoring their activity. David S. Lawrence and colleagues designed functionalized peptide libraries for the identification of efficient biosensor systems for protein kinases. Sensing of Src kinase was based on phosphorylation-driven disruption of stacking interactions between an extrinsic fluorophore and the target tyrosine residue in a peptide substrate [39,40]. In a different design, an

environmentally sensitive fluorophore was covalently attached to a tyrosine-containing peptide substrate recognized by Src kinase and the assay was performed in the presence of the phosphotyrosine binding domain Lck-SH2 [41]. Upon tyrosine phosphorylation, the fluorophore experienced changes in the local environment caused by the peptide binding to Lck-SH2 (Scheme 1). A similar approach was used for the detection of serine phosphorylation by the cAMP-dependent protein kinase [42]. Barbara Imperiali and colleagues designed a generic kinase sensor containing a variable enzyme recognition sequence and a fluorescent amino acid residue, Sox (from 8-hydroxy-5-(N,N-dimethylsulfonamido)-2-methylquinoline), which displays chelation-enhanced emission when binding Mg^{2+}. Phosphorylation of a target serine, threonine or tyrosine residue increased the affinity of Sox for the metal ion, which resulted in enhanced fluorescence intensity [43,44].

Fluorescent peptide reporters for histone acetyltransferase were designed by synthesizing a 20-residue peptide corresponding to the N-terminal part of histone H4 followed by functionalization with dansyl or fluorescein [45]. Charge reduction of the peptide following acetylation of target lysines resulted in a small increase in the emission from the fluorophores. Along similar lines, biosensor peptides for arginine methyltransferase 1 were also designed [46].

Scheme 1. Fluorescent sensing of Src protein kinase based on binding of an SH2 domain to the sensor peptide containing the kinase recognition sequence and a target tyrosine. The affinity of the SH2 domain for the peptide is increased upon phosphorylation, and SH2 binding induces a change in the chemical environment surrounding the fluorophore. From [41].

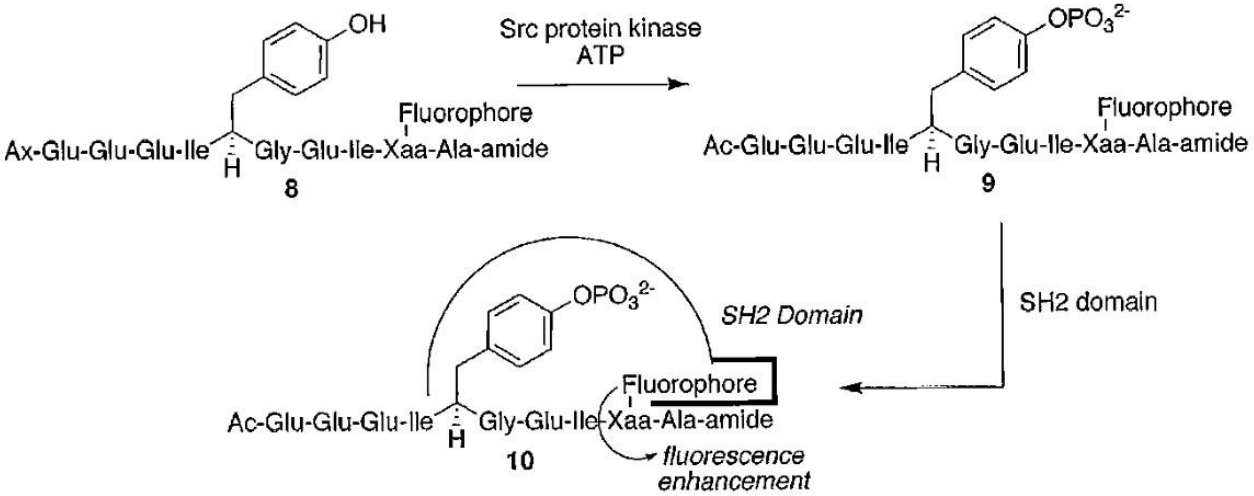

2.2. Construction of Peptide Biosensors

2.2.1. Strategies for the incorporation of fluorescent dye in the peptide

Two main strategies for covalent incorporation of the fluorophore in the peptide can be distinguished. The first one involves post-synthetic coupling at the N-terminal amine [21-23,28,30] or at the side chains of cysteines [19,29] or lysines [24-27,31].

The second strategy involves the incorporation of unnatural fluorescent amino acids during peptide synthesis. Barbara Imperiali's group has developed the functionalized amino acids DANA [33] and 4-DAPA (4-N,N-dimethylaminophtalimidoalanine, [35]), and used them to probe the phosphorylation-dependent binding of an octapeptide to a 14-3-3 protein. The 14-3-3 proteins are essential intermediates in cell cycle regulation, acting through phosphorylation-dependent protein-protein interactions. A caged fluorescent octo-phospho-peptide was synthesized that exposed a phosphoserine residue upon irradiation, allowing the peptide to bind to the 14-3-3 protein and modulate the emission properties of the fluorescent amino acid (Scheme 2). A shift in the maximum emission wavelength was observed, along with a 4- and 6-fold increase in the emission intensity for the DANA- and 4-DAPA-containing peptides, respectively.

Scheme 2. Probing of the phosphorylation-dependent binding of an octapeptide containing the fluorescent amino acid DANA to a 14-3-3 protein. **A)** The caged phosphopeptide is unable to bind 14-3-3. The maximum emission wavelength (λ_{em1}) of DANA is 522 nm. **B)** Irradiation of the caged phosphopeptide releases free phosphoserine-containing peptide. **C)** Released phosphoserine-peptide binds to the protein, thereby modulating the fluorescence properties of DANA (λ_{em2} = 501 nm). From [33].

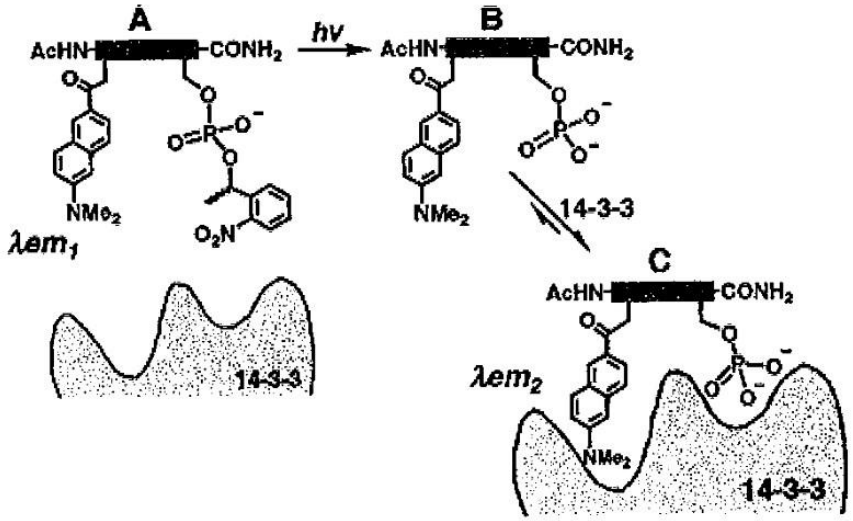

The amino acid 6-DMNA (6-N,N-dimethylamino-2,3-naphtalimidoalanine) was introduced adjacent to the conserved binding determinants of several peptides and exhibited up to an 11-fold change in fluorescence emission intensity upon binding to selected Src homology 2 (SH2) phosphotyrosine binding domains [37]. Much larger signal enhancements were observed for the binding of peptides containing 4-DAPA (470-fold) and 6-DMNA (1100-fold) to class II MHC proteins [38] (Figure 2). In two other papers, DANA was introduced in place of a phenylalanine to construct a fluorescent δ-opioid antagonist [32] and at three positions of a CCK-binding peptide to provide insights into distinct modes of binding and activation of type A and B CCK receptors [34].

Figure 2. Fluorescence emission spectra of a) a (6-DMNA)-peptide and b) a (4-DAPA)-peptide (**b**) and their complexes with a class II MHC protein (DR) are shown. Free peptide spectra are shown also on an expanded scale. Note the shift in emission wavelength λ_{max} upon binding of the peptide to protein, as well as the increase in the emission intensity. From [38], reprinted by permission from Macmillan Publishers Ltd (licence number 2341811044647).

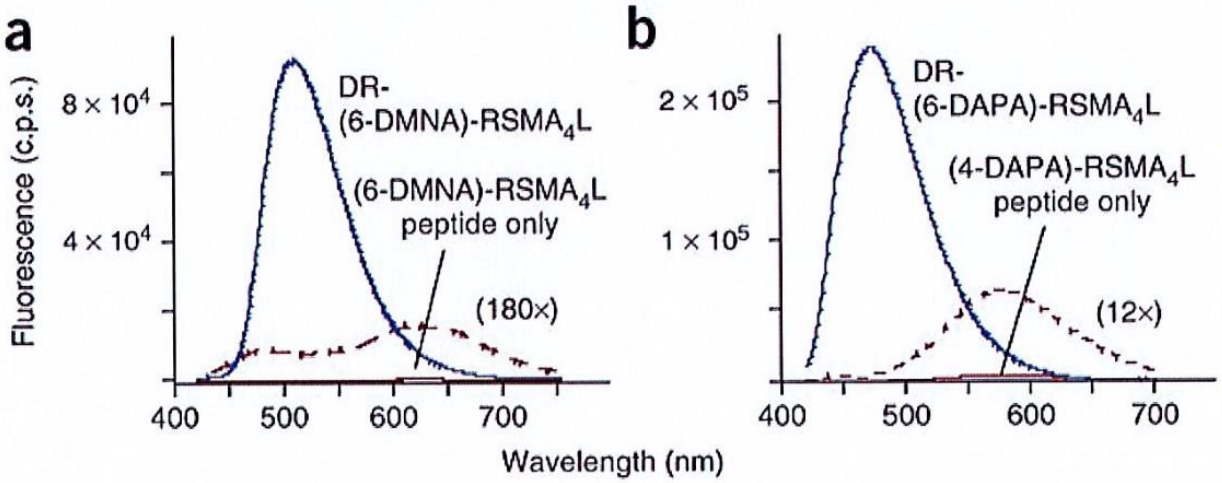

2.2.2. Position of the fluorophore in the amino acid sequence

It is difficult to predict the optimal position for labeling. It should be chosen so that the microenvironment of the fluorophore is altered upon analyte binding. In protein biosensors, this is achieved either (i) by analyte-dye contacts in or (ii) near the analyte binding site, or (iii) by conformational effects occurring over substantially longer intra-protein distances, affecting a fluorophore located distantly from the analyte binding site [47,48]. The design of a molecular sensor thus requires some knowledge about the interaction, gained from structural or functional studies, in order to identify positions for which fluorescent labeling allows analyte detection without perturbing its binding. Not only the position, but also the nature of the dye plays a critical role in the performance of a biosensor. It has been observed that simply changing the fluorophore at the same site of a protein can lead to differences in

binding parameters [8,18,49,50]. A combinatorial approach with various fluorophores is recommended to optimize sensitivity [51] and affinity.

Site-dependent differences in fluorescence response upon analyte binding to a peptide biosensor were quantified in three different studies.

Enander *et al.* [29] constructed a peptide-based ratiometric biosensor for the detection of an antibody fragment. Based on a detailed characterization of the functional epitope corresponding to residues 134–151 of the tobacco mosaic virus protein (TMVP), two positions were targeted (Figure 3A) for labeling with a two-band fluorophore, one in the immediate vicinity of positions mapped as essential for binding (position 146) and one in the C-terminus (position 151). Only one out of these two constructs behaved as a biosensor. When the peptide was labeled in the C-terminus, seven amino acids away from the essential residues of the epitope, the intensity ratio of the two emission bands changed by 40% upon analyte binding, while labeling two amino acids away from the residues most important for binding resulted in a construct that completely lacked ratiometric sensing ability. Choulier *et al.* [30] performed a similar study on a different antigen-antibody system. Three peptides, corresponding to the N-terminal sequence of the oncoproteine E6 of human papillomavirus (HPV) 16, were labeled at different distances from the epitope (Figure 3B): zero, two and five residues away from the first position in the sequence mapped as important for binding of the antibody fragment. One of these three peptidic constructs possessed sensing properties, namely the peptide for which the dye was coupled two residues away from the epitope. Addition of the antibody fragment to this peptide caused a 47 % decrease in the ratio of its two emission bands.

These two examples indicate that the fluorescence response largely depends on the site of fluorophore incorporation, and also that its distance to residues essential for analyte binding cannot be used as a simple parameter for sensor optimization. Similar results have been presented for protein biosensors earlier [48,50,52-58].

Recently, Sainlos *et al.* [36] developed a general screening strategy in the design of environmentally sensitive peptidic probes for PDZ domains. The design strategy includes two steps: (1) development of a peptide library to screen for the optimal site for fluorophore attachment and (2) screening of different peptide sequences for improved affinity and specificity while keeping a fixed fluorophore position. The initial library, consisting of 11 decamer peptides derived from the C-terminal sequence of stargazin ($^{-9}$NTANRRTTPV^{0}) that included 4-DAPA derivatives in eight different positions, was screened against three PDZ constructs. Positions 0 and -2 were not tested as they are essential for binding. Further optimization was carried out by adjusting the length of the linker bearing the dye (from one to three methylene groups). After this first step, out of eight coupling locations, three produced sensors with a <10-fold increase in fluorescence, two with a 10-20-fold increase and three with a >25-fold increase. Maximum fluorescence increase was obtained with the fluorescent amino acid in position -5, bearing a 2-methylene linker (β). In a second step, this position and linker size were kept fixed in the C-terminal sequences of a series of four known PDZ binders. The highest fluorescence increase was 265-fold for the GluR1 sequence ($^{-9}$SGδPβGATGV^{0}, δ being norleucine) with the PDZ domain Shank3. Both the nature of the fluorophore and its site of conjugation seem important for maximal signal change.

Figure 3. Sequences of the peptides corresponding to A) amino acids 134-151 of the TMV protein [29], and **B)** amino-acids 4-17, 7-17 and 9-17 of oncoprotein E6 [30]. Residues most important for analyte binding are shown in red, while positions targeted for fluorophore labeling are shown in green. Post-synthetic coupling of the fluorophore was performed **A)** at the side chains of cysteines replacing residues S146 and V151, and **B)** at the N-terminal amine.

A. TMVP sequence

	134																	151
pTMVP-S146C	R	G	T	G	S	Y	**N**	**R**	**S**	**S**	**F**	E	**S**	S	S	G	L	V
pTMVP-V151C	R	G	T	G	S	Y	**N**	**R**	**S**	**S**	**F**	E	S	S	S	G	L	**V**

B. E6 sequence

	4													17
pE6-4-17	**K**	R	T	A	M	F	**Q**	**D**	**P**	Q	E	R	P	R
pE6-7-17				**A**	M	F	**Q**	**D**	**P**	Q	E	R	P	R
pE6-9-17						**F**	**Q**	**D**	**P**	Q	E	R	P	R

3. Synthetic Peptide Sensors: Recognition Element Grafted on a Peptide Scaffold

In the examples given in Section 2, the sequence of the peptide was chosen in order to provide the recognition site for the analyte. A different role for the peptide has been presented in a series of papers by the groups of Akihiko Ueno and Lars Baltzer. Here, the folding propensity of polypeptides is a key property that makes them useful as scaffolds, onto which non-peptidic molecules for recognition can be grafted along with fluorophores for signaling. A well-defined structure provides directionality of incorporated groups, which is an important parameter in the design and optimization of biosensor performance. Also, the distance between recognition unit and fluorophore can be systematically varied by addressing different amino acid side chains in the scaffold.

A number of biosensor molecules based on a 17-residue, *de novo* designed α-helical peptide were presented, where different cyclodextrins were employed for recognition of bile acids and aliphatic alcohols [59-67]. The sensing principle was based on the disruption of an inclusion complex between cyclodextrin and a fluorophore upon binding of the analyte (guest). In the simplest design, dansyl or dimethylaminobenzoyl was attached in position i, i + 4 or i, i + 7 with respect to a β-cyclodextrin moiety, which corresponds to the two groups being separated by one or two turns of the helix scaffold while oriented similarly in space [59,65]. This arrangement allowed the fluorophore to interact with the hydrophobic interior of the cyclodextrin moiety. Upon introduction of a guest molecule, e.g., ursodeoxycholic acid, displacement of the fluorophore was reflected in quenching of its emission. In a different construct, α- or

β-cyclodextrin was coupled to the scaffold along with pyrene and its quencher nitrobenzene [63,66]. The signaling principle was based on nitrobenzene and the analyte competing for the binding site inside cyclodextrin, affecting the distance between fluorophore and quencher and thus the fluorescence intensity (Figure 4). Yet another design approach involved functionalization with two molecules of naphthalene or pyrene, and analyte binding was monitored from excimer fluorescence [60-62,64]. Bile acids and ring-structured alcohols were sensed using constructs with β- [59,63-65,67] or γ-cyclodextrin [60-62] while α-cyclodextrin was used for short chain aliphatic alcohols [66].

In a similar approach, *de novo* designed helix-loop-helix polypeptides that dimerize into four-helix bundles upon folding were functionalized to become molecular biosensors for protein analytes. In the initial design, dansyl and a benzenesulfonamide derivative were attached to separate helices of the scaffold [68,69]. The presence of carbonic anhydrase, which binds specifically to benzenesulfonamide, was accompanied by a disruption of the dimer [70] and a significant intensity increase of the dansyl fluorescence.

Figure 4. Schematic representation of a scaffold-based biosensor with β-cyclodextrin (β-CD) acting as the recognition element. Upon binding of the analyte (guest), the quencher nitrobenzene (NB) is displaced from the β-CD binding site and the emission from the fluorophore (pyrene, Py) is enhanced. From [63], with permission from the American Chemical Society.

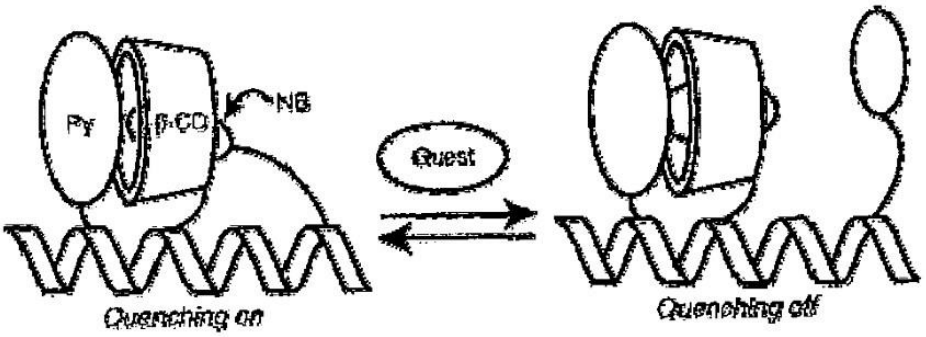

4. Affinity Characterization of the Interaction between Biosensor and Analyte

The equilibrium dissociation constant (K_D) of interactions between peptide biosensors and their analytes can be determined from the hyperbolic binding curves obtained by titration of a constant concentration of peptide biosensor with increased concentrations of analyte [13,19,20,27,31,35]. Affinities determined in this way vary from low nM to 500 μM depending on the system under study. In two studies [30,36], competition binding assays with non-fluorescent peptides recognizing the same analyte as the peptide biosensor further complemented titration experiments and allowed for determination of the relative affinities of unlabeled peptides for their protein analytes. The binding affinities were also independently evaluated by using non-fluorescence-based methods; isothermal titration calorimetry

(ITC, [36]) and surface plasmon resonance (SPR, [30]). In both cases, K_D values determined by ITC or SPR were in the same range as those determined by fluorescence-based procedures.

Based on the helix-loop-helix scaffolds designed by Baltzer and colleagues, biosensors with affinities towards carbonic anhydrase spanning three orders of magnitude were designed by varying the length of an aliphatic spacer attached to the benzenesulfonamide moiety [69,71]. Although interactions between the spacer and a hydrophobic pocket in the protein contributed to binding, the scaffold itself played an important role in providing both sterical constraints and chemical functionalities that affected the affinity [71].

5. Limit of Detection

Singly labeled reagentless biosensors based on proteins and used for analyte quantification displayed limits of detection (LOD) in the submillimolar range for maltose [54], and in the submicromolar range for glucose [72], glutamine [17,73], and β-lactam antibiotic [74].

The LOD of analyte by peptide biosensors was reported only in a few cases. The protein detection method established with folded peptides (see Section2.1) allowed for the detection of 5 μg/mL (# 90 nM) of α-amylase [24]. The LOD of the antibody fragment $scFv1F4_{Q34S}$ by the pE6 peptide biosensor [30] was 15 nM in buffer, and 50–100 nM in a more complex medium (bovine serum albumin (BSA) 100 μg/mL). Normal concentrations of specific antibodies and BSA in serum are around 50 μg/ml (330 nM) and 35-50 mg/ml, respectively.

6. Perspectives for Peptide Biosensors

The performances of peptide and protein sensors were recently compared [30] based on various antigen-antibody interactions that display affinities in the 0.1-20 nM range. In these studies, the receptor was either an antibody [52,53], or a peptide antigen [29,30], but the analytes were large in all cases (between 14 and 54 kDa). A biosensor was defined as operational if it showed a >35% fluorescence intensity variation upon analyte binding. Out of the total number of sensors constructed in each study (maximum 10 for antibody receptors and 3 for peptide receptors), 20–50% behaved as biosensors. In these studies, the proportion of efficient fluorescent sensors was therefore in the same range whether the receptor was a protein or a peptide. This observation makes peptide biosensors promising tools for developing new applications. With the availability of automatedchemical synthesis of long peptide fragments at high scale (100 mg of a 100 amino acid peptide can be routinely synthesized at >99% purity) and low price, rational or combinatorial peptide libraries can be straightforwardly produced for the optimization of recognition sites and positions for fluorophore attachment. However, the main challenge in the future will be to make peptide-based fluorescent biosensors useful for sensitive detection of bio-analytes in complex media (e.g., serum). In order to accomplish this, problems with interference from non-analyte components in the sample have to be addressed. Specifically, the possibility of enzymatic peptide degradation and of non-specific binding of sample components to the peptide, causing irrelevant sensor signals, has to be taken into consideration. The frequent problem of autofluorescence can be

avoided by employing long-wavelength dyes, which are usually very bright although they may be less sensitive to environmental changes compared to fluorophores excited in the UV region. Ratiometric sensor peptides, where the relative rather than the absolute intensity change upon analyte binding is monitored, should also be very useful in this respect.

In conclusion, fluorescent sensor peptides have already proven useful in a number of applications, ranging from analyte detection to elucidation of molecular details of protein-peptide and protein-protein interactions. It is expected that their general applicability with respect to analyte quantification – beyond proof-of-concept – will be expanded by combining combinatorial methods for peptide design with further improvement of fluorophores and fluorescent amino acids in terms of sensitivity to environmental changes. The most robust protein detection system will then probably rely on fingerprints obtained from arrayed sensor peptides.

Acknowledgements

We are grateful to Danièle Altschuh for valuable comments on the manuscript.

References

1. Hellinga, H.W.; Marvin, J.S. Protein engineering and the development of generic biosensors. *Trends. Biotechnol.* **1998**, *16*, 183-189.
2 Loving, G.S.; Sainlos, M.; Imperiali, B. Monitoring protein interactions and dynamics with solvatochromic fluorophores. *Trends Biotechnol.* **2010**, *28*, 73-83.
3. Wang, H.; Nakata, E.; Hamachi, I. Recent progress in strategies for the creation of protein-based fluorescent biosensors. *Chembiochem.* **2009**, *10*, 2560-2577.
4. Mims, M.P.; Sturgis, C.B.; Sparrow, J.T.; Morrisett, J.D. Acrylodan can label amino as well as sulfhydryl groups: results with low-density lipoprotein, lipoprotein[a], and lipid-free proteins. *Biochemistry*. **1993**, *32*, 9215-9120.
5. Yem, A.W.; Epps, D.E.; Mathews, W.R.; Guido, D.M.; Richard, K.A.; Staite, N.D.; Deibel, M.R. Sitespecific chemical modification of interleukin-1-beta by acrylodan at cysteine-8 and lysine-103. *J. Biol. Chem.* **1992**, *267*, 3122–3128.
6. Cohen, B.E.; McAnaney, T.B.; Park, E.S.; Jan, Y.N.; Boxer, S.G.; Jan, L.Y. Probing protein electrostatics with a synthetic fluorescent amino acid. *Science* **2002**, *296*, 1700-1703.
7. Bock, P.E. Active-site-selective labeling of blood coagulation proteinases with fluorescence probes by the use of thioester peptide chloromethyl ketones. *J. Biol. Chem.* **1992**, *267*, 14974-14981.
8. Verhamme, I.M.; Olson, S.T.; Tollefsen, D.M.; Bock, P.E. Binding of exosite ligands to human thrombin. Re-evaluation of allosteric linkage between thrombin exosites I and II. *J. Biol. Chem.* **2002**, *277*, 6788-6798.
9. Pollack, S.J.; Nakayama, G.R.; Schultz, P.G. Introduction of nucleophiles and spectroscopic probes into antibody combining sites. *Science* **1988**, *242*, 1038-1040.

10. Hamachi, I.; Nagase, T.; Shinkai, S. A general semisynthetic method for fluorescent saccharide-biosensors based on a lectin. *J. Am. Chem. Soc.* **2000**, *122*, 12065-12066.
11. Nakata, E.; Nagase, T.; Shinkai, S.; Hamachi, I. Coupling a natural receptor protein with an artificial receptor to afford a semisynthetic fluorescent biosensor. *J. Am. Chem. Soc.* **2004**, *126*, 490-495.
12. Nakata, E.; Wang, H.; Hamachi, I. Ratiometric fluorescent biosensor for real-time and label-free monitoring of fine saccharide metabolic pathways. *ChemBioChem.* **2008**, *9*, 25-28.
13. Ojida, A.; Tsutsumi, H.; Kasagi, N.; Hamachi, I. Suzuki coupling for protein modification. *Tetrahedron Lett.* **2005**, *46*, 3301-3305.
14. Becker, C.F.W.; Hunter, C.L.; Seidel, R.P.; Kent, S.B.H.; Goody, R.S.; Engelhard, M. A sensitive fluorescence monitor for the detection of activated Ras: total chemical synthesis of site-specifically labeled Ras binding domain of c-Raf1 immobilized on a surface. *Chem. Biol.* **2001**, *8*, 243-252.
15. Viljanen, J.; Larsson, J.; Larsson, A.; Broo, K.S. A multipurpose receptor composed of promiscuous proteins. Analyte detection through pattern recognition. *Bioconjugate Chem.* **2007**, *18*, 1935-1945.
16. de Lorimier, R.M.; Tian, Y.; Hellinga, H.W. Binding and signaling of surface-immobilized reagentless fluorescent biosensors derived from periplasmic binding proteins. *Protein Sci.* **2006**, *15*, 1936-1944.
17. Wada, A; Mie, M.; Aizawa, M.; Lahoud, P.; Cass, A.E.G.; Kobatake, E. Design and construction of glutamine binding proteins with a self-adhering capability to unmodified hydrophobic surfaces as reagentless fluorescence sensing devices. *J. Am. Chem. Soc.* **2003**, *125*, 16228-16234.
18. Gilardi, G.; Zhou, L.Q.; Hibbert, L.; Cass, A.E.G. Engineering the maltose binding protein for reagentless fluorescence sensing. *Anal. Chem.* **1994**, *66*, 3840-3847.
19. Schmid, D.; Baici, A.; Gehring, H.; Christen, P. Kinetics of molecular chaperone action. *Science* **1994**, *263*, 971-973.
20. Fekkes, P; den Blaauwen, T.; Driessen, A.J. Diffusion-limited interaction between unfolded polypeptides and the Escherichia coli chaperone SecB. *Biochemistry* **1995**, *34*, 10078-10085.
21. Harikumar, K.G.; Pinon, D.I.; Wessels, W.S.; Prendergast, F.G.; Miller, L.J. Environment and mobility of a series of fluorescent reporters at the amino terminus of structurally related peptide agonists and antagonists bound to the cholecystokinin receptor. *J. Biol. Chem.* **2002**, *277*, 18552-18560.
22. Harikumar, K.G.; Clain, J.; Pinon, D.I.; Dong, M.; Miller, L.J. Distinct molecular mechanisms for agonist peptide binding to types A and B cholecystokinin receptors demonstrated using fluorescence spectroscopy. *J. Biol. Chem.* **2005**, *280*, 1044-1050.
23. Harikumar, K.G.; Hosohata, K.; Pinon, D.I.; Miller, L.J. Use of probes with fluorescence indicator distributed throughout the pharmacophore to examine the peptide agonist-binding environment of the family B G protein-coupled secretin receptor. *J Biol Chem.* **2006**, *281*, 2543-2550.
24. Takahashi, M.; Nokihara, K.; Mihara, H. Construction of a protein-detection system using a loop peptide library with a fluorescence label. *Chem Biol.* **2003**, *10*, 53-60.

25. Usui, K.; Ojima, T.; Takahashi, M.; Nokihara, K.; Mihara, H. Peptide arrays with designed secondary structures for protein characterization using fluorescent fingerprint patterns. *Biopolymers* **2004**, *76*, 129-39.
26. Tomizaki, K.; Mihara, H. A novel fluorescence sensing system using a photochromism-based assay (P-CHROBA) technique for the detection of target proteins. *J. Mater. Chem.* **2005**, *15*, 2732-2740.
27. Usui, K.; Tomizaki, K.Y.; Ohyama, T.; Nokihara, K.; Mihara, H. A novel peptide microarray for protein detection and analysis utilizing a dry peptide array system. *Mol. Biosyst.* **2006**, *2*, 113-121.
28. Wearsch, P.A.; Voglino, L.; Nicchitta, C.V. Structural transitions accompanying the activation of peptide binding to the endoplasmic reticulum Hsp90 chaperone GRP94. *Biochemistry* **1998**, *37*, 5709-5719.
29. Enander, K.; Choulier, L.; Olsson, A.L.; Yushchenko, D.A.; Kanmert, D.; Klymchenko, A.S.; Demchenko, A.P.; Mely, Y.; Altschuh, D. A peptide-based, ratiometric biosensor construct for direct fluorescence detection of a protein analyte. *Bioconjugate Chem.* **2008**, *19*, 1864-1870.
30. Choulier, L.; Shvadchak, V.V.; Naidoo, A.; Klymchenko, A.S.; Mély, Y.; Altschuh, D. A peptide-based fluorescent ratiometric sensor for quantitative detection of proteins. *Anal. Biochem.* (in press).
31. Thompson, M. Synthesis, photophysical effects, and DNA targeting properties of oxazole yellow-peptide bioconjugates. *Bioconjugate Chem.* **2006**, *17*, 507-513.
32. Chen, H.; Chung, N.N.; Lemieux, C.; Zelent, B.; Vanderkooi, J.M.; Gryczynski, I.; Wilkes, B.C.; Schiller, P.W. [Aladan^3]TIPP: A fluorescent δ-opioid antagonist with high δ-receptor binding affinity and δ selectivity. *Biopolymers*. **2005**, *80*, 325-331.
33. Vázquez, M.E.; Nitz, M.; Stehn, J.; Yaffe, M.B.; Barbara Imperiali, B. Fluorescent caged phosphoserine peptides as probes to investigate phosphorylation-dependent protein associations. *J. Am. Chem. Soc.* **2003**, *125*, 10150-10151.
34. Harikumar, K.G.; Pinon, D.I.; Miller, L.J. Fluorescent indicators distributed throughout the pharmacophore of cholecystokinin provide insights into distinct modes of binding and activation of type A and B cholecystokinin receptors. *J. Biol. Chem.* **2006**, *281*, 27072-27080.
35. Vázquez, M.E.; Rothman D.M.; Imperiali, B. A new environment-sensitive fluorescent amino acid for Fmoc-based solid phase peptide synthesis. *Org. Biomol.Chem.* **2004**, *2*, 1965-1966.
36. Sainlos, M.; Iskenderian, W.S.; Imperiali, B. A general screening strategy for peptide-based fluorogenic ligands: probes for dynamic studies of PDZ domain-mediated interactions. *J. Am. Chem. Soc.* **2009**, *131*, 6680-6682.
37. Vázquez, M.E.; Blanco, J.B.; Imperiali, B. Photophysics and biological applications of the environment-sensitive fluorophore 6-N,N-dimethylamino-2,3-naphthalimide *J. Am. Chem. Soc.* **2005**, *127*, 1300-1306.
38. Venkatraman, P.; Nguyen, T.T.; Sainlos, M.; Bilsel, O.; Chitta, S.; Imperiali, B.; Stern, L.J. Fluorogenic probes for monitoring peptide binding to class II MHC proteins in living cells. *Nat. Chem. Biol.* **2007**, *3*, 222-228.
39. Wang, Q.; Cahill, S.M.; Blumenstein, M.; Lawrence, D.S. Self-reporting fluorescent substrates of protein tyrosine kinases. *J. Am. Chem. Soc.* **2006**, *128*, 1808-1809.

40. Wang, Q.; Dai, Z.; Cahill, S.M.; Blumenstein, M.; Lawrence, D.S. Light-regulated sampling of protein tyrosine kinase activity. *J. Am. Chem. Soc.* **2006**, *128*, 14016-14017.
41 Wang, Q.; Lawrence, D.S. Phosphorylation-driven protein–protein interactions: a protein kinase sensing system. *J. Am. Chem. Soc.* **2005**, *127*, 7684-7685.
42. Sharma, V.; Agnes, R.S.; Lawrence, D.S. Deep quench: an expanded dynamic range for protein kinase sensors. *J. Am. Chem. Soc.* **2007**, *129*, 2742-2743.
43. Shults, M.D.; Imperiali, B. Versatile fluorescence probes of protein kinase activity. *J. Am. Chem. Soc.* **2003**, *125*, 14248-14249.
44. Shults, M.D.; Carrico-Moniz, D.; Imperiali, B. Optimal Sox-based fluorescent chemosensor design for serine/threonine protein kinases. *Anal. Biochem.* **2006**, *352*, 198-207.
45. Wu, J.; Zheng, Y.G. Fluorescent reporters of the histone acetyltransferase. *Anal. Biochem.* **2008**, *380*, 106-110.
46. Feng, Y.; Xie, N.; Wu, J.; Yang, C.; Zheng, Y.G. Inhibitory study of protein arginine methyltransferase 1 using a fluorescent approach. *Biochem. Biophys. Res. Commun.* **2009**, *379*, 567-572.
47. de Lorimier, R.M.; Smith, J.J.; Dwyer, M.A.; Looger, L.L., Sali, K.M.; Paavola, C.D.; Rizk, S.S.; Sadigov, S.; Conrad, D.W.; Loew, L.; Hellinga, H.W. Construction of a fluorescent biosensor family. *Protein Sci.* **2002**, *11*, 2655-2675.
48. Medintz, I.L.; Mauro, J.M. Use of a cyanine dye as a reporter probe in reagentless maltose sensors based on *E. coli* maltose binding protein. *Anal. Lett.* **2004**, *37*, 191-202.
49. Sherman, D.B.; Pitner, J.B.; Ambroise, A.; Thomas, K.J. Synthesis of Thiol-derivative, long-wavelength fluorescent phenoxazine derivatives for biosensor applications. *Bioconjugate Chem.* **2006**, *17*, 387-392.
50. Tian, Y.; Cuneo, M.J.; Changela, A.; Höcker, B.; Beese, L.S.; Hellinga, H.W. Structure-based design of robust glucose biosensors using a Thermotoga maritima periplasmic glucose-binding protein. *Protein Sci.* **2007**, *16*, 2240-2250.
51. Morii, T.; Sugimoto, K.; Makino, K.; Otsuka, M.; Imoto, K.; Mori, Y. A new fluorescent biosensor for inositol trisphosphate. *J. Am. Chem. Soc.* **2002**, *124*, 2002, 1138-1139
52. Renard, M.; Belkadi, L.; Hugo, N.; England, P.; Altschuh, D.; Bedouelle, H. Knowledge-based design of reagentless fluorescent biosensors from recombinant antibodies. *J. Mol. Biol.* **2002**, *318*, 429-442.
53. Renard, M.; Belkadi, L.; Bedouelle, H. Deriving topological constraints from functional data for the design of reagentless fluorescent immunosensors. *J. Mol. Biol.* **2003**, *326*, 167-175.
54. Marvin, J.S.; Corcoran, E.E.; Hattangadi, N.A.; Zhang, J.V.; Gere, S.A.; Hellinga, H.W. The rational design of allosteric interactions in a monomeric protein and its applications to the construction of biosensors. *Proc. Natl. Acad. Sci. USA* **1997**, *94*, 4366-4371.
55. Choi, E.J.; Mao, J.; Mayo, S.L. Computational design and biochemical characterization of maize nonspecific lipid transfer protein variants for biosensor applications. *Protein Sci.* **2007**, *16*, 582-588.

56. Rizk, S.S.; Cuneo, M.J.; Hellinga, H.W. Identification of cognate ligands for the Escherichia coli phnD protein product and engineering of a reagentless fluorescent biosensor for phosphonates. *Protein Sci.* **2006**, *15*, 1745-1751.
57. Thomas, J.; Sherman, D.B.; Amiss, T.J.; Andaluz, S.A.; Pitner, J.B. Synthesis and biosensor performance of a near-IR thiol-derivative fluorophore based on benzothiazolium squaraine. *Bioconjugate Chem.* **2007**, *18*, 1841-1846.
58. Dattelbaum, J.D.; Looger, L.L.; Benson, D.E.; Sali, K.M.; Thompson, R.B.; Hellinga, H.W. Analysis of allosteric signal transduction mechanisms in an engineered fluorescent maltose biosensor. *Protein Sci.* **2005**, *14*, 284-291.
59. Matsumura, S.; Sakamoto, S.; Ueno, A.; Mihara, H. Construction of α-Helix peptides with β-cyclodextrin and dansyl units and their conformational and molecular sensing properties. *Chem. Eur. J.* **2000**, *6*, 1781-1788.
60. Hossain, M.A.; Hamasaki, K.; Mihara, H.; Ueno, A. Association and guest-induced dissociation of a novel α-helix peptide bearing pyrene and γ-cyclodextrin in the side chains. *Chem. Lett.* **2000**, *29*, 252-253.
61. Hossain, M.A.; Matsumura, S.; Kanai, T.; Hamasaki, K.; Mihara, H.; Ueno, A. Association of α-helix peptides that have γ-cyclodextrin and pyrene units in their side chain, and induction of dissociation of the association dimer by external stimulant molecules. *J. Chem. Soc. Perkin Trans.* **2000**, *2*, 1527-1533.
62. Toyoda, T.; Matsumura, S.; Mihara, H.; Ueno, A. Guest-responsive excimer emission in an α-helix peptide bearing γ-cyclodextrin and two naphthalene units. *Macromol. Rapid Commun.* **2000**, *21*, 485-488.
63. Hossain, M.A.; Hamasaki, K.; Takahashi, K.; Mihara, H.; Ueno, A. Guest-induced diminishment in fluorescence quenching and molecule sensing ability of a novel cyclodextrin-peptide conjugate. *J. Am. Chem. Soc.* **2001**, *123*, 7435-7436.
64. Yana, D.; Shimizu, T.; Hamasaki, K.; Mihara, H.; Ueno, A. Double naphthalene-tagged cyclodextrin-peptide capable of exhibiting guest-induced naphthalene excimer fluorescence. *Macromol. Rapid. Commun.* **2002**, *23*, 11-15.
65. Toyoda, T.; Mihara, H.; Ueno, A. Fluorescent cyclodextrin/peptide hybrids with a novel guest-responsive chemosensor in the peptide side chain. *Macromol. Rapid. Commun.* **2002**, *23*, 905-908.
66. Hossain, M.A.; Takahashi, K.; Mihara, H.; Ueno, A. Molecule-responsive fluorescent sensors of α-helix peptides bearing α-cyclodextrin, pyrene and nitrobenzene units in their side chains. *J. Inclusion Phenom. Macrocyclic Chem.* **2002**, *43*, 271-277.
67. Furukawa, S.; Mihara, H.; Ueno, A. Sensing behavior of fluorescent cyclodextrin/peptide hybrids bearing a macrocyclic metal complex. *Macromol. Rapid Commun.* **2003**, *24*, 202-206.
68. Enander, K.; Dolphin, G.T.; Andersson, L.K.; Liedberg, B.; Lundstrom, I.; Baltzer, L. Designed, folded polypeptide scaffolds that combine key biosensing events of recognition and reporting. *J. Org. Chem.* **2002**, *67*, 3120-3123.

69. Enander, K.; Dolphin, G.T.; Liedberg, B.; Lundström, I.; Baltzer, L. A versatile polypeptide platform for integrated recognition and reporting: affinity arrays for protein-ligand interaction analysis. *Chem. Eur. J.* **2004**, *10*, 2375-2385.
70. Enander, K.; Dolphin, G.T.; Baltzer, L. Designed, functionalized helix-loop-helix motifs that bind human carbonic anhydrase II: A new class of synthetic receptor molecules. *J. Am. Chem. Soc.* **2004**, *126*, 4464-4465.
71. Andersson, T.; Lundquist, M.; Dolphin, G.T.; Enander, K.; Jonsson, B-H.; Nilsson, J.W.; Baltzer, B. The binding of human carbonic anhydrase II by functionalized folded polypeptide receptors. *Chem. Biol.* **2005**, *12*, 1245-1252.
72. Salins, L.L.E.; Ware, R.A.; Ensor, C.M.; Daunert, S. A novel reagentless sensing system for measuring glucose based on the galactose/glucose-binding protein. *Anal. Biochem.* **2001**, *294*, 19-26.
73. Lam, H.; Kostov, Y.; Rao, G.; Tolosa, L. Low-cost optical lifetime assisted ratiometric glutamine sensor based on glutamine binding protein. *Anal. Biochem.* **2008**, *383*, 61-67.
74. Chan, P.H.; Liu, H.B.; Chen, Y.W.; Chan, K.C.; Tsang, C.W.; Leung, Y.C.; Wong, K.Y. Rational design of a novel fluorescent biosensor for β-lactam antibiotics from a class A β-lactamase. *J. Am. Chem. Soc.* **2004**, *126*, 4074-4075.

Article 1

Choulier, L.*[#], Schvadchak[#], VV., Naidoo, A., Klymchenko, AS., Mély, Y & Altschuh, D. (2010). A peptide-based fluorescent ratiometric sensor for quantitative detection of proteins. *Anal. Biochem.* **401**, 188-195. ([#]co-first authors, *corresponding author)

Analytical Biochemistry 401 (2010) 188–195

Contents lists available at ScienceDirect

Analytical Biochemistry

journal homepage: www.elsevier.com/locate/yabio

A peptide-based fluorescent ratiometric sensor for quantitative detection of proteins

Laurence Choulier [a,*,1], Volodymyr V. Shvadchak [b,1], Aletia Naidoo [a], Andrey S. Klymchenko [b], Yves Mély [b], Danièle Altschuh [a]

[a] Biosensor Group, CNRS/Université de Strasbourg, IREBS, 67412 Illkirch Cedex, France
[b] Laboratoire de Biophotonique et Pharmacologie, UMR-CNRS 7213, Faculté de Pharmacie, Université de Strasbourg, 67401 Illkirch, France

ARTICLE INFO

Article history:
Received 12 November 2009
Received in revised form 22 February 2010
Accepted 23 February 2010
Available online 25 February 2010

Keywords:
Detection
Fluorescence
Peptide biosensor
Quantification
Ratiometric dye
Surface plasmon resonance

ABSTRACT

A ratiometric fluorescent sensor was obtained by solid-phase synthesis of a peptide singly labeled at its N-terminus with a 3-hydroxychromone (3HC) derivative, an environmentally sensitive fluorophore with a two-band emission. The construct contains the binding site recognized by an antibody fragment, scFv1F4$_{Q34S}$, with nanomolar (nM) affinity. The dye only marginally affected the kinetic and equilibrium binding parameters of the scFv–peptide interaction, as measured by surface plasmon resonance. On interaction with the antibody fragment, the sensor showed up to 47% change in the ratio of its two emission bands, indicating an enhanced screening of the 3HC fluorophore from bulk water. Competition with two unlabeled peptides of different lengths led to a dynamic displacement of the construct governed by the relative binding constants. Calibration showed that the response is proportional to the ratio of scFv1F4$_{Q34S}$ to labeled peptide. The detection limit of scFv1F4$_{Q34S}$ was 15 nM. In a more complex medium (100 μg/ml bovine serum albumin), the scFv could be detected in the 50- to 100-nM range. This work demonstrates that, with the perspective of further improvements of the dye spectroscopic properties, fluorescent ratiometric sensing based on small synthetic peptides represents a promising tool for quantitative target detection.

Conventional assays for protein quantification are indirect approaches that rely on a labeled reporter molecule for detection and include several steps. As an interesting alternative, biosensors allow the detection of interactions as they take place without the need for third interactants. In biosensors, a biological receptor is associated with a transducer able to convert the recognition event between the receptor and its target into a measurable signal. The receptors are typically enzymes or antibodies, but it is theoretically possible to use any type of receptor so long as complex formation induces signal transduction.

Among the large variety of transducing principles that have been developed (e.g., electrochemical, optical, thermometric, piezoelectric), fluorescence-based detection presents a number of advantages, including sensitivity, simplicity, and diversity in fluorescence parameters and associated transduction strategies that can be used for sensing [1]. In particular, environmentally sensitive fluorescent dyes can provide signal transduction. When the dye is coupled near the binding site of a receptor or in a region of a receptor, which undergoes a conformational change in concert with target binding, its environment and thus its fluorescence properties change on complex formation [2]. The recognition (receptor) and transduction (fluorophore) modules, are therefore assembled into a single molecule that has been called the "molecular biosensor" [3].

The feasibility of reagentless fluorescent molecular sensors based on environmentally sensitive dyes has been demonstrated mainly on three types of protein receptors: bacterial periplasmic binding proteins (PBPs)[2] [2,4–6], antibody fragments [7–9], and lipid transfer proteins [10]. A fluorescent artificial molecule needs to be introduced into the ligand binding protein. The labeling procedure of proteins [11] presents difficulties at two levels. First, the

* Corresponding author. Fax: +33 368854683.
E-mail address: laurence.choulier@unistra.fr (L. Choulier).
[1] These authors contributed equally to this work.

[2] *Abbreviations used:* PBP, periplasmic binding protein; TMVP, tobacco mosaic virus protein; Fab, antibody binding fragment; 3HC, 3-hydroxychromone; ESIPT, excited state intramolecular proton transfer; scFv, single-chain variable fragment; HPV, human papillomavirus; Fmoc, fluorenylmethoxycarbonyl; NMP, *N*-methyl-2-pyrrolidone; HBTU, [2-(1*H*-benzo-triazole-1-*yl*)-1,1,3,3-tetramethyluronium; HOBt, 1-hydroxybenzotriazole; DMF, dimethylformamide; DIEA, diisopropylethylamine; TFA, trifluoroacetic acid; TIS, triisopropylsilane (iPr3SiH); HPLC, high-performance liquid chromatography; LB, Luria–Bertani; IPTG, isopropyl thiogalactoside; EDTA, ethylenediaminetetraacetic acid; HBS, Hepes-buffered saline; MBP, maltose binding protein; SDS–PAGE, sodium dodecyl sulfate–polyacrylamide gel electrophoresis; SPR, surface plasmon resonance; CFCA, calibration free concentration analysis; RU, resonance unit; UV, ultraviolet; I_{N^*}/I_{T^*}, intensity ratio of the normal (N^*) and tautomer (T^*) emission bands; BSA, bovine serum albumin; LOD, limit of detection; MM, molecular mass; HEL, hen egg white lysozyme; MalE–DE1–His6, dengue virus envelope protein with the MalE protein and a His tag; IANBD, *N*-((2-(iodoacetoxy)ethyl)-*N*-methyl)amino-7-nitrobenz-2-oxa-1,3-diazole.

0003-2697/$ - see front matter © 2010 Elsevier Inc. All rights reserved.
doi:10.1016/j.ab.2010.02.029

choice of the appropriate labeling site is not straightforward. The dye should be close enough to the binding site to "sense" complex formation but should not compromise the interaction between the receptor and its target. Second, achieving 100% site-directed chemical labeling of a biological molecule while keeping it active and stable is a challenge. Even when a successful strategy has been developed, large-scale production of a fluorescent protein biosensor represents a costly and labor-intensive task.

Synthetic peptides provide many advantages over proteins for sensor production. Their synthesis is straightforward and cost-effective, so that peptide–dye constructs can be manufactured on a large scale. Peptides are also robust. However, it is not obvious that environmental changes on complex formation would be as substantial when the dye is located at a peptide–target interface compared with a larger and more structured protein–target interface. The ability of a peptide-based fluorescent biosensor to detect a protein target was demonstrated recently [12] using the well-characterized high-affinity model interaction between an 18-amino-acid peptide of tobacco mosaic virus protein (TMVP) and a recombinant antibody fragment, Fab 57P [13–15]. In addition to using a peptide instead of a protein as receptor, a dye belonging to the 3-hydroxychromone (3HC) family was used as reporter. 3HCs are environmentally sensitive small fluorophores that, due to excited state intramolecular proton transfer (ESIPT), show variations in their dual emission in response to changes of polarity and hydration in their environment [16]. A ratiometric signal is preferable to absolute intensities for quantitative measurements because it is independent of probe concentration. The dye 2-(2-furanyl)-3-hydroxychromone was used in a previous study [12] due to its two-color ratiometric response optimized in the polar range, which provided a 40% decrease in the ratio of its two emission bands on addition of a saturating amount of Fab target to the peptide sensor. This dye also recently allowed the detection of protein conformational changes [17] and protein–oligonucleotide interactions [18].

In this study, we applied the strategy of 3HC labeling of a peptide receptor for sensing a different target. The objectives were (i) to verify that the concept of peptidic biosensor can be extended to another peptide receptor, (ii) to validate N-terminal labeling, which is easier to perform by solid-state peptide synthesis compared with labeling other peptide positions, (iii) to evaluate the potential of the ratiometric sensor for quantitative detection of both unlabeled peptide and target, and (iv) to investigate the behavior of the peptidic sensor in a complex medium. The model system consists of a recombinant antibody fragment, scFv1F4$_{Q34S}$, specific for E6 of human papillomavirus (HPV) 16 and interacting with a peptide corresponding to the N-terminal sequence of the protein [19]. Based on a previous study [20] that led to the identification of the peptide epitope (binding site) recognized by scFv1F4$_{Q34S}$, we designed three ratiometric peptides with the label located at different distances from the epitope. This was achieved by N-terminal labeling of peptides that differed in length. One of these three peptidic constructs possessed sensing properties. Thus, we confirm that efficient ratiometric peptide-based biosensors can be readily designed and synthesized, and demonstrate their potential for quantitative target detection, in direct and competition assays.

Materials and methods

Peptide synthesis and fluorophore coupling

Reagents were obtained from Merck, Sigma–Aldrich, or Applied Biosystems (USA). Fmoc-protected amino acids were obtained from Neosystem (France).

The fluorescent label, *N*-(2-furan-2-*yl*-3-hydroxychromon-6-*yl*)-succinamic acid, was prepared from 6-amino-2-furan-2-*yl*-3-hydroxychromone [21] as described previously [18].

Peptides were synthesized by solid-phase peptide synthesis on a 433A synthesizer (Applied Biosystems). The synthesis was performed on a 0.1-mmol scale using the standard fluorenylmethoxycarbonyl (Fmoc)–amino acid coupling protocol starting from 0.44 mmol/g LL-HMP resin. At the end of the synthesis, 100 mg of Fmoc-deprotected peptidyl resin was isolated and washed twice by *N*-methyl-2-pyrrolidone (NMP). Then 4 eq of the label, *N*-(2-furan-2-*yl*-3-hydroxychromon-6-*yl*)-succinamic acid, was mixed with 4 eq of HBTU/HOBt coupling solution (in dimethylformamide [DMF]) and 5 eq of diisopropylethylamine (DIEA). This mixture was immediately added to the peptidyl resin and stirred at room temperature for 18 h. The resin was filtrated and washed by NMP, methanol, and dichloromethane.

Cleavage of the peptidyl resin and deprotection were performed for 2 h using a 10-ml trifluoroacetic acid (TFA) solution containing water (3.5%, v/v), triisopropylsilane (TIS, iPr_3SiH, 1%, v/v), and ethanedithiol (2.5%, v/v). The solution was concentrated in vacuo, and the peptide was precipitated using ice-cold diethyl ether and pelleted by centrifugation. The pellet was then washed with diethyl ether and dried before solubilization with aqueous TFA (0.05%, v/v). Purification by high-performance liquid chromatography (HPLC) was carried out on a C8 column (Uptisphere 300A, 5 μm, 250 × 10 mm, Interchim, France) in a water/acetonitrile mixture containing 0.05% TFA with a linear gradient from 10% to 50% of acetonitrile for 30 min and was monitored at 360 nm (3HC dye absorption). Molecular masses obtained by ionspray mass spectrometry were 2188, 1863, 1803, 1478, and 1275 for 3HC–4–17, 4–17, 3HC–7–17, 7–17, and 9–17, respectively, in agreement with the expected theoretical masses. Prior to use, peptides were dissolved in distilled water, aliquoted, and stored at −20 °C. Concentrations of the labeled peptides were determined from the label absorbance at 360 nm using $\varepsilon = 16{,}000\ M^{-1}\ cm^{-1}$. Solutions of nonlabeled peptides were prepared by dissolving a known amount (~4 mg) of the powder.

Expression and purification of scFv1F4$_{Q34S}$

An scFv1F4 mutant, with Gln34 replaced by Ser (scFv1F4$_{Q34S}$) [22], was chosen as protein target because it is produced in higher yield than the wild-type fragment. Both scFvs recognize the same peptide antigen. ScFv1F4$_{Q34S}$ was produced as described previously for scFv1F4 [19] with some modifications. Briefly, BL21(DE3) transformed cells were grown at 37 °C in Luria–Bertani (LB) medium supplemented with 100 μg/ml ampicillin, and expression was induced by adding 1 mM isopropyl thiogalactoside (IPTG) at an OD_{600} of approximately 1.0. After 16–18 h at 27 °C, cells were pelleted by centrifugation. Both supernatant and pellet were collected. Supernatant fraction was concentrated approximately 20 times against dry poly(ethylene glycol). The periplasmic fraction of the cells was obtained by resuspending the cell pellet in ice-cold 30 mM Tris–HCl (pH 8.0), 20% sucrose, and 1 mM ethylenediaminetetraacetic acid (EDTA) (buffer A) and was incubated on ice for 1 h. Then 5 ml of ice-cold buffer A, 5 ml of ice-cold sterile water, and 250 μl of lysozyme at 3 mg/ml were added. The mixture was incubated on ice for 1 h. The periplasmic supernatant containing scFv was recovered after centrifugation and dialyzed against Hepes-buffered saline (HBS) containing 100 μM phenylmethanesulfonyl fluoride.

ScFv1F4$_{Q34S}$ was affinity purified using unlabeled peptide 4–17 (corresponding to amino acids 4–17 of the E6 sequence from HPV type 16 with an additional C-terminal cysteine) (Fig. 1A) coupled to CNBr-activated Sepharose 4B (Amersham Biosciences, USA) or using MBP-E6 fusion protein (amino acids 1–18 of E6 linked to

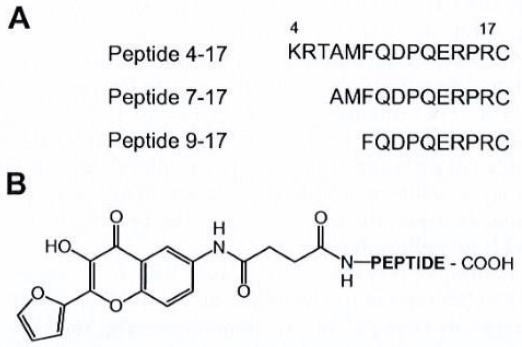

Fig. 1. (A) Sequences of the three peptides used for sensor development, corresponding to amino acids 4–17, 7–17, and 9–17 of the E6 sequence. A cysteine was added at the C-terminus for coupling on SPR sensor chips. (B) Structure of the ratiometric fluorophore *N*-(2-furan-2-*yl*-3-hydroxychromon-6-*yl*)-succinamic acid coupled at the N-terminus of the peptide.

the maltose binding protein) [19] coupled to an amylose resin (New England Biolabs, USA). Then 2 mg of peptide 4–17 dissolved in 0.1 M $NaHCO_3$ and 0.5 M NaCl (pH 8.3) was added to 3 ml of washed gel and coupling was allowed for 1 h at room temperature. Blocking of unreacted CNBr groups by 0.1 M Tris–HCl (pH 8.0) was performed for 2 h at room temperature. The gel was then washed according to the manufacturer's instructions. The coupling of the MBP-E6 to the amylose resin was performed following the manufacturer's instructions. Cell extracts containing scFv1F4$_{Q34S}$ were applied to the two types of columns following equilibration at pH 7.4. The protein was eluted with 10 mM glycine (pH 2.2) and immediately neutralized with 1 M Tris–HCl (pH 8.3) to give a final pH of 7.4. Fractions of purified proteins were checked on sodium dodecyl sulfate–polyacrylamide gel electrophoresis (SDS–PAGE) gels.

SPR experiments

Surface plasmon resonance (SPR) experiments were performed with Biacore 2000 and T100 instruments (GE Healthcare Biacore, Sweden) at 25 °C using HBS buffer (10 mM Hepes, 150 mM NaCl, and 3.4 mM EDTA, pH 7.4) containing 0.005% P20 as a running buffer. The immobilization of unlabeled and labeled peptides by thiol chemistry on carboxylated dextran matrix of sensor surfaces was performed as described previously [23]. The concentration of active scFv1F4$_{Q34S}$ was determined with the Biacore T100 by varying the flow rate under conditions of partial mass transport limitation [24–26] using the calibration free concentration analysis (CFCA) facility implemented in the Biacore T100 evaluation software (version 2.0.1, GE Healthcare Biacore). This method allows the determination of active scFv concentrations without the need for a calibration curve. After its concentration had been determined in this way, the scFv preparation was used to establish a calibration curve that allowed the rapid determination of scFv concentration in all solutions prepared for kinetic runs as described previously [27].

Between 4.5 and 19 resonance units (RU) of peptides were immobilized for kinetic measurements. Control surfaces were obtained by treating the surface as for peptide immobilization except that peptide injection was omitted. The scFv1F4$_{Q34S}$ was injected at concentrations ranging from 0.6 to 40 nM at a constant flow rate of 30 μl/min in HBS buffer either with the conventional method, where serial injections of solutions with different analyte concentrations are followed by a regeneration step (pulse of NaOH = 20 mM), or with the titration method, where these solutions are injected over the surfaces without regeneration [28]. Data were analyzed with the global fitting algorithm of BIAevaluation software (version 4.1) or Biacore T100 evaluation software (version 2.0.1) for experiments realized on Biacore 2000 or T100, respectively. At least two independent surfaces were used for each peptide–scFv1F4$_{Q34S}$ interaction. In 86% of the studied cases the χ^2/ fitted R_{max} was below 0.09 RU, and in 14% of the cases it was between 0.09 and 0.18 RU.

Fluorescence experiments

Absorption spectra were recorded with a Cary 4000 ultraviolet (UV)–visible spectrophotometer (Varian, USA). Fluorescence spectra were recorded on FluoroMax3 and FluoroLog spectrofluorimeters (Jobin Yvon, USA) equipped with thermostated cell compartments. Quantum yields were calculated using quinine sulfate in 0.5 M sulfuric acid ($\varphi = 0.577$) as a reference [29].

The excitation wavelength was 350 nm, and emission was monitored in the range of 370–700 nm. Excitation and emission slits were 3 and 9 nm, respectively. All experiments were performed in HBS buffer at room temperature (20 °C). All spectra were corrected for Raman scattering and background fluorescence measured before the addition of the labeled peptide. The intensity ratio at the maximum of the normal (N^*) band (~430 nm) and the tautomer (T^*) band (~510 nm), I_{N^*}/I_{T^*}, was calculated for each sample.

The binding properties of labeled peptides were checked by measuring the emission spectrum of 0.2 μM peptides in the presence of 0.2 μM scFv1F4$_{Q34S}$ or of an unrelated goat anti-rabbit F(ab')$_2$ fragment (Sigma–Aldrich, reference R9130).

In competition assays, 0–0.5 μM unlabeled peptides (4–17 and 7–17) were incubated with a mixture of 0.1 μM peptide 3HC–7–17 and 0.1 μM scFv1F4$_{Q34S}$. Fluorescence spectra were recorded for eight concentrations of unlabeled peptides. To determine the equilibrium dissociation constant of the interaction between scFv1F4$_{Q34S}$ and unlabeled peptides, the concentration–response data were fit to the following equation:

$$R = R_0 - \frac{x(R_0 - R_f)}{x + C_0 \times K_0/K_C}, \quad (1)$$

where R is the band ratio at competitor concentration x, R_f and R_0 are the I_{N^*}/I_{T^*} band ratio of the fully bound and free 3HC–7–17, respectively, C_0 is the initial concentration of the 3HC–7–17/antibody complex, and K_0/K_C is the ratio of the equilibrium dissociation constants of scFv1F4$_{Q34S}$ for 3HC–7–17 and competitor, respectively. An unrelated unlabeled peptide (C19V: CRGTGSYNRSSFESSSGLV) was also tested as a negative control at one concentration (1.25 μM).

The calibration curve was obtained by titration of the 3HC–7–17 peptide by scFv1F4$_{Q34S}$. Two series of experiments were performed with 75 and 200 nM peptide 3HC–7–17. Concentrations of scFv1F4$_{Q34S}$ were from 15 to 165 nM and from 40 to 300 nM, respectively. The binding curves were fitted to the rewritten Scatchard equation:

$$R = R_0 - \frac{(R_0 - R_f)}{P} \times \frac{(1 + (P + nA)K_a) - \sqrt{(1 + (P + nA)K_a)^2 - 4PnAK_a^2}}{2K_a}, \quad (2)$$

where R is the signal (emission band ratio) at a given antibody concentration, P is the total concentration of peptide, n is the binding stoichiometry (found to be 1 ± 0.1), A is the total antibody concentration, and K_a is the apparent affinity constant. The limit of detection was defined as the lowest scFv1F4$_{Q34S}$ concentration that gives 20% variation of the I_{N^*}/I_{T^*} ratio for a biosensor (3HC–7–17) concentration where the intensity at the short-wavelength band (432 nm) is threefold larger than that of the blank. The short-wavelength

band was selected for this criterion because it is much more affected by the blank than is the long-wavelength band. For experiments in a complex medium, various concentrations (15–200 nM) of scFv1F4$_{Q34S}$ were added in HBS buffer with bovine serum albumin (BSA) at 100 μg/ml in the absence or presence of peptide 3HC–7–17 at 0.1 μM. Spectra were corrected for the background fluorescence recorded prior to the addition of scFv1F4$_{Q34S}$ and peptide 3HC–7–17.

Results

Design of peptidic fluorescent constructs

To confer sensing properties to a receptor, the dye must be located in such a way that its environment changes when the target binds, but it should not interfere with binding. The design of a molecular sensor, therefore, requires some knowledge about the interaction, gained from structural or functional studies, to identify positions that are close to the binding interface. The molecular interaction between scFv1F4$_{Q34S}$ and peptides corresponding to the N-terminal sequence of the E6 protein of HPV 16 has been well characterized by phage display, spot peptide synthesis on cellulose membranes, and SPR kinetic measurements [20]. The functional epitope for scFv binding has been mapped to positions 9–14 of the E6 sequence.

Three positions were chosen for labeling: zero, two, and five residues away from position 9, which is the first position in the E6 sequence mapped as important for scFv binding. Because the dye was coupled at the N-terminus of the peptides, three peptides of different lengths resulted from this design, corresponding to amino acids 4–17, 7–17, and 9–17 of the E6 sequence. A cysteine was added at the peptide C-terminus to allow chemical thiol coupling on Biacore sensor chips. Positions important for scFv binding (9–14) remain untouched in the two longer peptides. The carboxylic acid derivative of the 3HC fluorophore 2-(2-furanyl)-3-hydroxychromone (3HC in Fig. 1B) was chosen as the reporter dye.

Binding properties of labeled and unlabeled peptides interacting with scFv1F4$_{Q34S}$

The association (k_a), dissociation (k_d), and equilibrium (K_D) binding parameters for the interaction of labeled and nonlabeled peptides 4–17 and 7–17 with scFv1F4$_{Q34S}$ were determined by SPR using the conventional and titration approaches (see Materials and methods). For all experiments, the fitted curves ran close to the experimental data, as illustrated in Fig. 2. The interaction of the unlabeled peptide 9–17 with scFv1F4$_{Q34S}$ (Fig. 2C) appears to be much less stable than other interactions (Fig. 2A and B), indicating that the presence of the fluorophore on residue F9, which belongs to the previously identified epitope recognized by the scFv, or deletion of amino acids Ala7 and Met8 has a strong negative impact on affinity. Therefore, we decided not to use this peptide for further SPR investigations.

Kinetic and affinity parameters for the labeled and unlabeled peptides 4–17 and 7–17 are listed in Table 1. The values of the kinetic parameters of the four peptides are comparable. K_D values are in the same range, varying from 0.39 to 0.98 nM.

Sensor properties of labeled peptides

Comparison of different peptide constructs

To check whether the peptide constructs exhibit sensing properties, the fluorescence signal of each labeled peptide alone was compared with that in the presence of equimolar amounts of scFv1F4$_{Q34S}$ or of an unrelated antibody fragment F(ab')$_2$ (Fig. 3). The intensity ratio at the maximum of the N* band and the T* band, I_{N^*}/I_{T^*}, was calculated for each sample.

The fluorescence spectra of all three peptide constructs in buffer showed dual emission typical for 3HC dyes. In the case of 3HC–4–17 and 3HC–7–17, the I_{N^*}/I_{T^*} values (1.13 and 1.34, respectively) are close to the value for the free label in water (1.47) [18], indicating an efficient exposure of the label to the bulk water. For 3HC–9–17, the I_{N^*}/I_{T^*} value is significantly lower (0.61), suggesting an interaction between the 3HC label and the peptide that screens the label from bulk water.

The addition of scFv1F4$_{Q34S}$ to peptide 3HC–7–17 caused a 47% decrease in the ratio of its two emission bands (I_{N^*}/I_{T^*}), indicating an enhanced screening of the 3HC fluorophore (Fig. 3B). Thus, complex formation leads to the exclusion of water molecules from the peptide labeling site. In contrast, the addition of a negative control F(ab')$_2$ (Fig. 3A and B) did not modify the dual emission of the peptide, indicating that the response is specific for the target.

Peptides 3HC–4–17 (Fig. 3A) and 3HC–9–17 (Fig. 3C) did not behave as biosensors given that no significant spectral change was observed in the presence of scFv1F4$_{Q34S}$. The biosensor properties of 3HC–7–17 were further investigated by competition and titration experiments.

Competition with unlabeled peptides

The addition of different concentrations (0, 50, 100, 150, 200, 300, 400, and 500 nM) of unlabeled peptide 4–17 or 7–17 to a 3HC–7–17/scFv1F4$_{Q34S}$ mixture (at 0.1 μM each) sets up a competition between the labeled and unlabeled peptides for scFv1F4$_{Q34S}$ binding, as shown by the change of the I_{N^*}/I_{T^*} ratio as a function of the unlabeled peptide concentration (Fig. 4).

A fit of the data using Eq. (1) provided K_D values of 0.21 and 1.34 nM for the interaction between scFv1F4$_{Q34S}$ and peptides 4–17 and 7–17, respectively, in the same range as the K_D values determined by SPR (Table 1). The unrelated peptide C19V at 1.25 μM did not change the spectra of peptide 3HC–4–17 or 3HC–7–17 complexed to scFv1F4$_{Q34S}$ (data not shown).

Calibration experiments

For calibration experiments, increasing concentrations of scFv1F4$_{Q34S}$ were added to a constant concentration of peptide 3HC–7–17. Two experiments were performed with scFv1F4$_{Q34S}$ concentrations ranging from 15 to 165 nM for a 3HC–7–17 concentration of 75 nM and with scFv1F4$_{Q34S}$ concentrations ranging from 40 to 300 nM for a 3HC–7–17 concentration of 200 nM. Fig. 5 presents the I_{N^*}/I_{T^*} ratio of the 3HC–7–17 peptide versus [scFv1F4$_{Q34S}$]/[3HC–7–17]. The graph is linear over the range of concentration ratio from 0 to 1 and shows saturation above. Analysis of the linear part shows that the dynamic range for scFv1F4$_{Q34S}$ calibration is between 15 and 70 nM for [3HC–7–17] = 75 nM and between 30 and 180 nM for [3HC–7–17] = 200 nM, with a limit of detection (LOD) of 15 nM.

Fluorescence measurements in 100 μg/ml BSA

We then checked whether the 3HC–7–17 construct could be used for detection of scFv1F4$_{Q34S}$ in the same buffer as for other fluorescence experiments, to which BSA was added at 100 μg/ml. This concentration is 350–500 times lower than the concentration of BSA in bovine serum (35–50 mg/ml).

Fig. 6 shows the fluorescence spectra of 0.1 μM peptide 3HC–7–17 in the absence and presence of 50 and 100 nM scFv1F4$_{Q34S}$ before and after subtraction of the background fluorescence of BSA. The strong background is due mainly to the limited brightness of the 3HC dye and to the UV excitation that produces a strong autofluorescence. However, it was still possible to detect a change in the I_{N^*}/I_{T^*} value in the presence of 50 or 100 nM scFv1F4$_{Q34S}$.

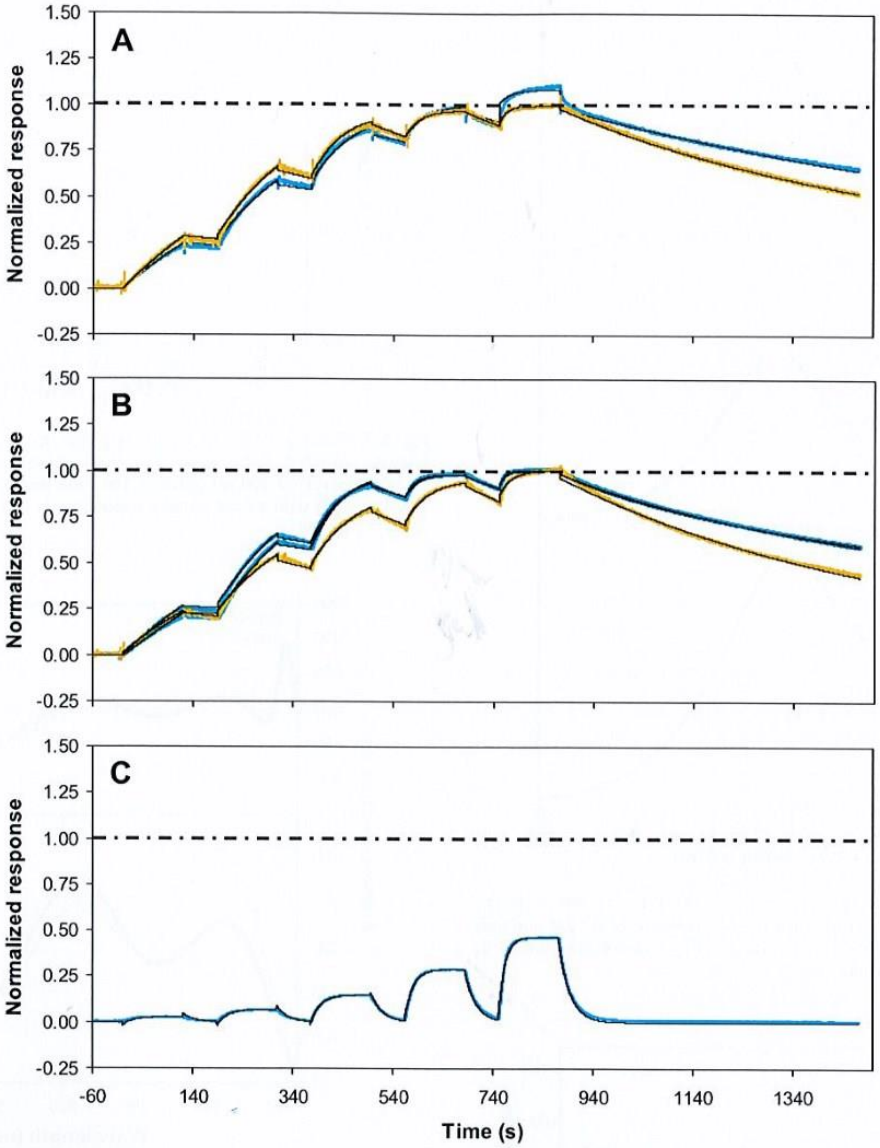

Fig. 2. SPR titration curves (blue and orange) and fitted curves (black) for the interaction of scFv1F4$_{Q34S}$ with immobilized unlabeled (blue) and labeled (orange) peptides 4–17 (A), 7–17 (B), and 9–17 (C). A replicate of scFv injection on peptide 7–17 is shown in panel B (lighter blue). The scFv was injected at concentrations ranging from 2.5 to 40 nM. Responses were normalized as *R*/fitted R_{max} to take into account differences in peptide immobilization levels, with R_{max} being the response at surface saturation (dashed line). R_{max} values for peptides 4–17, 3HC–4–17, 7–17, 3HC–7–17, and 9–17 were 64, 36, 46 (blue) and 191 (lighter blue), 76, and 375 RU, respectively.

Table 1
Binding parameters for interaction of scFv1F4$_{Q34S}$ with unlabeled and labeled peptides 4–17 and 7–17, as determined by SPR.

Peptide	k_a (10^6 M^{-1} s^{-1})	k_d (10^{-3} s^{-1})	K_D (10^{-9} M)	Number of independent experiments
4–17	2.1 ± 0.8	0.7 ± 0.1	0.40 ± 0.13	8
3HC–4–17	2.5 ± 0.7	1.2 ± 0.3	0.48 ± 0.11	12
7–17	3.2 ± 1.1	1.2 ± 0.4	0.39 ± 0.09	12
3HC–7–17	1.6 ± 0.4	1.5 ± 0.2	0.98 ± 0.35	6

Discussion

The concept of a peptide receptor coupled to a two-color ratiometric dye for the direct detection of an antibody fragment [12] was confirmed in this study by the successful development of a new singly labeled fluorescent peptide sensor. Its sensing properties were characterized in detail, allowing a comparison of its performance with the performances of previously published protein sensors.

The properties of environmentally sensitive protein sensors have been described previously for two receptor families: PBPs [2,5,6] and antibodies [7–9]. The construction procedures and performances of PBP-based sensors are not directly comparable with those of our peptide sensors. PBPs recognize small ligands such as sugars (e.g., maltose, glucose, arabinose) or amino acids, dipeptides, anions, and cations (with molecular mass [MM] < 400 Da), with low affinity (K_D = 0.1–1 μM) in the case of wild-type proteins [2,4,5], although engineered PBPs with higher affinity have been described previously [6]. The reporter dye is often coupled in a region that undergoes a conformational change when the ligand binds, thereby avoiding perturbations at the ligand–receptor interface. Here we compare construction procedures, activities, and per-

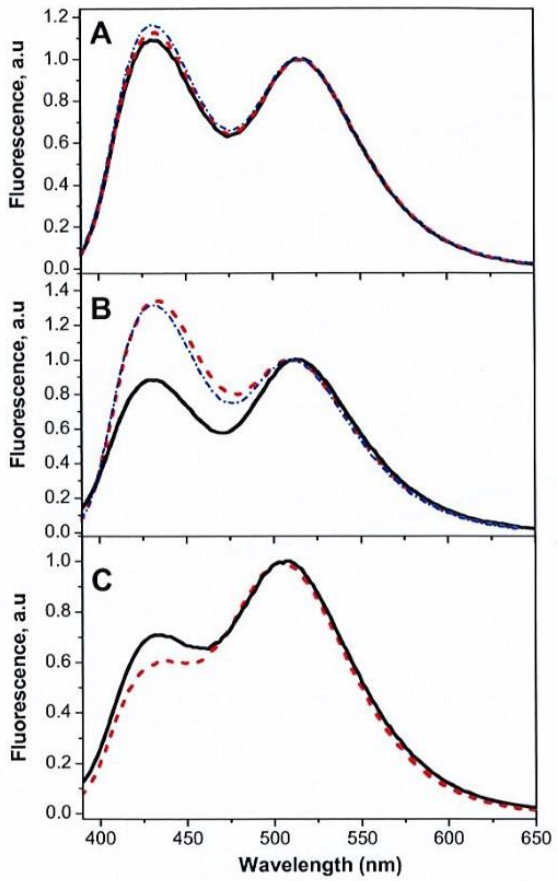

Fig. 3. Normalized fluorescence spectra of 0.2 μM 3HC–4–17 (A), 3HC–7–17 (B), and 3HC–9–17 (C) in the absence (dashed line) or presence of 0.2 μM antibody fragments scFv1F4$_{Q34S}$ (thick line) or unrelated F(ab′)$_2$ (dash-dotted line). The excitation wavelength was 350 nm.

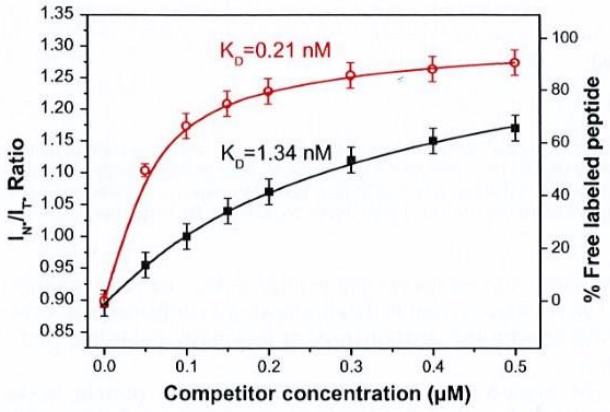

Fig. 4. Competitive binding of the nonlabeled peptides 4–17 (open circles) and 7–17 (squares) added to the 3HC–7–17/scFv1F4$_{Q34S}$ complex, as monitored by the ratio of the 3HC emission bands. Lines represent the fit of the data to Eq. (1), yielding K_D values for the scFv1F4$_{Q34S}$–competitor peptide interactions. The right axis shows the percentage of free labeled peptide in solution corresponding to observed $I_{N'}/I_{T'}$ values.

formances of antibody and peptide sensors. Both are based on antigen–antibody interactions, with the receptor being either the antibody [7,8] or the peptide antigen (see Ref. [12] and this study).

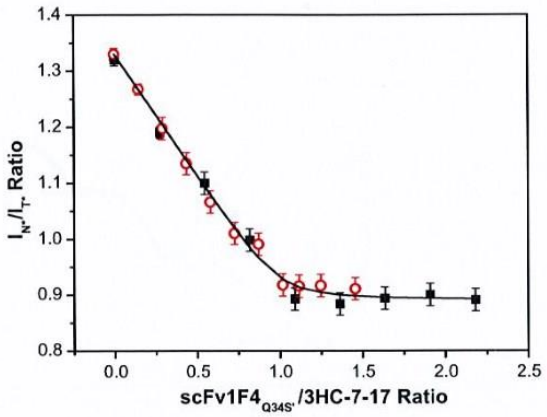

Fig. 5. Calibration of the 3HC–7–17 response ($I_{N'}/I_{T'}$ ratio) as a function of the [scFv1F4$_{Q34S}$]/[3HC–7–17] ratio. The concentration of peptide 3HC–7–17 was 75 nM (squares) or 200 nM (circles). The solid line corresponds to the fit of the data to Eq. (2) with a fixed binding stoichiometry of 1:1. The calculated K_D value was 1.5 ± 0.7 nM.

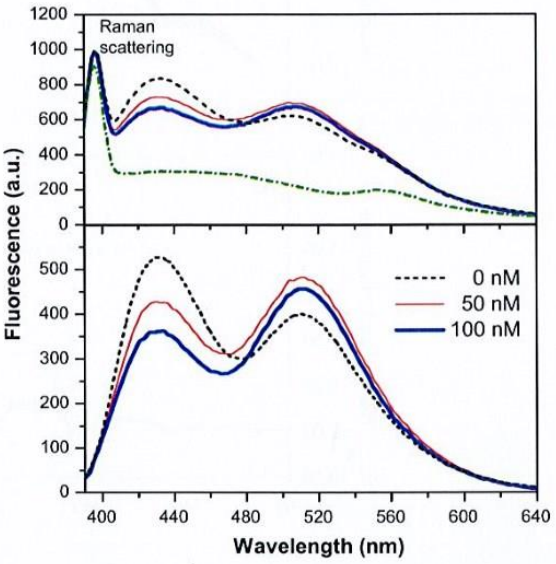

Fig. 6. Uncorrected (upper panel) and corrected (bottom panel) fluorescence spectra of 0.1 μM peptide 3HC–7–17 in the absence (dashed lines) or presence of 50 nM (thin lines) or 100 nM (thick lines) scFv1F4$_{Q34S}$ in the presence of 100 μg/ml BSA. The spectrum of 100 μg/ml BSA (dash-dotted line) was used for curve corrections.

Dyes are coupled near the binding interfaces, and all systems display affinities in the 0.1-nM range. Compared with the targets recognized by PBPs, the targets of antibody and peptide sensors are large (Table 2): hen egg white lysozyme (HEL) [7], residues 296–400 of the dengue virus envelope protein with the MalE protein and a His tag (MalE–DE1–His6) [8], and antibody fragments (Fab 57P [12] and scFv1F4 [this study]).

Renard and coworkers [7,8] characterized five steps or properties during biosensor development. The first three refer to sensor construction: expression level of cysteine mutants, reaction yield (protein remaining soluble after the coupling procedure), and coupling yield (molecular ratio of dye to protein). The remaining two properties refer to sensor activity: binding affinity for the target and variation in fluorescence on target binding. Finally, sensor performance can be evaluated from the dynamic range of calibration curves and from the sensitivity limit. These steps or properties

Table 2
Comparison of construction procedures, activities, and performances of antibody and peptide biosensors.

	Renard et al. [7]	Renard et al. [8]	Enander et al. [12]	This study
System characteristics				
Receptor	scFv D1.3	scFv 4E11	Peptide 134–151 of the TMVP	Peptide 7–17 of the E6 protein
Target	HEL	MalE-DE1-His6	Fab 57P	scFv1F4$_{Q34S}$
Molecular mass (Da)	14,300	54,000	49,000	29,000
K_D of unlabeled receptor–target complex (nM)	16	0.35	1.6	0.39
Number of sensors designed	10	8	2	3
Type of fluorescence response	Intensiometric	Intensiometric	Ratiometric	Ratiometric
Sensor construction				
Method of receptor construction	Recombinant protein	Recombinant protein	Synthetic peptide	Synthetic peptide
Labeling method	SH group protein labeling	SH group protein labeling	SH group labeling on resin	N-terminal labeling on resin
Sensor activities and performances				
Active sensors (>35% response)	2/10	3/8	1/2	1/3
Number of conjugates characterized in more detail for target quantification	2	3	0	1
K_D of biosensor–target complex as measured by SPR (nM)	14 and 15	0.21, 0.36, and 0.37	ND	0.98
Fluorescence signals at saturation (%)	55 and 26	45, 182, and 74	40	47
Dynamic range (nM)	10–400	10–100	ND	15–180
Limit of detection (nM)	10[a]	10[a]	ND	15[b]

Note. ND, not determined.
[a] Value reported by the authors.
[b] Value corresponding to a 20% change in the signal of the biosensor at a biosensor concentration giving a fluorescence intensity threefold larger than the blank.

are compared for the four systems in Table 2 and are discussed below.

Proteic and peptidic sensor construction

With a few exceptions, expression levels of cysteine mutants of the protein receptors were similar to those of the wild type and coupling yields were close to 100% [7,8]. However, reaction yields were typically low (~20%) due to protein precipitation during chemical coupling. This low reaction yield and relatively low protein expression levels (a few hundred μg/L culture) clearly represent limiting factors in protein sensor construction compared with synthetic sensors that can be easily produced in milligram (mg) or larger amounts. The dyes can be readily incorporated into synthetic peptides before cleaving them from the resin either by coupling to the thiol of a cysteine residue [12] or by direct N-terminal labeling (this study), yielding pure and 100% single-site labeled molecules. Of the five peptide sensors designed (two in Ref. [12] and three in this study), sensor synthesis and solubilization was problematic in only one case (peptide 9–17 in this study) where the peptide was shortened by two residues compared with the shortest known active form, corresponding to residues 7–17 [20].

Protein versus peptide sensor activity

The studies available so far suggest that, once the dye–receptor conjugates are constructed, the proportion of efficient fluorescent sensors lies in the same range whether the receptor is a protein or a peptide, with the limiting factor being the sensing capacity of the constructs but not their target binding affinity. However, additional examples are needed in the future to support this conclusion. Binding affinities of the protein receptors were not severely affected by the cysteine mutations, probably as a consequence of the careful choice of coupling sites based on prior functional or structural knowledge of the binding site. Partly for these same reasons, binding affinities were only marginally affected by the presence of the dye [7,8], with K_D values being 0.6 to 1.3 times those measured with the corresponding unlabeled proteins. Accommodation of the dye at the interfaces may also be facilitated by the flexibility of the aliphatic arm of the dye *N*-((2-(iodoacetoxy)ethyl)-*N*-methyl)amino-7-nitrobenz-2-oxa-1,3-diazole (IANBD) used in protein sensors [7] as well as the inherent flexibility of peptide sensors. However, although the binding affinity is preserved, only a fraction of the constructs (20–50%) show greater than 35% biosensing abilities (Table 2). A similar proportion of efficient peptide sensors was recently observed based on the low (μM) affinity binding of peptides to PDZ domains. Of eight coupling locations in a decamer, three provided sensors with a less than 10% increase in fluorescence, two with a 10–20% increase, and three with a greater than 25% increase [30].

The 3HC–7–17 peptide sensor did not behave well in 100 μg/ml BSA, in contrast to antibody sensors using IANBD as reporter [7,8]. Indeed, the limited brightness of the 3HC label and its excitation in the UV region (350 nm) make it highly sensitive to background fluorescence and prevented measurements at low peptide concentrations in a more complex medium.

Protein versus peptide sensor performance for target quantification

We showed that the peptide sensor 3HC–7–17 can be used for detecting unlabeled peptides in competition experiments, for evaluating their affinity for the scFv1F4$_{Q34S}$, and for direct target detection.

Competition experiments for detecting unlabeled peptide are fast, require relatively low amounts of material, and yield affinity data. Indeed, a single competition experiment consumes 400 pmol of unlabeled competitor peptide and 80 pmol of peptide biosensor and scFv, and it requires 10–15 min. The K_D values obtained (0.21 and 1.34 nM for peptides 4–17 and 7–17, respectively) are in the same range as those determined by SPR (0.40 and 0.39 nM for peptides 4–17 and 7–17, respectively). The titration curve of the peptide 3HC–7–17 was linear for scFv1F4$_{Q34S}$ concentrations ranging from 0 to 61 nM with [3HC–7–17] = 75 nM and from 0 to 190 nM with [3HC–7–17] = 200 nM, with a detection threshold of 15 nM in buffer and in the 50- to 100-nM range in a buffer containing 100 μg/ml BSA. These values are in the same range as those reported for antibody sensors (Table 2). Whereas biosensors commonly respond to the analyte binding by changes in the intensity (intensiometric), the current biosensor shows changes in the ratio of its two emission bands (ratiometric response). This ratio directly

describes the ratio between the concentrations of free and bound forms of the biosensor. Thus, it is independent of the instrumental factors that affect the fluorescence intensities, and it allows adjustment of receptor and target concentrations.

Conclusion

This study has shown that peptides perform as well as protein receptors in the design of singly labeled environmentally sensitive fluorescent sensors. Formation of complexes with their targets can provide significant environmental changes for the dye despite the smaller size and likely increased flexibility of a peptide–target interface compared with a protein–target interface. Prediction of the optimal labeling site remains a major issue regardless of whether peptide or protein receptors are used. The problem can be circumvented by constructing series of conjugates labeled at different sites and screening for operational sensors, and this is obviously much easier in the case of synthetic peptides. Further improvements of ratiometric sensors include the development of optimized dyes, which are brighter (higher fluorescence quantum yields and extinction coefficient) to increase the sensitivity of detection and display higher photostability and red-shifted absorption and emission maxima, so as to decrease the interference from a complex medium.

Acknowledgments

This work was supported by the Agence Nationale de la Recherche (ANR blanc 07-BLAN-0287), the Centre National de la Recherche Scientifique (CNRS), the Université de Strasbourg, and an Eiffel fellowship for V.V.S.

References

[1] D. Altschuh, S. Oncul, A.P. Demchenko, Fluorescence sensing of intermolecular interactions and development of direct molecular biosensors, J. Mol. Recognit. 19 (2006) 459–477.
[2] R.M. de Lorimier, J.J. Smith, M.A. Dwyer, L.L. Looger, K.M. Sali, C.D. Paavola, S.S. Rizk, S. Sadigov, D.W. Conrad, L. Loew, H.W. Hellinga, Construction of a fluorescent biosensor family, Protein Sci. 11 (2002) 2655–2675.
[3] H.W. Hellinga, J.S. Marvin, Protein engineering and the development of generic biosensors, Trends Biotechnol. 16 (1998) 183–189.
[4] J.S. Marvin, E.E. Corcoran, N.A. Hattangadi, J.V. Zhang, S.A. Gere, H.W. Hellinga, The rational design of allosteric interactions in a monomeric protein and its applications to the construction of biosensors, Proc. Natl. Acad. Sci. USA 94 (1997) 4366–4371.
[5] S.S. Rizk, M.J. Cuneo, H.W. Hellinga, Identification of cognate ligands for the *Escherichia coli* phnD protein product and engineering of a reagentless fluorescent biosensor for phosphonates, Protein Sci. 15 (2006) 1745–1751.
[6] Y. Tian, M.J. Cuneo, A. Changela, B. Höcker, L.S. Beese, H.W. Hellinga, Structure-based design of robust glucose biosensors using a *Thermotoga maritima* periplasmic glucose-binding protein, Protein Sci. 16 (2007) 2240–2250.
[7] M. Renard, L. Belkadi, N. Hugo, P. England, D. Altschuh, H. Bedouelle, Knowledge-based design of reagentless fluorescent biosensors from recombinant antibodies, J. Mol. Biol. 318 (2002) 429–442.
[8] M. Renard, L. Belkadi, H. Bedouelle, Deriving topological constraints from functional data for the design of reagentless fluorescent immunosensors, J. Mol. Biol. 326 (2003) 167–175.
[9] M. Renard, H. Bedouelle, Improving the sensitivity and dynamic range of reagentless fluorescent immunosensors by knowledge-based design, Biochemistry 43 (2004) 15453–15462.
[10] E.J. Choi, J. Mao, S.L. Mayo, Computational design and biochemical characterization of maize nonspecific lipid transfer protein variants for biosensor applications, Protein Sci. 16 (2007) 582–588.
[11] H. Wang, E. Nakata, I. Hamachi, Recent progress in strategies for the creation of protein-based fluorescent biosensors, ChemBioChem 10 (2009) 2560–2577.
[12] K. Enander, L. Choulier, A. Linnéa-Olsson, D.A. Yushchenko, D. Kanmert, A.S. Klymchenko, A.P. Demchenko, Y. Mély, D. Altschuh, A peptide-based ratiometric biosensor construct for direct fluorescence detection of a protein analyte, Bioconjug. Chem. 19 (2008) 1864–1870.
[13] J. Chatellier, N. Rauffer-Bruyère, M.H. Van Regenmortel, D. Altschuh, E. Weiss, Comparative interaction kinetics of two recombinant Fabs and of the corresponding antibodies directed to the coat protein of tobacco mosaic virus, J. Mol. Recognit. 9 (1996) 39–51.
[14] L. Choulier, N. Rauffer-Bruyère, M. Ben Khalifa, F. Martin, T. Vernet, D. Altschuh, Kinetic analysis of the effect on Fab binding of identical substitutions in a peptide and its parent protein, Biochemistry 38 (1999) 3530–3537.
[15] L. Choulier, D. Laune, G. Orfanoudakis, H. Wlad, J.-C. Janson, C. Granier, D. Altschuh, Delineation of a linear epitope by multiple peptide synthesis and phage display, J. Immunol. Methods 249 (2001) 253–264.
[16] A.P. Demchenko, Y. Mély, G. Duportail, A.S. Klymchenko, Monitoring biophysical properties of lipid membranes by environment-sensitive fluorescent probes, Biophys. J. 96 (2009) 3461–3470.
[17] C. Boudier, A.S. Klymchenko, Y. Mely, A. Follenius-Wund, Local environment perturbations in α_1-antitrypsin monitored by a ratiometric fluorescent label, Photochem. Photobiol. Sci. 8 (2009) 814–821.
[18] V.V. Shvadchak, A.S. Klymchenko, H. de Rocquigny, Y. Mely, Sensing peptide–oligonucleotide interactions by a two-color fluorescence label: application to the HIV-1 nucleocapsid protein, Nucleic Acids Res. 37 (2009) e25.
[19] C. Giovane, G. Travé, A. Briones, Y. Lutz, B. Wasylyk, E. Weiss, Targetting of the N-terminal domain of the human papillomavirus type 16 E6 oncoprotein with monomeric ScFvs blocks the E6-mediated degradation of cellular p53, J. Mol. Recognit. 12 (1999) 141–152.
[20] L. Choulier, G. Orfanoudakis, P. Robinson, D. Laune, M. Ben Khalifa, C. Granier, E. Weiss, D. Altschuh, Comparative properties of two peptide–antibody interactions, as deduced from epitope delineation, J. Immunol. Methods 259 (2002) 77–86.
[21] A.S. Klymchenko, V.V. Shvadchak, D.A. Yushchenko, N. Jain, Y. Mely, Excited-state intramolecular proton transfer distinguishes microenvironments in single- and double-stranded DNA, J. Phys. Chem. B 112 (2008) 12050–12055.
[22] N. Hugo, M. Weidenhaupt, M. Beukes, B. Xu, J.C. Janson, T. Vernet, D. Altschuh, VL position 34 is a key determinant for the engineering of stable antibodies with fast dissociation rates, Protein Eng. 16 (2003) 381–386.
[23] M. Khalifa, M. Weidenhaupt, L. Choulier, J. Chatellier, N. Rauffer-Bruyère, D. Altschuh, T. Vernet, Effects on interaction kinetics of mutations at the VH–VL interface of Fabs depend on the structural context, J. Mol. Recognit. 13 (2000) 127–139.
[24] P.M. Richalet-Sécordel, N. Rauffer-Bruyère, L.L. Christensen, B. Ofenloch-Haehnle, C. Seidel, M.H. Van Regenmortel, Concentration measurement of unpurified proteins using biosensor technology under conditions of partial mass transport limitation, Anal. Biochem. 249 (1997) 165–173.
[25] L.L. Christensen, Theoretical analysis of protein concentration determination using biosensor technology under conditions of partial mass transport limitation, Anal. Biochem. 249 (1997) 153–164.
[26] K. Sigmundsson, G. Másson, R. Rice, N. Beauchemin, B. Obrink, Determination of active concentrations and association and dissociation rate constants of interacting biomolecules: an analytical solution to the theory for kinetic and mass transport limitations in biosensor technology and its experimental verification, Biochemistry 41 (2002) 8263–8276.
[27] M. Weidenhaupt, M.B. Khalifa, N. Hugo, L. Choulier, D. Altschuh, T. Vernet, Functional mapping of conserved, surface-exposed charges of antibody variable domains, J. Mol. Recognit. 15 (2002) 94–103.
[28] R. Karlsson, P.S. Katsamba, H. Nordin, E. Pol, D.G. Myszka, Analyzing a kinetic titration series using affinity biosensors, Anal. Biochem. 349 (2006) 136–147.
[29] J.W. Eastman, Quantitative spectrofluorimetry: the fluorescence quantum yield of quinine sulfate, Photochem. Photobiol. 6 (1967) 55–72.
[30] M. Sainlos, W.S. Iskenderian, B. Imperiali, A general screening strategy for peptide-based fluorogenic ligands: probes for dynamic studies of PDZ domain-mediated interactions, J. Am. Chem. Soc. 131 (2009) 6680–6682.

B. *Identification de ligands de cibles thérapeutiques par criblages de chimiothèques*

Articles 2 & 3

Résumé :

Au sein de l'UMR 7242 (IREBS), pour identifier de nouveaux ligands de cibles d'intérêt thérapeutique, nous avons développé différentes stratégies de criblage de petites et moyennes chimiothèques (comprenant jusqu'à 1120 composés) par SPR ('surface plasmon resonance'). Cette technique permet de détecter des interactions entre molécules non marquées et, notamment, d'avoir accès à leurs paramètres cinétiques d'interaction.
Nous avons réalisé trois criblages sur trois cibles différentes :

- sur l'adrénomédulline, un criblage direct : les molécules d'une très petite banque ont été injectées successivement sur l'adrénomédulline immobilisée. Cette étude nous a permis de valider la faisabilité d'un criblage direct par SPR.

- sur la tyrosine phosphatase-1b (PTP-1b), un criblage direct (Article 2) avec les 1120 composés de la banque de Prestwick Chemical, connue pour ses composés de grande diversité chimique et pharmacologique. Les meilleurs ligands de la PTP-1b ont été sélectionnés. Parmi eux, un inhibiteur connu de la PTP-1b a été retrouvé, la sanguinarine.

- sur l'interaction entre le domaine PDZ de MAGI1 et un peptide mimant l'extrémité terminale de l'oncoprotéine E6 du papillomavirus de type 16, un criblage indirect, par inhibition, avec les 1120 composés de la banque de Prestwick Chemical. De nouveaux ligands inhibant l'interaction ont été identifiés, ainsi que des pistes pour simuler la conception de criblages par inhibition sur d'autres systèmes d'interactions moléculaires.

Les données ont permis d'obtenir des informations sur l'affinité de l'interaction, d'éliminer les composés aggrégés (facilement détectables par SPR), d'éviter les faux positifs souvent problématiques lors des criblages à haut débit, et donc de générer des données à haut contenu informatif.

Dès la fin des années 1980, les entreprises pharmaceutiques ont énormément investi dans le criblage à haut debit (HTS : 'high throughput screening'). Des robots analysent des milliers de petits composés chimiques d'origine naturelle ou non, pour détecter des molécules actives 'hits', susceptibles d'être efficaces contre telle ou telle pathologie. La méthode exige un nombre considérable de molécules à passer au crible. Les laboratoires et centres de recherche ont donc étoffé au fil des années, leurs collections, les techniques de criblage et leur débit. Pourtant ces approches de HTS n'ont pas eu autant de succès qu'escompté. L'une des raisons vient du fait que les avantages dus au criblage de très grandes chimiothèques sont contrebalancés par la fréquence des faux-positifs. Les entreprises pharmaceutiques se sont donc progressivement tournées vers des méthodes biophysiques permettant un criblage à haut contenu informatif (Huber, 2005; Lundqvist, 2005), pour limiter les faux-positifs. Les appareils Biacore (GE Healthcare, Uppsala, Suède) sont des biocapteurs optiques qui utilisent le phénomène de résonance plasmonique de surface (SPR) pour détecter l'interaction de molécules non marquées, en temps réel (*Figures 1 & 2*). La technologie SPR ('surface plasmon resonance') est une technique à haut contenu informatif. Ces appareils permettent notamment la mesure précise des paramètres cinétiques d'association (k_{on}) et de dissociation (k_{off}), du K_D et d'avoir accès à la stochiométrie de la liaison. Les appareils Biacore ne sont pas dédiés au criblage de chimiothèques de millions de molécules. Par contre, ils sont très souvent utilisés dans les entreprises pharmaceutiques pour confirmer ou infirmer les 'hits' résultant d'un criblage en plaque ou de 'leads'

A l'IREBS, en collaboration avec trois équipes de recherche d'Illkirch et de Madrid et avec la société Prestwick Chemical, nous avons développé différentes stratégies de criblages de petites/moyennes chimiothèques par SPR : criblage direct pour lequel les molécules de la banque sont injectées successivement sur la cible immobilisée, permettant de générer directement des informations sur l'affinité de l'interaction et de sélectionner les meilleurs ligands (Löfas et al., 2011), et criblage par inhibition. L'appareil utilisé est le Biacore T100, automatisé, rapide, sensible, et dont les logiciels sont adaptés à l'évaluation de grandes quantités de données. L'objectif est de combiner les analyses d'activité de liaison, la modélisation moléculaire et l'approche SAR (Structure Activity Relationship), pour apprendre à développer efficacement des ligands spécifiques de diverses cibles. La technologie SPR permet de discriminer entre liaison spécifique et artéfacts lors de d'identification de nouveaux ligands. D'autre part, l'analyse en temps réel permet de mettre en évidence des interactions de faible affinité. Une cause fréquente des résultats faux-positifs, générés par des approches classiques,

est liée à la tendance des molécules synthétiques ou semi-synthétiques à s'agréger, en particulier aux fortes concentrations nécessaires pour détecter des liaisons de faible affinité. Des indicateurs quantitatifs permettent d'éliminer ces artéfacts en analyse SPR, si la conception expérimentale et l'exploitation des données sont correctes.

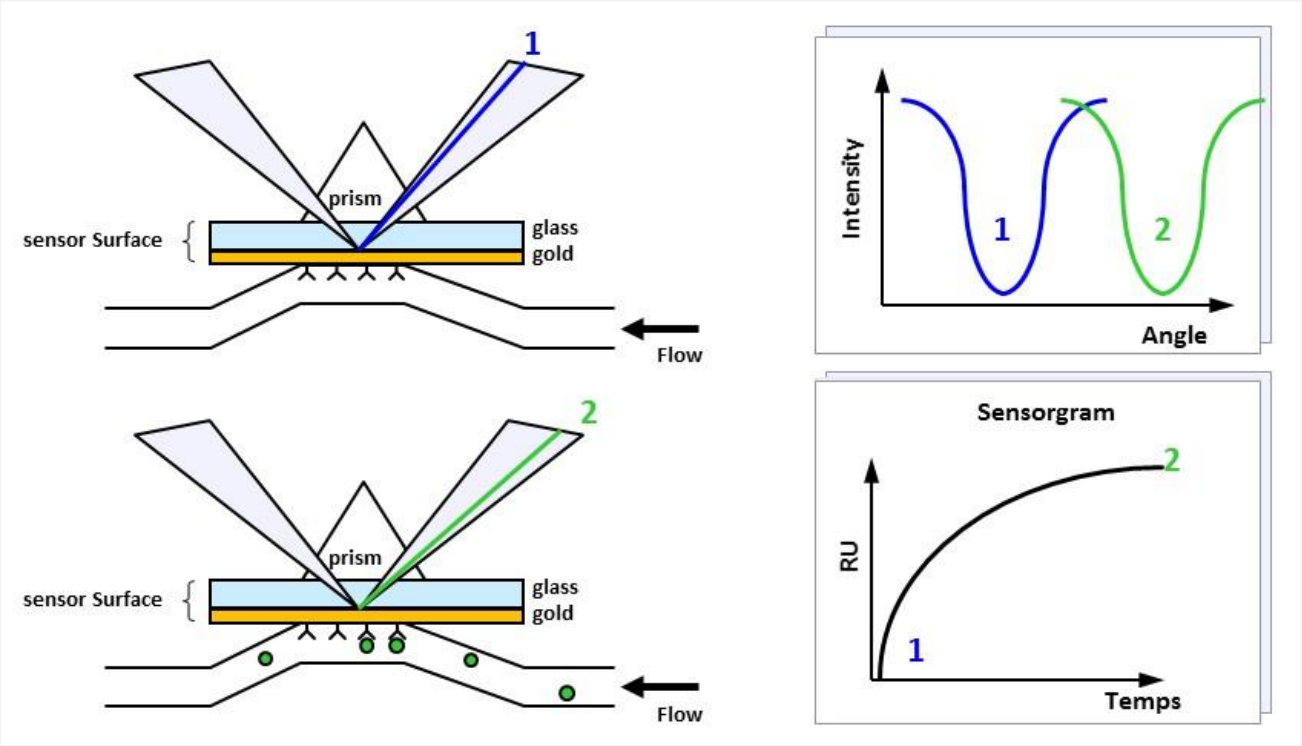

Figure 1. **Détection par résonance plasmonique de surface des interactions moléculaires**. Lorsqu'un faisceau de lumière polarisée monochromatique illumine une interface entre deux milieux d'indices de réfraction différents, une partie de la lumière incidente est réfléchie sur l'interface et l'autre partie est réfractée à travers l'interface. Selon l'angle d'incidence du faisceau, toute la lumière incidente peut être réfléchie. Le système de détection optique des appareils de la gamme Biacore est calibré pour que le faisceau lumineux rencontre l'interface biospécifique dans des conditions dites de réflexion interne totale. Le phénomène de SPR se produit lorsqu'une fine couche de métal, riche en électrons libres, est déposée à l'interface. Une couche d'or de 50 nm est utilisée pour recouvrir les surfaces *sensor* (bonne réponse SPR et inertie chimique). Les photons du faisceau incident entrent en résonance avec les plasmons du métal. Une conséquence énergétique de cette résonance est une chute d'intensité à un angle défini du faisceau réfléchi. Cet angle d'intensité minimum est l'angle de résonance. Il varie en fonction de l'indice de réfraction du milieu environnant le point d'impact du faisceau incident, indice qui lui-même est proportionnel aux changements de masse locale résultant de la fixation des molécules injectées sur la surface *sensor*. Le ligand (représenté par un anticorps noir) est immobilisé sur la surface *sensor* et l'analyte est injecté (représenté en vert) dans un flux continu à l'aide d'un circuit microfluidique. L'enregistrement de la variation de l'angle permet de suivre en temps réel l'association ou la dissociation des complexes. Le signal de résonance est quantifié en unités de résonance (RU). Une variation de 1000 RU correspond à une déviation de l'angle de résonance de 0,1° et à une fixation de 1 ng de protéine par mm^2 de surface. L'enregistrement du signal s'appelle un sensorgramme.

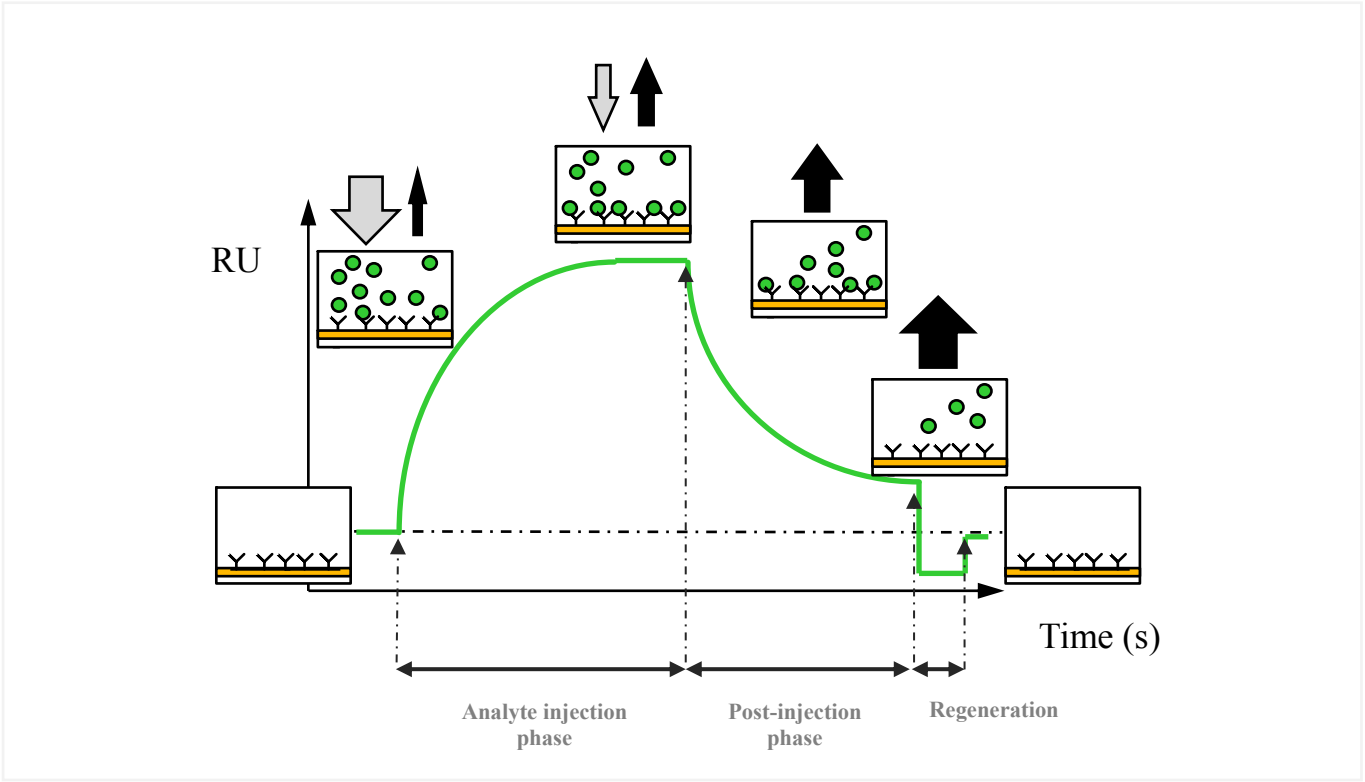

Figure 2. **Un sensorgramme : enregistrement de l'interaction ligand-analyte**. La ligne de base au début de l'expérience correspond à un débit de tampon sur une matrice déjà greffée avec le ligand. Lorsque l'analyte est injecté, la formation des complexes est suivie par l'augmentation de la réponse en RU. La dissociation est observée lorsque le tampon de réaction remplace l'analyte dans le circuit microfluidique. Puis, une solution de régénération peut être injectée pour décrocher l'analyte et idéalement revenir à la même ligne de base qu'au début du sensorgramme. C'est l'exploitation de la mesure en temps réel qui va permettre d'obtenir une cinétique de l'interaction donnant accès aux paramètres dynamiques d'association et de dissociation et d'en déduire l'affinité de l'interaction.

B1. Criblage direct sur adrénomédulline

Ce projet a été partiellement financé dans le cadre d'un Partenariat Hubert Curien franco-espagnol - PICASSO 2010-2011, intitulé 'Design, synthesis and 3D-QSAR study of small molecules targeting adrenomedullin in several diseases', en collaboration avec ma partenaire espagnole Sonsoles Martin Santamaria (University San Pablo-CEU, Madrid) et a donné lieu à une publication (Roldós et al., 2008).

L'AM est une hormone peptidique de 52 acides aminés dont la fonction biologique est reliée à plusieurs maladies, comme le diabète, l'hypertension, le cancer (Garcia et al., 2006). Des taux élevés d'AM sont corrélés à un effet protecteur dans des maladies rénales et cardiovasculaires, mais à un effet négatif pour la progression du diabete de type 2 et de plusieurs cancers (Zudaire et al., 2003). L'objectif du projet adrénomédulline (AM), était de découvrir de nouveaux

composés chimiques non-peptidiques, modulateurs négatifs de l'AM, à activité anti-angiogénique et anti-tumorale.

Dans une étude de criblage de la chimiothèque du National Cancer Institute (USA), par ELISA à haut débit, des modulateurs de l'AM, possédant une activité hypotensive et anti-tumorale, avaient déjà été identifiés (Martinez et al., 2004 ; Julián et al., 2005). Dans notre étude, l'un de ces composés (composé 1, un modulateur négatif de l'AM) a été utilisé comme point de départ au développement d'une série d'une vingtaine d'analogues. Une fois synthétisés (Organic Synthesis Laboratory, Université San Pablo-CEU, Madrid), ces composés ont été criblés séquentiellement sur l'AM immobilisée covalemment sur une surface *sensor* CM5 du Biacore T100. Différentes concentrations de chacun des composés chimiques ont été injectées. Les composés ont été solubilisés dans du DMSO. Le DMSO donne de grands indices de réfraction par SPR, toujours plus grands que le signal très faible obtenu avec les petits composés chimiques de faible affinité pour leur cible. Des courbes de calibration précises doivent être réalisées pour ne pas sur-interpréter les sensorgrammes obtenus. Bien que les réponses SPR soient faibles, les composés ont pu être classés en fonction de leur liaison : pas de liaison (*Figure 3a*) ou liaison (*Figure 3b & 3c*) à l'AM. Parmi ces derniers, cinq composés ont une meilleure affinité que le composé 1 d'origine. Des composés agrégés ont également été mis en évidence par SPR (*Figure 3d*). A la suite de ces résultats, une étude 3D-QSAR ('quantitative structure-activity relationship') a permis de mettre en évidence les groupements chimiques des composés importants pour leur liaison à l'AM (tels que la présence d'un groupement donneur de liaison hydrogène et d'un groupement aromatique).

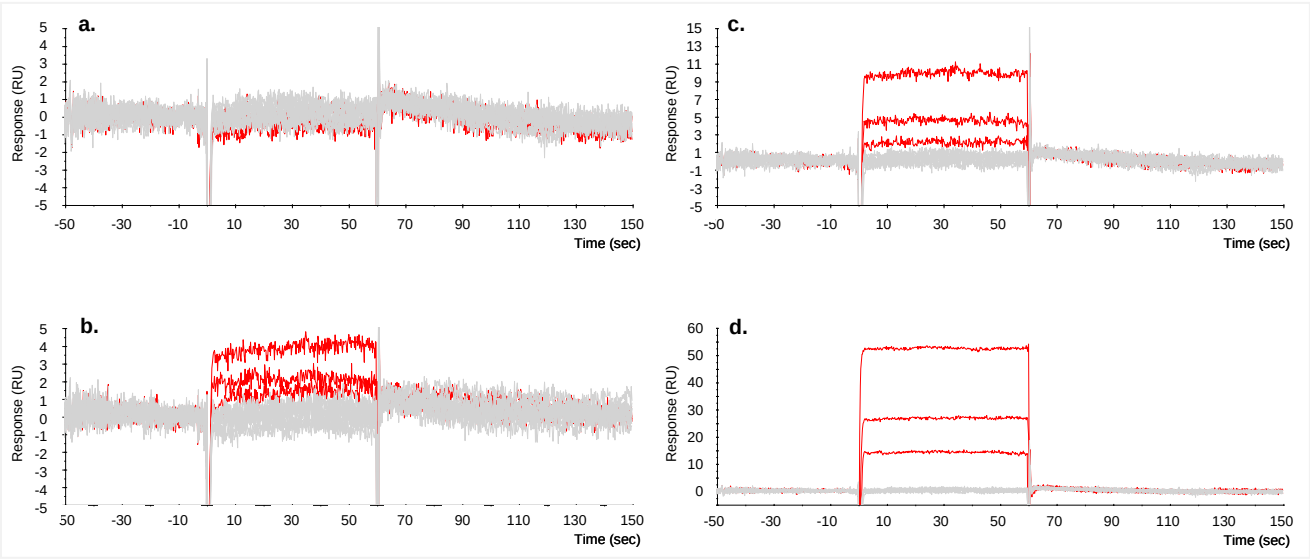

Figure 3. **Exemples de sensorgrammes** obtenus après soustraction d'une surface de référence et correction DMSO, correspondant à 60 secondes d'injection sur l'AM de 4 composés à différentes concentrations : 0 (gris), 50, 100 et 200 nM (rouge). **a.** Composé négatif. **b et c.** Composés positifs d'affinités différentes pour l'AM, le niveau de réponse étant plus faible pour b. que c. à poids moléculaire similaire. **d.** Composé agrégé, la réponse expérimentale excédant la réponse théorique attendue pour une liaison 1 :1.

B2. Criblage direct sur la tyrosine phosphatase-1b (PTP-1b)

Le projet précédent nous a permis de montrer qu'un criblage de petites molécules par SPR était envisageable, que des ligands peuvent être identifiés, même s'ils ont de faibles affinités pour leur cible. Nous avons ensuite réalisé un autre criblage direct, avec un plus grand nombre de composés, en collaboration avec Alberto Podjarni (UMR 7104, IGBMC, Illkirch), Marie-Louise Jung et Bruno Didier (Prestwick Chemical, Illkirch) sur une autre cible : la tyrosine phosphatase-1b (PTP-1b). Les PTP sont des molécules de signalisation qui régulent notamment la croissance cellulaire, la différentiation, le cycle mitotique. La PTP-1b est une protéine cytoplasmique impliquée dans la voie de régulation de l'insuline et de la leptine par déphosphorylation des résidus phosphotyrosines des récepteurs à l'insuline et à la leptine (*Figure 4*). Elle est également impliquée dans le développement de certains cancers (cancers du sein notamment). La protéine PTP-1b est une cible thérapeutique d'intérêt en oncologie, et pour le traitement du diabète de type 2 et de l'obésité (Delibegovic & Mody., 2009 ; Elchebly et al., 2000) .

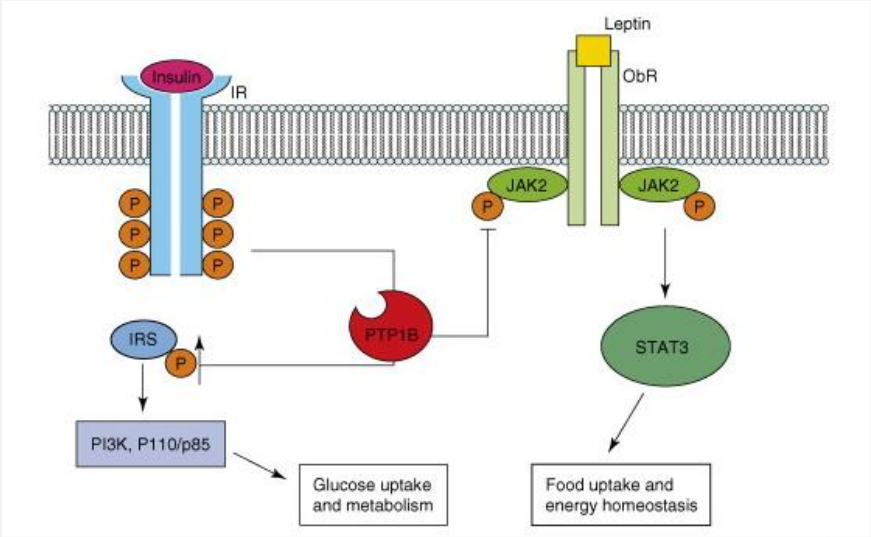

Figure 4. **Rôle de la PTP-1b dans les voies de signalisation de l'insuline et de la leptine.** Dans la voie de signalisation de l'insuline, la PTP-1b s'associe et déphosphoryle le récepteur à l'insuline (IR) ou le substrat du récepteur à l'insuline (IRS). Dans la voie de signalisation de la leptine, la PTP-1b déphosphoryle JAK2, protéine elle-même associée au récepteur de la leptine, ObR. (Zhang et Zhang, 2007).

Les objectifs de ce projet étaient (i) de voir s'il était possible de réaliser un criblage direct par SPR d'une banque de taille moyenne, (ii) d'établir des procédures optimisées générant des données quantitatives fiables en un nombre minimum d'expériences et (iii) de découvrir de nouveaux ligands de la PTP-1b.

La banque utilisée est celle de Prestwick Chemical (Illkirch, http://www.prestwickchemical.com/prestwick-chemical-library.html). Lorsque nous l'avons utilisé, elle contenait 1120 composés, de grandes diversités chimique et pharmacologique. Elle en comprend maintenant 1280. Cette chimiothèque est constituée à 95% de molécules approuvés par la FDA ('food and drug administration'), l'EMA ('european medecines agency') ou d'autres agences du médicament. Elle est généralement utilisée pour valider des tetst biologiques, pour identifier des faux-positifs, pour préciser la stratégie 'post-criblage' ou pour découvrir de nouvelles applications pour des principes actifs déjà connus. Les 1120 composés de la banque ont des PM ('poids moléculaires') variant de 102 à 1662 Da, la moyenne étant de 386 Da. La solubilité des composés et la taille de cette banque rendent cette étude adéquate à une analyse SPR. D'autre part, les inhibiteurs connus de la PTP-1b n'avaient qu'un succès relatif car trop chargés ou ayant un effet toxique. Les composés de la banque de Prestwick Chemical étant pour la plupart des médicaments, ont les propriétés désirées pour s'affranchir en partie de ce genre de problème.

Les composés de la banque de Prestwick Chemical ont été injectés successivement sur la PTP-1b immobilisée covalemment sur une surface *sensor* du Biacore T100, mais également sur une surface de référence ne contenant ni peptide ni protéine et sur deux molécules utilisées en tant que témoins négatifs pour évaluer la sélectivité de liaison : la protéine hAR ('human aldose reductase') et un peptide nommé C12V correspondant aux 11 acides aminés en C-terminal de la protéine E6 du virus du papillome humain de type 16. Nous avions préalablement simulé les conditions optimales du criblage permettant la détection de molécules d'affinité de 10-100 µM. Ainsi, les composés ont été injectés successivement à 0,5 puis à 10 µM. Plus de 90% des composés ne donnent aucun signal détectable. Parmi les 30 composés identifiés en tant que ligands, 22 se lient à au moins deux cibles de cette étude. Ils ne sont donc pas spécifiques de la PTP-1b. Huit composés se lient spécifiquement à la PTP-1b avec un K_D de l'ordre de 10^{-5} M, dont la sanguinarine, un inhibiteur connu de la PTP-1b, identifiée sans avoir de connaissance préalable de sa présence au sein de la chimiothèque de Prestwick. Six d'entre eux ont été confirmés en tant que ligands de la PTP-1b par des tests d'inhibition et des expériences SPR de dépendance en concentration. L'un d'entre eux, le fluspirilen a été utilisé pour proposer un modèle basé sur une relation structure-activité (SAR) à partir des analyses quantitatives obtenues avec tous les analogues structuraux du fluspirilen de la chimiothèque. Ce modèle de relation structure-activité (SAR) pourrait être utile au développement ultérieur de nouveaux inhibiteurs de la PTP-1b.

Cette étude a donné lieu à une publication (Zeder-Lutz et al., 2012) insérée à la fin de ce paragraphe (Article 2).

B3. Criblage par inhibition de l'interaction PDZ1 de MAGI1-$E6_{peptide}$

Les deux criblages décrits précédemment étaient des criblages directs de petits composés injectés successivement sur une cible immobilisée. Ce type de criblage permet de sélectionner des ligands sans connaître le site de liaison à leur cible. Pour identifier des ligands du site actif de la cible, une possibilité est de cribler séquentiellement une chimiothèque de petits composés, injectés en même temps que la cible, sur une surface immobilisée avec un inhibiteur connu du site actif.

En collaboration avec l'équipe de Gilles Travé (équipe Oncoprotéine, UMR 7242, Illkirch), l'objectif de ce projet était de trouver de petits composés chimiques inhibant l'interaction entre le domaine PDZ (abréviation des trois premières protéines identifiées contenant ce domaine :

PSD-95, Dlg, and ZO-1) de la protéine MAGI-1 (‘membrane-associated guanylate kinase (MAGUK) inverted protein 1’) et l’oncoprotéine E6. Les domaines PDZ sont des domaines d’interactions protéiques trouvés dans des protéines cytoplasmiques impliquées dans les voies de signalisation et dans le transport subcellulaire. Ils jouent un rôle dans la croissance, la polarité et l’adhésion cellulaire. Les protéines virales ciblent souvent les domaines PDZ, perturbant ainsi le cycle cellulaire au bénéfice du cycle viral. Les oncoprotéines des papillomavirus humains (HPVs) sont responsables des cancers du col de l’utérus et sont également impliquées dans un nombre croissant d'autres cancers épithéliaux (tête et cou, anus, peau...). L’oncoprotéine E6 reconnaît et provoque la dégradation cellulaire de plusieurs domaines PDZ impliqués dans le contrôle de la signalisation et des contacts intercellulaires. Cette perturbation d’un réseau d’interactions cellulaires médiée par les protéines ciblées apparaît comme un évènement clé de l’oncogenèse induite par HPV. Les PDZ reconnaissent des motifs spécifiques à l’extrémité C-terminale de leurs partenaires cellulaires (Kiyono et al., 1997). L’interaction entre l’extrémité C-terminale de E6 et le domaine PDZ1 de la protéine MAGI-1 est bien caractérisée du point de vue biochimique, fonctionnel et structural (Fournane et al., 2011 ; Charbonnier et al., 2011 ; *Figure 5*).

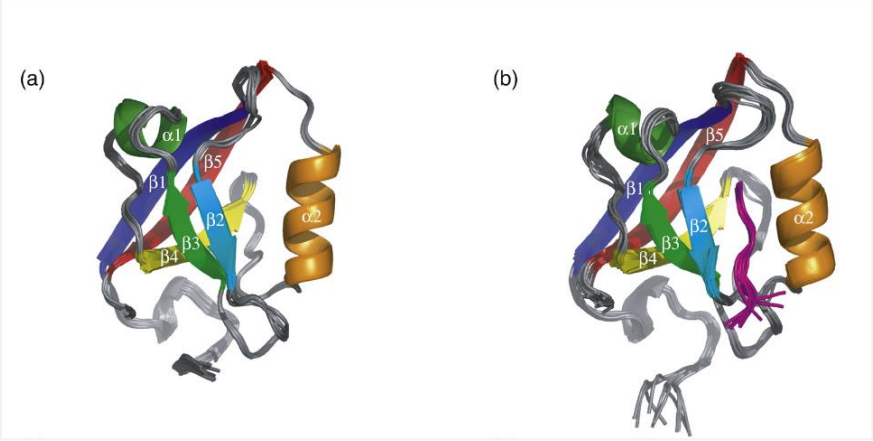

Figure 5. **Structure tridimentionnelle par RMN du domaine PDZ1 de MAGI-1 (a) seul et (b) en interaction avec E6$_{peptide}$.** Les éléments de la structure secondaire du domaine PDZ sont colorés (β1 en violet, β2 en bleu, β3 en vert clair, β4 en jaune, β5 en rouge et les hélices α1 et α2 en vert foncé et orange, respectivement). Le squelette du peptide lié est représenté en magenta. (Charbonnier et al., 2011)

J’ai entrepris un criblage par inhibition de l’interaction entre le domaine PDZ1 de MAGI-1 (nommé PDZ ci-dessous) et un peptide correspondant aux 11 résidus de l’extrémité C-terminale de E6, (nommé E6$_{peptide}$). La chimiothèque utilisée est celle de Prestwick Chemical, constituée de 1120 composés solubles dans le DMSO, décrite précédemment. Nous savions donc déjà qu’utilisés à 10 µM les composés de cette banque sont adaptés à un criblage par SPR :

pas ou peu d'aggrégation et seuls 22 composés interagissent aspécifiquement avec plusieurs cibles.

Après avoir simulé notre modèle et déterminé théoriquement les conditions optimales de notre criblage par inhibition, notre stratégie a consisté à immobiliser covalemment le peptide $E6_{peptide}$ sur une surface *sensor* du Biacore T100, et à injecter successivement les 1120 composés de la banque à 10 µM en présence de la protéine PDZ à 1 µM, sachant que le K_D de l'interaction PDZ-$E6_{peptide}$ est proche de 1 µM (0,78 µM). Si un composé se lie au domaine PDZ sur le site de liaison du peptide E6, la réponse PDZ-composé sera diminuée par rapport à la réponse de la PDZ seule. On mesure alors un pourcentage d'inhibition. Plusieurs contrôles ont été réalisés, tels que l'utilisation d'une surface de référence (sans peptide), l'utilisation de différentes concentrations de $E6_{peptide}$ immobilisé, l'injection régulière de PDZ seule sur $E6_{peptide}$ (indicateur de la reproductibilité des réponses dans le temps) et l'injection des composés chimiques en absence de PDZ pour déterminer des ligands directs de $E6_{peptide}$. Sur les 1120 composés de la chimiothèque, 1084 ne sont pas inhibiteurs. Ils n'ont aucun effet sur l'interaction PDZ-$E6_{peptide}$. Vingt composés inhibent l'interaction PDZ-$E6_{peptide}$ à plus de 5% et 16 composés ont un comportement variable en fonction de la quantité de $E6_{peptide}$ utilisée pour les tests d'inhibition. Les meilleurs inhibiteurs, confirmés par des expériences de dose-dépendance, ont une affinité pour le domaine PDZ de 10-50 µM.

Ces données furent difficiles à générer, mais surtout à interpréter compte tenu de la variabilité des réponses obtenues en fonction des quantités de peptides immobilisés et de la perte d'activité du domaine PDZ en fonction du temps. Les quantités de composés à injecter ne devaient pas être trop élevées pour éviter de boucher le circuit microfluidique du Biacore, mais pas non plus trop faibles pour espérer quantifier une inhibition. Pourtant, malgré ces contraintes et grâce aux simulations qui ont été d'une grande aide pour identifier les conditions expérimentales optimales, nous avons démontré pour la première fois qu'un criblage par inhibition d'une chimiothèque de taille moyenne est faisable par SPR et des pistes sont suggérées pour aider à la conception de criblages par inhibition d'une interaction d'affinité différente que celle de l'interaction PDZ-$E6_{peptide}$.

La publication résultant de ces données (Choulier et al., 2013) figure ci-dessous (Article 3).

Article 2

Zeder-Lutz, G., Choulier, L., Besse, M., Cousido-Siah, A., Figueras, FXR., Didier, B., Jung, ML., Podjarny, A. & Altschuh, D. (2012). Validation of SPR screening of a diverse chemical library for the discovery of protein tyrosine phosphatase 1b binders. *Anal. Biochem.* **421**, 417-427.

Analytical Biochemistry 421 (2012) 417–427

Contents lists available at SciVerse ScienceDirect

Analytical Biochemistry

journal homepage: www.elsevier.com/locate/yabio

Validation of surface plasmon resonance screening of a diverse chemical library for the discovery of protein tyrosine phosphatase 1b binders

Gabrielle Zeder-Lutz[a], Laurence Choulier[a], Marie Besse[a,1], Alexandra Cousido-Siah[b], Francesc Xavier Ruiz Figueras[b], Bruno Didier[c], Marie-Louise Jung[c], Alberto Podjarny[b], Danièle Altschuh[a,*]

[a] Biosensor Group, UMR 7242, CNRS–University of Strasbourg, 67412 Illkirch, France
[b] Structural Biology and Genomics Department, IGBMC, CNRS, INSERM, University of Strasbourg, 67404 Illkirch, France
[c] Prestwick Chemical, 67400 Illkirch, France

ARTICLE INFO

Article history:
Received 25 July 2011
Received in revised form 13 September 2011
Accepted 14 September 2011
Available online 29 September 2011

Keywords:
Surface plasmon resonance
Chemical library screening
New binders
Protein tyrosine phosphatase 1b

ABSTRACT

We investigated the suitability of surface plasmon resonance (SPR) for providing quantitative binding information from direct screening of a chemical library on protein tyrosine phosphatase 1b (PTP1B). The experimental design was established from simulations to detect binding with $K_D < 10^{-4}$ M. The 1120 compounds (cpds) were injected sequentially at concentrations [*C*(cpd)] of 0.5 or 10 μM over various target surfaces. An optimized evaluation procedure was applied. More than 90% of cpds showed no detectable signal in four screens. The 30 highest responders at *C*(cpd) = 10 μM, of which 25 were selected in at least one of three screens at *C*(cpd) = 0.5 μM, contained 22 promiscuous binders and 8 potential PTP1B-specific binders with $K_D \sim 10^{-5}$ M. Inhibition of PTP1B activity was assayed and confirmed for 6 of these, including sanguinarine, a known PTP1B inhibitor. *C*(cpd) dependence studies fully confirmed screening conclusions. The quantitative consistency of SPR data led us to propose a structure–activity relationship (SAR) model for developing selective PTP1B inhibitors based on the ranking of 10 aryl-butylpiperidine analogs.

High-information content biophysical methods that provide detailed information on binding should facilitate decision making during the drug development process [1,2]. Surface plasmon resonance (SPR)[2]-based biosensing is among the most informative technologies for this purpose, giving access to binding affinity, kinetics, and stoichiometry. Furthermore, SPR is particularly suited for detection of the low-affinity interactions expected in compound screening because complex formation is monitored while it happens. Therefore, a signal is observed even if total complex dissociation occurs when one of the interacting partners is removed. Two SPR screening strategies are applied. In SPR-based array imaging, the target is injected over a matrix of 400 to 10,000 fixed compounds [3] and the results are analyzed simultaneously. In channel-based SPR instruments, the compounds are injected sequentially over a surface carrying the target with a throughput of a few thousand molecules. Despite the small signals generated, the later assay design proved to be suitable to detect and quantify the weak-affinity binding (K_D up to mM range) of small molecules (down to ~100 Da) to immobilized targets [4–6] and is used largely for hit validation after primary high-throughput screening. However, published examples of its application to the screening of more than 500 chemical compounds, which can be fragments, remain scarce [7–10].

In this study, we have used a Biacore T100 instrument (GE Healthcare Biacore, Uppsala, Sweden) to screen the Prestwick Chemical Library® (Prestwick Chemical, Illkirch, France) on protein tyrosine phosphatase 1b (PTP1B). The objectives were to investigate the suitability of SPR for sequential screening of a chemical library, to establish optimized procedures that provide reliable quantitative data based on a minimal number of experiments, and possibly to discover new PTP1B binders. The Prestwick Chemical Library contains 1120 compounds (cpds) with molecular masses (MWs) ranging between 102 and 1665 Da (mean MW = 386 Da). The cpds are soluble in dimethyl sulfoxide (DMSO) at 5 mM, and approximately half of them are water soluble. The small size of the library, combined with the solubility of its cpds, makes it adequate for SPR screening. PTP1B is a monomeric protein with MW 34,630 Da. PTP1B has been identified as a major and

* Corresponding author.
E-mail address: daniele.altschuh@unistra.fr (D. Altschuh).
[1] Current address: UMR 6600, CNRS–UTC, 60200 Compiègne, France.
[2] *Abbreviations used:* SPR, surface plasmon resonance; PTP1B, protein tyrosine phosphatase 1b; cpd, compound; MW, molecular weight; DMSO, dimethyl sulfoxide; HPV, human papilloma virus; hAR, human aldose reductase; cDNA, complementary DNA; IPTG, isopropyl β-D-1-thiogalactopyranoside; EDTA, ethylenediaminetetraacetic acid; DTT, dithiothreitol; EDC, *N*-ethyl-*N*′-(3-dimethylaminopropyl)-carbodiimide hydrochloride; NHS, *N*-hydroxysuccinimide; PDEA, 2-(2-pyridimyldithioethaneamine); HBS, Hepes-buffered saline; RU, resonance units; *C*(cpd), compound concentration; FO, fractional occupancy; pNPP, *p*-nitrophenyl phosphate.

0003-2697/$ - see front matter © 2011 Elsevier Inc. All rights reserved.
doi:10.1016/j.ab.2011.09.015

relevant pharmaceutical target as it acts as a regulator of the signaling pathways associated with diabetes and obesity [11]. However, the intensive current work on PTP1B inhibitors has led to only a few promising results because proposed inhibitors are too charged and/or toxic due to action on the related phosphatases. The cpds from the Prestwick Chemical Library®, being essentially existing drugs, already have the desired properties to circumvent these problems. Therefore, the library represents a promising starting point for PTP1B inhibitor development and could provide initial structure–activity relationship (SAR) information if binders can be reliably identified and ranked.

The implementation of screening and data analysis procedures that would provide quantitative information, in particular in case of low-affinity binding, is not straightforward [12]. The high target densities and cpd concentrations [C(cpd)], which are required to detect low-affinity binding and also the DMSO typically used to solubilize compounds, may generate significant noise. High-affinity binders are identified from the slow complex dissociation, which is readily visualized in real-time binding curves [8]. In the case of weak binding ($K_D > 10^{-6}$ M), careful reference and DMSO correction procedures must be applied to extract the SPR signal due to complex formation [13]. This signal recorded before the end of cpd injection, which should reflect the equilibrium response, lies in a narrow range between noise and a fraction of surface saturation. Therefore, it is important to assess its quantitative value in direct screening, from comparing experimental signals with those expected from simulations and from comparing the responses in different experimental conditions. We show that signal ranking is sufficiently reliable to distinguish among the strongest responders, weaker responders, and nonresponders. Therefore, a SAR model was proposed based on the ranking of nine analogs of one of the selected PTP1B binders.

Materials and methods

Peptides and chemical library

Peptide C12V (sequence: CRSSRTRRETQV, MW = 1478 Da, pI = 11.5) corresponding to the last 11 C-terminal residues of human papilloma virus 16 (HPV16) E6 and bearing an additional N-terminal cysteine for immobilization, was synthesized by P. Eberling (Chemical Peptide Synthesis Service, IGBMC, Illkirch, France), as described previously [14]. The chemical library was obtained from Prestwick Chemical (Illkirch, France).

hAR production

The open reading frame (ORF) of the human aldose reductase (hAR) gene (accession GenBank/embl Data Bank No. J05017) was amplified by polymerase chain reaction (PCR) from its complementary DNA (cDNA) and cloned into the T7 RNA polymerase-based vector pET15b (Novagen). Expression of the His6–hAR in the *Escherichia coli* strain BL21(DE3) (Novagen) is induced by isopropyl β-D-1-thiogalactopyranoside (IPTG, Euromedex) during a 3-h culture at 37 °C. The pellet from a 4-L culture was disrupted by sonication and centrifuged. The supernatant was applied on a Talon metal affinity column (Clontech). After thrombin cleavage of the hexahistidine extension, the detagged protein was loaded on a DEAE Sephadex A-50 column (Pharmacia) and eluted with an NaCl gradient.

PTP1B production

Bacteria containing the cDNA for the PTP1B in pET23b plasmid (Novagen) were grown in *E. coli* BL21(DE3). An overnight culture of the transformed BL21(DE3) cells was diluted 2:100 into 1 L of Luria–Bertani (LB) medium containing 100 μg/ml ampicillin. The culture was grown at 37 °C until the absorbance at 600 nm reached 0.6, at which point the cells were induced with 1 mM IPTG for 3 h. The cells were harvested by centrifugation at 4 °C for 20 min at 4000*g*. The cell pellet was resuspended in 70 ml of 100 mM 2-(4-morpholino)-ethane sulfonic acid (pH 6.5) (buffer A), sonicated for 20 min, and centrifuged for 1 h at 40,000 rpm. The supernatant was then loaded onto a CM-Sephadex column (30-ml bed volume, Pharmacia) and washed with 10 bed volumes of buffer A. PTP1B was eluted from the column by a linear gradient from 0 to 0.5 M NaCl. Approximately 25 mg of PTP1B (95% pure as estimated by sodium dodecyl sulfate–polyacrylamide gel electrophoresis [SDS–PAGE]) was recovered from a 3-L culture.

SPR instrument and buffers

All experiments were performed on a Biacore T100 instrument at 20 °C. The sCM5 sensor surfaces (BR-1006-68) and Biacore consumables were obtained from GE Healthcare. DMSO was purchased from Sigma–Aldrich (cat. no. 472301). The composition of running buffers was as follows:

HBS-EP: 10 mM Hepes (pH 7.4), 150 mM NaCl, 3.4 mM ethylenediaminetetraacetic acid (EDTA), and 0.05% (v/v) surfactant P20;
HBS-A: 10 mM Hepes (pH 7.4), 150 mM NaCl, 3.4 mM EDTA, 2 mM dithiothreitol (DTT), and 0.005% (v/v) Tween 20;
HBS-B: 10 mM Hepes (pH 7.4), 150 mM NaCl, 3.4 mM EDTA, 1 mM DTT, 0.005% Triton, and 5% DMSO;
HBS-C: 10 mM Hepes (pH 7.4), 150 mM NaCl, 0.05% Triton, and 2% DMSO.

Sensor surface preparation

PTP1B and hAR were immobilized using the standard amine coupling protocol (Amine Coupling Kit, BR-1000-50, GE Healthcare) and HBS-A as running buffer. The proteins (PTP1B [200 μg/ml] diluted in 10 mM acetate, pH 5.6, with 1 mM DTT; hAR [100 μg/ml] diluted in 10 mM acetate, pH 5.0) were injected during 7 min on surfaces that had been activated (7 min) with a 1:1 mix of 0.2 M *N*-ethyl-*N'*-(3-dimethylaminopropyl)-carbodiimide hydrochloride (EDC) and 0.05 M *N*-hydroxysuccinimide (NHS). Remaining reactive groups on the matrix were blocked by treatment with 1 M ethanolamine–HCl at pH 8.5. Peptide C12V was immobilized using the thiol activation chemistry (Thiol Coupling Kit, BR1000-58, GE Healthcare) and HBS-EP as running buffer at a flow rate of 10 μl/min. Surfaces were activated by successive injections of a 1:1 EDC/NHS mixture (10 min), 2-(2-pyridimyldithioethaneamine) (PDEA) at 80 mM in 0.1 M Na borate (pH 8.5) (4 min), and 1 M ethanolamine–HCl (pH 8.5) (4 min). The peptide was injected at concentrations varying between 5 and 200 μg/ml in HBS-EP or Na acetate at 10 mM (pH 3.2). Inactivation of free PDEA groups was achieved by injecting 0.1 M L-cysteine and 1 M NaCl in 0.1 M Na formate (pH 4.3) (10 min). Empty control surfaces were obtained by treating them as for target immobilization except that target injection was omitted.

Screening experiments

All assays were run at 25 °C at a flow rate of 40 μl/min. An initial series of buffer injections was carried out on empty (reference) and target surfaces to equilibrate the system. For screening on PTP1B and hAR surfaces, the running buffer was HBS-B. Each cycle consisted of a 60-s injection of cpd at a concentration of 0.5 or 10 μM, followed by a 140-s postinjection phase, a carryover control (running buffer, 30 s), and a wash of the flow system with a 1:1

mixture of DMSO and water. For screening on peptide surfaces, the running buffer was HBS-C. Each cycle consisted of a 60-s injection of cpd at a concentration of 10 μM, followed by a 120-s postinjection phase, one or two 30-s washing steps with 5 mM NaOH, and a wash of the flow system with a 1:1 mixture of DMSO and water. All screening experiments comprised two eight-point DMSO injections, run just before and just after the set of 80 cpd and control injection cycles performed for each plate, to produce a DMSO calibration curve in order to correct for differences in solvent effects on empty and target surfaces [13]. They consisted of 30-s injections of eight solutions containing either 4.5% to 5.8% DMSO (proteins) or 1.0% to 2.8% DMSO (peptide).

Data processing

Data were XY-zeroed, referenced, and calibrated using Biacore T100 evaluation software (version 2.0.2, GE Healthcare Biacore). Signals on control surfaces were subtracted from those recorded on target surfaces, and the DMSO correction was applied. SPR responses (R, expressed in resonance units [RU]) used for data analysis correspond to the corrected response recorded 5 s before the end of buffer or cpd injections. The SPR signal depends on factors that determine the amount of complex formed (target density, C(cpd), and binding affinity) and on the molecular mass of the bound cpd (MW_{cpd}). To facilitate data comparison, responses were normalized relative to target density and MW_{cpd} as fractional occupancy of target sites (FO):

$$FO = R/R_{max},$$

where R is the response generated by cpd injection and R_{max} (maximal binding capacity) is the theoretical response expected when each target molecule has bound 1 cpd molecule:

$$R_{max} = R_{target} \times MW_{cpd}/MW_{target},$$

where R_{target} is the target immobilization level and MW_{target} and MW_{cpd} are the molecular masses of target and cpd, respectively.

Dose dependence experiments

A subset of cpds was assayed on PTP1B surfaces in a four- or five-sample concentration series using a 2- or 4-fold dilution starting at 40 or 20 μM. Experiments were set up and processed as for screening experiments. Binding curves were prepared by applying DMSO correction and double referencing (subtraction of signals produced by the sample on the reference surface and by buffer on the target surface) [15].

Enzymatic assay and IC_{50} determination

The capacity of the compounds to inhibit PTP1B activity was assayed in 100 mM Hepes and 5 mM EDTA (pH 6.8) at 37 °C in a final p-nitrophenyl phosphate (pNPP) concentration of 2 mM. EDTA was excluded for vanadate determination. The enzyme was diluted to a concentration of 8 μg/ml with enzyme dilution buffer (10 mM Tris–HCl, 25 mM NaCl, and 5 mM DTT, pH 7.5). A typical 50-μl reaction system contained 5 μl of pNPP, 4 μl of enzyme, 5 μl of inhibitor dissolved in DMSO, and 36 μl of H_2O. After the mixture, without pNPP, had been incubated at 37 °C for 10 min, the enzyme reaction was initiated by the addition of pNPP. After 5 min at 37 °C, the reaction was quenched by the addition of 0.5 M NaOH (0.95 ml) with the absorbance at 405 nm measured to quantify the p-nitrophenol produced. The IC_{50} values of the inhibitors were determined by measuring the pNPP hydrolase activity of PTP1B in a range of different inhibitor concentrations. The kinetic data were analyzed using the GraFit 5.0 program (Erithacus Software), and each value is given as mean of three experiments ± standard deviation.

Results

Simulation of response levels

Simulations were performed to help with the design of screening experiments. SPR equilibrium responses (R) expected for K_D in the 10^{-7} to 10^{-3} M range for C(cpd) of 0.5 (dotted lines) and 10 μM (black lines) and surface binding capacities (R_{max}) of 75, 150, and 300 RU are shown in Fig. 1A. An average cpd molecular mass (MW_{cpd}) of 350 Da was used. The corresponding normalized responses ($FO = R/R_{max}$) are shown in Fig. 1B for C(cpd) = 0.5 and 10 μM. In contrast to the SPR response (R), normalized responses (FO) are independent of MW_{cpd} and target density.

The experimental noise in direct screening is likely to be significant when injecting samples with high C(cpd) on high-density protein surfaces. The gray circles in Fig. 1A indicate a response of 10 RU, which should be readily measurable. They are reported in Fig. 1B to indicate the corresponding FO and K_D values and visualize how the detection sensitivity varies with C(cpd) and target density.

Experimental screening conditions

Fig. 1B shows that screening at C(cpd) = 0.5 and 10 μM should allow the detection of cpds binding with K_D at approximately 10^{-5} and

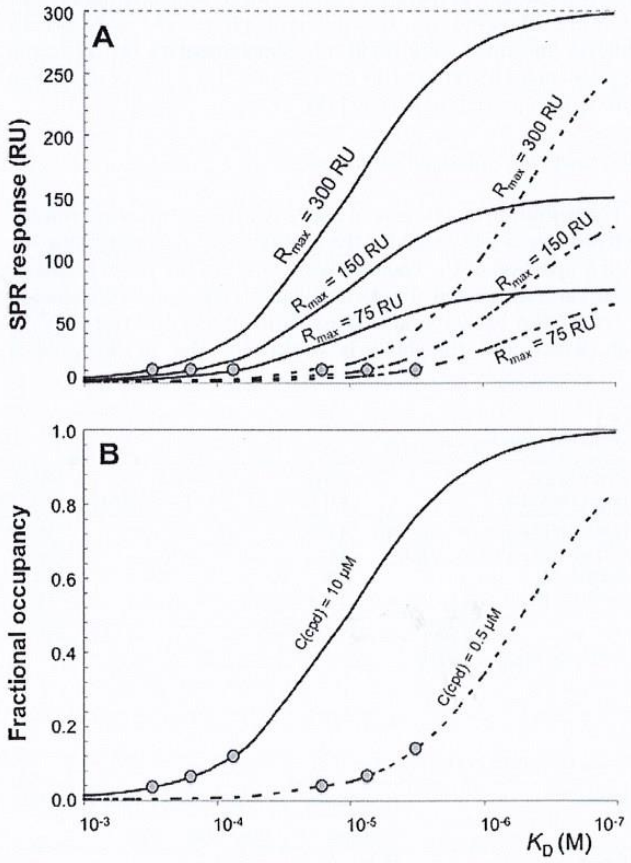

Fig. 1. Detection sensitivity as a function of screening conditions. Equilibrium responses were simulated for K_D in the 10^{-3} to 10^{-7} M range (with $k_{on} = 10^5\ M^{-1}\ s^{-1}$ and k_{off} varied between 100 and 0.01 s^{-1}). Compound concentrations were 0.5 μM (dotted lines) and 10 μM (black lines). Surface binding capacities (R_{max}) were 75, 150, and 300 RU. Equilibrium responses are expressed as SPR responses (RU) assuming MW_{cpd} = 350 Da (A) and as fractional occupancy of ligand sites ($FO = R/R_{max}$) (B). The gray circles indicate a threshold of 10 RU (A) and corresponding detection sensitivity (B).

10^{-4} M, respectively, if the target density is sufficient (R_{max} > 75 and 150 RU, respectively). Lower C(cpd) would not be appropriate because of the small SPR responses expected and because of possible mass transport limitations on high-density surfaces. Experimental screening conditions applied in this study are summarized in Table 1. Screening was performed at C(cpd) = 0.5 μM at different PTP1B densities (screens A-Fc2, A-Fc4, B-Fc2, and B-Fc4) with theoretical R_{max} values ranging from 78 to 332 RU (assuming MW_{cpd} = 350 Da). The aim of these screens was to evaluate the influence of target density on detection sensitivity. The library was also screened at C(cpd) = 10 μM on three targets: PTP1B (screen C-Fc2), hAR (screen C-Fc4), and a peptide corresponding to the 11 C-terminal residues of E6 of the human papilloma virus 16 (Pept: screen D-Fc3). The aim of these screens was to identify low-affinity binders and evaluate binding selectivity.

Controls

In the initial screen performed at C(cpd) = 0.5 μM (A-Fc2), sanguinarine was identified as a PTP1B binder and then found to be a published PTP1B inhibitor [16]. Therefore, it was used as a positive control in screens B and C to evaluate possible changes in surface capacity with injection cycles. Buffer was used as a negative control. These controls consisted of 12 evenly distributed recurring injections of sanguinarine (1 or 10 μM) and buffer for each plate. With a few exceptions that could be attributed to problems with sample preparation, similar mean sanguinarine FO values were observed for the different plates and Stds on 12 replicate injections were small (see Supplementary Fig. S1 in the supplementary material). This indicates good stability of the PTP1B surface, as reported previously [17].

Background and threshold calculations

The definition of a threshold above which responses are considered positive is a key step for the evaluation of screening data. If a large proportion of the cpds show no binding, the mean response (Mean) and associated standard deviation (Std) can be considered to reflect the background and experimental noise, respectively, from which the threshold is evaluated. The presence of a significant proportion of outliers or imperfect data normalization across independent experiments may significantly affect Mean and Std, in which case a more elaborate threshold definition is required. Responses were corrected for the background (FO_{cor} = FO − Mean) and the threshold was set to 3Std, with Mean and Std calculated in three ways:

(i) Over FO of all cpds after excluding those with FO > 1 [in this case, the same background ($Mean_{all}$) and threshold ($3Std_{all}$) is used for evaluating all data (from all 14 plates)].
(ii) Over FO of the 80 cpds of each plate (after excluding those with FO > 1) [in this case, the background ($Mean_{plate}$) and threshold ($3Std_{plate}$) differ for each plate].
(iii) Over FO of each plate after excluding the five highest and five lowest FO values [here also, the background ($Mean_{6-75}$) and threshold ($3Std_{6-75}$) differ for each plate].

Mean and Std values (multiplied by 100 to facilitate reading) are listed in Supplementary Table 1. The mean is reasonably close to 0 in screens A, B [low C(cpd)], and D (low mass of fixed Pept) but varies in the −9 to 25 range in screen C-Fc2 (PTP1B) and in the −5 to 99 range in screen C-Fc4 (hAR), most likely because of imperfect DMSO corrections at high target density and C(cpd). Std_{all} is higher than Std_{plate} or Std_{6-75} because the mean signal varies from plate to plate (plates were analyzed in independent experiments). Std_{6-75} is significantly lower than Std_{plate} for some of the plates and screens (see plates 2 and 5 in all screens or plates 6–10 in screen C-Fc2). Thus, the background and noise vary significantly for different experiments and calculation methods, with resulting variations in threshold and cpd selection.

Defining the selection procedure

The ranking of sanguinarine was used as a criterion to define an optimized cpd selection procedure. Its ranking, together with number of cpds with $FO_{cor} \geqslant$ threshold, are reported in Table 2 for Mean and Std calculated in the three ways described above. The lowest PTP1B density and C(cpd) assayed (screen A-Fc4: R_{max} = 78 RU, C(cpd) = 0.5 μM) did not allow sanguinarine selection. In other screens, procedures 2 and 3 performed better for its selection than

Table 1
Experimental screening conditions.

Screen name	A-Fc2	A-Fc4	B-Fc2	B-Fc4	C-Fc2		C-Fc4		D-Fc3	
Target (MW, Da)	PTP1B (35,310)	PTP1B (35,310)	PTP1B (35,310)	PTP1B (35,310)	PTP1B[a] (35,310)		hAR[a] (36,140)		Peptide[a] (1478)	
Target immobilization level (RU)	18,853	7862	30,253	33,524	9375	18,870	3181	8545	705	695
Average theoretical R_{max} (RU)[b]	187	78	300	332	93	187	31	83	167	165
C(cpd) (μM)	0.5	0.5	0.5	0.5	10	10	10	10	10	10
Prestwick plates	1–14	1–14	1–14	1–14	1–8	9–14	1–8	9–14	1–7D	7H–14

[a] Two sensor surfaces with different target immobilization levels were used.
[b] Assuming MW_{cpd} = 350 Da.

Table 2
Sanguinarine ranking in PTP1B screens.

Screen	Sanguinarine ranking/No. of responses above threshold		
	Procedure 1 ($Mean_{all}$, Std_{all})	Procedure 2 ($Mean_{plate}$, Std_{plate})	Procedure 3 ($Mean_{6-75}$, Std_{6-75})
A-Fc2[a]	10/11	7/25	9/58
A-Fc4[b]	26/15	265/19	72/49
B-Fc2	47/14	13/23	14/51
B-Fc4	19/10	14/18	16/48
C-Fc2[c]	49/23	28/28	25/71

[a] Data for 3 cpds missing because of responses lying outside the DMSO calibration curve.
[b] Data for 4 cpds missing because of responses lying outside the DMSO calibration curve.
[c] Data for 3 cpds missing because of responses lying outside the DMSO calibration curve and plate 8 excluded because of high Std.

procedure 1, as judged from its lower ranking. Procedure 3 selected more cpds than procedure 2 because Std_{6-75} is lower than Std_{plate}. Procedure 3 may favor the selection of false positives, whereas weak binders may be overlooked using procedure 2. As a compromise, procedure 3 was applied for further evaluations, but considering only the 30 highest responders; cpds are selected if the two conditions ($FO_{cor} \geqslant$ threshold and rank $\leqslant 30$) are satisfied, with $FO_{cor} = FO - Mean_{6-75}$ and threshold $= 3Std_{6-75}$.

Identification of specific PTP1B binders

All data were evaluated except those from screen A-Fc4 because of responses within noise (as judged from sanguinarine response [Table 2]) and from plate 8 in screen C because of high Std (Supplementary Table 1). FO_{cor} patterns observed at $C(cpd) = 0.5$ μM (screen A-Fc2) and 10 μM (screen C-Fc2) are illustrated in Supplementary Fig. S2. They are similar, but most of the "obvious" signals are overstoichiometric and also appeared on control surfaces (not shown). Signals above threshold (of which the 30 highest identified selected cpds) are best visualized as positive values in (FO_{cor} – threshold) plots (Fig. 2). Cpds that were selected in at least one of the PTP1B screens were divided into four groups, of which three are listed in Table 3, with cells highlighted in black if responses are overstoichiometric and in gray otherwise. The first group contains 13 cpds selected in all PTP1B screens and should represent the strongest binders. The second group contains 12 cpds selected in PTP1B screen C-Fc2 [$C(cpd) = 10$ μM] and in at least one of screens A-Fc2, B-Fc2, or B-Fc4 [$C(cpd) = 0.5$ μM], which suggests weaker binding. The third group contains 5 cpds selected in screen C-Fc2 only. The fourth group contains 25 cpds selected at $C(cpd) = 0.5$ μM only (screens A and/or B only; see Supplementary data). Cpds from groups 3 and 4 are likely to be false positives or very weak binders. Among the 30 highest responders in screen C-Fc2 (Table 3, groups 1–3), 22 also reacted with hAR and/or Pept and were considered as promiscuous binders. These include all 12 cpds with overstoichiometric responses. Therefore, 8 potential PTP1B-specific binders were identified: fluspirilen, sanguinarine, and kaempferol in group 1; diethylstilbestrol, merbromin, and dienestrol in group 2; and chlorpromazine hydrochloride and thioridazine hydrochloride in group 3.

Concentration dependence of binding

$C(cpd)$ dependence studies were performed for a subset of the cpds and were consistent with the classifications proposed from screening data. The six cpds from groups 1 and 2 (Fig. 3, two first rows), assumed to be the most promising candidates, were confirmed as PTP1B binders in at least one of the duplicate assays. Two cpds from group 3 and one cpd from group 4 (Fig. 3, last row), assumed to be weak binders or false positives, showed weak or unclear dose dependencies. Except for sanguinarine, all binders showed complex kinetics such as absence of surface saturation or multiphasic postinjection phase, as observed by others [18,19], suggesting molecular heterogeneity or a tendency of cpds to aggregate at high concentrations. Nevertheless, the $C(cpd)$ dependence studies confirmed the interactions or absence of interactions concluded from screening.

Relationship between physicochemical properties of cpds and PTP1B binding

Several selected molecules belong to distinct chemical families (arylbutylpiperidines, flavones, and stilbenes). A substructure search in the Prestwick Chemical Library® allowed us to select other compounds with similar scaffolds in order to propose a SAR model based on their binding activities.

We considered the family of fluspirilen because compounds in this family are structurally homogeneous (Table 4). They are composed of two subgroups: the diarylbutylpiperidines (**1**, **3**, and **9**) and the monoarylbutylpiperidines (**2**, **4**–**8**, **10**, and **11**). Table 4 reports responses above background (fourth column) and above threshold (last column) recorded in the four screens for these cpds,

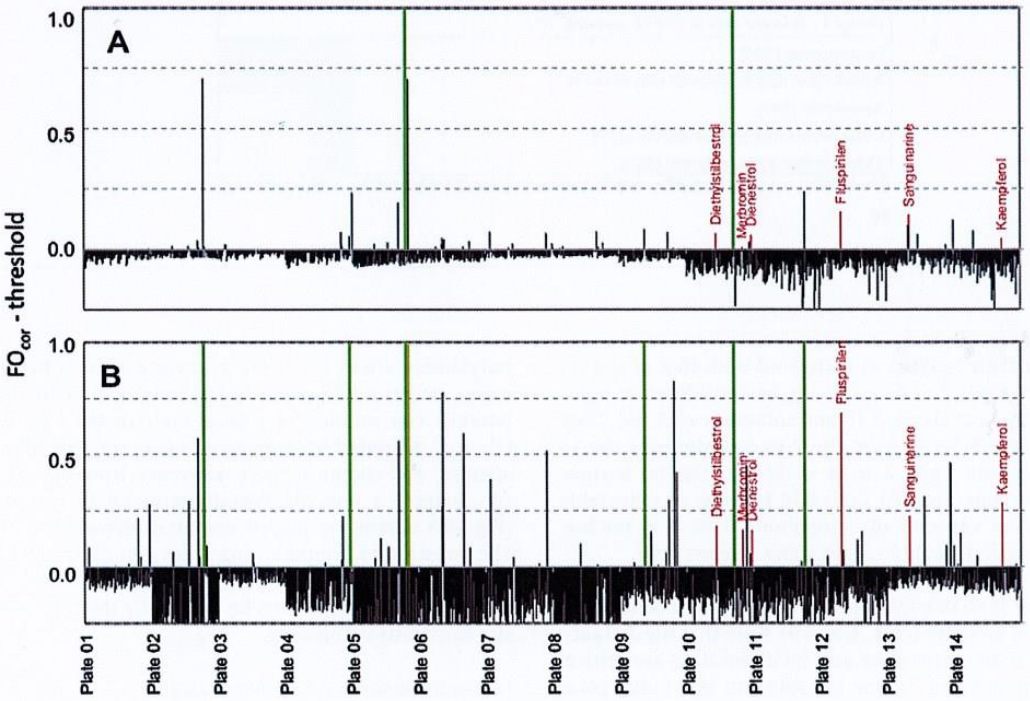

Fig.2. Responses above threshold (FO_{cor} – threshold > 0) for the 1120 cpds in screens A-Fc2 (A) and C-Fc2 (B). Overstoichiometric responses are shown in green, and those of six potentially PTP1b-selective cpds are shown in red. (For interpretation of the references to color in this figure legend, the reader is referred to the web version of this article.)

Table 3
Selected PTP1B binders.

Selected PTP1B binders

Screen	A-Fc2	B-Fc2	B-Fc4	C-Fc2	C-Fc4	D-Fc3
Target	PTP1B				hAR	Pept
Cpd chemical Name (MW)	C (cpd) (μM)					
	0.5	0.5	0.5	10	10	10
Group 1: Selected in all PTP1B screens (A-Fc2, B-Fc2, B-Fc4 and C-Fc2)						
Mitoxantrone dihydrochloride (517)						
Dequalinium dichloride (528)						
Chlorhexidine (505)						
Alexidine dihydrochloride (582)						
Quinacrine dihydrochloride dihydrate (509)						
Raloxifene hydrochloride (510)						
Astemizole (459)						
Tetrandrine (623)						
Clofazimine (473)						
Pentamidine isethionate (593)						
Fluspirilen (476)						
Sanguinarine (332)						
Kaempferol (286)						
Group 2: Selected in PTP1B screen C-Fc2 and at least one of screens A, B						
Cholecalciferol (385)						
Lysergol (254)						
Colistin sulfate (1352)						
Propidium iodide (668)						
Alcuronium chloride (738)						
Methyl benzethonium chloride (462)						
Hexestrol (270)						
Benzethonium chloride (448)						
Roxatidine Acetate HCl (385)						
Diethylstilbestrol (268)						
Merbromin (805)						
Dienestrol (266)						
Group 3 : Selected only in PTP1B screen C-Fc2						
Perphenazine (404)						
Amodiaquin dihydrochloride dihydrate (465)						
Apramycin (540)						
Chlorpromazine hydrochloride (355)						
Thioridazine hydrochloride (407)						

Black: $FO_{cor} > 1$; grey: $1 \geq FO_{cor} \geq$ threshold and rank ≤ 30; white: $FO_{cor} <$ threshold or rank > 30.

and Fig. 4A shows their ranking as compared with that of the six highest responders. Cpds **2** to **4** can clearly be considered as binders based on responses at C(cpd) = 10 and sometimes 0.5 μM. They are not listed in Table 3 because we chose to consider only the 30 highest responders, but cpds **2** to **4** ranked in the 80 highest responders in all screens (Fig. 4A). Cpds **9** to **11** show no detectable binding. The binding capacity of compounds **5** to **8** is unclear because they responded weakly and in some screens only.

Molecule **9** shows conclusively that the piperidine ring should be substituted by at least one hydrophobic group and accompanied by a hydrogen bond acceptor (cf. **1**, **3**, and **9**). Note that the distance between this group and piperidine and its orientation are critical (cf. **1** and **3** and then **4** and **7**). The introduction of a bulky polar group is highly unfavorable despite the common group attached to the piperidine ring (cf. **2** and **11**, replacing a methyl by a carboxylic acid). We cannot conclude about the requirement of a flexible butylamine chain for binding; levocabastine (**10**) introduces too many structural changes to be compared with the other compounds. The number of similar cpds in the Prestwick Chemical Library® is limited because its aim is to propose diversity in "therapeutic" and chemical space. However, from our observations, we can suggest a possible two-dimensional pharmacophore model (Fig. 4B) where we placed essential elements in the molecules. The substituted aromatic ring shown in the model could bind to the entry of the active site, notably to Tyr46, like the substrate. The inhibition would then be caused by the blocking of the active site for substrate binding.

Enzymatic assay and IC_{50} determination

Four of the six PTP1B-specific binders identified by SPR, together with two binders and one nonbinder among arylbutylpi-

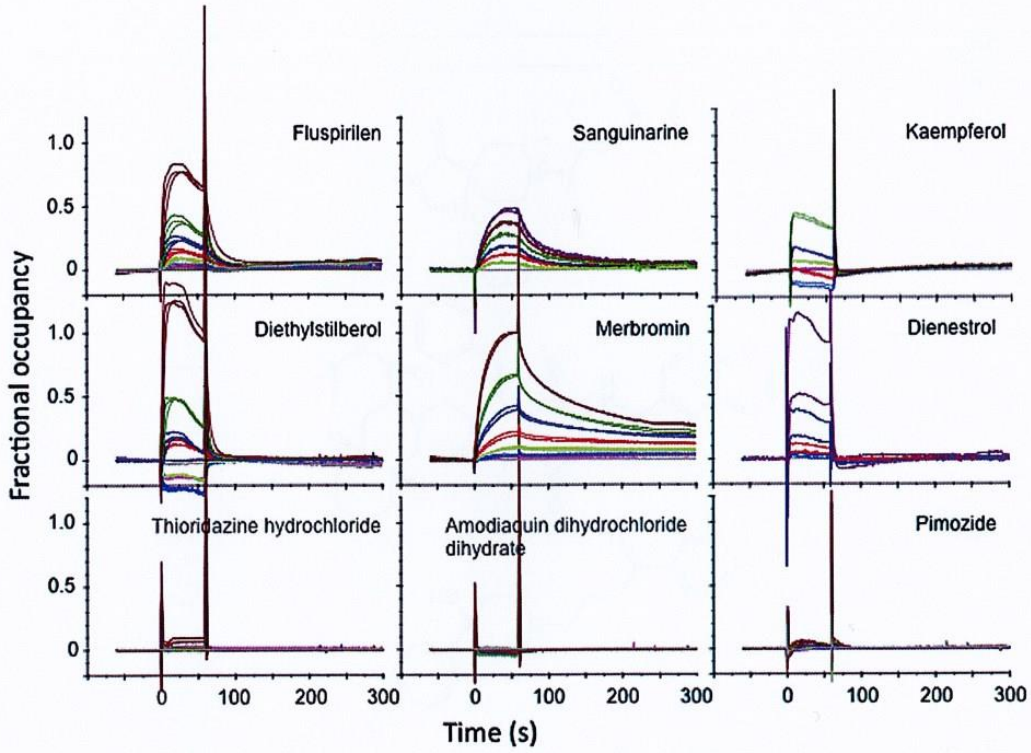

Fig.3. *C*(cpd) dependence of signals in the 0.6 to 40 μM range for fluspirilen, sanguinarine, kaempferol, diethylstilberol, merbromin, dienestrol, thioridazine hydrochloride, amodiaquin dihydrochloride dihydrate, and pimozide. Duplicate or triplicate sensorgrams are shown.

Table 4
Structure and responses of arylbutylpiperidines.

Number	Name	Structure	$FO_{cor} > 0$	$FO_{cor} \geqslant$ threshold
1	Fluspirilen	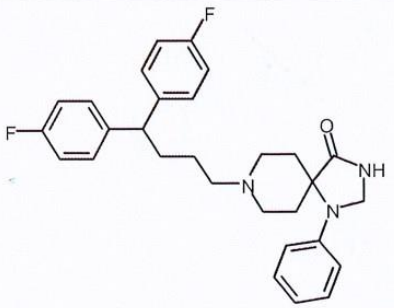	++ ++ ++ ++	++ ++ ++ ++
2	Terfenadine	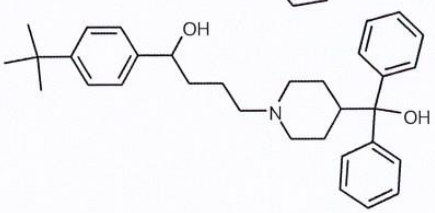	+ ++ ++ ++	+ + – ++
3	Pimozide	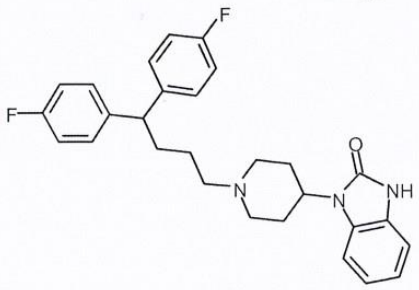	++ + + ++	++ + + +

(*continued on next page*)

Table 4 (*continued*)

Number	Name	Structure	$FO_{cor} > 0$	$FO_{cor} \geqslant$ threshold
4	Spiperone	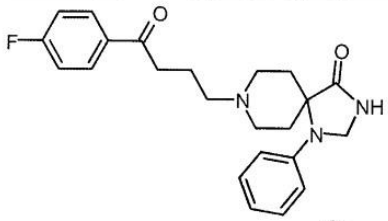	+ + + ++	+ – – +
5	Saquinavir	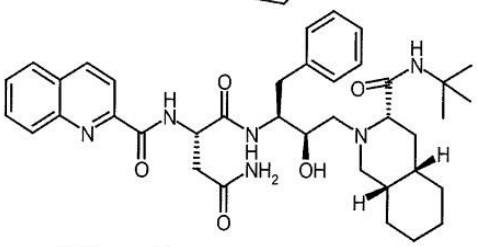	+ + + ++	– – – +
6	Haloperidol	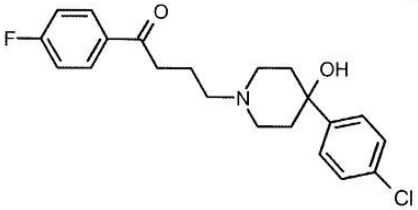	+ – – ++	– – – –
7	Benperidol	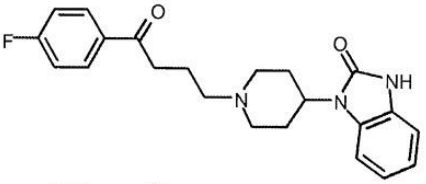	+ + + +	– – – –
8	Bromperidol	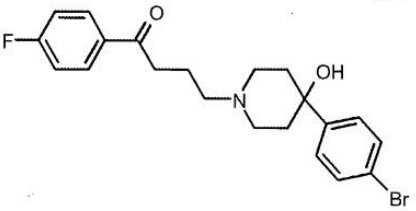	+ + + ++	+ – – –
9	Diphenidol	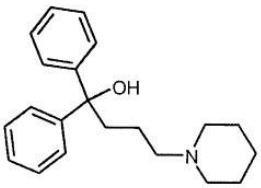	+ – – –	– – – –
10	Levocabastine	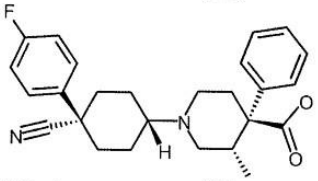	– + + –	– – – –
11	Fexofenadine	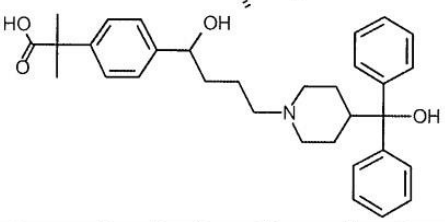	+ – + –	– – – –

Note. In the last two columns, the four lines correspond to the four screens A-Fc2, A-Fc4, B-Fc2, B-Fc4, C-Fc2. ++: FO_{cor} or [FO_{cor} – threshold] $\geqslant 0.05$; +: $0 \leqslant FO_{cor} < 0.05$; –: $FO_{cor} < 0$.

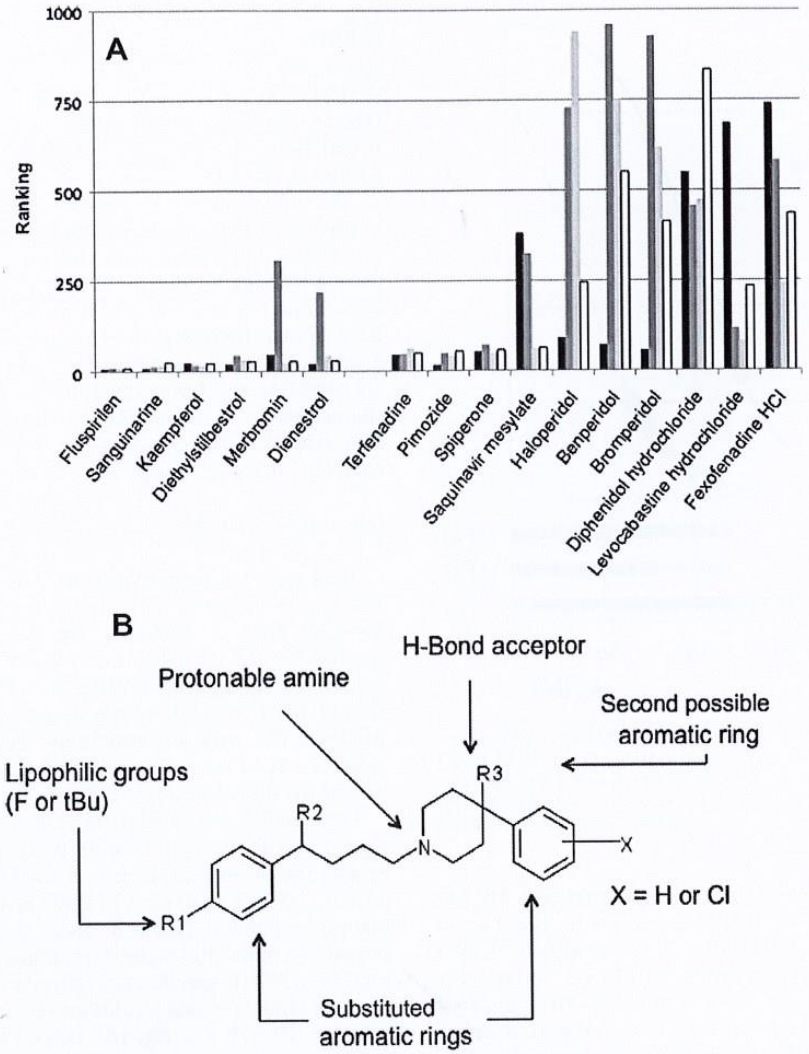

Fig.4. SAR model based on the responses of fluspirilen analogs. (A) Ranking for the cpds in four screens compared with that of the six most promising binders. (B) SAR model.

peridines (Table 4), were tested for their ability to inhibit PTP1B enzymatic activity. Vanadate, a known PTP1B inhibitor [20], was used as a positive control, and the nonbinder diphenidol (molecule **9** in Table 4) was used as a negative control. The ranking of IC_{50} values presented in Table 5 is consistent with published data [16,20] and with observed SPR response levels. The most potent inhibitors were vanadate and sanguinarine, with IC_{50} values of 0.029 and 1.36 μM, respectively. IC_{50} values between 10 and 50 μM were observed for all other binders. Diphenidol hydrochloride showed marginal PTP1B inhibition, if any.

Table 5
IC_{50} values as determined from enzymatic assay.

Inhibitor	IC_{50} vs. PTP1B (μM)
Fluspirilen	23.9 ± 2.7
Terfenadine	50 ± 0.2
Dienestrol	10 ± 0.7
Kaempferol	21 ± 3
Sanguinarine	1.36 ± 0.05
Vanadate	0.029 ± 0.004
Diphenidol hydrochloride	28% activity inhibition at 500 μM

Discussion

Detection sensitivity

The detection limits (expressed as K_D range) are illustrated for screens A-Fc2, B-Fc2, and C-Fc2 in Fig. 5. For example, Std_{6-75} lies between FO = 0.008 and 0.03 for the 14 plates of screen A-Fc2 (Supplementary Table 1), which results in a threshold between 0.024 and 0.09 ($3Std_{6-75}$), corresponding to K_D between 2×10^{-5} and 5×10^{-6} M. The threshold lies between 0.05 and 0.28 in screen C-Fc2, which corresponds to K_D between 0.2×10^{-5} and 2.6×10^{-5} M. FO_{cor} values recorded for the six most promising PTP1B binders are also reported in Fig. 5. They lie between 0.3 and 0.8 at $C(cpd) = 10$ μM and between 0.02 and 0.2 at $C(cpd) = 0.5$ μM, indicating K_D of approximately 10^{-5} M. The 2- to 5-fold difference in responses at the two cpd concentrations is slightly below the 3- to 10-fold difference expected for K_D in the 10^{-5} to 10^{-6} range and can be attributed to uncertainties on small responses, $C(cpd)$, or R_{max} (e.g., due to the presence of inactive fixed molecules).

Fig. 5 shows that screening at $C(cpd) = 0.5$ and 10 μM allowed the detection of binders with K_D of approximately 10^{-5} and

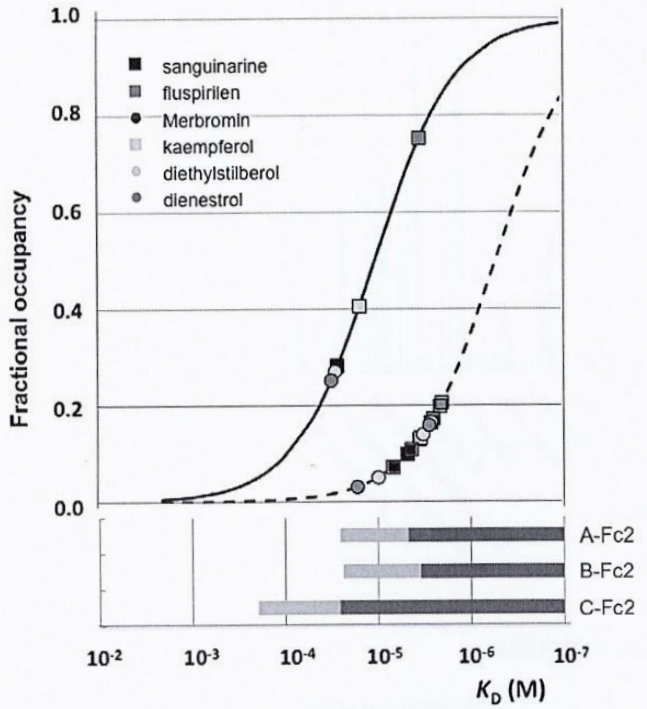

Fig.5. Experimental detection sensitivity. FO = $f(K_D)$ plots at C(cpd) = 0.5 μM (dotted line) and 10 μM (black line), indicating the signals (FO_{cor}) calculated for the six potential PTP1B-specific binders. The horizontal bars indicate the K_D range detectable in screens A-Fc2, B-Fc2, and C-Fc2. Black: K_D detectable whatever the plate; gray: range of detection limits (K_D corresponding to threshold) for the 14 plates of each screen.

10^{-4} M, respectively, which is in the expected range (Fig. 1B) but with significant variations in different experiments. The gain in sensitivity expected at high C(cpd) (C-Fc2) is slightly offset by a higher noise. The threshold also varies with target surface. For example, it was higher on hAR surfaces (not shown) compared with PTP1B surfaces, presumably because of the presence of denatured proteins in the hAR sample. It was low on the peptide surface (not shown), which contains a low mass of material compared with protein surfaces. Cpd size did not appear as a limiting factor for the detection of binding because three of the six best candidates have a MW < 300 Da.

Optimal screening procedure

Despite a gain in sensitivity that is slightly less than expected, screening at high rather than low C(cpd) provides several advantages. Overstoichiometric binders are more readily identified; eight such binders were identified on PTP1B surfaces at C(cpd) = 10 μM as compared with less than three at C(cpd) = 0.5 μM. Furthermore, signals generated by responders were more easily distinguishable from noise. This is because an interaction with K_D of approximately 10^{-5} M, as calculated for these interactions, is expected to generate a 10-fold signal increase at C(cpd) = 10 μM compared with 0.5 μM (Fig. 1B), whereas the increase in noise was approximately 3-fold, as judged from Std values (Supplementary Table 1). The lower signal/noise ratio observed at C(cpd) = 0.5 μM also favored the selection of likely false positives (25 cpds were selected at C(cpd) = 0.5 but not 10 μM).

A single screen at C(cpd) at approximately 10 μM on a sensor surface carrying a reference, the target of interest, and two unrelated proteins at high densities should be sufficient to discriminate among promiscuous, overstoichiometric, and potentially selective binders with $K_D < 5 \times 10^{-5}$ M and to identify the highest responders. It should be noted that high cpd concentrations are of little benefit if binders with $K_D < 10^{-6}$ M are sought; the theoretical signal increase when screening at 10 μM compared with 0.5 μM is only 3-fold at $K_D = 10^{-6}$ M and negligible at $K_D = 10^{-7}$ M (Fig. 1B). Data should be evaluated using a plate-by-plate approach if variations of mean response are observed in different experiments, as was the case here.

The time needed to screen one 96-well plate and retrieve a list of MW corrected responses is approximately 14 h using automated procedures implemented in the T100 instrument and software. Once a strategy for threshold definition is established, automated algorithms can be developed using dedicated software to retrieve a list of hits. Therefore, the 14 plates can be screened within 2 to 3 weeks. Other high-information content screening approaches are available and have sometimes been compared [21,22,6]. The characteristics of the interaction system under study are particularly critical in the choice of the most appropriate among these complementary technologies.

Quantitative reliability

Data were consistent with simulations despite the small level and narrow range of measured SPR signals (FO_{cor} between 0.03 and 0.4). First, as predicted (Fig. 1B), the screen performed at C(cpd) = 0.5 μM on a low-density PTP1B surface (R_{max} = 83 RU) did not allow discriminating between binding and noise (Table 2). Second, more than 90% of the signals were within the noise level whatever the screening conditions (Fig. 2). Finally, responses at C(cpd) = 10 μM were always higher than those at C(cpd) = 0.5 μM even if the difference is slightly less than expected (Fig. 1B).

Cpd ranking was found to be a reliable indicator for discriminating among the strongest binders, weaker binders, and non binders. Among the 90 measurements at low C(cpd) recorded for cpds of groups 1, 2 and 3 (30 cpds in three screens), 56 ranked in the 30 highest responders (Table 3, gray), but 20 more (in total 76 of 90) ranked in the 100 highest responders. In particular, the 6 most promising PTP1B-specific cpds ranked in the 50 highest responders whatever the screening conditions except for merbromin and dienestrol in screen B-Fc2 (Fig. 4A). This exception can be explained by the high noise observed for plate 7 to which these cpds belong, possibly due to insufficient surface conditioning with buffer before starting the experiment (Supplementary Table 1).

Chemical library and PTP1B binders

The Prestwick Chemical Library® was fully suitable for SPR screening. All 1120 compounds were sufficiently soluble to allow SPR analysis at a concentration of 10 μM. Very few carryover effects were observed, and ⩾90% of the compounds were not identified as binders, whatever the screening conditions and target surfaces. At C(cpd) = 10 μM, only 12 cpds showed overstoichiometric responses, indicating that they bind either in the form of aggregates or at multiple sites of the target. It can be noted that all 12 also showed promiscuous binding, as expected for compounds that easily adsorb to molecular surfaces (Table 3).

Chemical consistency of data is observed at several levels. Among cpds identified as potential PTP1B-specific binders, sanguinarine is a known PTP1B inhibitor [16]. Five cpds of the library present a benzene-OH moiety homologous to the Tyr side chain naturally bound by PTP1B (Supplementary Table 2). Three of these are structurally similar (kaempferol, dienestrol, and diethylstilberol) and were selected as binders. The two others differ from the former by a more flexible anchor for the benzene-OH group and never showed binding. Four members belonging to the arylbutylpiperidine family ranked in the 80 highest responders in all screens (Fig. 4A). Three of these (fluspirilen, terfenadine, and pimozide)

were assayed and confirmed as PTP1B inhibitors. Another member of this family (benperidol) showed neither binding nor inhibition activity.

Conclusions

Our results demonstrate the reliability of SPR data obtained from the direct screening of a focused chemical library on PTP1B, leading us to propose a SAR model for PTP1B binding. Eventually, this will help the synthesis of new compounds with good affinity and selectivity for PTP1B.

Acknowledgments

This work was supported by the CNRS (Centre National de la Recherche Scientifique), University of Strasbourg, INSERM (Institut National de la Science et de la Recherche Médicale), and, the Hôpital Universitaire de Strasbourg (H.U.S) and ARC (Association pour la Recherche sur le Cancer) (Grant 3171). The authors thank Isabelle Hazemann for hAR production.

Appendix A. Supplementary data

Supplementary data associated with this article can be found, in the online version, at doi:10.1016/j.ab.2011.09.015.

References

[1] W. Huber, A new strategy for improved secondary screening and lead optimization using high-resolution SPR characterization of compound–target interactions, J. Mol. Recognit. 18 (2005) 273–281.
[2] T. Lundqvist, The devil is still in the details: driving early drug discovery forward with biophysical experimental methods, Curr. Opin. Drug Discov. Dev. 8 (2005) 513–519.
[3] T. Neumann, H.D. Junker, K. Schmidt, R. Sekul, SPR-based fragment screening: advantages and applications, Curr. Top. Med. Chem. 7 (2007) 1630–1642.
[4] M. Strandh, B. Persson, H. Roos, S. Ohlson, Studies of interactions with weak affinities and low-molecular-weight compounds using surface plasmon resonance technology, J. Mol. Recognit. 11 (1998) 188–190.
[5] R. Karlsson, M. Kullman-Magnusson, M.D. Hämäläinen, A. Remaeus, K. Andersson, P. Borg, E. Gyzander, J. Deinum, Biosensor analysis of drug–target interactions: direct and competitive binding assays for investigation of interactions between thrombin and thrombin inhibitors, Anal. Biochem. 278 (2000) 1–13.
[6] M. Kobayashi, K. Retra, F. Figaroa, J.G. Hollander, E. Ab, R.J. Heetebrij, H. Irth, G. Siegal, Target immobilization as a strategy for NMR-based fragment screening: comparison of TINS, STD, and SPR for fragment hit identification, J. Biomol. Screen. 15 (2010) 978–989.
[7] M.D. Hämäläinen, A. Zhukov, M. Ivarsson, T. Fex, J. Gottfries, R. Karlsson, M. Bjorsne, Label-free primary screening and affinity ranking of fragment libraries using parallel analysis of protein panels, J. Biomol. Screen. 13 (2008) 202–209.
[8] M. Elinder, H. Nordstrom, M. Geitmann, M. Hämäläinen, L. Vrang, B. Oberg, U.H. Danielson, Screening for NNRTIs with slow dissociation and high affinity for a panel of HIV-1 RT variants, J. Biomol. Screen. 14 (2009) 395–403.
[9] I. Navratilova, A. Hopkins, Fragment screening by surface plasmon resonance, ACS Med. Chem. Lett. 1 (2010) 44–48.
[10] S. Perspicace, D. Banner, J. Benz, F. Muller, D. Schlatter, W. Huber, Fragment-based screening using surface plasmon resonance technology, J. Biomol. Screen. 14 (2009) 337–349.
[11] M. Elchebly, A. Cheng, M.L. Tremblay, Modulation of insulin signaling by protein tyrosine phosphatases, J. Mol. Med. 78 (2000) 473–482.
[12] U.H. Danielson, Fragment library screening and lead characterization using SPR biosensors, Curr. Top. Med. Chem. 9 (2009) 1725–1735.
[13] A. Frostell-Karlsson, A. Remaeus, H. Roos, K. Andersson, P. Borg, M. Hämäläinen, R. Karlsson, Biosensor analysis of the interaction between immobilized human serum albumin and drug compounds for prediction of human serum albumin binding levels, J. Med. Chem. 43 (2000) 1986–1992.
[14] S. Charbonnier, G. Stier, G. Orfanoudakis, B. Kieffer, R.A. Atkinson, G. Trave, Defining the minimal interacting regions of the tight junction protein MAGI-1 and HPV16 E6 oncoprotein for solution structure studies, Protein Expr. Purif. 60 (2008) 64–73.
[15] D.G. Myszka, Improving biosensor analysis, J. Mol. Recognit. 12 (1999) 279–284.
[16] A. Vogt, A. Tamewitz, J. Skoko, R.P. Sikorski, K.A. Giuliano, J.S. Lazo, The benzo[c]phenanthridine alkaloid, sanguinarine, is a selective, cell-active inhibitor of mitogen-activated protein kinase phosphatase-1, J. Biol. Chem. 280 (2005) 19078–19086.
[17] P. Stenlund, A. Frostell-Karlsson, O.P. Karlsson, Studies of small molecule interactions with protein phosphatases using biosensor technology, Anal. Biochem. 353 (2006) 217–225.
[18] A.M. Giannetti, B.D. Koch, M.F. Browner, Surface plasmon resonance based assay for the detection and characterization of promiscuous inhibitors, J. Med. Chem. 51 (2008) 574–580.
[19] C. Kreatsoulas, K. Narayan, Algorithms for the automated selection of fragment-like molecules using single-point surface plasmon resonance measurements, Anal. Biochem. 402 (2010) 179–184.
[20] X.L. Guo, K. Shen, F. Wang, D.S. Lawrence, Z.Y. Zhang, Probing the molecular basis for potent and selective protein–tyrosine phosphatase 1B inhibition, J. Biol. Chem. 277 (2002) 41014–41022.
[21] A. Boettcher, S. Ruedisser, P. Erbel, D. Vinzenz, N. Schiering, U. Hassiepen, P. Rigollier, L.M. Mayr, J. Woelcke, Fragment-based screening by biochemical assays: systematic feasibility studies with trypsin and MMP12, J. Biomol. Screen. 15 (2010) 1029–1041.
[22] C. Dalvit, NMR methods in fragment screening: theory and a comparison with other biophysical techniques, Drug Discov. Today 14 (2009) 1051–1057.

Article 3

Choulier, L.*, Nominé, Y., Zeder-Lutz, G., Charbonnier, S., Didier, B., Jung, M.L. & Altschuh, D.* (2013). Chemical library screening using a SPR-based inhibition in solution assay: simulations and experimental validation. *Anal. Chem.* **85**, 8787-95. (*corresponding authors).

analytical chemistry

Article

pubs.acs.org/ac

Chemical Library Screening Using a SPR-Based Inhibition in Solution Assay: Simulations and Experimental Validation

Laurence Choulier,*[†,§] Yves Nominé,[†] Gabrielle Zeder-Lutz,[†] Sebastian Charbonnier,[†] Bruno Didier,[‡] Marie-Louise Jung,[‡] and Danièle Altschuh*[†]

[†]Biotechnologie et Signalisation Cellulaire, Université de Strasbourg, CNRS, ESBS, Boulevard Sébastien Brant BP10413, 67412 Illkirch, France

[‡]Prestwick Chemical, Bd Gonthier d'Andernach, Parc d'Innovation, 67400 Illkirch, France

Supporting Information

ABSTRACT: We have developed a surface plasmon resonance (SPR)-based inhibition in solution assay (ISA) to search for inhibitors of the medium affinity (K_D = 0.8 μM) interaction between an E6-derived peptide ($E6_{peptide}$) immobilized on the sensor and a PDZ domain (MAGI-1 PDZ1) in the mobile phase. DZ domains are widespread protein-protein interaction modules that recognize the C-terminus of various partners. Simulations indicated that relatively low compound concentrations (10 μM) and limited peptide densities (R_{max} < 200 resonance units) should allow the detection of inhibitors with a target affinity close to 100 μM, which was then demonstrated experimentally. ISA screening, carried out on the Prestwick Chemical Library® (1120 compounds), identified 36 compounds that inhibited the interaction by more than 5%. Concentration-dependent ISA, carried out on a subset of 19 potential inhibitors, indicated that 13 of these indeed affected the interaction between MAGI-1 PDZ1 and the $E6_{peptide}$. No effect was observed for 84 compounds randomly chosen among noninhibitors. One of the four best inhibitors was a peptide binder, and three were PDZ binders with K_D in the 10−50 μM range. We propose that a medium (μM) affinity between the target and surface-bound partner is optimal for SPR-based ISA screening.

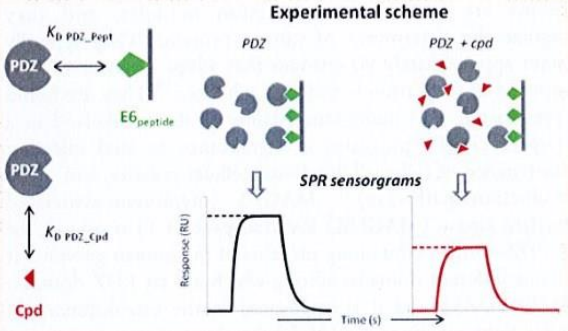

Surface plasmon resonance (SPR) biosensors provide information-rich data on molecular recognition with relatively low material consumption. The technology has been implemented in several steps of the drug discovery process, from the characterization of target−compound binding to the screening of small libraries.[1−5] Libraries of several hundred up to a few thousand compounds or fragments (together called here low molecular weight (LMW) compounds) were so far screened in SPR-based direct binding assays (DBA) where they are injected sequentially over target surfaces.[6−14] DBA screening selects all binders, whether they interact with the active site or with other regions of the fixed target. Several assay formats were, therefore, designed to identify active-site binders. The LMW compounds can be injected in parallel on the active form of the target and on an inactive form, in which the binding site is either mutated or blocked by a high-affinity inhibitor.[1,6,7] Active-site binders can also be distinguished from those binding elsewhere on the target in surface competition assays (SCA)[7,8,12,13] or inhibition in solution assays (ISA).[15−17] In SCA, the target is immobilized, and a known active-site binder, called the target definition compound (TDC), is injected in mixture with the compound under study. Nonadditive responses are expected if the two molecules compete for the same active site. In ISA, the TDC is immobilized, and a target−compound mixture is injected over the surface. If the compound recognizes the active site, the signal is decreased compared to that produced by the target alone.

Competition and inhibition assays were applied so far for hit characterization after screening the library in a direct assay, but to the best of our knowledge, they were not used for hit identification in the initial screen. Their disadvantages compared to DBA are that a TDC is required, that the experiments last longer, and that no information is obtained about the kinetics of compound−target binding. SCA, as well as DBA, presents drawbacks related to target immobilization. The high target density required to detect LMW and weak-affinity binders is typically achieved through covalent coupling. The binding activity of the target may be significantly affected by its covalent immobilization on the surface and by regeneration steps sometimes necessary after each compound injection to remove target- or surface-bound compounds. The assay design used in ISA represents an attractive alternative because the compound−target interaction occurs in solution. The immo-

Received: June 28, 2013
Accepted: August 9, 2013
Published: August 9, 2013

bilized TDC can be a synthetic molecule, likely to be more resistant to immobilization/regeneration conditions compared to proteins. Finally, detection sensitivity should be higher because the SPR signal generated by complex formation is related to the MW of the injected molecule and is, therefore, larger in ISA (target in solution) compared to SCA (compound in solution). Gerschwindner et al.[16] compared the outcome on trypsin inhibitor identification of different assay formats, among which are DBA and ISA, using optical waveguide grating (OWG) platforms. The library contained known active and nonactive compounds and frequent hitters. DBA was found to identify a large number of false positives, as compared to ISA. In contrast, results from ISA showed a good correlation with the enzymatic assay.

Here, we apply ISA to identify compounds that inhibit the interaction between a PDZ domain and a peptide. The term PDZ is an abbreviation for the first three proteins found to share this structural domain: PSD-95, Dlg, and ZO-1. PDZ domains are widespread interaction modules, and they recognize the C-terminus of various proteins. They typically contain approximately 90 residues that adopt a conserved fold composed of six β-strands and two α-helices.[18] They are found in cytoplasmic and membrane-adapter proteins involved in a variety of cellular processes of significance to viral infection (maintenance of cell–cell junctions, cellular polarity, and signal transduction pathways).[19] MAGI-1 (membrane-associated guanylate kinase (MAGUK) inverted protein 1) is one of the 160 PDZ-domain-containing proteins of the human genome. It contains different domains among which are six PDZ domains (PDZ0–PDZ5), and it is implicated in the establishment of cellular tight junctions.[20] MAGI-1 has been shown to interact with several cellular and viral proteins,[19] among which is the E6 oncoprotein of the high-risk mucosal human papillomavirus (HPV) type 16. In human cells, the latter interaction leads to the proteasome-mediated degradation of MAGI-1, which promotes tight junction disruption in epithelial cells with a likely role in cell differentiation and cell proliferation processes.[21] MAGI-1 is, therefore, a potential target in cancer therapy,[22] and specific inhibitors of the MAGI-1 interaction with viral proteins have been investigated.[22−25]

We first defined appropriate conditions for the SPR-based ISA from simulations before applying them to search for inhibitors of the target–TDC interaction. The target was a recombinant protein corresponding to the MAGI-1 PDZ1 domain (the second of the six PDZ domains of MAGI-1), hereafter called PDZ. This protein cannot be used in a DBA where the compounds are injected over the surface-bound PDZ because it is too fragile to withstand immobilization or regeneration steps. The TDC was a peptide corresponding to the 11 C-terminal residues of the E6 oncoprotein of HPV16 with a L/V replacement of the last residue, called $E6_{peptide}$. The compound library was the Prestwick Chemical Library® (Prestwick Chemical, Illkirch, France) composed of 1120 compounds (MW between 102 and 1665 Da, average of 386 Da). We have previously used the library to identify protein tyrosine phosphatase 1b binders in a direct assay.[14] This work showed that the compounds of the Prestwick Chemical library are well-behaved (no obvious aggregation or carry-over, only 22 promiscuous binders) at a concentration of 10 μM, a concentration sufficient to detect inhibitors with a PDZ affinity up to 100 μM, according to the simulations. The 1120 compounds were, therefore, screened in ISA at 10 μM, where the signal corresponding to the injection of a compound–PDZ mix over $E6_{peptide}$ surfaces was compared to that generated by PDZ alone (Figure 1A). They were also screened in DBA

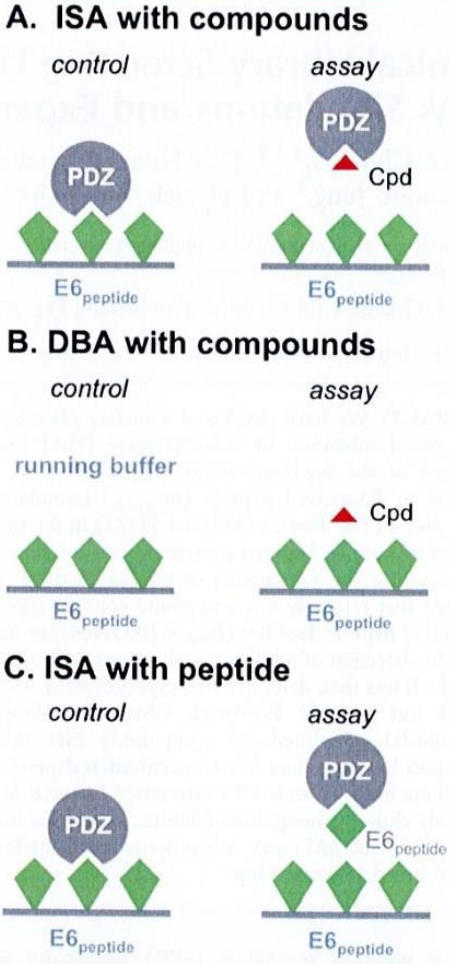

Figure 1. Experimental design. $E6_{peptide}$ is immobilized on the sensor. (A) ISA: compound–PDZ mix is injected over the surface, and the response is compared to that produced by PDZ alone. (B) DBA: compound is injected alone, and the response is compared to that produced by buffer. (C) Control ISA: peptide–PDZ mix is injected, and the response is compared to that produced by PDZ alone.

(compound alone injected over $E6_{peptide}$ surfaces, signal compared to that generated by buffer, Figure 1B) in order to distinguish between $E6_{peptide}$ and PDZ binders among $E6_{peptide}$–PDZ inhibitors. The quality of the surfaces and PDZ was assessed from an ISA using the $E6_{peptide}$ as an inhibitor in solution (Figure 1C). The conclusions of the ISA screen were challenged with compound concentration-dependent ISA carried out for a subset of the compounds.

■ EXPERIMENTAL SECTION

PDZ Expression and Purification. The construct of MAGI-1 PDZ1 called PDZ, comprising residues 456–580 (MW 13 856 Da) of human MAGI-1, was cloned into the pETM-41 expression vector providing a N-terminal His6-maltose binding protein (MBP) tag and a tobacco etch virus (TEV) protease cleavage site.[26] Proteins were expressed in BL21 DE3 *Escherichia coli* cells and purified, as previously

dx.doi.org/10.1021/ac4019445 | *Anal. Chem.* 2013, 85, 8787–8795

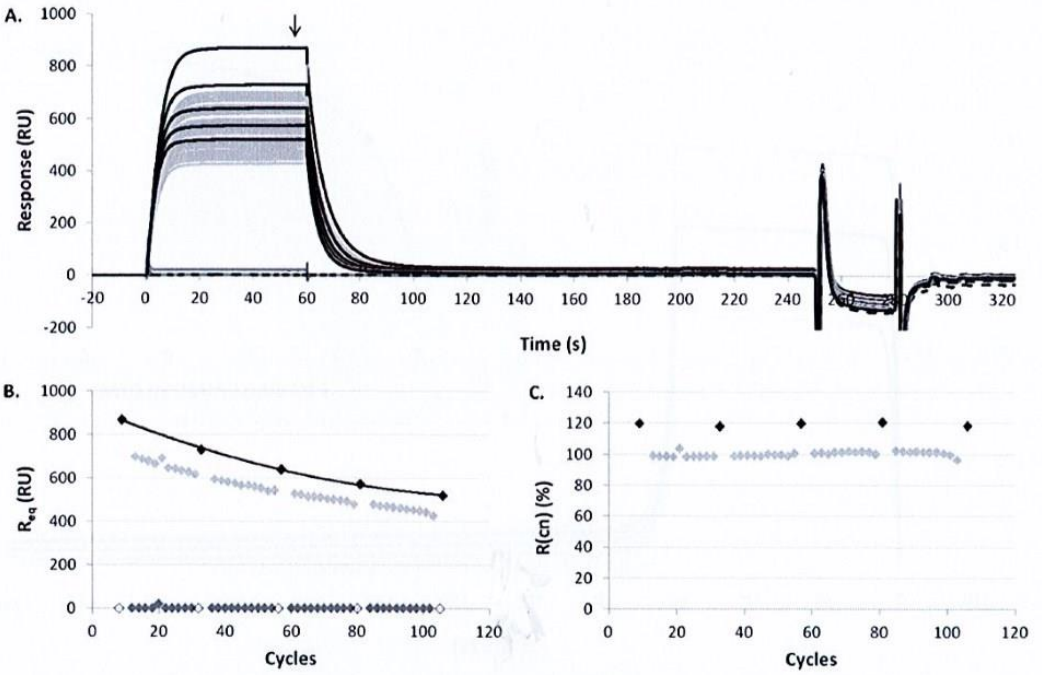

Figure 2. Illustrative half-plate screening data. (A) *XY*-zeroed, reference subtracted curves recorded on a surface immobilized with 700 RU of $E6_{peptide}$. PDZ and running buffer injections, performed every 20 cycles, are shown as plain and dotted black lines, respectively. PDZ–compound and compound injections are in light and dark gray, respectively. (B) Responses recorded 5 s before the end of injection (arrow in (A)) are plotted for each cycle. Plain and open black diamonds represent PDZ and buffer responses, respectively. Light and dark gray diamonds represent PDZ–compound and compound alone responses, respectively. Decrease in $R_{eq(PDZ)}$ was fitted to a two-parameter polynomial (black line, $R^2 = 0.99$) used to correct all responses for the loss of surface binding capacity. Corrected responses were then normalized relative to the mean of the 40 PDZ–compound responses. (C) Corrected and normalized responses for the injections of PDZ ($R_{cn(PDZ)}$, plain black diamonds) and PDZ–compound ($R_{cn(PDZ\_Cpd)}$, plain light gray diamonds).

described.[27] Briefly, PDZ extracts were loaded on an amylose column (New England Biolabs) and eluted with a buffer supplemented with 10 mM maltose. The MBP tag was cleaved with recombinant TEV protease at 8 °C overnight and removed by loading the digestion mix on a Ni–NTA (nickel–nitrilotriacetic acid) resin (QIAGEN). The resulting flow-through was finally subjected to a final gel-filtration step on a Sephadex HiLoad 16/60 75 pg column (GE Healthcare) to ensure a high-purity-degree sample.

Peptide Synthesis. $E6_{peptide}$ (sequence: CRSSRTRRETQV; MW: 1478 Da; pI: 11.52) corresponding to the last 11 C-terminal residues of HPV16 E6 with the C-terminal L replaced by V and bearing an additional N-terminal cysteine for immobilization was synthesized by P. Eberling (Chemical Peptide Synthesis Service, IGBMC, France), as previously described.[27]

SPR Experiments. All experiments were performed on a Biacore T100 instrument (GE Healthcare Biacore, Uppsala, Sweden) at 25 °C. Sensor surfaces and other Biacore consumables were purchased from GE Healthcare Biacore. Running buffers were filtered through a 0.22 μm membrane. Dimethyl sulfoxide (DMSO) was purchased from Sigma Aldrich (ref no. 472301). The chemical library was obtained from Prestwick Chemical, Inc. (Illkirch, France).

Peptide Immobilization. The running buffer was HEPES-buffered saline (HBS) (0.01 M HEPES, pH 7.4, 0.15 M NaCl) supplemented with 0.005% v/v, Surfactant P20. The $E6_{peptide}$ was immobilized on flow cells (Fc) 2, 3, and 4 of CM5 surfaces (BR-1005-30, GE Healthcare Biacore) through the sulfydryl group of its N-terminal cysteine using the thiol coupling chemistry. The flow rate was 10 μL/min. Surfaces were activated by successive injections of a 1:1 mix of 0.2 M *N*-ethyl-*N*′-(3-dimethylaminopropyl)-carbodiimide hydrochloride (EDC) and 0.05 M *N*-hydroxysuccinimide (NHS) for 10 min and 2-(2-pyridimyldithioethaneamine) (PDEA) at 18 mg/mL in 0.1 M Na borate (pH 8.5) for 240 s. Deactivation was achieved by a 240 s injection of 1 M ethanolamine-HCl (pH 8.5). Peptides at concentrations varying from 5 to 200 μg/mL were injected in 10 mM formate (pH 3.2). Immobilization levels were between 50 and 1700 resonance units (RU). Inactivation of free PDEA groups was achieved by injecting 0.1 M L-cysteine and 1 M NaCl in 0.1 M Na formate (pH 4.3) for 10 min. Reference surfaces (Fc1) were treated similarly except that peptide injection was omitted.

Determination of PDZ–$E6_{peptide}$ Affinity. PDZ samples at concentrations in the 40 nM to 10 μM range were serially injected for 60 s over reference and $E6_{peptide}$ surfaces. Each PDZ injection was followed by a 120 s buffer flow and a 30 s, 5 mM NaOH injection for surface regeneration. The flow rate was 40 μL/min. Sensorgrams were corrected for signals from the reference Fc. The equilibrium response (R_{eq}) was recorded 5 s before the end of the PDZ injection (time window: 5 s). The K_D was determined by fitting the R_{eq} versus the [PDZ] curve to a simple 1:1 interaction model with the Biacore T100 2.0.2 evaluation software (GE Healthcare).

Screening Experiments. The running buffer, freshly prepared before starting each method, was HBS supplemented with 0.05% Triton and 2% DMSO. We verified by SPR that the

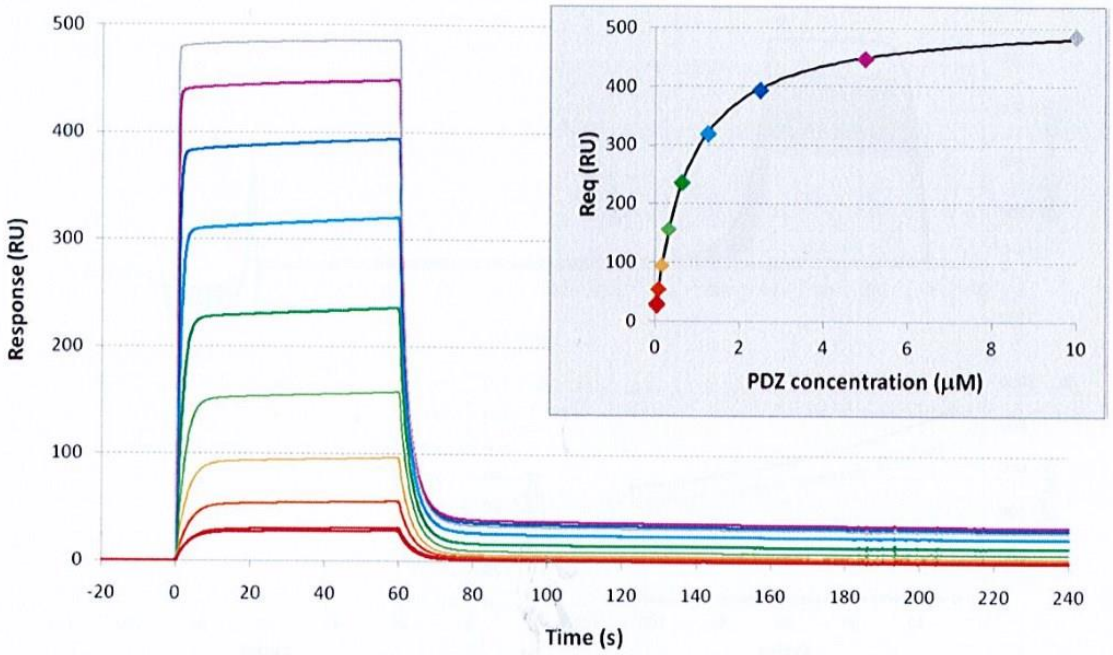

Figure 3. Determination of the equilibrium affinity of the PDZ–$E6_{peptide}$ interaction. Concentration-dependent binding of PDZ (40 nM to 10 μM range) to the covalently immobilized $E6_{peptide}$. Fit of the equilibrium response (R_{eq}) versus [PDZ] to a 1:1 binding isotherm (inset) indicates a $K_{D(PDZ\_pept)}$ of 0.78 μM.

PDZ binding activity was not affected in the presence of 2% DMSO (data not shown). In the initial ISA screen, PDZ at 1 μM was injected in the presence of the 1120 compounds at 10 μM over the reference (Fc1, empty) and peptide (Fc2, 3, and 4, increasing peptide densities) channels for 60 s, at a flow rate of 40 μL/min. A 120 s buffer flow was followed by one or two 30 s washing steps using 5 mM NaOH and by an extra wash of the flow system for 30 s with 50% DMSO. The compounds at 10 μM were also injected alone over the surfaces in order to identify peptide binders. The controls included buffer, PDZ alone, and in some cases, PDZ in the presence of $E6_{peptide}$ at 0.1 and 1 μM. The 1120 compounds of the Prestwick Chemical library are supplied in 14 96-well plates (P01–P14). Half a plate (40 compounds) was screened in a typical experiment. The corresponding automated method programmed the following injections: [controls], $[(\text{compound}_x, \text{compound}_x + \text{PDZ})_{x=1-10}]$, [controls], $[(\text{compound}_x, \text{compound}_x + \text{PDZ})_{x=11-20}]$, [controls], $[(\text{compound}_x, \text{compound}_x + \text{PDZ})_{x=21-30}]$, [controls], $[(\text{compound}_x, \text{compound}_x + \text{PDZ})_{x=31-40}]$, [controls]. Six startup cycles (buffer injections) were performed at the beginning of each method for conditioning the sensor surfaces. Two eight-point DMSO calibration curves (running buffer with 1 to 2.8% DMSO) were included before and after a set of 80 injections to correct for possible excluded-volume effects.

Data Processing. SPR data were processed using the Biacore T100 evaluation 2.0.2 software. Sensorgrams were automatically *XY*-zeroed before the injection start and corrected for signals recorded on the empty reference surface. The overlaid sensorgrams of a typical experiment are shown in Figure 2A. Responses recorded 5 s before the end of injection were further processed by subtracting the average of the five running buffer responses (double referencing). The double-referenced equilibrium responses were called $R_{eq(Cpd)}$, $R_{eq(PDZ)}$, and $R_{eq(PDZ\_Cpd)}$, for the compound, PDZ, and the PDZ–compound mix, respectively. A plot of these responses in a typical experiment is shown in Figure 2B. Results obtained when including DMSO correction were superimposable to those obtained without DMSO correction. Consequently, DMSO correction was not needed.

The $R_{eq(PDZ)}$ and $R_{eq(PDZ\_Cpd)}$ signals recorded in successive cycles were monotonously decreasing, indicating a loss of surface binding capacity and/or of PDZ binding activity (Figure 2B). Therefore, the five $R_{eq(PDZ)}$ values acquired within each experiment were fitted using a two-parameter polynomial, and the subsequent function was used to correct the responses over the entire sample set. These corrected responses were further normalized relative to the average response as follows. The averages of the five corrected $R_{eq(PDZ)}$ and of the 40 corrected $R_{eq(PDZ\_Cpd)}$ should be similar because few, if any, inhibitors of the PDZ–peptide interaction are expected in each half-plate. In our experiments, $R_{eq(PDZ)}$ was higher than $R_{eq(PDZ\_Cpd)}$ (Figure 2B). This discrepancy in active PDZ concentration may possibly result from differences in pipeting volumes and in containers; the control PDZ sample was prepared as a large volume in a glass tube, while PDZ–compound samples were prepared as small volumes in plastic wells. We chose to normalize responses relative to the mean of $R_{eq(PDZ\_Cpd)}$ in order to facilitate the detection of compounds which led to signal variations. The resulting corrected and normalized responses were called R_{cn}. A plot of $R_{cn(PDZ)}$ and $R_{cn(PDZ\_Cpd)}$ in a typical experiment is shown in Figure 2C.

Simulation of the Inhibition Level. Equations were previously described by Morelock et al.[28] and de Mol,[29] and they are developed in Figure S1 of the Supporting Information using a terminology adapted to our interaction system. The assumption underlying the equations is that the pre-established PDZ–compound complex present in the injected mix does not

dx.doi.org/10.1021/ac4019445 | Anal. Chem. 2013, 85, 8787–8795

dissociate during the time needed for the injected sample to cross the cell length; therefore, the equilibrium is not shifted toward the PDZ–peptide (surface-bound) interaction.[29,30] The contact time of the sample with the surface is about 90 ms at a flow rate of 40 μL/min, the volume of a Biacore T100 Fc being 60 nL. The half-life of the PDZ–compound complex is ≥90 ms if k_{off} < 8 s^{-1}. Assuming a typical k_{on} of 10^5 $M^{-1}\cdot s^{-1}$, PDZ–compound complexes with $K_{D(PDZ\_Cpd)}$ stronger than 80 μM should not dissociate during the injection time. For the simulations, we consider a higher $K_{D(PDZ\_Cpd)}$ limit of 100 μM. Step 1 in Figure S1 describes the interaction that occurs in solution between PDZ and the compound, in order to calculate the free PDZ left in the mix. Step 2 in Figure S1 describes the interaction between this free PDZ and the surface-bound peptide in order to calculate the corresponding SPR equilibrium response R_{eq}.

Concentration-Dependent ISA. Compounds were assayed in five-sample concentration series using 2-fold dilutions starting at a compound concentration of 40 μM, using a PDZ concentration of 1 μM.

RESULTS AND DISCUSSION

Determination of the Affinity of the PDZ–$E6_{peptide}$ Interaction. We measured a $K_{D(PDZ\_pept)}$ of 0.78 μM for the interaction of PDZ with the covalently coupled synthetic $E6_{peptide}$ using a steady-state approach (Figure 3). This value is in agreement with the value of 0.8 ± 0.2 μM previously determined in SPR experiments using the 16E6 L_0/V (RSSRTRRETQV) peptide sequence produced as recombinant fusion with the glutathione-S-transferase (GST) and immunocaptured on CM5 sensor surfaces.[26]

Simulation-Based Experimental Design. The experimental conditions (PDZ and compound concentrations, peptide density) must be adjusted so that the difference in response recorded for PDZ in the absence and presence of the compound ($R_{eq(PDZ)} - R_{eq(PDZ\_Cpd)}$) is large enough to be measurable. Two conditions must be met for this purpose. First, the compound should bind the largest possible fraction of PDZ, leading to a drop in the free PDZ concentration (see step 1, Figure S1 of the Supporting Information). This condition depends on the affinity of the PDZ–compound interaction ($K_{D(PDZ\_Cpd)}$) and total concentrations of compound ($[Cpd_t]$) and PDZ ($[PDZ_t]$). The compound concentration should be as large as possible to favor PDZ–compound binding even at weak affinity and obviously larger than $[PDZ_t]$; otherwise, only a fraction of the PDZ will be blocked when the totality of the compound is engaged in the complex. The second condition is that the variation in free PDZ concentration resulting from the formation of PDZ–compound complexes should induce a detectable variation in SPR response (step 2, Figure S1 of the Supporting Information). This condition requires working in the steep part of the curve $R_{eq}(PDZ) = f([PDZ])$, namely, at a PDZ concentration in the same range as the affinity of the PDZ–$E6_{peptide}$ interaction (Figure 3, Figure S2 of the Supporting Information). The $E6_{peptide}$ density influences the magnitude of R_{eq}, and therefore of ($R_{eq(PDZ)} - R_{eq(PDZ\_Cpd)}$) (Figure S2 of the Supporting Information). In contrast, the relative response variation ($(R_{eq(PDZ)} - R_{eq(PDZ\_Cpd)})/R_{eq(PDZ)}$) is independent of peptide density (Figure S2, inset, of the Supporting Information).

In theory, a PDZ concentration in the micromolar range, together with high peptide density and compound concentration, should be optimal for ISA screening. In practice, high molecular concentrations are known to favor artifacts such as unspecific absorptions, aggregation, and partial inaccessibility of the densely immobilized peptide. We have evaluated the lowest peptide density (expressed as R_{max}) that should allow the detection of compounds with $K_{D(PDZ\_Cpd)}$ up to 100 μM. Weaker affinities may be detectable, as observed by Gerschwindner et al.[17] in an empirical optimization of ISA on a OWG platform, but a competition between the compound and the surface-bound peptide for PDZ binding may occur in our assay setup. Furthermore, it is unlikely that compounds with weaker target affinity can be developed into efficient inhibitors. Figure 4A shows a simulation of the inhibition level

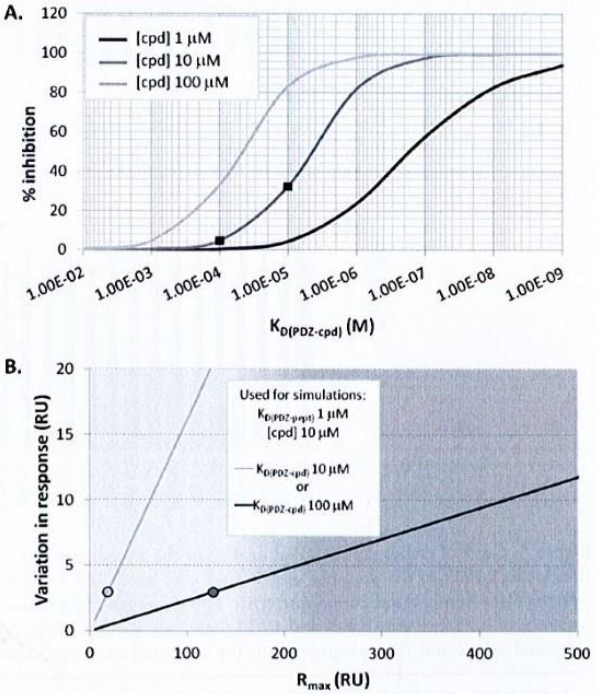

Figure 4. Simulation of the effect of (A) PDZ–compound affinity and (B) surface binding capacity on inhibition of the PDZ–$E6_{peptide}$ interaction. (A) Inhibition levels ($100 \times (R_{eq(PDZ)} - R_{eq(PDZ\_Cpd)})/R_{eq(PDZ)}$) as a function of $K_{D(PDZ\_Cpd)}$ for $[Cpd_t]$ = 1, 10, and 100 μM. Squares on the plot of [Cpd] = 10 μM represent inhibition levels of 5 and 32% for $K_{D(PDZ\_Cpd)}$ = 100 and 10 μM, respectively. (B) Variation in response ($R_{eq(PDZ)} - R_{eq(PDZ\_Cpd)}$) as a function of peptide density (expressed as R_{max} for $[Cpd_t]$ = 10 μM). Circles highlight a signal variation of 3 RU.

($100(R_{eq(PDZ)} - R_{eq(PDZ\_Cpd)})/R_{eq(PDZ)}$) as a function of $K_{D(PDZ\_Cpd)}$ for $[Cpd_t]$ = 1, 10, and 100 μM, with $[PDZ_t]$ = $K_{D(PDZ\_pept)}$ = 1 μM. We have shown previously that the compounds of the Prestwick Chemical library are well-behaved at a concentration of 10 μM.[14] At this concentration, the calculated inhibition levels are 32 and 5% for $K_{D(PDZ\_Cpd)}$ = 10 and 100 μM, respectively (black squares in Figure 4A). Figure 4B illustrates the signal variation ($R_{eq(PDZ)} - R_{eq(PDZ\_Cpd)}$) corresponding to these inhibition levels, as a function of peptide density (R_{max}). As a signal variation of 3 RU can be detected on a Biacore T100 device, R_{max} levels of 20 and 130 RU should be sufficient to identify inhibitors with $K_{D(PDZ\_Cpd)}$ of 10 and 100 μM, respectively (circles in Figure 4B).

dx.doi.org/10.1021/ac4019445 | Anal. Chem. 2013, 85, 8787–8795

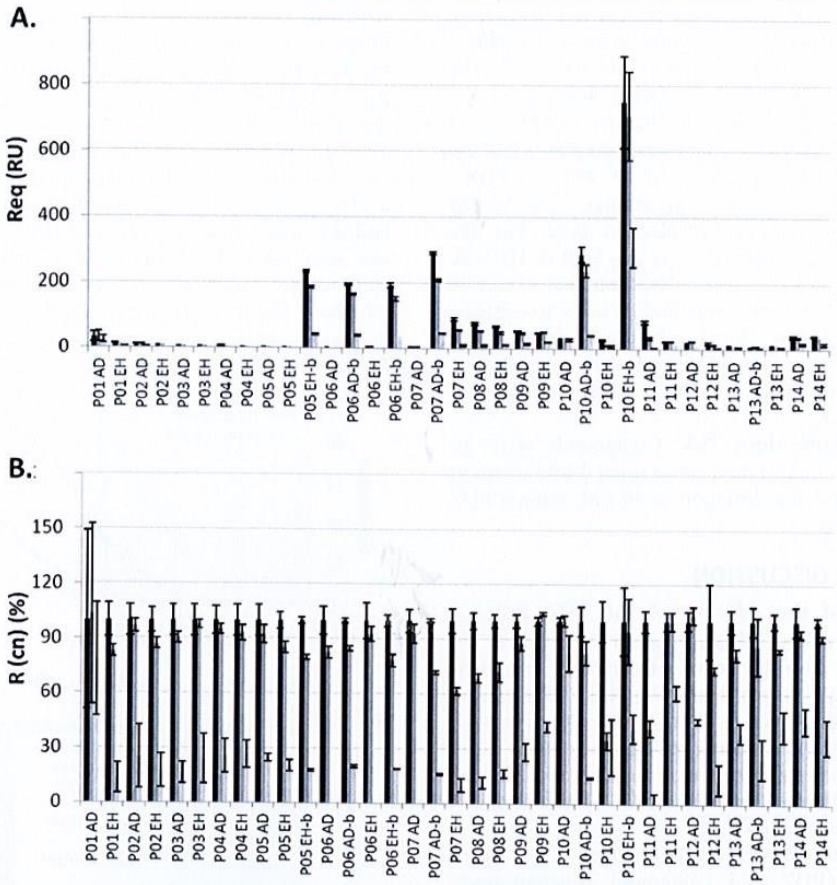

Figure 5. Control responses recorded on Fc2 in the 35 experiments. (A) Mean of five R_{eq} measurements and error bars are shown for PDZ alone (black bars), PDZ in the presence of 0.1 (dark gray bars), and 1 μM peptide (light gray bars). The names of the 35 experiments given on the x-axis refer to plate number and compound rows. (B) Corresponding corrected and normalized responses (R_{cn}) for PDZ alone (black bars), PDZ in the presence of 0.1 (dark gray bars), and 1 μM (light gray bars) peptide. Error bars are computed by considering the standard deviation of the triplicated corrected values and then propagated to the corrected and normalized values.

Inhibition Screening of the Full Library. The Prestwick Chemical library was screened at $[Cpd_t] = 10$ μM and $[PDZ_t] = 1$ μM. The peptide was immobilized at increasing densities on Fc2, 3, and 4, leading to PDZ responses between 2.5 and 1840 RU. Each experiment (Biacore method consisting of controls, compound, and PDZ–compound injections) was designed to screen 40 compounds (half of a Prestwick plate) in ISA and DBA, meaning that 28 experiments were needed to screen the 14 plates. Since seven half-plates were screened twice, the 10 μM ISA assay comprised 35 experiments. These were named according to plate number and compound rows (P01 AD: first half of plate 1, P01 EH: second half of plate 1....), with replicates labeled "b" (e.g., P05 EH-b).

The controls, consisting of injections of PDZ alone and PDZ in the presence of 0.1 and 1 μM peptide, were performed every 20 cycles (five controls per experiment) and then averaged over the entire experiment. The 35 mean control responses recorded in the 35 experiments on Fc2 are represented as histograms in Figure 5A. They indicate that surface binding capacities differed widely in the different experiments and flow cells. The corrected and normalized responses (R_{cn}) are shown in Figure 5B (Fc2) and Figure S3, panels a (Fc3) and b (Fc4), of the Supporting Information. The responses recorded for PDZ in the presence of peptide were reasonably stable in the 35 experiments performed on Fc2 (lowest peptide densities, Figure 5B), with $R_{cn(PDZ-Pept)}$ ~85 and 27% in the presence of 0.1 and 1 μM peptide, respectively. The corresponding inhibition levels of ~15 and 73% are higher than expected from simulations (2.5 and 25%, respectively), presumably because of an error on peptide concentration, estimated from weighing a small amount of peptide powder. The $R_{cn(PDZ-Pept)}$ values calculated on Fc3 or 4 were less stable (Figure S3 of the Supporting Information). Therefore, data recorded on Fc2 were used for identifying inhibitors.

It would be surprising that a library of 1120 compounds contains numerous inhibitors of the PDZ–$E6_{peptide}$ interaction. Therefore, we considered only the two best inhibitors (lowest $R_{cn(PDZ\_Cpd)}$) in each experiment. Among the 70 compounds (2 compounds in 35 experiments), 36 showed $R_{cn(PDZ\_Cpd)}$ <95% (inhibition >5%). They were named $Inh_{10\ \mu M}$ and are listed in Table 1 (classified according to the results of concentration-dependent experiments, see below). Among the 36 compounds selected on Fc2, 20 also showed inhibition on Fc3 and/or Fc4 (light gray in Table 1), while $R_{cn(PDZ\_Cpd)}$ was >125% for seven compounds (dark gray in Table 1). The other 1084 compounds were considered as noninhibitors (named $NonInh_{10\ \mu M}$).

Concentration-Dependent Inhibition Experiments. In order to evaluate the validity of our selection procedure, 103

Table 1. Inhibitors of the PDZ–E6$_{peptide}$ Interaction Identified in the 10 μM ISA and Behavior of 19 of These in C-Dep ISA

Compound		10 μM ISA screen			C-dep ISA
Name [1]	MW	Corrected and normalized responses $R_{cn(PDZ\_Cpd)}$		$R_{cn(PDZ)}$ on Fc2	Effect
		10 μM compound	1 μM pept		
Gallamine triethiodide	892	85	17	9	Inhibition
Methimazole[2]	114	92	41	750	Inhibition
Methacycline hydrochloride[2]	479	30	25	9	Inhibition
Thioguanosine	299	73	25	4	Inhibition
Carbimazole	186	81	ND [3]	3	Inhibition ±
Verteporfin	737	81	37	40	Inhibition ±
Menadione[2]	172	87	19	191	Inhibition ±
Nabumetone	228	88	*45*	22	Increase
Cefoperazone dihydrate	682	66	25	4	Increase
Daunorubicin hydrochloride	564	86	ND	3	Increase
Kawain	230	93	24	6	Increase
Disulfiram	297	87	25	11	Increase
Thioperamide maleate	409	77	13	17	Increase
Meclofenamic acid sodium salt monohydrate	336	91	24	6	None
Hemicholinium bromide	574	91	21	4	None
(+)-Isoproterenol (+)-bitartrate salt	361	90	*45*	22	None
Diethylstilbestrol	*268*	*78*	*83* [4]	*34*	*None*
Monensin sodium salt	*693*	*77*	*83* [4]	*34*	*None*
Simvastatin	*419*	*91*	*61* [4]	*24*	*None*
Denatonium benzoate[2]	447	63	25	9	ND [3]
Idazoxan hydrochloride	241	79	13	17	ND
Mebhydroline 1,5-naphtalenedisulfonate	841	81	ND	3	ND
Isocarboxazid	231	83	31	27	ND
Cloperastine hydrochloride	366	84	31	27	ND
Pyrazinamide	123	89	ND	3	ND
Pilocarpine nitrate	271	89	ND	3	ND
Myricetin[2]	318	91	19	191	ND
Ketotifen fumarate	426	91	21	4	ND
Calciferol	397	91	ND	3	ND
Imipenem[2]	299	92	16	290	ND
Ethamsylate	263	93	43	14	ND
Azapropazone	300	93	43	14	ND
Nystatine[2]	926	94	16	290	ND
Niflumic acid	282	94	26	5	ND
Glafenine hydrochloride	409	94	27	4	ND
Sulfachloropyridazine	285	94	42	48	ND

[1]Light gray cells: $R_{cn(PDZ\_Cpd)}$ < 95 (inhibition >5%) on Fc3 and/or Fc4. Dark gray cells: $R_{cn(PDZ\_Cpd)}$ >125 on Fc3 and/or Fc4. [2]Identified in experiment b. [3]ND = not determined. [4]Italics indicate that inhibition levels in the presence of 1 μM peptide were lower than average.

compounds (19 Inh$_{10\mu M}$ and 84 NonInh$_{10\mu M}$) were assayed in a concentration-dependent (C-dep) ISA. The experiments were repeated two and up to six times for 30 of these. The correlation between the 10 μM ISA and C-dep ISA data was satisfactory; none of the 84 NonInh$_{10\mu M}$ compounds showed C-dep inhibition (data not shown), and 13 out of the 19 Inh$_{10\mu M}$ compounds affected (inhibited or increased) the PDZ–E6$_{peptide}$ interaction in at least one experiment (Figure S4 of the Supporting Information). Results for these 19 Inh$_{10\mu M}$ compounds are summarized in the last column of Table 1. The K_D of the four best inhibitors (gallamine triethiodide, methimazole, methacycline hydrochloride, thioguanosine) was estimated in the 10 to 50 μM range from the compound concentration needed to achieve 50% inhibition (Figure S4,

panels A–D, of the Supporting Information). Inhibition may result from the compound interacting with either PDZ or the $E6_{peptide}$. The 10 μM DBA (data not shown) indicated that one of the four inhibitors was a peptide binder (methacycline hydrochloride), yielding a SPR signal (RU) >5 times higher than the buffer signal. Three among the 19 Inh_{10uM} compounds showed weak and irreproducible inhibition (Figure S4, panels E–G, of the Supporting Information) and six showed increases in signal (Figure S4, panels H–M, of the Supporting Information). Among the latter, four also showed increased signals on Fc3 and Fc4 in the 10 μM ISA (Table 1). Finally, among the six compounds that showed no inhibition (Figure S4, panels N–S, of the Supporting Information), three were selected in initial ISA experiments performed in nonoptimal conditions, as judged from the low inhibition level ($R_{cn(PDZ\text{-}Pept)}$ >50%) recorded in the presence of 1 μM peptide (italics in Table 1).

Despite the nonideal behavior of our TDC–target interaction (decay of the binding capacity of peptide surfaces and/or loss of PDZ binding activity, effects on TDC–target interaction depending on TDC density), we demonstrate that SPR-based ISA screening is feasible using a Biacore T100 instrument. Extremely small signal variations were detectable (for example $R_{eq(PDZ)} - R_{eq(PDZ\_Cpd)}$ was 4 − 3 = 1 RU for compound thioguanosine, Table 1). Consequently, the TDC density can be kept low, a condition that favored inhibitor detection in our case, while high TDC densities promoted signal increases in the presence of compound. Gerschwindner et al.[17] also observed that high TDC density favored unspecific TDC-inhibitor binding for an ISA developed on an OWG platform. The detection of inhibitors with affinity weaker than 100 μM is complicated by a possible competition between the immobilized TDC and the compound in solution for target binding.

CONCLUSION

The conditions of SPR-based ISA screening must be adjusted depending on the target–TDC affinity. When the affinity of the target–TDC interaction is in the micromolar range, as here, or higher, equilibrium is reached within seconds and the complex fully dissociates in the buffer flow (Figure 6, green and gray curves). SPR responses are recorded at equilibrium, with target concentration ([T]) ~$K_{D(T\_TDC)}$ and [Cpd_t] > [T]. Surface regeneration is not mandatory. At TDC–target affinity weaker than μM, the high target and compound concentrations required increase material consumption and adverse effects such as aggregation and nonspecific binding. In case of a strong (nM) target–TDC affinity the response recorded at the end of a 1 min injection would be far from equilibrium and small if [T] were kept around $K_{D(T\_TDC)}$. Therefore [T] (Figure 6, red curve) and/or TDC density (R_{max}) must be increased. Variations in target concentration are easily measured in conditions of [T] ≫ $K_{D(T\_TDC)}$ when the initial (and not equilibrium) response is recorded. The concentration of target–TDC complex is then negligible, and the reaction rate mainly depends on association kinetics and therefore concentration of free target. Nevertheless, the slow dissociation of the target–TDC complex requires a regeneration step, which may limit surface recycling. In conclusion, a medium target–TDC affinity appears as a favorable compromise for SPR-based ISA screening because drawbacks associated with high molecular concentrations (weak affinity) and drastic surface regeneration (strong affinity) are avoidable.

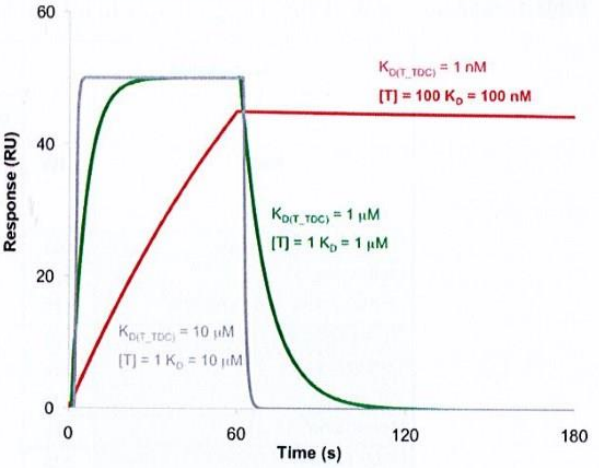

Figure 6. Simulated SPR binding curves for target–TDC affinity 10 μM (gray), 1 μM (green), and 1 nM (red) for a surface binding capacity of 100 RU. Target concentrations relative to $K_{D(T\_TDC)}$ are indicated.

ASSOCIATED CONTENT

Supporting Information

Additional information as noted in text. This material is available free of charge via the Internet at http://pubs.acs.org.

AUTHOR INFORMATION

Corresponding Authors

*E-mail: daniele.altschuh@unistra.fr (D.A.).
*E-mail: laurence.choulier@unistra.fr (L.C.).

Present Address

§Laboratoire de Biophotonique et Pharmacologie, Université de Strasbourg, CNRS, 74, Route du Rhin, 67401 Illkirch, France.

Notes

The authors declare no competing financial interest.

ACKNOWLEDGMENTS

This work was supported by the CNRS (Centre National de la Recherche Scientifique) and the University of Strasbourg, the Association pour la Recherche contre le Cancer (ARC) (no. 3171), and the Agence Nationale de la Recherche (ANR-MIME-2007 EPI-HPV-3D). S.C. was supported by ANR. We warmly thank Bruno Kieffer for constructive discussions.

REFERENCES

(1) Hämäläinen, M. D.; Zhukov, A.; Ivarsson, M.; Fex, T.; Gottfries, J.; Karlsson, R.; Björsne, M. *J. Biomol. Screening* **2008**, *13*, 202–209.
(2) Danielson, U. H. *Curr. Top. Med. Chem.* **2009**, *18*, 1725–1735.
(3) Holdgate, G. A.; Anderson, M.; Edfeldt, F.; Geschwindner, S. *J. Struct. Biol.* **2010**, *172*, 142–157.
(4) Navratilova, I.; Hopkins, A. L. *Future Med. Chem.* **2011**, *3*, 1809–1820.
(5) Hennig, M.; Ruf, A.; Huber, W. *Top. Curr. Chem.* **2012**, *317*, 115–143.
(6) Nordström, H.; Gossas, T.; Hämäläinen, M.; Källblad, P.; Nyström, S.; Wallberg, H.; Danielson, U. H. *J. Med. Chem.* **2008**, *51*, 3449–3459.
(7) Perspicace, S.; Banner, D.; Benz, J.; Müller, F.; Schlatter, D.; Huber, W. *J. Biomol. Screening* **2009**, *14*, 337–349.
(8) Elinder, M.; Nordström, H.; Geitmann, M.; Hämäläinen, M.; Vrang, L.; Oberg, B.; Danielson, U. H. *J. Biomol. Screening* **2009**, *14*, 395–403.

(9) Navratilova, I.; Hopkins, A. L. *ACS Med. Chem. Lett.* **2010**, *1*, 44–48.
(10) Rich, R. L.; Myszka, D. G. *Anal. Biochem.* **2010**, *402*, 170–178.
(11) Elinder, M.; Geitmann, M.; Gossas, T.; Källblad, P.; Winquist, J.; Nordström, H.; Hämäläinen, M.; Danielson, U. H. *J. Biomol. Screening* **2011**, *16*, 15–25.
(12) Geitmann, M.; Elinder, M.; Seeger, C.; Brandt, P.; de Esch, I. J.; Danielson, U. H. *J. Med. Chem.* **2011**, *54*, 699–708.
(13) Pollack, S. J.; Beyer, K. S.; Lock, C.; Müller, I.; Sheppard, D.; Lipkin, M.; Hardick, D.; Blurton, P.; Leonard, P. M.; Hubbard, P. A.; Todd, D.; Richardson, C. M.; Ahrens, T.; Baader, M.; Hafenbradl, D. O.; Hilyard, K.; Bürli, R. W. *J. Comput.-Aided Mol. Des.* **2011**, *25*, 677–687.
(14) Zeder-Lutz, G.; Choulier, L.; Besse, M.; Cousido-Siah, A.; Figueras, F. X.; Didier, B.; Jung, M. L.; Podjarny, A.; Altschuh, D. *Anal. Biochem.* **2012**, *421*, 417–427.
(15) Karlsson, R.; Kullman-Magnusson, M.; Hämäläinen, M. D.; Remaeus, A.; Andersson, K.; Borg, P.; Gyzander, E.; Deinum, J. *Anal. Biochem.* **2000**, *278*, 1–13.
(16) Geschwindner, S.; Carlsson, J. F.; Knecht, W. *Sensors* **2012**, *12*, 4311–4323.
(17) Geschwindner, S.; Dekker, N.; Horsefield, R.; Tigerström, A.; Johansson, P.; Scott, C. W.; Albert, J. S. *J. Med. Chem.* **2013**, *56*, 3228–3234.
(18) Doyle, D. A.; Lee, A.; Lewis, J.; Kim, E.; Sheng, M.; MacKinnon, R. *Cell* **1996**, *85*, 1067–1076.
(19) Javier, R. T.; Rice, A. P. *J. Virol.* **2011**, *85*, 11544–11556.
(20) Murata, M.; Kojima, T.; Yamamoto, T.; Go, M.; Takano, K.; Chiba, H.; Tokino, T.; Sawada, N. *Cell Tissue Res.* **2005**, *319*, 341–347.
(21) Kranjec, C.; Banks, L. *J. Virol.* **2011**, *85*, 1757–1764.
(22) Chi, C. N.; Bach, A.; Strømgaard, K.; Gianni, S.; Jemth, P. *Biofactors* **2012**, *38*, 338–348.
(23) Shan, J.; Zhang, X.; Bao, J.; Cassell, R.; Zheng, J. J. *Chem. Biol. Drug Des.* **2012**, *79*, 376–383.
(24) Wang, N. X.; Lee, H. J.; Zheng, J. J. *Drug News Perspect.* **2008**, *21*, 137–141.
(25) Dev, K. K. *Nat. Rev. Drug Discovery* **2004**, *3*, 1047–1056.
(26) Fournane, S.; Charbonnier, S.; Chapelle, A.; Kieffer, B.; Orfanoudakis, G.; Travé, G.; Masson, M.; Nominé, Y. *J. Mol. Recognit.* **2011**, *24*, 511–523.
(27) Charbonnier, S.; Stier, G.; Orfanoudakis, G.; Kieffer, B.; Atkinson, R. A.; Travé, G. *Protein Expression Purif.* **2008**, *60*, 64–73.
(28) Morelock, M. M.; Ingraham, R. H.; Betageri, R.; Jakes, S. *J. Med. Chem.* **1995**, *38*, 1309–1318.
(29) de Mol, N. J. *Methods Mol. Biol.* **2010**, *627*, 101–111.
(30) Nieba, L.; Krebber, A.; Plückthun, A. *Anal. Biochem.* **1996**, *234*, 155–165.

PROJETS DE RECHERCHE ACTUELS

Aptamères ciblant des cellules de glioblastome exprimant l'intégrine α5β1

A. Aptamères et SELEX

***Résumé** :*

Les aptamères sont de petits oligonucléotides simple brin, de 30 à 80 bases. Leur variété de repliement leur permet de reconnaître leurs cibles (acides aminés, nucléotides, peptides, protéines…) avec une forte affinité et sélectivité. Leur taille, leur propriétés physico-chimiques, leur faible coût de synthèse, leur caractère non-immunogène, en font une alternative pertinente aux anticorps, auxquels ils sont souvent comparés.

Ils sont sélectionnés par un criblage nommé SELEX ('selective evolution of ligands by exponential enrichment') pour lequel toutes les molécules d'une très grande banque (10^{14} molécules) sont mises en contact en même temps avec leur cible. Les aptamères peuvent être sélectionnés par cell-SELEX (SELEX dont les cibles sont des cellules) et se lier à des cibles cellulaires, souvent des biomarqueurs protéiques exprimés à la surface de cellules tumorales. Ils peuvent alors être utilisés en tant qu'agents diagnostiques ou thérapeutiques. S'ils ciblent un récepteur membranaire, ils peuvent être internalisés, et s'ils sont couplés à un agent thérapeutique, ils peuvent servir de véhicule pour le délivrer à l'intérieur des cellules. Les aptamères internalisés peuvent ainsi délivrer des agents cytotoxiques, des siRNA, des nanoparticules… au sein des cellules qu'ils ciblent spécifiquement.

A1. Aptamères

Outre leur rôle d'agents de l'expression génique, les acides nucléiques peuvent également être des partenaires d'interactions moléculaires. L'exploitation des propriétés de liaison des acides nucléiques a conduit à la découverte d'une nouvelle classe de molécules : les aptamères.

Les aptamères, du latin ‘aptus’ signifiant ‘correspondre à’ et du suffixe grec ‘mer’, sont des oligonucléotides ADN ou ARN capables de se lier avec une grande affinité et une grande spécificité à leur cible. De nombreux aptamères ont été identifiés contre un grand nombre de molécules cibles. Ils représentent une alternative aux anticorps monoclonaux dans les domaines analytique, diagnostique et thérapeutique.

Un brin d’histoire :

de la découverte des aptamères naturels…

Dans les années 80,

(i) il a été montré que certains génomes viraux (virus de l’immunodéficience humaine HIV-1 et adénovirus) codent pour de petits ARN structurés ayant la propriété de se lier aux protéines virales ou cellulaires avec une forte affinité et spécificité. Par définition, ce sont des aptamères. Pour HIV-1, il s’agit d’un petit ARN structuré en ‘épingle à cheveux’, appelé élément TAR (‘trans-activation response’), localisé dans la région 5’ non-traduite de l’ARNm. Il est essentiel à la transcription du génome rétroviral, et donc à la réplication du HIV-1, par liaison à la protéine Tat (Sullenger et al. 1990, *Figure 6*).

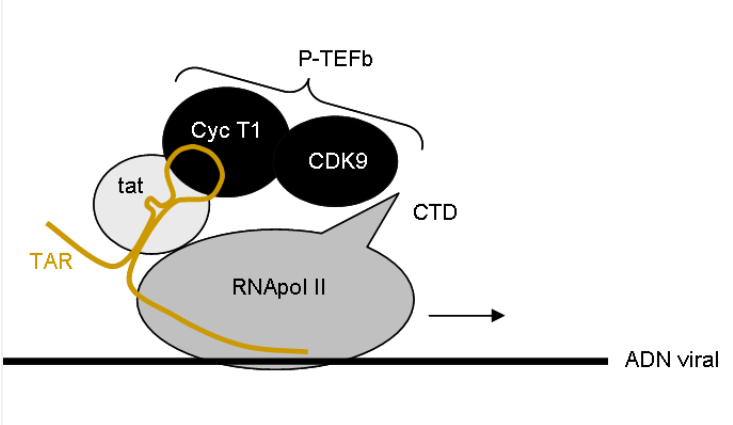

Figure 6. **Complexe d'élongation**. Le P-TEFb, cofacteur cellulaire d'élongation positif, est composé des sous-unités Cyc T1 et CDK9 (kinase CTD). Cyc T1 permet la formation du complexe tat/TAR en augmentant l'affinité de TAR pour tat. CDK9 phosphorolyse le domaine C-terminal (CTD) de la RNApol II permettant ainsi la transcription. Source : http://www.imgt.org

Quant aux adénovirus, ils produisent naturellement l’ARN VA (‘virus-associated’) qui inhibe la fonction de la protéine PKR (‘protéin kinase R’) et permet ainsi de poursuivre la production de protéines virales par la machinerie de traduction de la cellule hôte. (O'Malley et al. 1986).

(ii) la découverte de l’épissage des introns du groupe I a montré que l’ARN peut se lier à de petites molécules, la guanosine ou l’un de ses dérivés, qui est un cofacteur obligatoire et spécifique de la réaction d’excision. (Bass and Cech 1984, *Figure 7*)

Un aptamère doté de fonction catalytique est nommé ribozyme (pour 'ribonucleotide enzyme'). Le prix Nobel de chimie en 1989 a été attribué à Sidney Altman et Thomas R. Cech pour leur découverte indépendante en 1982 des propriétés catalytiques des ARN. Les ribozymes sont des molécules d'ARNs catalytiques, fonctionnant dans l'eau, en présence de sels (K^+, Na^+, Mg^{2+}) et en absence de facteurs protéiques.

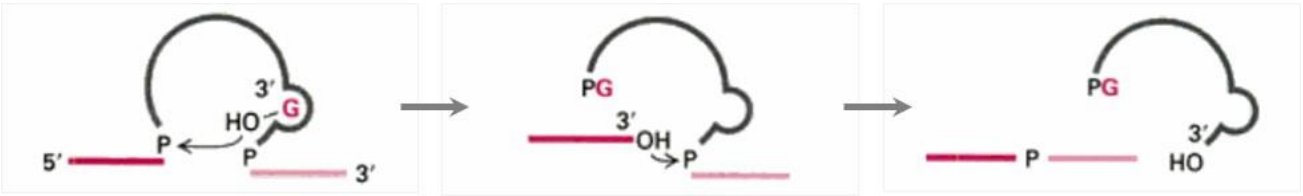

Figure 7. **Mécanisme de l'épissage par les introns du groupe I, doués d'auto-excision.** L'intron est représenté en noir et les exons à relier en rose. Un cofacteur, la guanosine (G), s'associe au site actif. Le groupement 3' hydroxyle de la guanosine participe à une réaction de trans-estérification avec le phosphate de l'extrémité 5' de l'intron. (Lodish et al., 2005).

… à la sélection d'aptamères artificiels

La découverte des aptamères naturels a donné naissance, en 1990, à la technique nommée SELEX ('selective evolution of ligand by exponential enrichment'), simultanément par trois équipes américaines indépendantes :

- Larry Gold et son étudiant en fin de thèse, Craig Tuerk (Université du Colorado, Boulder), ont utilisé le terme SELEX pour leur procédé de sélection d'ARN, ligands de la T4 ADN polymérase (Tuerk & Gold, 1990).
- Andy Ellington et Jack Szostak (Massachusetts General Hospital, Boston) ont publié une technique qu'ils ont nommé 'sélection *in vitro*' pour sélectionner des ARNs dirigés contre différents colorants organiques. Andy Ellington a donné le nom aux 'aptamères' (Ellington & Szostak, 1990).
- Gerald Joyce et Debra Robertson (Scripps Institute, La Jolla, Californie) ont sélectionné le premier ribozyme ('RNA enzyme') artificiel, doué de propriétés catalytiques par clivage spécifique d'un ADN simple brin (Robertson & Joyce, 1990).

A2. SELEX

Le SELEX est une technique de sélection *in vitro* (ou d'évolution *in vitro*) pour la production d'aptamères, qui permet le criblage de grandes banques d'acides nucléiques

(comprenant jusqu'à 10^{15} séquences différentes synthétisées de façon aléatoire) contre des cibles diverses (qui peuvent ou non être des molécules liant naturellement des acides nucléiques), telles que : ions, petites molécules organiques (théophylline, dopamine…), nucléotides et dérivés, antibiotiques, oligonucléotides, acides aminés, peptides, protéines, sucres, virus, parasites, bactéries, cellules... Lors de cette technique de criblage, les composés de la banque sont tous mis en contact en même temps avec la cible, contrairement aux criblages décrits dans la première partie de ce document, où les composés étaient injectés successivement sur la cible.

La méthode SELEX consiste à réaliser des cycles successifs de sélection (de plus en plus stringents) et d'amplification permettant d'enrichir la population en candidats possédant les propriétés requises. Clonage et séquençage permettent d'identifier les ligands oligonucléotidiques (aptamères) ayant de fortes affinités pour leurs cibles (*Figure 8*).

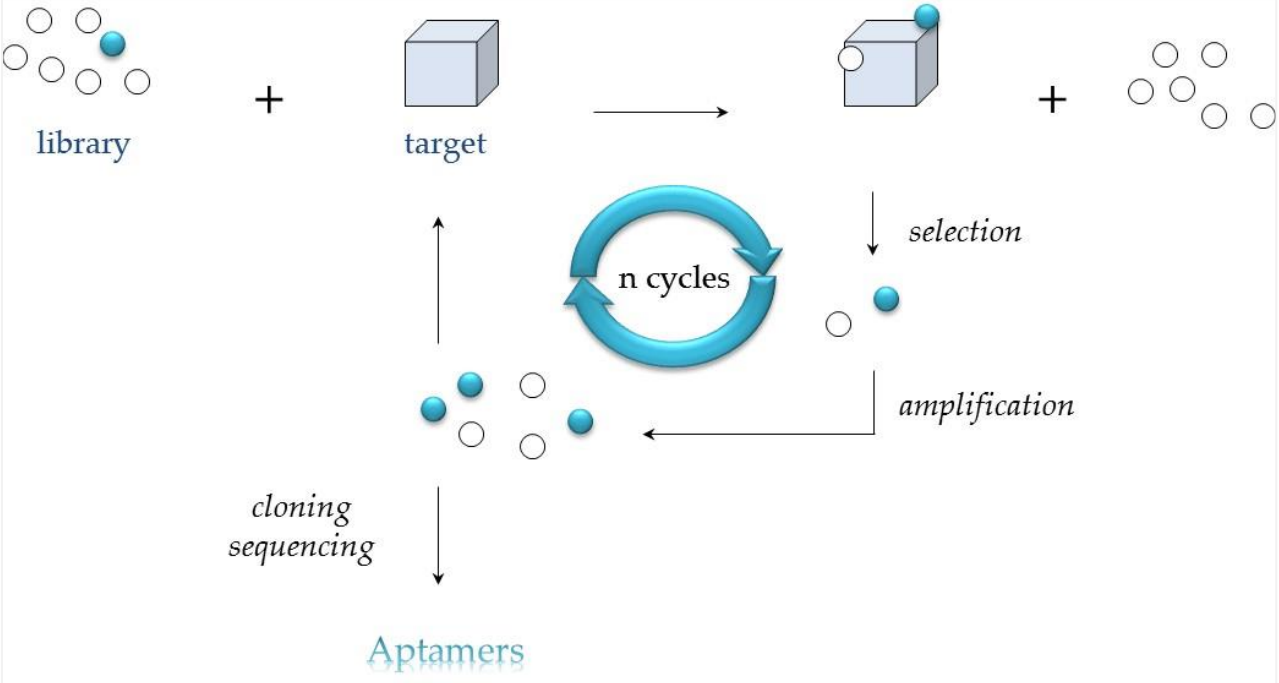

Figure 8. **Principe du SELEX**.

A3. Aptamères versus anticorps

Les aptamères sont des acides nucléiques capables de lier une cible avec une forte spécificité et une grande affinité. Ils sont généralement comparés aux anticorps. De poids moléculaire variant en moyenne de 8 à 25 kDa, les aptamères sont de taille intermédiaire entre

les anticorps (150 kDa) et les petits peptides (1-5 kDa). Etant des polyanions, les aptamères sont de composition différente des anticorps. En tant que molécules synthétiques, les aptamères peuvent être facilement modifiés chimiquement.

Dans la littérature, on leur prête bien des qualités par rapport aux anticorps, telles que leur plus petite taille, leur facilité et faible coût de synthèse, leur caractère non immunogène et leur faible toxicité, leur stabilité. En outre, les aptamères sont identifiés grâce à un processus de sélection *in vitro*, qui ne nécessite pas l'utilisation d'animaux ou de cellules. De ce fait, ils peuvent être générés contre des toxines ou des molécules n'engendrant pas de réponse immunitaire (*Tableau 1*).

Aptamers	**Antibodies**
Size: > 10 000 Da	Size: 150 000 Da
K_D: low nM - pM range	K_D: low nM - pM range
Selection is an *in vitro* process that can target any small molecule, biopolymer or cell	Selection requires a biological organism and is inefficient with toxins (not tolerated by animals) and small non-immunogenic molecules
Selection is an iterative process and usually requires 5-10 rounds or more (varied from target to target)	Screening of mAb is expensive and time consuming
Uniform activity regardless of the batch	Activity of antibodies varies from batch to batch
Wide variety of chemical modifications are introduced to diversify properties and functions	Very limited modifications
Return to original conformation after temperature insult (reversibly denatured)	Temperature sensitive. Irreversible denaturation
Unlimited shelf-life	Limited shelf-life
No evidence of immunogenicity	Significant immunogenicity
Cross-reactive compounds can be isolated using toggle strategy to facilitate preclinical studies	No method for isolating cross-reactive compound
Aptamer-specific antidote can be developed to reverse the inhibitory activity of the drug	No rational method to reverse molecules

Tableau 1. **Comparaison anticorps - aptamères** (adapté de Jayanesa, 1999 et Nimjee et al., 2017).

Il faut toutefois noter que :

- sélection et caractérisation d'aptamères ne sont pas si rapides ni si simples, surtout dans le cas d'un SELEX sur cellules (cell-SELEX)
- à l'heure actuelle, la preuve de la faible immunogénicité et de la moindre toxicité des aptamères semble être basée uniquement sur des essais cliniques de phase I et de phase II du produit 'Mucagen' (voir ci-dessous).
- les aptamères sont modifiables pour augmenter leur stabilité et leur résistance à l'action des nucléases. L'impact de cette augmentation de stabilité en santé humaine et sur l'environnement n'est pas connu.

Aptamères et anticorps sont plutôt complémentaires qu'opposables. Mais alors, pourquoi le marché des anticorps est-il tellement prometteur alors que le marché des aptamères n'en est qu'à ses prémices ?

- Les nombreux brevets technologiques sur le SELEX et ses applications ont probablement freiné les 20 premières années de développement des aptamères en diagnostique et clinique, par rapport à la technologie non brevetée des anticorps monoclonaux.
- Des milliers de laboratoire développent ou utilisent en routine des anticorps monoclonaux, et ce depuis des années. Les aptamères doivent donc franchir des fossés pour se faire une place.
- Malgré le nombre d'aptamères disponibles contre des milliers de cibles de natures différentes, la procédure de sélection des aptamères n'est pas toujours efficace. On estime à 30% le nombre de SELEX infructueux. Un SELEX pourrait ne pas être fructueux à cause de contre-sélections non efficaces, ou à cause des 'tags' (utilisés pour immobiliser les protéines ciblées dans certains processus de sélection), eux aussi potentiellement 'aptagènes', ou parce que les acides nucléiques sont chargés négativement et donc difficiles à sélectionner contre des cibles acides. Ce chiffre de 30% n'a jamais été publié. Il est d'ailleurs invérifiable. Mais il est régulièrement avancé par les spécialistes des aptamères.
- On avance souvent le fait que les acides nucléiques ne fonctionnent qu'à un code à 4 lettres (nucléotides), ce qui restreindrait leurs caractéristiques biophysiques comparé aux protéines dont le code comprend 20 lettres (acides aminés). Toutefois, les spécificités et caractéristiques des aptamères ne sont pas directement déterminées par la séquence primaire mais bien par leur structure tertiaire. Les aptamères peuvent adopter un grand nombre de conformations, ce qui explique leur faculté à se lier à différentes cibles. D'autre part, la chimie des acides nucléiques connaît ces dernières années des progrès fulgurants (*Figure 9*). De nombreuses équipes de recherche créent de nouveaux nucléotides synthétiques, nommés XNA ('xeno nucleic acid'), entraînant ainsi une 'explosion' du code génétique ('expanded genetic code', Pinheiro & Holliger, 2014). Le marché des aptamères n'a probablement pas encore livré tous ses secrets.

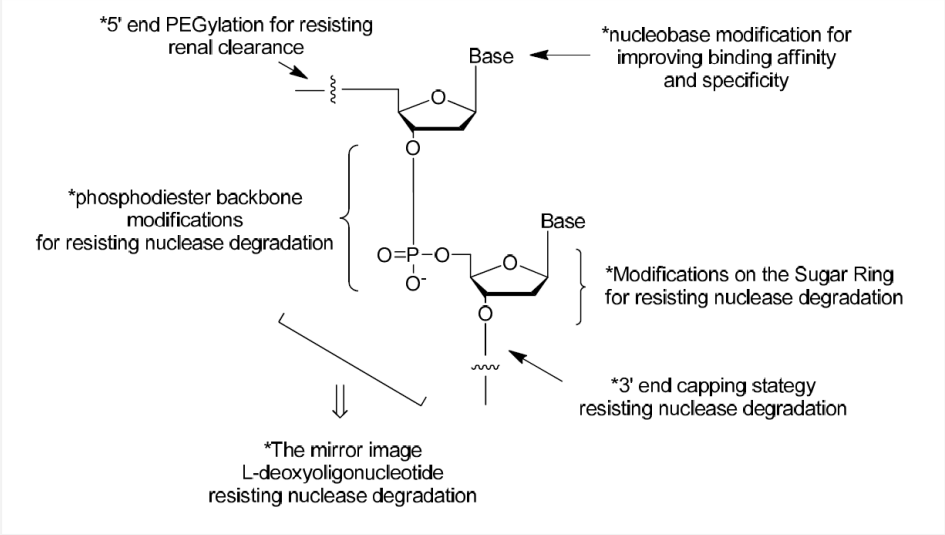

Figure 9. Diversité des modifications chimiques des aptamères (Ni et al., 2017).

A4. Aptamères en développement clinique

Les aptamères, en tant qu'agents thérapeutiques alternatifs aux anticorps, ont déjà trouvé leur place dans diverses applications thérapeutiques. Un médicament est sur le marché, et une douzaine sont en phase clinique, en tant qu'agents anti-angiogéniques, anti-coagulants, en oncologie, pour le traitement du diabète ou de l'hémophilie (*Tableau 2*).

Name	**Target**	**Form & Modifications**	**ClinicalTrials.gov identifier (current status)** ph means 'phase'	**Indication**	**Company**
Macular degeneration					
Macugen pegaptanib sodium	**$VEGF_{165}$**	27-nt **RNA** 2′-fluoropyrimidines 2′-*O*-methyl purines 3′-inverted dT 40 kDa PEG	NCT00021736 (ph II/III,completed) NCT00040313 (ph II, completed) NCT00056199 (ph I, completed) NCT00312351 (ph IV, terminated) NCT00321997 (ph II/III, completed) NCT01487070 (ph I, completed)	Age-related macular degeneration ; Diabetic macular oedema ; Proliferative diabetic retinopathy	Eyetech Pharmaceuticals Inc / Pfizer
ARC1905	**C5**	38-nt **RNA** 2′-fluoropyrimidines 2′-*O*-methyl purines 3′-inverted dT 40 kDa PEG	NCT00709527 (ph I, completed) NCT00950638 (ph I, completed) NCT02397954 (ph II, completed) NCT02686658 (ph II/III, recruiting)	Age-related macular degeneration ; Idiopathic polypoidal choroidal vasculopathy ; Geographic atrophy	Ophthotech Corp. / Archemix Corp.
E-10030	**PDGF**	29-nt **DNA** 2′-*O*-methyl purines 3′-inverted dT 40 kDa PEG	NCT00569140 (ph I, completed) NCT01089517 (ph II, completed) NCT02387957 (ph II, recruiting) NCT02591914 (ph I, ongoing) NCT01940887 (ph III, recruiting) NCT01940900 (ph III, ongoing) NCT01944839 (ph III, recruiting)	Age-related macular degeneration	Ophthotech Corp. / Archemix Corp. / Retinal Consultants of Arizona

Coagulation					
REG1 anticoagulation system (RB006 plus RB007)	**Coagulation factor IXa**	RB006 (drug): 31-nt **RNA** aptamer 2′-ribo purine or 2′-fluoropyrimidine 40 kDa PEG RB007 (antidote): 15-nt 2′-*O*-methyl	NCT00113997 (ph I, completed) NCT00715455 (ph II, completed) NCT00932100 (ph II, completed) NCT01872572 (ph I, completed) NCT01848106 (ph III, terminated, clinical hold owing to serious anaphylactic reactions)	Acute coronary syndrome ; Cardiac catheterization (intravenous form) ; Coronary artery disease ; Percutaneous coronary intervention	Regado Biosciences / Archemix Corp.
ARC1779	**A1 domain of von Willebrand factor**	39-nt **DNA** 3′-inverted dT 2′-*O*-methyl with a single phosphorothioate linkage 20 kDa PEG	NCT00432770 (ph I, completed) NCT00507338 (ph II, terminated) NCT00632242 (ph II, completed) NCT00694785 (ph II, withdrawn prior to enrolment) NCT00742612 (ph II, terminated)	von Willebrand disease ; Thrombotic thrombocytopaenic purpura ; von Willebrand disease type 2b ; Acute myocardial infarction ; Percutaneous coronary intervention ; Thrombosis	Archemix Corp.
NU172	**Thrombin**	26-nt **DNA** Unmodified	NCT00808964 (ph II, unknown)	Heart disease (for example, used during cardiopulmonary bypass to maintain steady state of anticoagulation)	ARCA Biopharma / Archemix Corp.
ARC 183 (HD1 ; G15D ; HTQ)	**Thrombin**	15-nt **DNA** G-rich DNA Unmodified	phI, completed, but not in development	Acute cardiovascular settings	Archemix Corp. / Nuvelo
ARC19499 (BAX499)	**TFPI**	32-nt **RNA** 2′-*O*-methyl purine 3′-inverted dT 40 kDa PEG	NCT01191372 (ph I, terminated)	Haemophilia	Baxalta US / Archimex
Oncology					
AS1411 (AGRO001)	**Nucleolin**	26-nt **DNA** G-rich DNA Pegylated	NCT00512083 (ph II, completed) NCT00740441 (ph II, unknown) NCT00881244 (ph I, completed) NCT01034410 (ph II, terminated)	Acute myeloid leukaemia ; Metastatic renal cell carcinoma ; Advanced solid tumour	Antisoma / Archemix Corp.
NOX-A12	**CXCL12**	45-nt **RNA** (Spiegelmer) L-ribonucleic acid Pegylated	NCT00976378 (ph I, completed) NCT01194934 (ph I, completed) NCT01521533 (ph II, completed) NCT01486797 (ph II, ongoing, but not recruiting)	Multiple myeloma and non-Hodgkin lymphoma ; Chronic lymphocytic leukaemia ; Autologous stem cell transplantation ; Haematopoietic stem cell transplantation	NOXXON Pharma
Inflammation					
NOX-E36	**CCL2**	40-nt **RNA** (Spiegelmer) L-ribonucleic acid Pegylated	NCT00976729 (ph I, completed) NCT01085292 (ph I/II, completed) NCT01372124 (ph I, completed) NCT01547897 (ph II, completed)	Chronic inflammatory diseases ; Type 2 diabetes mellitus ; Systemic lupus erythematosus ;	NOXXON Pharma

				Albuminuria ; Renal impairment	
NOX-H94	**Hepcidin peptide hormone**	44-nt **RNA** (Spiegelmer) L-ribonucleic acid Pegylated	NCT01372137 (ph I, completed)2 NCT01522794 (ph I, completed) NCT01691040 (ph II, completed) NCT02079896 (ph I/II, completed)	Anaemia ; End-stage renal disease ; Anaemia of chronic diseases ; Inflammation	NOXXON Pharma

Tableau 2. **Aptamères dans les différentes phases de développement clinique** (d'après Esposito et al., 2011a ; Ni et al. 2011 ; Sundaram et al., 2013 ; Sun et al., 2014 ; Darmostuk et al., 2015 ; Gopinath et al., 2016 ; Camorani & Cerchia, 2015 ; Zhou & Rossi., 2017).

Le pegaptanib sodium (Macugen), commercialisé par Eyetech Pharmaceuticals/Pfizer, est le premier aptamère approuvé par la FDA ('Food and Drug Administration'), en décembre 2004, pour traiter les patients atteints de dégénérescence maculaire liée à l'âge (DMLA) de forme humide. Cette maladie touche la partie centrale de la rétine (la macula), à l'arrière de l'oeil, et provoque une perte de la vision centrale, pouvant aller jusqu'à la cécité. La forme humide de la maladie est provoquée par le développement de vaisseaux sanguins anormaux sous la rétine et la macula qui peuvent saigner et conduire à un épanchement, entraînant une perte de la vision. Le pegaptanib est un aptamère ARN (*Figure 10*) ciblant le VEGF-165 ('vascular endothelial growth factor'), facteur pro-angiogénique (néovascularisation occulaire pathologique et perméabilité vasculaire), avec un K_D de 0.1 nM (Ng et al., 2006).

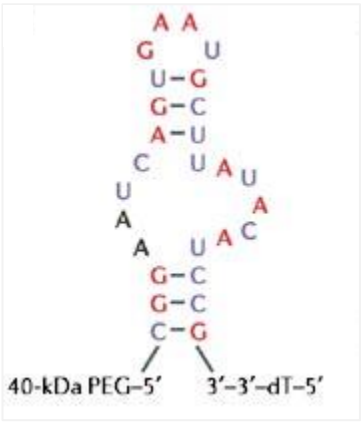

Figure 10. **Séquence du pegaptanib sodium**, ARN de 28 nucléotides. Quatre années ont été nécessaires pour modifier l'aptamère, le rendre résistant aux dégradations enzymatiques et augmenter sa biodisponibilité. Les deux ribonucléotides non modifiés sont en noir. Les purines substituées par des groupements 2'-O-méthyls et les pyrimidines substituées par des groupements 2'-fluoro sont en rouge et bleu, respectivement. L'extrémité 5' de l'ARN contient deux chaînes de PEG ('polyethylene glycol') de 20 kDa, et à l'extrémité 3', une thymidine est liée par un lien 3'-3' à la méthoxyguanosine qui la précède.

La date de l'AMM ('Autorisation de Mise sur le Marché') européenne date du 31 janvier 2006 et sa commercialisation en France date de juin 2006. Depuis l'évaluation initiale de son intérêt thérapeutique, aucune étude n'a comparé le pegaptanib aux autres anti-VEGF, mais les données cliniques ont montré que les anti-VEGF les plus récents (ranibizumab et aflibercept) amélioraient l'acuité visuelle alors que le pegaptanib permettait seulement de diminuer la perte d'acuité visuelle (http://www.has-sante.fr/portail/jcms/c_1714255/en/macugen-pegaptanib-anticorps-monoclonal-anti-vegf). En conséquence, le pegaptanib n'a plus de place dans la prise

en charge de la DMLA exsudative et sa commercialisation en France s'est arrêtée le 17 octobre 2014. Il a néanmoins ouvert la voie des aptamères thérapeutiques.

'Regado Bioscience' a mis au point un médicament, REG1 (*Figure 11*), testé dans des essais cliniques de phase III lors d'angioplasties. REG1 est composé de deux éléments :

- Pegnivacogin (RB006), l'aptamère ciblant le facteur de coagulation IXa
- Anivamersen (RB007), l'oligonucléotide complémentaire antidote (antisens) au RB006

L'antidote agit comme compétiteur. Il permet de dissocier l'aptamère de sa cible protéique et donc de contrôler les hémorragies (effet secondaire de l'anti-coagulant). Les molécules antidotes complémentaires d'aptamères sont faciles à concevoir. Elles pourraient trouver intérêt dans diverses applications thérapeutiques.

L'essai clinique de phase III (NCT01848106) de comparaison de l'aptamère pegnivacogin à la bivalirudine (un inhibiteur direct et spécifique de la thrombine) s'est toutefois terminé à un stade précoce, à cause de réactions allergiques importantes rapportées chez 1% des patients recevant le pegnivacogin (Povsic et al., 2016 ; Lincoff et al., 2016 ; Verheugt 2016). Il semblerait toutefois que ni l'acide nucléique ni ses produits de dégradation ne soient responsables des réactions allergiques. Elles seraient vraisemblablement dues au groupement polyéthylène glycol (PEG), couplé à l'extrémité de l'aptamère. De forts taux d'anticorps anti-PEG ont été quantifiés chez les patients ayant développé des réactions allergiques (Ganson et al., 2016).

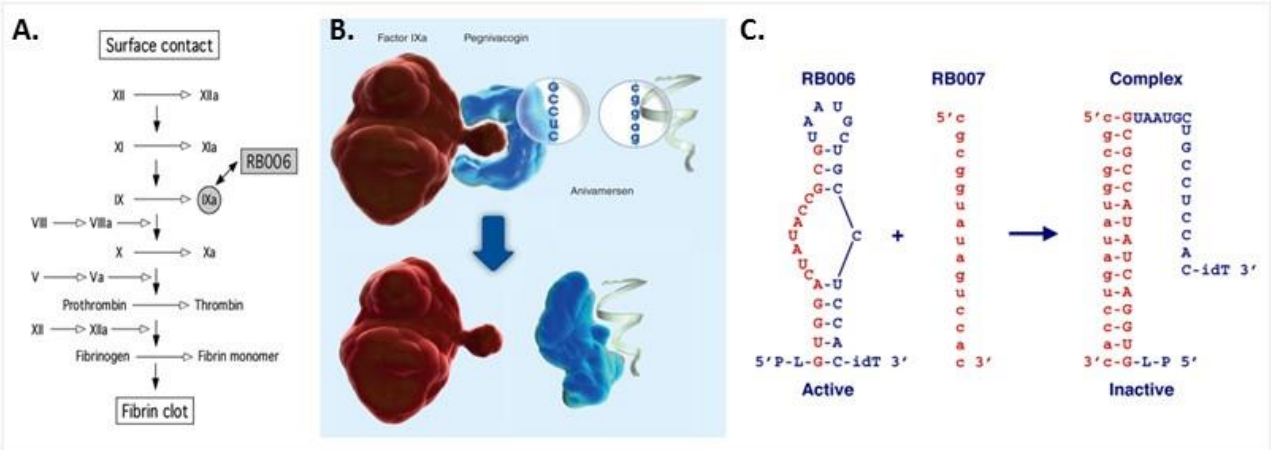

Figure 11. **REG1**. **A.** Cascade de coagulation sanguine. **B.** Schéma illustrant le mode d'action du REG1. **C.** Mode d'action plus détaillé de l'interaction entre le pegnivacogin (RB006) et l'anivamersen (RB007). (d'après Vallalle & Cohen, 2012 ; Rusconi et al., 2004).

A5. Aptamères - un vaste domaine en pleine expansion

Une analyse des publications scientifiques recensées dans PubMed permet d'évaluer l'importance des travaux de recherche sur le sujet. Fin 2017, on compte sur cette base 7612 et 2000 publications pour des recherches avec les mots 'aptamer' et 'SELEX', respectivement. 50% des publications sont recensées depuis 2013 (*Figure 12*).

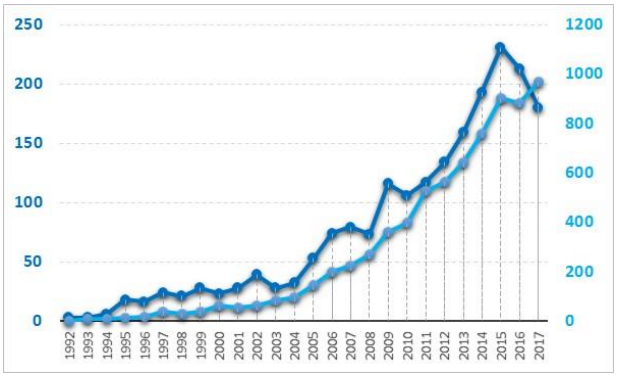

Figure 12. **Nombres de publications** répertoriées dans Pubmed jusqu'à fin 2017, avec les mots clés '**SELEX**' et '**aptamer**'.

Les aptamères intéressent les grandes sociétés du domaine médical et pharmaceutique ainsi que les entreprises axées sur les biotechnologies. 441 brevets sur les aptamères sont recensés sur la base française de l'INPI ('Institut National de la Propriété Intellectuelle') et plus de 3600 brevets sur la base européenne de l'EPO ('European Patent Office').

La littérature concernant les aptamères est extrêmement diversifiée. Certaines applications biochimiques, diagnostiques et thérapeutiques des aptamères (Gijs et al., 2015 ; Xiang et al., 2015b ; Zhou et al., 2016) seront commentées dans la discussion de ce manuscrit, lorsqu'elles ont rapport aux perspectives de mon projet de recherche actuel. Ci-dessous, j'ai tout de même souhaité commenter des travaux, qui présentent, à titre personnel, un intérêt particulier, du monde à ARN il y a 3,8 milliards d'années, à la thérapie du futur.

'RNA world'

L'hypothèse du monde à ARN ('RNA world', Gilbert, 1986) arrive en tête dans les scénarii de l'évolution (Maurel, 2005). L'ARN, aux origines du vivant il y a 3,8 milliards d'années, serait le précurseur de toutes les macromolécules biologiques, puisqu'il permet à la fois

d'assurer des fonctions métaboliques (catalyseur) et d'être le support d'une information génétique. En effet, l'ARN est la seule molécule qui soit à la fois mémoire et action.

L'hypothèse du monde à ARN suggère qu'à une certaine étape de l'évolution, la réplication et l'expression de l'information génétique (continuité génique) dépendent d'ARN ayant une fonction enzymatique (ribozymes). Le SELEX, technique d'évolution moléculaire dirigée *in vitro*, a d'ores et déjà permis la sélection de ribozymes synthétiques capables de catalyser plusieurs réactions chimiques telles que clivage, liaison (de nucléotides les uns aux autres ; d'acides aminés à l'ARN), oxydo-réduction... Récemment, Horning et Joyce (2016) ont rapporté l'évolution *in vitro* d'un ribozyme ayant une fonction de polymérase à ARN capable de synthétiser des molécules d'ARN structurées fonctionnelles et de répliquer de courtes séquences d'ARN (riboPCR), à partir d'un ARN matrice structuré et riche en C.

Les expériences tentant de faire naître la vie dans un tube à essai et les preuves démontrant l'hypothèse d'un monde à ARN sont de plus en plus nombreuses et fructueuses. Dans l'hypothèse du monde à ARN, il resterait à comprendre l'apparition des premiers nucléotides.

SOMAmers ('slow off-rate modified aptamers')

Larry Gold, l'un des pères du SELEX, a fondé NeXagen (devenue plus tard NeXstar Pharmaceuticals, avant de fusionner en 1999 avec Gilead Sciences, Inc.), puis, en 2000, SomaLogic (Boulder, http://www.somalogic.com). SomaLogic® commercialise des essais SOMAscan® (une technologie de découverte et validation de biomarqueurs) associés aux SOMAmers® ('slow off-rate modified aptamers', spécifiques de protéines).

Les SOMAmers sont des aptamères ADN :

- obtenus de banques modifiées par des dUTPs (*Figure 13*). Cette modification permet la sélection de SOMAmers contre des cibles protéiques qualifiées de 'difficiles' car la sélection d'aptamères non modifiés n'avait jamais abouti contre ces cibles. Cette modification leur confère, en outre, une forte affinité, puisque la plupart des SOMAmers sélectionnés ont des K_D < nM (Gold et al., 2010)
- sélectionnés pour des k_{off} > 30 min. Ce temps de dissociation long permet de détruire sélectivement les interactions non-spécifiques par compétition avec un large excès de compétiteur poly-anionique (sulfate de dextran), et donc d'augmenter leur spécificité

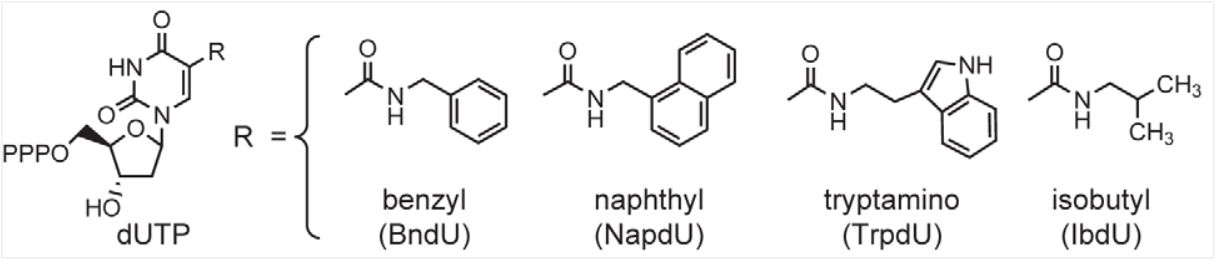

Figure 13. **Nucléotides modifiés** (Gold et al., 2010). Analogues de nucléotides triphosphates modifiés en position 5 (R) de l'uridine (dUTP): 5-benzylaminocarbonyl-dU (BndU); 5-naphthylmethylaminocarbonyl-dU (NapdU): 5-tryptaminocarbonyl-dU (TrpdU); et 5-isobutylaminocarbonyl-dU (iBudU).

Le principe du SOMAscan est représenté ci-dessous (*Figure 14*).

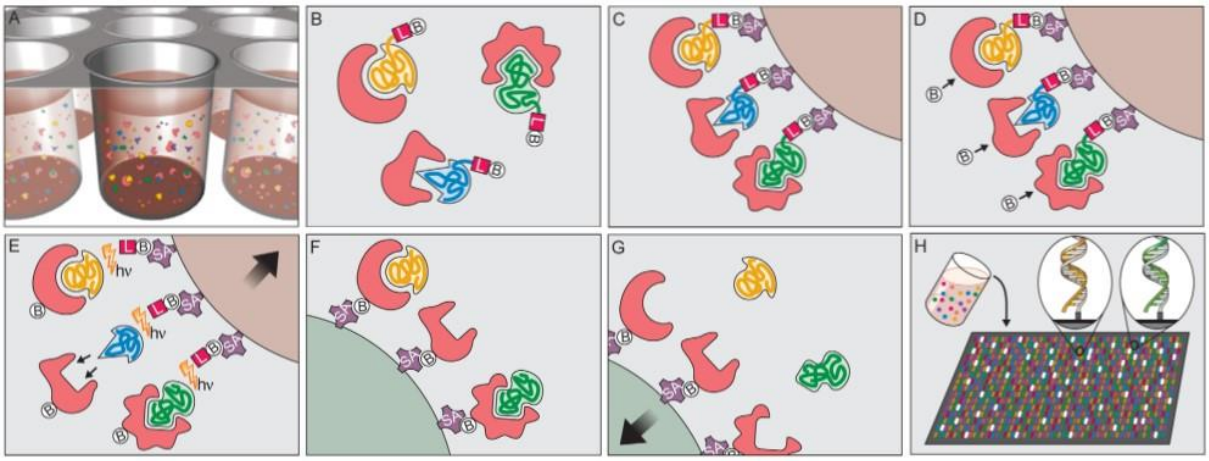

Figure 14. **Principe du SOMAscan** (Gold et al., 2010). **A**. SOMAmers et échantillons sont mis en contact dans des plaques de 96 puits. Les interactions moléculaires peuvent avoir lieu. **B**. Liaison entre les SOMAmers (en jaune, vert et bleu) et les protéines de l'échantillon (en rouge). Les SOMAmers sont biotinylés (B), contiennent une liaison photo-clivable (L) et un 'tag' fluorescent. Les SOMAmers représentés en vert et jaune forment des complexes avec leur protéine cible. Le SOMAmer bleu forme un complexe avec une protéine qui n'est pas sa protéine cible. **C**. Les SOMAmers sont capturés sur des billes greffées par des streptavidines (SA). Les protéines non complexées sont lavées. **D**. Les protéines sont 'taggées' avec un groupement biotine-NHS (B). **E**. Le lien (L) est clivé sous UV, et les SOMAmers sont libérés des billes de streptavidine. Un compétiteur anionique (sulfate de dextran) est ajouté pour dissocier les complexes de faibles K_D (ici le complexe avec le SOMAmer bleu). **F**. Les complexes protéines-SOMAmers restant sont capturés sur les billes greffées par des avidines. Les SOMAmers non complexés sont lavés. **G**. Les SOMAmers sont dissociés des complexes à pH élevé. **H**. Les SOMAmers restant sont quantifiés par hybridation (microarray) à des sondes d'ADN simple brin complémentaires aux séquences des SOMAmers. La double hélice ainsi formée est détectée par le tag fluorescent.

A l'heure actuelle, les SOMAmers permettent de détecter et quantifier environ 4000 protéines humaines à partir de petits volumes (15 µl) d'échantillons biologiques humains tels que sang, urine, tissus… Une grande étude de recherche de biomarqueurs, à partir de matrices saines ou malades (maladies cardiaques, Alzheimer, myopathie de Duchenne, plusieurs cancers, régimes divers…) est en cours à SomaLogic.

Associé à l'Université d'Oxford (GB) depuis août 2016, SomaLogic a comme objectif de surveiller la santé d'un individu dans le temps en mesurant les modifications de la composition protéique d'échantillons biologiques par le suivi de groupes de marqueurs. Ainsi pourraient être détectées rapidement les signatures protéiques de plusieurs maladies. Par exemple, les biomarqueurs de cancers pourraient être détectés dans le sang. Il serait également possible de mesurer l'effet de régimes, l'état physique, la réponse à diverses thérapies... Ces analyses permettraient, d'après Larry Gold, à chaque individu, de surveiller son état de santé dans le temps et donc d'améliorer sa qualité de vie, pour un coût estimé à 100 $/ année et un test éventuellement réalisé à la maison à partir d'une goutte de sang.

A6. Aptamères ciblant des biomarqueurs cellulaires

Revue 2

Les protéines membranaires représentent environ 30% des protéines codées par le génome eukaryote (Fry, & Clemons., 2018). Elles sont les acteurs primaires de communication entre les cellules et leur environnement externe. Les interactions entre ces protéines et leurs ligands conditionnent la réponse cellulaire via différentes voies de signalisation. Contrairement aux protéines intracellulaires, les protéines de surface sont très facilement accessibles à des ligands extracellulaires. Elles sont donc les cibles privilégiées des molécules thérapeutiques et diagnostiques. Selon le réseau DT-networks (‘drug target networks’, 60% des médicaments approuvés par la FDA (‘food and drug administration’) et 40% des molécules en phases expérimentales ciblent des protéines membranaires (*Figure 15*).

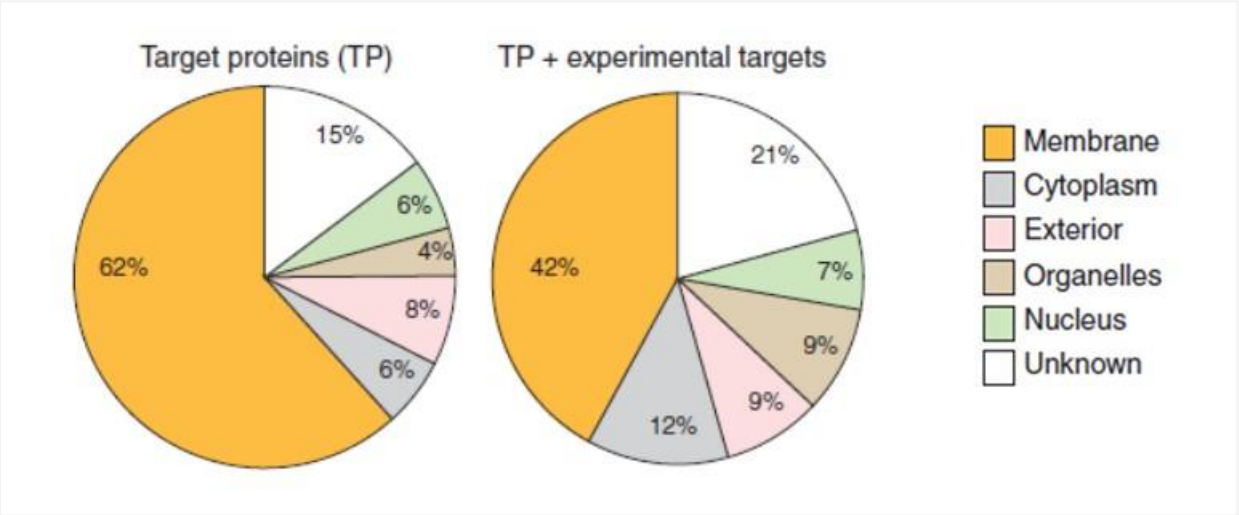

Figure 15. **Distribution cellulaire des cibles** de molécules approuvées par la FDA et expérimentales (Yildirim et al., 2007).

Plusieurs aptamères ciblant des biomarqueurs tumoraux de surface cellulaire ont été identifiés, principalement par ‘cell-SELEX’ et par SELEX classique (‘protein-SELEX’). Nous les avons récemment décrits dans une revue, ainsi que les avantages et désavantages de ces deux principales techniques de criblage, les applications des aptamères et les aptamères en phase clinique en oncologie. Cette revue (Mercier et al., 2017) est insérée ci-dessous (Revue 2).

Par rapport au SELEX classique pour lequel la cible est généralement une molécule isolée (souvent une protéine recombinante), la technique du cell-SELEX consiste à utiliser une cellule

entière et vivante en tant que cible. Cette méthode est beaucoup plus proche des conditions *in vivo* puisque les cibles sont dans leur forme native et dans leur environnement cellulaire.

La contre-sélection (ou sélection négative) est une étape du SELEX, décrite pour la première fois en 1994 (Jenison et al., 1994). Elle permet de s'affranchir des artéfacts de la sélection, à savoir les aptamères non-spécifiques de la cible (par exemple les séquences de la banque ayant la capacité de se fixer sur un filtre ou à une molécule de la colonne de chromatographie utilisée pour immobilier la cible, ou à un 'tag' de la protéine ciblée…) qui conduisent à sélectionner des séquences non désirées. Lors de la ou des étape(s) de contre-sélection, la banque est mise en contact avec l'élément ou la molécule non-désirée (typiquement le filtre ou la colonne de chromatographie sans cible, ou le 'tag' seul…). Les acides nucléiques qui ne s'y lient pas sont ensuite récupérés. Les cycles de sélection 'positive' sont réalisés de manière classique. Les étapes de contre-sélection sont évidemment particulièrement importantes lors d'un cell-SELEX, bien plus complexe qu'un SELEX classique.

Le terme 'cell-SELEX' est un peu ambigu. Il est important de différencier 2 manières différentes de l'appréhender, en fonction du ciblage d'une protéine prédéfinie, on non.

- Lorsque la cible est une cellule, ou plus précisément une lignée cellulaire :

Chaque lignée cellulaire affichant une signature moléculaire qui lui est propre, les aptamères sélectionnés sont décrits comme étant spécifiques d'une lignée cellulaire donnée. Ainsi des aptamères spécifiques des lignées de GBM U87-MG, U251, U118 et A-172 ont été rapportés (Cerchia et al., 2009 ; Kang et al., 2012 ; Bayrac et al., 2011). *A posteriori*, la cible spécifique d'un des aptamères sélectionné peut être déterminée par spectroscopie de masse (par exemple la protéine pigpen à partir de cellules endothéliales de rat YPEN-1, Blank et al., 2001 ou la tenascine-C, Daniels et al., 2003…).

- Lorsque la sélection vise une cible bien déterminée, généralement une protéine membranaire ayant une partie extracellulaire accessible, mais aussi d'autres cibles :

Les lignées cellulaires utilisées comme cibles sont généralement modifiées pour sur-exprimer la protéine d'intérêt. Ainsi des aptamères ciblant le variant III du récepteur à l'EGF ('Epidermal Growth Factor'), EGFRvIII, ont été sélectionnés sur des cellules U87-MG sur-exprimant cette protéine. La contre-sélection a été réalisée contre les cellules U87-MG 'wild-type'. Camorani et al (2014) ont utilisé la lignée cellulaire U87-MG exprimant la protéine PDGFRβ. Dans ce cas, il ne s'agit donc pas d'une lignée cellulaire sur-exprimant la protéine ciblée. Mais la même lignée cellulaire, sous-exprimant PDGFRβ (par extinction de gènes) a été utilisée pour la contre-sélection. D'autres aptamères A1-A6 (Kim et al., 2013) spécifiques de CD133, un biomarqueur de cellules souches, ont été sélectionnés en utilisant des cellules initiatrices de tumeurs (TIC)

en tant que cible. L'aptamère TTA1 est un ligand de la tenascine-C. Les cellules U251 expriment cette protéine. Aucune étape de contre-sélection n'a été réalisée. Mais une autre méthode, nommée 'cross-over SELEX', également nommé 'hybrid-SELEX', a été appliquée pour sélectionner des ligands spécifiques de la tenascine-C. En plus des cycles de cell-SELEX, quelques cycles de SELEX 'classique' sur la protéine purifiée ont été réalisés (Hicke et al., 2001). Un cross-over SELEX a également été utilisé pour sélectionner un aptamères ADN ciblant la sous-unité β4 de l'intégrine α6β4 (Berg et al., 2016).

Beaucoup de protéines membranaires ont été ciblées par des aptamères, soit par un SELEX 'classique' en utilisant des protéines recombinantes comme cible, soit par un cell-SELEX en déterminant la cible *a posteriori* (Dua et al., 2011). Un article décrit un cell-SELEX pour lequel la cible pré-déterminée n'a pourtant pas été la cible des aptamères sélectionnés. Cibiel et al. (2014) ont réalisé un cell-SELEX ciblant la protéine ET_BR ('Endothelin type B receptor') sur-exprimée à la surface des cellules CHO-K1. Malgré plusieurs étapes de contre-sélection sur les cellules CHO-K1, plusieurs aptamères ont été identifiés, mais aucun ne permettait de discriminer parmi les deux types cellulaires. Une recherche de cible de l'aptamère ACE4 *a posteriori* a donc été entreprise. La cible déterminée s'avère être l'annexin-2, une protéine sur-exprimée à la surface de plusieurs cellules tumorales.

Revue 2

Mercier, M.-C., Dontenwill, M. & Choulier, L.* (2017). Selection of nucleic acid aptamers targeting tumor cell-surface protein biomarkers. *Cancers*. **9**(6), pii: E69. doi: 10.3390/cancers9060069. (*corresponding author).

cancers

MDPI

Review

Selection of Nucleic Acid Aptamers Targeting Tumor Cell-Surface Protein Biomarkers

Marie-Cécile Mercier, Monique Dontenwill and Laurence Choulier *

UMR 7213 CNRS, Laboratoire de Biophotonique et Pharmacologie, Tumoral Signaling and Therapeutic Targets, Université de Strasbourg, Faculté de Pharmacie, 67401 Illkirch, France;
marie-cecile.mercier@unistra.fr (M.-C.M.); monique.dontenwill@unistra.fr (M.D.)
* Correspondence: laurence.choulier@unistra.fr; Tel.: +33-36885-4197; Fax: +33-36885-4313

Academic Editor: Samuel C. Mok
Received: 9 May 2017; Accepted: 13 June 2017; Published: 21 June 2017

Abstract: Aptamers are nucleic acids referred to as chemical antibodies as they bind to their specific targets with high affinity and selectivity. They are selected via an iterative process known as 'selective evolution of ligands by exponential enrichment' (SELEX). Aptamers have been developed against numerous cancer targets and among them, many tumor cell-membrane protein biomarkers. The identification of aptamers targeting cell-surface proteins has mainly been performed by two different strategies: protein- and cell-based SELEX, when the targets used for selection were proteins and cells, respectively. This review aims to update the literature on aptamers targeting tumor cell surface protein biomarkers, highlighting potentials, pitfalls of protein- and cell-based selection processes and applications of such selected molecules. Aptamers as promising agents for diagnosis and therapeutic approaches in oncology are documented, as well as aptamers in clinical development.

Keywords: aptamer; SELEX; cell-surface biomarker

1. Introduction

Nucleic acid aptamers are single stranded DNA (ssDNA) or RNA molecules. They are selected through a fully in vitro well-established iterative process known as 'selective evolution of ligands by exponential enrichment' (SELEX) [1–3]. A large library of 10^{14}–10^{15} ssDNA or RNA sequences of 20–50 variable bases is combined with a target, under temperature and buffer conditions dependent on requirements. During the partitioning step, nucleic acid molecules which bind to the target are selected while the vast majority of sequences which do not bind are washed away. Binding molecules are amplified thanks to the fixed primer-binding sequences flanking the variable region, by PCR or RT-PCR according to the nature of the oligonucleotide, ssDNA or RNA. Double-stranded DNA molecules are then separated from ssDNA in DNA-SELEX, or in vitro transcribed in RNA-SELEX by means of a T7-RNA polymerase binding site in the fixed region. The three steps (selection, partitioning and amplification) constitute a round of SELEX. Negative selection to environmental elements (usually supports of the SELEX process, like filters, beads ...) and/or counter selection to target's counterparts (like related proteins or cells) is usually performed, either before or after the positive selection, to eliminate non-specific binding nucleic acids. The rounds of selection are repeated several times, increasing stringency progressively, until molecules with the desired binding properties are cloned and sequenced. Those selected oligonucleotides are named aptamers, from the greek aptus ("to fit") and the suffix "-mer". Databases dedicated to aptamers provide information on targets of specific aptamers, length, molecular weight, extinction coefficient, GC (guanine-cytosine) content, chemistry, primary sequences, predictive secondary structures, as well as affinities, assay buffers ... (for example, [4–6]).

More than 900 aptamers have been generated from SELEX [7] towards a wide range of targets such as inorganic ions, small organic ligands, amino-acids, nucleotides and derivatives, oligonucleotides, antibiotics, peptides, proteins, sugars, parasites, virus, cells and tissues; the most common targets remaining proteins. In oncology, the aptamer field is rapidly expanding. On 3 May 2017, Medline listed 1398 entries for 'aptamer and cancer', including 167 reviews, with more than half entries published in the last 4 years. Deregulation of cell-surface membrane protein expressions and activities are hallmarks of cancer cells. Receptors that are uniquely expressed, overexpressed or mutated in tumors are major pharmaceutical targets for therapies in the era of personalized medicine. Advances in genomic, proteomic, metabolomic techniques led to the discovery of tumor biomarkers including cell surface receptors (tyrosine kinase receptors, cell adhesion receptors, cell death receptors) [8–10]. A vast majority of drugs are currently designed to target such proteins/receptors and to inhibit their oncogenic activities [11]. Recent data emphasized the high inter-and intra-tumoral heterogeneity of histologically similar tumors, at genomic but also protein levels of relevant targets [12,13]. Failure of clinical trials for targeted therapies in non-stratified patient populations may be linked to this underappreciated tumor heterogeneity. Highly specific tools, such as aptamers, may represent molecular probes for labeling the targets on tumor samples and thus helping to patient stratification. In addition, accessibility of cell surface receptors for targeting with aptamers will allow not only molecular imaging but also the direct delivery of drugs to relevant cancer cells [14].

The success of a SELEX process relates to the identification of aptamers of high affinities and specificities for their targets. Identification of aptamers is more complex for cell-surface proteins which activities depend on their conformation and on their cellular environment than for non-amphipatic molecules. To target cell surface biomarkers, it can therefore be important when possible to choose selection conditions and processes mimicking as far as possible the targets natural environment. This review will thus focus on the main selection strategies which have been used to identify aptamers to tumor cell-surface proteins, highlighting differences, success, and limitations of the SELEX processes. Tumor cell-surface biomarkers used as targets for SELEX are listed in Table 1. This review includes three more tables describing characteristics and applications of aptamers identified by protein- and cell-based SELEX, for which targets are proteins and cells, respectively. For cell-based SELEX, a distinction has been made between pre- and post-identified targets. Powerful potential applications of aptamers as diagnostic and therapeutic agents in the field of oncology will be briefly discussed and recent developments of the few aptamers already in clinical trials in oncology described.

Table 1. Major functions of biomarkers cited in this review.

Biomarker	Major Functions of Biomarker in Cancer
Cell-adhesion molecules	
Epithelial cell adhesion molecule-EpCAM (CD326)	EpCam is a pleiotropic molecule able to promote and prevent epithelial cell-cell adhesion. Induces proliferation, up-regulates proto-oncogene (c-myc, cyclins A/E) and is involved in migration, proliferation, differentiation and metastasis. Circulating tumor cell marker Implicated in self-renewal of stem cells
Carcinoembryonic antigen-CEA (CD66e)	Implicated in cell adhesion, anoikis resistance, promotion of metastasis
Integrin αvβ3	Essential for endothelial cell survival. Involved in cell growth and migration, tumor invasion, metastasis and angiogenesis
Integrin α6β4	Implicated in tumor cell growth, invasion and metastasis
Integrin αv	Endothelial adhesion receptor. Implicated in angiogenesis
Integrin α4	Prognostic marker in lymphocytic leukemia
E-and P-Selectin	Implicated in tumor cell adhesion to vascular endothelium, migration, proliferation of cancer cells and step of metastasis formation
L-Selectin	Roles in cell adhesion and in initiation of cell-cell interaction in vasculature system. Initiates events leading to leukocyte extravasations for the blood. Biomarker of naïve T cells

Table 1. *Cont.*

Biomarker	Major Functions of Biomarker in Cancer
Tyrosine kinase receptors	
EGFR	EGFR is a receptor tyrosine kinase expressed at the surface of cell. Involved in proliferation, invasion, angiogenesis and metastasis. Associated with poor prognosis
EGFRVIII	The most common form of EGFR mutation. Associated with poor survival of patients. Promotes tumor cell motility
PDGFR β	Cell surface tyrosine kinase receptor. Implicated in proliferation, migration and angiogenesis
HER-2	Belongs to ErbB family (EGFR, ErbB2). Implicated in formation, progression of human tumor, aggressiveness and resistance to therapy. Implicated in poor prognosis
HER-3	Member of the receptor tyrosine kinase. Contributes to increased drug resistance in HER2 cells
c-MET	Receptor tyrosine kinase involved in development and progression of cancer. Induces cell proliferation, cell survival, cell motility and invasion
Receptor tyrosine kinase-RET^{C634Y}	Mutated form of RET (proto-oncogene)
Neurotrophin receptor TrkB	Cancer cell resistance to chemotherapy. Promotes growth of cancer cells. Implicated in cell proliferation, differentiation, survival, and invasion
TGFβ III receptor	Role in signal transduction. Role in disease is poorly understood but correlates with higher tumor grade
Protein Tyrosine Kinase 7-PTK7	Biomarker for leukemia
Insulin Receptor	Receptor tyrosine kinase. Implicated in activation of MAPK/ERK and PI3K/AKT pathways
Axl	Implicated in cancer development and progression Belongs to TAM family of tyrosine kinase receptors. Implicated in invasiveness and metastasis
Cell membrane-associated enzyme	
Prostate specific membrane antigen-PSMA	Prostate tumor cell marker
Mucines	
MUC-1	Cell surface mucin glycoprotein
Tumor necrosis factor receptor (TNF-R) and co-stimulatory receptors	
T-cell receptor OX40	Member of TNF family receptors. Co-stimulatory receptor on CD4+ T cells. Increases immune response to cancer and foreign entities. Implicated in exacerbating effects of inflammation through the increased cytokine production (IL2) and in cell survival of CD4+ OX40+ T cells
T-cell receptor 4-1BB	Co-stimulatory receptor implicated in survival and expansion of activated T cells
Receptor activator of NF-κB-RANK	NFkB is a member of the tumor necrosis factor (TNF) receptor family. Implicated in osteoclast differentiation and in focal bone erosion and bone malignancies
CD28	Co-stimulatory receptor implicated in activation of T lymphocytes
Surface transmembrane glycoproteins	
CD133	Cancer stem cells marker
CD30 TNFRSF8	Hematological malignancies biomarker
Others	
Cytotoxic T cell antigen-4-CTLA-4	Receptor expressed on activated T cells. Reduction in T-cell responses and activation
B-cell–activating factor (BAFF)-receptor (BAFF-R)	BAFF is a member of the tumor necrosis factor (TNF) family cytokines. BAFF receptor is expressed on B-cells. Implicated in proliferation, maturation and cell survival of cancer B cells
CD124 (IL-4Rα)	Implicated in survival and in suppressor activity of myeloid derived suppressor cells
VCAM-1	Member of the immunoglobulin-like super family. Implicated in recruitment of immune cells to inflammation sites
Toll-like receptor 3 ectodomain	Implicated in the production of INF-β and inflammatory cytokine
hyaluronic acid (HA) binding domain of CD44	Belongs to the proteoglycan family of transmembrane glycoproteins. Receptor for hyaluronic acid. Role in tumor growth and metastasis. Marker for subpopulations of tumor initiating cells and implicated in chemo resistance
Angiopoietin-1	Promotes endothelial cell survival and vascular impermeability. Prevents increase in endothelial cell adhesion molecule expression
Angiopoietin-2	Potentialisation of proangiogenic growth factors
CD71	Responsible for cellular iron transport. Rapidly proliferative cells require more iron. Cofactor for enzyme involved in DNA synthesis of proliferative cells
Multidrug resistant-associated protein 1-MRP1	MRP1 correlates with chemotherapy drug resistance. Expressed in cancer stem cells
CD16α	Implicated in antibody dependent cellular cytotoxicity and recruitment of NK cells. NK cells are important for suppressing tumor metastasis and outgrowth
Alkaline phosphatase placental-like 2-ALPPL-2	Implicated in cell growth and invasion. Ectopically expressed on cell surface and in cell secretion
Nucleolin	Multifunctional protein interacting with DNA and RNA. Involved in rRNA maturation, ribosome assembly and exportation of ribosome components to the cytoplasm Role in mRNA stabilization (example: role in stabilization of bcl-2 mRNA in human leukemia). Overexpressed on the surface of certain cancer cells
Immunoglobulin heavy mu chain	Major component of the B-cell antigen receptor in Burkitt-s lymphoma cells Implicated in transforming healthy cells and in cancer progression

2. Generalities on Aptamers

Owing to their three-dimensional conformation and the strong shape complementarity between aptamers and their targets, aptamers are known to recognize their specific target with high affinity and selectivity. Analogous to antibodies in their range of target recognition and variety of applications, they are referred as 'chemical antibodies' [15]. Aptamers though possess several advantages over antibodies: Temperature stability, self-refolding, easy production, and presumably lack of immunogenicity/toxicity ... Due to their molecular weight, which is comprised between 10 and 30 Da, aptamers penetrate tissues faster and more efficiently than the 150 kDa antibodies [16]. Aptamers are chemically synthetized, rapidly, at reasonable cost, with no or low variation from batch to batch, and independently of any biological systems. Risks of viral and bacterial contamination are thus eliminated. Aptamers are thermally stable. Denatured at 95 °C, they refold into their correct three-dimensional conformation when cooled down to room temperature. To date, aptamers have never elicited toxicity in therapeutic applications.

RNA aptamers fold into more diverse three-dimensional structures than ssDNA aptamers, because of their 2′-hydroxyl (2′-OH) group on ribose and the non-Watson-Crick base pairing. The chemical production of ssDNA aptamers is easier and cheaper than RNA aptamers. But the preparation of ssDNA molecules during the SELEX process is more challenging than RNAs [17,18]. Nucleic aptamers suffer from two major disadvantages: their nuclease sensitivity, especially for RNA aptamers that can be cleared from the circulation within minutes or seconds [19], which limits their development as pharmaceuticals. Further, the chemical diversity of a 4 nucleotides based DNA and RNA library may be limited compared to that of a 20 amino acids based library. Developments allowed overcoming these weaknesses. The 2′-OH group is the naturally occurring cleavage site prone to nucleophilic attack. Typical modifications that can be inserted during the SELEX process include masking the nuclease-sensitive 2′OH group by replacing it with 2′fluoro (2′-F) or 2′-amino (2′-NH2). Such modified pyrimidines are incorporated via an efficient engineered mutant T7 RNA polymerase [20]. Other modified nucleotides can also be incorporated in SELEX libraries like 2′-O-methyl nucleotides, locked nucleic acid (LNA), hexitol nucleic acid (HNA) [21–25]. Modifications, if they do not alter much specificity and target binding properties of aptamers, can be introduced post-selection. Those modifications include 2′-F, 2′-NH2, 2′-thio (2′-SH), 2′-azido (2′-N3), 2′-hydroxymethyl (2′-CH_2OH) or 2′-methoxy (2′-O-Me) groups, LNA [26]. Synthetic nucleic acids, named xeno nucleic acids (XNA), increase the resistance and also the diversity of such modified aptamers [27,28]. Gold et al. [29] demonstrated that the success rate of a conventional SELEX on difficult proteins is lower than 30% and improved this rate up to 84%, by the incorporation of four modified nucleotide triphosphate analogs: 5-benzylaminocarbonyl-dU(BndU), 5-naphthylmethylaminocarbonyl-dU (NapdU), 5- tryptaminocarbonyl-dU (TrpdU), and 5-isobutylaminocarbonyl-dU (iBudU). The idea was to expand the chemical diversity of aptamers by adding functional groups that mimic amino acid side chains [30]. These modifications enhance protein binding through direct hydrophobic contacts with the target protein, resulting in increased binding affinities and slower complex dissociation rates compared to unmodified aptamers. So called Slow Off-rate Modified Aptamers (SOMAmers), are developed by the SomaLogic Company (Boulder, CO, USA) to currently more than 1300 proteins. SOMAmers are used in SOMAscan™ assay, a highly sensitive proteomic tool for discovering and validation of biomarkers. Capping aptamers with inverted nucleotides is another alternative to reduce exonuclease degradation [31]. The native phosphodiester backbone of nucleotides can also be modified with boranophosphate or phosphorothioates [32–34]. The company NOXXON Pharma AG (Berlin, Germany) takes advantage of spiegelmers ('spiegel' means 'mirror' in German) to prevent enzymatic degradation in biological fluids [19,35]. Spiegelmers are artificial RNA-like molecules built from L-ribose units, images of natural D-units, highly resistant to nuclease degradation and much more stable in vivo, with lifetimes greater than 60 hours in plasma. The SELEX is performed with D-RNA libraries combined with mirror images of peptides or small proteins artificially synthesized with D-aminoacids. Once aptamers are identified, they are converted to stable L-RNAs and they bind to the

natural L-form of peptide or protein targets with equally high affinities. Three spiegelmers are actually in clinical trials, of which one in oncology (described in Section 5). This process is however limited to artificially synthesized targets. To increase their size, consequently reducing their systemic clearance and prolonging their in vivo half-lives, ssDNA and RNA aptamers are often coupled to bulky groups, such as poly (D,L-lactic-co-glycolic acid) (PLGA), poly ethylene glycol (PEG), liposomes, steptavidin or cholesterol [36–41].

3. Protein- and Cell-Based SELEX Processes

Different SELEX processes have been developed for the selection of aptamers targeting tumor cell-surface protein biomarkers. Figure 1 illustrates the classical protein- and cell-based SELEX procedures, the two main methods that are used to identify aptamers to tumor cell-surface biomarkers for which targets are proteins and cells, respectively.

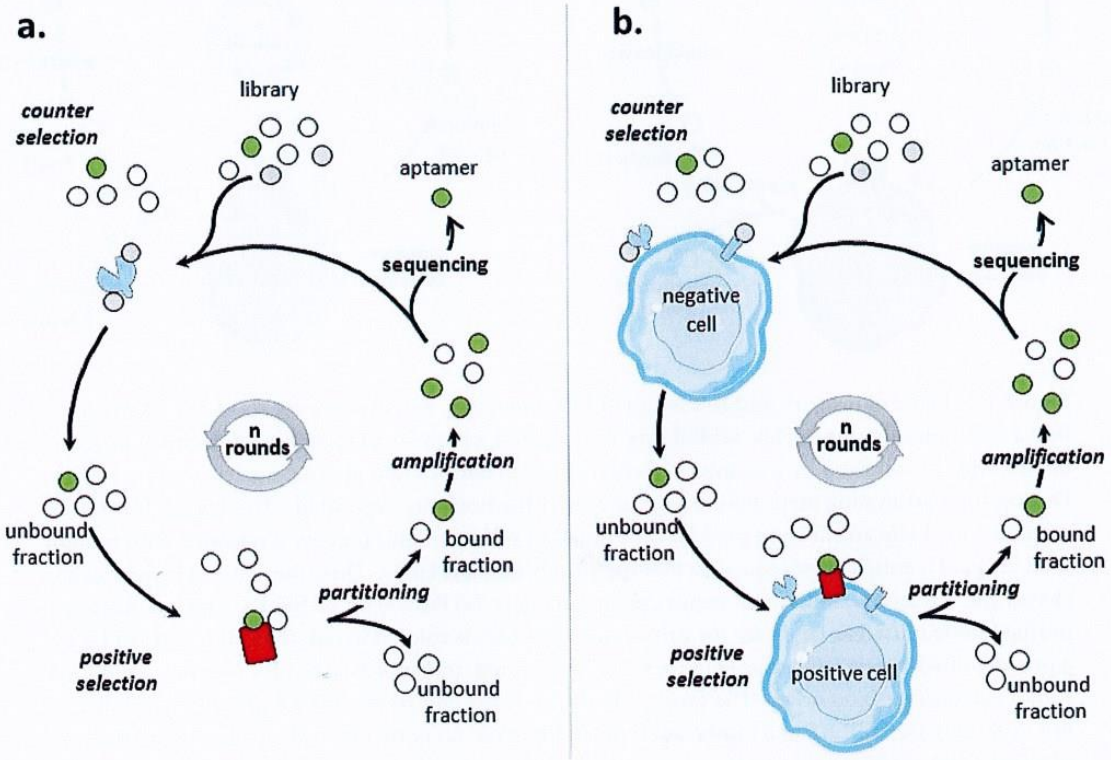

Figure 1. *Cont.*

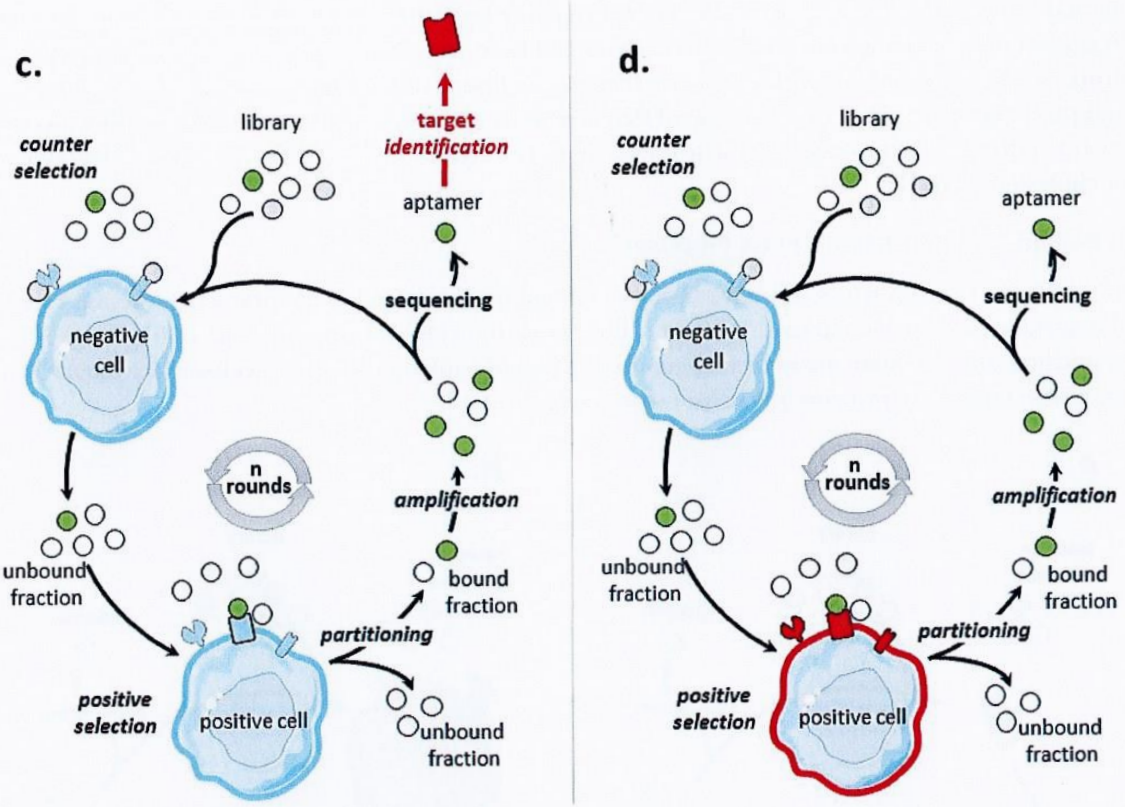

Figure 1. Scheme of protein- and cell-based SELEX processes. Briefly, the process of SELEX involves first a selection step: the nucleic acid library is incubated with a target (positive selection), which can be preceded or followed by a counter selection phase to remove non-specific nucleic acid molecules. During the partitioning step, bound and unbound fractions are separated. The bound fraction is amplified to obtain an enriched pool for next round of selection. This process is repeated for n rounds until the pool is enriched for sequences that specifically bind the target. These nucleic acid molecules are cloned and sequenced. Individual sequences are aptamers. (**a**) Protein-based SELEX. The pre-identified purified protein used as target for the protein-based SELEX is colored in red. (**b**) Cell-based SELEX on a pre-identified tumor cell-surface biomarker colored in red. (**c**) Cell-based SELEX on a post-identified tumor cell-surface biomarker. The target, identified at the end of the SELEX process, is colored in red. (**d**) Cell-based SELEX to a tumor cell type. In this case, no particular cell-surface biomarkers are identified and aptamers are specific to the cell's molecular signature. The whole cell used for positive selection is colored in red.

3.1. Aptamers Selected by Protein-Based SELEX

Protein SELEX is the simplest form of SELEX process (Figure 1a). Table 2 provides an inventory of most of tumor cell-surface protein biomarkers selected by protein-SELEX. Aptamers selected by protein-based SELEX have been reported for cell-adhesion molecules, tyrosine kinase receptors, cell membrane-associated enzymes, mucins, T-cell receptors, co-stimulator receptors, surface transmembrane glycoproteins ... Some of the biomarkers have been subjects to different SELEX procedures, like integrin αvβ3, MUC-1, L-selectin and CD44 and the tyrosine kinase receptors EGFR, HER-2, and c-Met. Many factors varied, like the nature and the number of random nucleotides of the library, the separation procedures, the numbers of selection rounds. All of these selection procedures lead to aptamers of high affinities for their targets, usually in the low nanomolar range.

Table 2. Aptamers to tumor cell-surface biomarkers selected by protein-based SELEX (updated since 2011 [42–44]).

Biomarker	Target Used for Protein-SELEX	Aptamer Library	Number of Variable Nucleotides	Number of Rounds of Selection	Separation Method	Name of Selected Aptamers	K_D	Applications	Year	References
Cell-adhesion molecules										
Epithelial cell adhesion molecule-EpCAM (CD326)	His-tagged C-terminal domain of EpCAM	2′F-RNA	40	12	affinity chromatography	Truncated EpCAM RNA aptamer	55 nM to human cells	Target stem cell marker. Potential applications: development of targeted cancer nanomedecine and molecular imaging agents	2011	[45]
EpCAM	His-tagged C-terminal domain of EpCAM	DNA	40	12	affinity chromatography	Truncated aptamer SYL3C	38 and 67 nM to cells	Imaging (confocal) Cancer cell capture	2013	[46]
Carcinoembryonic antigen- CEA (CD66e)	His-tagged recombinant protein of full-length CEA	2′F-RNA	40	17	affinity chromatography	Group I, II and III	low nM range	Inhibition of cell migration/invasion in vivo. Promotion of cell anoikis resistance in vitro Inhibition of liver metastasis in vivo	2012	[47]
Integrin αvβ3	purified αvβ3 integrin	2′F-RNA	50	15–17	affinity chromatography	Apt-avb3	nM range	Inhibition of endothelial cell adhesion and proliferation Reduction of endothelial cell tube formation Inhibition of cancer cell proliferation and adhesion (HUVEC) Increases endothelial cell apoptosis	2005	[48,49]
Integrin αvβ3	purified αvβ3 integrin	2′F-RNA	50	6	MAI-SELEX [1]	αV-1 and β3-1	8.9–10.5 nM	Recognizes distinct binding sites on a single target (αV or β3) with minimal cross-reactivity Potential applications: molecular diagnosis and targeted therapies	2012	[50]
E-and P-Selectin	recombinant human E-selectin/IgG-Fc-chimeras	DNA	50	17	affinity chromatography	SDA	100 nM	Inhibition of cancer cell adhesion Potential applications in therapies during metastasis formation	2014	[51]
L-Selectin	L-selectin-Ig chimera	2′-NH2 RNA	40	14	affinity chromatography	14.12	0.2–3 nM range	Preferential blokade of a specific selectin	1996	[52]
L-Selectin	L-selectin–IgG fusion protein	DNA	40	17	affinity chromatography	LD201, LD174 and LD196	1.8, 5.5 and 3.1 nM	Inhibition of lymphocyte rolling on endothelial cells	1996	[53]

Table 2. *Cont.*

Biomarker	Target Used for Protein-SELEX	Aptamer Library	Number of Variable Nucleotides	Number of Rounds of Selection	Separation Method	Name of Selected Aptamers	K_D	Applications	Year	References
Tyrosine kinase receptors										
EGFR	purified extracellular domain of human EGFR	RNA	62	12	not documented	J18	7 nM	Drug delivery (internalization of gold nanoparticules) Potential application: delivery of siRNA and cancer detection	2010	[54]
EGFR	human EGFR-Fc protein	2′F-RNA	62	9 + 7–9 rounds with a 30% doped sequence (from aptamer E01)	affinity chromatography	E07 Internalized	2.4 nM	Prevention of proliferation of tumor cells (blocks receptor autophosphorylation) Drug delivery (Gemcitabine) and induces cell death	2011	[55,56]
EGFR	purified extracellular domain of EGFR	DNA	40	11	affinity chromatography	Tutu-22	56 nM	Regognizes EGFR-positive cancer cells with strong affinity and selectivity Potential applications: development of novel targeted cancer detection, imaging and therapy	2014	[57]
EGFRVIII	histidine-tagged EGFRvIII ectodomain (*E. coli.* system)	2′F-RNA	40	12	affinity chromatography	E21	33 nM	Disruption of post-translational modifications of immature EGFRvIII Induction of apoptosis	2009	[58]
HER-2	recombinant glutathione S-transferase (GST)-tagged ErbB2 protein (22–122 amino acids)	2′F-RNA	50	15	affinity chromatography	SE15-8	low nM range	High specificity to ErbB2 and not to other members of the ErbB family Potential applications: drug delivery and imaging for in vivo diagnosis	2011	[59]
HER-2	peptide from the juxtamembrane region of HER2 extracellular domain	DNA	40	multiple	affinity chromatography	HB5	18.9 nM	Drug delivery (Doxorubicin)	2012	[60]
HER-2	20-amino acid HER2 peptide	Thio-DNA	21	12	affinity chromatography	HY6	172 nM	Potential application: targeted therapy	2015	[61]
HER-2	His-tagged Her2–extra cellular domain (*E. coli* system)	DNA	40	15	membrane filtration	ECD_Apt1	6.33 nM	Potential applications: theranostic (non invasive cancer diagnosis), therapeutics and monitoring patient compliance	2017	[62]
HER-3	extracellular domains of HER3 produced in S2 insect cells	RNA	49	15	membrane filtration and gel shift assay	A30	0.1 nM range	Inhibition of HER3 activation and growth of tumor cells Potential application: anticancer drug	2003	[63]
c-MET	c-Met-Fc	DNA	40	12	membrane filtration	CLN3 and CLN4	91 pm and 11 nM	Mediates tumor cell lysis Recruits NK cells to tumor and induces ADCC	2011	[64]
c-MET	c-Met-Fc	2′F-RNA	40	16	membrane filtration	CLN64	1 nM	Inhibition of tumor cell migration Potential application: therapeutics and diagnosis	2015	[65]

Table 2. *Cont.*

Biomarker	Target Used for Protein-SELEX	Aptamer Library	Number of Variable Nucleotides	Number of Rounds of Selection	Separation Method	Name of Selected Aptamers	K_D	Applications	Year	References
Cell membrane-associated enzyme										
Prostate specific membrane antigen-PSMA	706 extracellular amino acids of PMSA	2′F-RNA	40	6	affinity chromatography	A9, A10, A10-3 after minimization & optimization	low nM range	Promotion of tumor regression Delivery of siRNA Potential application: diagnosis and therapies	2002	[66,67]
Mucins										
MUC-1	MUC-1 peptides of 2 lenghts: 9 and 60 amino acids	DNA	25	10	affinity chromatography	S1.3/S2.2	low nM range to 0.1 nM	Potential application: detection by fluorescent microscopy	2006	[68]
MUC-1	His-tagged unglycosylated form of the MUC1 protein containing five tandem repeats of the VTR (*E. coli* system)	DNA	25	10	affinity chromatography	MUC1-5TR-1, 2, 3, 4	47–85 nM	Potential application: diagnosis assays for early or metastatic diseases	2008	[69]
Tumor necrosis factor receptor (TNF-R) and co-stimulatory receptors										
T-cell receptor OX40	extracellular domain of OX40-Fc fusion protein	2′F-RNA	40	9–11	affinity chromatography	9C7, 11F11	2-10 nM for purified OX40 protein and # 50 nM for OX40 on activated T cells	Increasing proliferation of T lymphocytes and production of IFN-γ. Potential application: therapeutics in association with dendritic cell-based vaccines (adoptive cellular therapy)	2013	[70]
T-cell receptor OX40	murine extracellular domain of OX40-Fc fusion protein	2′F-RNA	40	11	affinity chromatography	9.8	8 nM	Induces nuclear localization of NFκB, cytokine production and cell proliferation. Increases dendritic cell based tumor vaccine effects	2008	[71]
T-cell receptor 4-1BB	murine extracellular domain of 4-1BB-Fc fusion protein	2′F-RNA	40	12	affinity chromatography	M12-23 (multimeric aptamer)	40 nM	Inhibition of tumor growth in vivo. Potential application: therapeutic manipulation of the immune system	2008	[72]
Receptor activator of NF-κB-RANK	recombinant human soluble RANK/IgG_1Fc chimera	RNA	40	7	affinity chromatography	apt1, apt2 and apt3	0.33, 1.8 and 5.8 μM. 100 nM for the 2′-F version of aptamers	Potential application: therapeutics against osteoclastogenesis	2004	[73]
CD28 [2]	murine recombinant CD28-Fc fusion protein	2′F-RNA	25	9	affinity chromatography	CD28Apt2 and CD28Apt7	60 nM for CD28Apt7-dimer	Potentialisation of antitumor vaccine efficacy Reduction of tumor progression and increased overall survival (in vivo) Potential application: enhancing vaccine-induced immune responses	2013	[74]

Table 2. *Cont.*

Biomarker	Target Used for Protein-SELEX	Aptamer Library	Number of Variable Nucleotides	Number of Rounds of Selection	Separation Method	Name of Selected Aptamers	K_D	Applications	Year	References
Others										
Cytotoxic T cell Antigen-4-CTLA-4	murine CTLA-4/Fc fusion protein	2′F-RNA	40	9	membrane filtration	M9-9	30–60 nM	Increases tumor immunity (in vivo) Potential application: immunotherapy	2003	[75]
B-cell–activating factor (BAFF)-receptor (BAFF-R)	Human recombinant BAFF-R protein	2′F-RNA	50	12	membrane filtration	R-1, R-2 and R-14	47, 95 and 96 nM	Delivery of siRNA. Potential application: combinatorial therapeutics	2013	[76]
CD124 (IL-4Rα)	recombinant ILR4α protein enzymatically cleaved	2′F-RNA	40	5	affinity chromatography	cL42	14 nM for recombinant protein and 788 nM for MCS2 cells	Induction of MDSCS apoptosis Promotes CD8+ T cell infiltration and reduces the number of MDSCs infiltration. Reduction of tumor progression in vivo	2012	[77]
VCAM-1	N-terminal fragment of VCAM-1	2′F-RNA	40	12	affinity chromatography	12.11	10 nM	Potential application: imaging	2007	[78]
Toll-like receptor 3 ectodomain	Toll-like receptor 3 ectodomain with N-terminal FLAG and C-terminal His	RNA	40	7	membrane filtration	Family-I and Family II	# 3 nM	Aptamer without agonist and antagonist effects	2006	[79]
hyaluronic acid (HA) binding domain of CD44	HA-binding domain of human CD44 (cell-free expression system)	Thio-DNA	30	10	affinity chromatography	TA1-TA6	180–295 nM	Potential applications targeted therapy and imaging	2010	[80]
CD44	GST-tagged human recombinant full length CD44 protein	2′F-RNA	45	11	affinity chromatography	Apt1	81.3 nM	Potential applications therapeutic (targeted delivery againt stem cells) and diagnosis	2013	[81]
Angiopoietin-1	recombinant human Ang1	2′F-RNA	40	9	membrane filtration	ANG9-4	2.8 nM	Inhibition of cell endothelial cell survival	2008	[82]
Angiopoietin-2	recombinant human Ang2	2′F-RNA	40	11	membrane filtration	11-1 and truncated 11-1.41	3.1 and 2.2 nM	Inhibition of angiogeneis (in vivo)	2003	[83]

[1] Integrin αvβ3 is a heterodimeric transmembrane protein composed of α and β chains, for which the selection procedure of a 2′-fluoro aptamer has been patented [48]. In order to select for aptamers specific to homodimer αv and β3, Gong et al [50], developed a strategy called MAI-SELEX (MAI for multivalent aptamer isolation). Two distinct selection stages were employed, the first being a classical affinity selection on the purified full-length αvβ3 integrin. The second module, for specificity, leads selection to β3 as integrin αIIbβ3 served as a protein decoy. Two aptamers, specific for αv and β3 were identified with affinities in the low nanomolar range. This selection strategy applied to heterodimeric proteins is limited to the availability of decoy proteins. [2] Aptamer, GR1, targets CD28. This G-rich oligonucleotide, which, alike AS1411 [84], has not selected by SELEX, inhibits CD28 T cell responses in vitro and in vivo [85].

Cell surface proteins used as targets for protein-based SELEX are either full-length or truncated versions of full length proteins, generally recombinant ectodomains coupled to tags (His-tags, Fc fragments of antibody or GST), facilitating purification and selection by affinity. Peptides can also be used as targets. In that case, the advantages linked to the exact knowledge of the aptatope, and to the facility of production of large amounts of targets can be offset by the limitations of these peptides as protein mimics. Cell-surface proteins are amphipatic membrane proteins, and therefore not easily extracted from the lipidic membrane, purified and solubilized. Even though membrane proteins can be purified and solubilized, large amount of proteins are needed for a whole protein-SELEX procedure. Further, full-length membrane proteins or ectodomains, expressed in prokaryotic or lower eukaryotic systems, may lack or have different post-translational modifications (phosphorylation, glycosylation, ubiquitination, methylation, myristoylation, acetylation ...). For example, the 2′F-RNA aptamer E21, elicited against the EGFRvIII ectodomain produced in bacteria, did not bind to the native protein expressed from eucaryotic cells because glycosylation, a post-translational modification present only in eukaryotic systems, significantly alters the structure of the target protein [58].

Some of the biomarkers have been subjects to different SELEX, like MUC-1, that allowed comparison between aptamers targeting proteins and peptides mimics of proteins. For example, Ferreira et al. [68] selected ssDNA aptamers targeting two peptides of the native MUC1. They used the 9-amino-acid immune-dominant antibody-binding epitope APDTRPAPG which contains only part of the variable tandem repeat region of MUC-1, as well as a larger peptide (60 amino acids long) which comprised three complete tandem repeats of the MUC1 region. From a preceding experience with an antibody binding to MUC1, the short peptide was weakly binding to the antibody compared to longer peptides, possibly due to increased flexibility resulting in higher entropic cost [86]. The two SELEX on the two peptides of different lengths resulted in identical aptamer sequences with affinities as low as 0.1 nM. Moreover, aptamers selected on the short peptide have been shown to successfully recognize and bind to the native MUC1 at the surface of the MCF7 breast cancer cell line. In comparison, the same group has selected aptamers to the MUC-1 protein with higher K_D (47–85 nM) than those obtained for aptamers to peptides, which might be due to an unstructured MUC-1 protein [69].

Overall, the main disadvantage of protein SELEX is that purified and solubilized membrane proteins, recombinant proteins and peptides may not adopt the same state (in terms of lengths, conformation, post-translational modifications ...), than the cell-surface biomarker in its endogenous environment. Thus, some aptamers selected against purified membrane proteins failed to recognize their targets in whole cells [58,78], limiting their use for medical applications [87]. Moreover, some biomarkers like receptors require co-receptors for proper folding, that prevents the use of protein-SELEX. Other processes, like cell-based SELEX using whole living cells as targets may overcome these limitations.

3.2. Aptamers Selected by Cell-Based SELEX

The general process of cell-SELEX is shown in Figure 1b–d. In cell-based SELEX, the target of the selection is embedded in its native environment in cells. PubMed indicates 829 entries with 'cell SELEX' of which more than 1/3 are on 'cancer and cell SELEX'. There has been growing developments in cell-SELEX these last years. Recent reviews detail advances in aptamer selection technology, particularly the high-throughput next-generation sequencing and bioinformatics [88], the cell-SELEX process [89], the evolution of complex target SELEX [90]. For example, FACS (Fluorescence activated cell sorting) SELEX aims at removing, from the cell suspension, dead cells which could have an impact on the selection [91–93]. In Internalized cell-SELEX, aptamers are selected on their ability to bind to cell-surface target and to internalize in the cell [94–100]. Nucleic acid sequences which do not internalize are eliminated. To best mimic the natural environment of targets, Souza et al. [101] developed 3D cell-SELEX, in which aptamers are selected on spheroid cells in 3D cell culture by magnetic levitation method to mimic the tissue microenvironment in vitro.

3.2.1. Cell-Based SELEX to Identify Aptamers to Tumor Cell-Surface Protein Biomarkers

Depending on the objective, knowledge of the target identity prior to selection can be useful, or not. Therefore, different strategies can be distinguished:

Pre-Identified Tumor Cell-Surface Biomarkers

When the objective of a cell-based SELEX is the identification of aptamers to a clearly identified cell-surface biomarker (Figure 1b), the SELEX procedure is sometimes termed TECS-SELEX for 'target expressed on cell surface-SELEX' [102]. In Table 3, selections by cell-based SELEX realized on pre-identified tumor cell-surface biomarkers are described. Many identical tumor biomarkers, in particular tyrosine kinase receptors, EpCAM and integrins, were used as pre-identified targets for protein-and cell-based SELEX (Tables 2 and 3). As an example of solid tumor targeted by cell-based SELEX, Delac et al. [103] reviewed aptamers designed to target glioblastoma cells. Some of the key cell surface molecules that have been identified as glioblastoma biomarkers (transferrin receptor, $\alpha v\beta 3$ integrin, EGFR, EGFRvIII) [104], have already been targets of protein-and/or cell-based SELEX (Tables 2 and 3).

Different procedures have been developed to direct the recognition of the target by the aptamer. For example, ligand-guided selection (LIGS) SELEX guides the selection to a specific epitope of a known cell-surface target. Zumrut et al. [105,106] used antibodies as secondary ligands to elute specific aptamers. The antibody interacts with its cognate antigen to outcompete aptamers specific for a pre-determined cell-surface receptor and replace specific aptamers from an enriched SELEX pool. Immunoprecipitation (IP) SELEX is an approach combining cell-SELEX and protein-nucleic acid immunoprecipitation to ensure that aptamers bind to a pre-identified target [7,107]. Hybrid-SELEX, also called cross-over SELEX, is a combinatorial approach to guide selection towards a pre-identified target. Usually, the first rounds of selection are realized on cells which express the target by cell-SELEX, and then rounds of selection are realized on the same version of the target in its purified form by protein-based SELEX. A reverse hybrid-SELEX combines first protein-SELEX followed by cell-SELEX. Hybrid-or reverse hybrid-SELEX have been used to isolate aptamers targeting the RET^{C634Y} mutant receptor tyrosine kinase overexpressed in PC12 cells [108], the HER-2 tyrosine kinase receptor expressed in SKOV3 ovarian cancer cells [109], CD16α on Jurkat cells overexpressing CD16 alloforms [64], integrin $\alpha 6\beta 4$ on PC-3 cells [110], the transferrin receptor CD71 expressed in HeLa cells [94]. In this last example, a combination of protein-SELEX and cell-internalized SELEX was realised. Soldevilla et al. [111] used another variant of reverse hybrid-SELEX, combining cell-SELEX to peptide-SELEX. Ten rounds of selection were first realized by peptide-SELEX, followed by one round of cell-SELEX on a chemotherapy-resistant tumor cell line that highly express MRP1 (H69AR).

Cell-based SELEX involves positive selection to collect aptamers that interact specifically with the target cells and usually counter selection to eliminate nonspecific nucleic acid sequences binding to negative cells. Different human tumor cell lines have been used for positive selection: glioblastoma (U251, U87MG), breast carcinoma (SKBR-3, N202.1), ovarian cancer (SKOV3), gastric cancer (N87), lung carcinoma (A549, H69), lymphoma (Jurkat, K299T), liver cancer (HepG2), prostate adenocarcinoma (PC-3), cervical cancer (HeLa). The PC12 cell line derived from pheochromocytoma of the rat adrenal medulla has also been used, as well as other non-tumoral cells lines, like Chinese hamster ovary (CHO), Human embryonic kidney (HEK) cells. The choice of the couple of cells used for positive- and counter-selections is of great importance for cell-based SELEX on pre-identified cell-surface protein. The two cell type should display a high difference in target expression levels, so that aptamers interact specifically with the target on positive cells and does not interact with cells used for counter-selection which does not display or displays lower levels of the target protein. For positive selection, the pre-identified target can be naturally expressed or over-expressed at the surface of the cell line. Cells used for counter selection are chosen in light of positive cells. In the literature, cell lines used for counter selection were:

(i) isogenic to cells used for positive selection. Most of the cell-based SELEX process used cells overexpressing the target of interest for the positive selection, and the parental cell line for counter selection (Table 3). As an example over many others, a cell-based SELEX was realized on Chinese hamster ovary (CHO)-K1 cells ectopically expressing human transforming growth factor-β type III receptor while CHO-K1 cells were used for counter selection [102]. In two examples described in Table 3, both on integrins, cells used for counter-selection were under-expressing the target. In the first example, the parental isogenic cell lines are used for the positive selection. Berg et al. [110] used this strategy to select an ssDNA aptamer specific for α6β4 integrin in its native state. Five rounds of positive cell selection were realized on PC-3 cells. PC-3 β4 integrin (ITGB4) knockdown cells were used in a preselection step to deplete aptamers specific for cell surface marker other than β4 sub-unit. However, the counter-selection strategy was found to be insufficient. And seven more rounds of protein-SELEX were performed on a recombinant α6β4 protein to select for α6β4-specific aptamers. In the second example, HEK293 cells lines are used. For positive selection, HEK293 cells were manipulated to generate positive αv selection cells by overexpressing ITGAV. For counter selection, the same cell line was depleted in ITGAV with microRNA-mediated silencing. Takahashi et al. [112] named this strategy Icell-SELEX for isogenic cell SELEX.

(ii) unrelated to cells used for positive selection. Two studies [113,114] related the use for positive selection of the breast cancer cell line SK-BR3 modified to overexpress HER-2. For counter-selection, the human breast cell types MDA-MB-231 and MDA-MB-468, respectively underexpressing and negative for HER-2 were used. Twelve and sixteen rounds of selection were performed to select RNA- [113] and ssDNA- [114] aptamers. According to Dastjerdi et al. [114], the use of the HER2 underexpressing cell line (MDA-MB-231) in Kang et al's study [113], instead of a HER2-negative cell line may have compromised counter selection. A hybrid-SELEX strategy was used to get aptamers to the surface transmembrane glycoprotein CD30 [115]. For the cell-SELEX, lymphoma cells K299T and Jurkat cells were used for positive and counter-selection, respectively.

(iv) inexistent or not documented [116]. ssDNA aptamers to HER-2 have recently been selected through a hybrid-SELEX [109], combining 8 rounds a protein-SELEX using the His-tagged extracellular domain of HER-2 and 7 rounds of cell-SELEX on HER-2 over-expressed in SKOV3 cancer cells. Human serum albumin was used for negative screening in protein-SELEX and added to ssDNA pools during cell-SELEX, but no cells were used for counter-selection. Post-selection, HER2-negative MCF7, MDA-MB-435 and MDA-MB-231 cells were used to test the specificity of aptamers. Seven aptamer candidates from hybrid-SELEX were radiolabeled with ^{18}F and further screened in vivo by PET imaging in a SKOV3 tumor model. Two aptamers, Heraptamer-1 and-2 which had relatively high tumor uptake ratios, are promising ligands for HER-2 imaging in cancer. A similar approach was used by Wilner et al. [94]. Four rounds of protein-SELEX were performed using the His-tagged recombinant transferring receptor CD71 (TfR) as target, followed by 1 round of cell-SELEX on HeLa cells, a human cervical cancer cell line known to express TfR. Following the first round, a negative selection step was performed in which the library was pre-incubated with Ni-NTA agarose prior to the positive selection. But the cell-SELEX procedure did not include counter-selection steps.

Table 3. Aptamers selected by cell-based SELEX on pre-identified tumor cell-surface biomarkers.

Biomarker	Aptamer Library	Number of Variable Positions	K_D Range	Number of Positive Selection Rounds (*selection method*) [1]	Cells Used for Positive Selection	Cells Used for Counter-SELEX	Applications	References
Tyrosine kinase receptors								
EGFRvIII	DNA	30	0.62–37.57 nM	14	U87-EGFRvIII, U87-MG, GBM cells overexpressing EGFRvIII	U87-MG	Potential applications: delivery of chemical drug and diagnosis	[117]
EGFRvIII	DNA	40	3–16 nM	11	U87-MG, GBM cells overexpressing EGFRvIII	U87-MG	Imaging (radiolabeled 188Re, in vivo) Potential applications: diagnosis in stratifying patient and monitoring treatment	[118]
HER-2	RNA	40	94.6 nM	20	HER-2-overexpressing SK-BR-3 cell line	MDA-MB-231, a HER-2-underexpressing breast cancer cell line	Potential application: therapy	[113]
HER-2	2′F-RNA	20	46–82 nM	9 (*cell-internalization SELEX*)	N202.1A mammary carcinoma clonal cell lines expressing high levels of surface HER-2/neu.	N202.1 E clonal cell line has no detectable surface expression of the HER2/neu oncoprotein.	Drug delivery (Bcl-2 siRNA) Induces chemosensibilisation and reduces drug resistance	[100]
HER-2	DNA	50	Not documented	4 rounds	Cleared extract of ErbB-2-overexpressing N87 cells	Not documented	Acceleration of ErbB-2 degradation in lysosomes Inhibition of growth of tumor cell in vitro and tumor mass in vivo	[116]
HER-2	DNA	30	5–23 nM	8 rounds of protein SELEX followed by 7 rounds of cell -SELEX (*hybrid-SELEX*)	HER-2 overexpressed in SKOV3 ovarian cancer cells	No cells	PET imaging (radio labeled, in vivo)	[109]
HER-2	DNA	40	Not documented	16	HER2-overexpressing breast cancer cell line, SK-BR3	HER2 negative breast cancer cell line, MDA-MB468	Development of a new method to monitor the enrichment of aptamers in a given round of cell-SELEX	[114]
Receptor tyrosine kinase-RET^{C634Y}	2′F RNA	50	Tens of nM	15 rounds of selection on cells, followed by 7 rounds on purified protein (*hybrid-SELEX*)	RET^{C634Y} mutant receptor expressed in PC12 cells (PC12/MEN2A)	PC12	Potential applications: diagnosis, imaging and therapy	[108]
Neurotrophin receptor TrkB	2′F RNA	20	2 nM	4 (*cell-internalization SELEX*)	TrkB-expressing HEK cells	HEK	Neuroprotective effects Potential in therapy for neuro degenerative disease	[119]
Other kinase receptors								
TGFβ III receptor	2′F RNA	60	1 nM	11	TGFβ III receptor ectopically expressed on CHO-K1 cells	CHO-K1	Potential application: therapy through inhibition of TGFβIII receptor	[102]
Transferrin receptors (TfR)								
CD71	2′F-RNA	50	nM range	4 rounds of protein-SELEX on the His-tagged recombinant protein and 1 round on cells (*hybrid SELEX combined with cell-internalization SELEX*)	HeLa cells, a human cervical cancer cell line known to express TfR	NO cells	Delivery of siRNA Targets cell in liposomes	[94]
ATP-binding cassette (ABC) transporters								
Multidrug resistant-associated protein 1-MRP1	2′F-RNA	25	50 nM	10 rounds of peptide-SELEX followed by 1 round of cell-SELEX (*hybrid-SELEX*)	chemotherapy-resistant tumor cell line that has high MRP1 expression (H69AR)	Parental cell line H69	Reduction of cell growth in vitro and improved survival in vivo	[111]

Table 3. *Cont.*

Biomarker	Aptamer Library	Number of Variable Positions	K_D Range	Number of Positive Selection Rounds (*selection method*) [1]	Cells Used for Positive Selection	Cells Used for Counter-SELEX	Applications	References
Cell adhesion molecules								
Epithelial cell adhesion molecule-EpCAM (CD326)	DNA	40	µM range	7 (*FACS-SELEX*)	EpCAM over-expressed in HepG2 cells	HepG2 cells	Potential application: stem cell marker	[120]
Integrin α6β4	DNA	39	139 nM	5 rounds of cell-SELEX followed by 7 rounds of protein-SELEX (*hybrid-SELEX*)	PC-3 cells	PC-3 β4 integrin (ITGB4) knockdown cells	Imaging (confocal) Potential application: drug delivery	[110]
Integrin αv	RNA	35 & 40	359–408 nM	13 (*Isogenic cell-SELEX*)	Human HEK293 cells manipulated to generate positive αv selection cells by overexpressing ITGAV	Human HEK293 cells depleted in ITGAV with microRNA-mediated silencing.	Potential application: targeting channels, transporters . . .	[112]
CD16α	DNA	40	6–429 nM	9 rounds of protein-SELEX and 6 rounds of cell-SELEX (*hybrid-SELEX*)	Fc receptors CD16_-6His and CD16_ Val-158 or Phe-158 alloforms expressed on recombinant Jurkat cells	Jurkat E6.1 cell line	ADCC (tumor cell lysis)	[64]
Surface transmembrane glycoproteins								
CD133	2′F RNA	40	Not determined	6	HEK293T expressing CD133	His-tagged irrelevant protein expressed in HEK293T	Potential application: target cancer stem cells and molecular imaging	[121]
CD30 TNFRSF8	DNA	30	nM range	20 rounds of cell-SELEX followed by 5 rounds on purified His-tagged CD30 protein (*hybrid-SELEX*)	CD30-positive K299 T-cells lymphoma	Jurkat cells	Potential application: therapy	[115]

[1] Selection method is specified if it is different from classical cell-SELEX.

Post-Identified Tumor Cell-Surface Biomarkers—Discovery of Tumor Biomarkers

Aptamers are valuable tools to isolate tumor-specific biomarkers [122–124], as cell-based SELEX can also be used to identify targets after the selection (Figure 1c). The idea is first to select and identify aptamers specific for a tumor cell type, and then to use these high-affinity aptamers as probes to identify their cell-surface targets. These cell-surface targets, specific for tumor cells under study, are identified as (new) biomarkers. The main challenge is the identification of the protein target, usually by affinity purification followed by mass-spectrometry. The first post cell-SELEX identification of a tumor biomarker was realized in 2003 by Daniels et al. [125]. The U251 glioblastoma cell line was used as target for positive selection. Counter selection rounds were not included in SELEX. Twenty-one rounds of cell-SELEX using a 34 nucleotide long random library of ssDNA were performed to select aptamer GBI-10, shown to be the ligand for Tenascin-C, which is not a cell-surface receptor, but an extracellular matrix protein. Table 4 presents some (certainly not all) tumor cell-surface protein biomarkers which have been identified post-SELEX.

The ssDNA aptamer AS1411 in clinical trials as a novel treatment for cancer is original compared to all other aptamers cited in this review, as its discovery does not result from a SELEX approach. It is referred as an aptamer as its activity arises from binding to a specific target via shape-specific recognition. Briefly, Bates et al. [84], in the late 1990's, tested G-rich oligonucleotides (GRO) in a variety of cell lines and showed that they had unexpected anti-proliferative effect. AS1411 is a 26-nucleotide GRO, which forms quadruplex. It blocks the activation of secondary targets (NF-κB, and B-cell lymphoma 2, BCL2), sensitizes tumor cells to chemotherapy, has direct anti-proliferative effects in vitro, is efficiently internalized even at nanomolar doses ... [126,127]. Later, aptamer AS1411 was found to target nucleolin [127,128], a multifunctional protein that was first considered to be nucleolar. Nucleolin was found to be highly expressed by cancer cells, intracellularly but also at the cell surface. A recent review described uses and mechanisms of the G-quadruplex oligonucleotide AS1411 as a targeting agent [129].

Table 4. Aptamers Selected by Cell-Based SELEX on Post-Identified Tumor Cell-Surface Biomarkers.

Biomarker	Aptamer Library	Applications	References
EGFR	2′F-RNA	Induces EGFR-mediated signal pathways causing selective cell death Inhibits tumor growth in vivo Combined cetuximab-aptamer treatment shows clear synergy in inducing apoptosis in vitro and in vivo Potential application: translational therapy	[130]
PDGFR β	2′F-RNA	Inhibition of receptor signaling and of glioblastoma-derived tumor growth Inhibition of cell migration and proliferation Induction of differentiation	[99]
Alkaline phosphatase placental-like 2-ALPPL-2	2′F-RNA	Targets ALPPL-2 in both membrane bound and secretary forms Potential applications: diagnosis, imaging and therapy	[131]
selectin L and integrin α4	DNA	Potential application: therapeutic intervention	[132]
CD44/CD24	DNA	Potential applications: disruption of therapeutic resistance, invasion and angiogenesis	[133]
CD44	DNA	Potential applications: cancer detection, imaging and drug delivery	[134]
Protein Tyrosine Kinase 7-PTK7	DNA	Potential application: drug delivery	[135]
Insulin Receptor	2′-fluoro RNA	Inhibition of IR signaling Reduction of cell viability Potential applications: targeted therapies	[136]
Axl	2′F-RNA	Interferes with cell migration and invasion Inhibition of spheroid formation and cell transformation Inhibition of tumor growth	[137]
Nucleolin	DNA	Interferes with multiple biological activities in tumor cells Induction of apoptosis via down-regulation of bcl-2 proteins	[84,127–129]
Immunoglobulin heavy mu chain	DNA	Role in identification of cell membrane receptor with increased expression levels Potential applications: early diagnosis, targeted therapy and mechanistic studies	[138]

Berezovski et al. [139] described a technology for biomarker discovery, named aptamer-facilitated biomarker discovery (AptaBiD). It involves working with pool of aptamers rather than individual sequences. It is based on three steps: (i) cell-SELEX is performed to select ssDNA aptamers to biomarkers differentially expressed at the cell surfaces; (ii) a pool of biotinylated aptamers is used to isolate biomarkers from the cells, and then (iii) biomarkers are identified. AptaBiD was used to discover previously unknown surface biomarkers that distinguish live mature and immature dendritic cells [139] and to select DNA aptamers on lung adenocarcinoma cells derived from post-operative tissues [140].

Undetermined Targets

By cell-based SELEX process, aptamers have also been selected for tumor cell types (Figure 1d), without pre- or post-identification of targets. In this respect, aptamers are specific to the molecular signature of a tumor cell type. Such cell-based SELEX have been performed on several tumor cells, including breast cancer cells [141], colorectal cancer cells [142], small-cell lung cancer [143,144], non-small cell lung cancer [145], liver cancer cells [146], leukemia cells [147,148], gastric cancer cells [149], pancreatic ductal adenocarcinoma cells [150], prostate cancer cells [101], metastatic cells [151,152], and tumor initiating cells [153]. For example, J.N. Rich's team [153], identified tumor initiating cell (TIC) specific ssDNA aptamers. They used a cell-based SELEX approach with positive selection for CD133(+) TICs and counter selection for CD133(-) non-TICs both from human GBM xenografts in mice. In addition, counter selection was also made on human non-tumoral neural progenitor cells. Selected aptamers specifically bound to TICs with dissociation constants (K_D) in the low nanomolar range. These aptamers internalized into glioblastoma TICs that self-renew, proliferate, and initiate tumors.

3.2.2. Advantages and Limitations of Cell-Based SELEX

Aptamer binding is dependent on the target conformation which is conditioned by its environment. Full-length purified recombinant proteins, ectodomains or peptidic fragments of proteins used in protein-based SELEX may not be relevant targets if they have to be used in clinical developments. In cell-based SELEX, cell-surface targets post-translationally processed are in their endogenous environment, as close as possible to their natural distributions and conformations. Cell-based SELEX does not necessitate the production and purification steps usually required for protein-based SELEX and therefore the method may be useful to target proteins difficult to be produced and/or purified. Moreover, aptamers can be selected without prior knowledge of cell-surface targets. In that case, the aptamer acts as a bait to identify its target, which can be a new tumor protein biomarker.

But cell-based SELEX is a complex process, much more difficult than protein-based SELEX [122]. Cells lines need to be available, cultivable and stable. Aptamers might be difficult to generate for less expressed target proteins on cells. For most of the tumor cell-based selections described in this review, SELEX required modifications of cell lines, like over- and/or under-expression of the cell-surface protein target for selection and/or counter-selection. Over- or under-expression of a protein might deregulate expression of other proteins. This can trigger modifications to the cell line that might not represent anymore the disease cellular context. It is commonly admitted that more rounds of positive selection are performed in cell-SELEX compared to protein-SELEX and more rounds of counter selection are required to improve the selectivity of aptamers.

Post-SELEX characterization of the target is often required to check if the predetermined target is the 'real' target of selected aptamers, or to identify the target if it has not been identified prior selection. Selected aptamers are used as bait, a posteriori, to purify and then to identify their targets. Briefly, biotinylated-aptamers are used to retain whole live cells on streptavidin beads. The cell lysate is then loaded on a SDS-PAGE gel. After electrophoresis and silver staining, proteins that have a higher intensity than controls (extracted proteins with empty beads and extracted proteins with a scrambled nucleic acid sequence) are extracted from the gel and analyzed by nano-LC-MS/MS mass spectroscopy [132,154]. Aptamer-mediated target identification is not an easy process, due to the

inherent properties of lipid embedded proteins (hydrophobicity, poor solubility, resistance to digestion ...), even though significant advances have occurred to address these challenges [155].

Other methods, indirect compared to the method described above, have been used to identify a protein target post-cell-based SELEX. For example, Esposito et al. [130] used different techniques to characterize an aptamer's target. They realized a whole-cell-based SELEX strategy on human NSCLC to select 2′-fluoro RNA aptamers, which distinguish A549 cells (used for positive selection) from H460 cells (used for counter selection). The best candidate, CL4, was used to identify functional targets using a phospho-RTK array analysis, which provided convincing evidence that the target could likely be EGFR and/or ErbB3. To definitively identify the target, authors performed first a filter binding analysis with the soluble extracellular domains of EGFR and ErbB3, which showed a strong affinity for the EGFR protein (in its monomeric and dimeric forms), while no binding was observed for the ErbB3 protein. Binding of the radiolabeled CL4 aptamer to EGFR was confirmed on NIH3T3 cells overexpressing EGFR and compared to NIH3T3 cells. Binding to A549 cells was decreased by interfering with EGFR expression and by high concentration of EGF. Binding of radiolabeled CL4 on A549 cells was competed by soluble EGFR but not by soluble ErbB3. The specific interaction of CL4 with EGFR on cell surface was further analyzed by affinity purification on streptavidin coated beads of extracts from A549 cells treated with biotin-labeled CL4 followed by immunoblotting with anti-EGFR antibodies. Then, CL4 was detected on stable tumor derived cell lines that express high levels of EGFR. Later [156] this aptamer has been shown to bind to the EGFRvIII mutant, even though the mutant lacks most of domains I and III in the extracellular part of the protein. Other methods have been used to demonstrate the binding of CL4 to glioblastoma U87MG cells stably transfected with the EGFRvIII mutant: reverse transcription polymerase chain reaction, confocal microscopy with fluorescent FAM-labelled aptamer and flow cytometry. The binding was shown to inhibit EGFRvIII autophosphorylation and to affect migration, invasion and proliferation of glioblastoma cells.

Cell-based SELEX might lead to the selection of aptamers against other proteins than the pre-identified target. A cell-based SELEX was performed by Cibiel et al. [157] to identify aptamers against CHO-K1 cells expressing the Endothelin type B receptor (ET_BR), using the isogenic CHO-K1 cell line for counter selection rounds. None of the selected aptamers could discriminate between both cell lines. Nevertheless, the authors decided to study the 2′-fluoro RNA aptamer ACE4. The band excised from the PAGE-gel revealed that ACE4 did not interact with ET_BR, but with Annexin-2, a calcium dependent phospholipid-binding protein which is up-regulated in various tumor types and plays multiple roles in regulating cellular functions (angiogenesis, proliferation, cell migration and adhesion). The high affinity aptamer, although not initially planned to bind to the post-SELEX identified tumor biomarker Annexin A2, could however be a promising tool for biomedical applications. In another example [158], a panel of G-rich ssDNA aptamers was selected by cell-SELEX against EGFR-transfected A549 cell line, using A549 cells for counter selection, and their targets was suggested to be nucleolin.

4. Applications of Aptamers in Oncology

Besides their role for biomarker discovery above mentioned, aptamers have many applications in oncology. Some relevant applications of aptamers in the cancer field will be briefly described.

4.1. Aptamers as Detection and Imaging Reagent

Current approaches of protein biomarker detection include gel electrophoresis and conventional immunoassays (for capture and/or detection) such as enzyme-linked immunosorbent assay (ELISA), surface plasmon resonance, mass-sensing BioCD protein array, surface enhanced Raman spectroscopy (SERS), microfluidics and colorimetric, electrochemical and fluorescence assays (flow cytometry, europium or gold nanoparticle based detection, protein microarray, quantum dots ...). Most of these approaches still lack accuracy, sensitivity and specificity required for diagnostic application. Advantages and limitations of these methods have been compared for the prostate specific antigen (PSA) biomarker detection [159]. Different cancer biosensors and their characteristics were recently

reported [160]. Aptamers are a class of bio-recognition element which can be used as molecular tools for clinical diagnosis [161,162]. For localization of proteins on tissue sections to aid in histopathological diagnosis, aptahistochemistry methods have been developed [163]. Soluble tumor biomarkers (notably CEA, EGFR, HER2, MUC1, PSA) were detected on aptamer-based analytical platforms with low limits of detection [164]. Aptamers can be used in sufficiently sensitive diagnosis assays for the detection and capture of circulating tumor cells [165,166]. Upon the binding to their targets, conformational changes undergone by aptamers can be converted into measurable signals. So called aptasensors match the requirements of fast and portable molecular devices. The most current applications of aptasensors in oncology concerns biomarker detection [167]. A recent review reports the development of aptasensors for analysis of tumor biomarkers using electrochemical, electrochemoluminescence and photoelectrochemical transduction. In particular, nano-structure-based aptasensors significantly improved analytical performances [168]. Aptasensors can also be used to detect exoxomes [169]. Aptamers can be used as imaging agents [170–173], for example to track cell status and functions [174]. In particular, glioblastoma-specific aptamers were developed by either targeting the whole cell surface or known glioma biomarkers. Coupled with radionuclide or fluorescent labels, bioconjugates or nanoparticles, they represent a noninvasive manner for defining the tumor tissue border [103].

4.2. Aptamers in Therapy

Applications of aptamers as targeted therapeutics have been reviewed recently [15,175,176]. Nucleic acid aptamers can serve as antagonist or agonist and have therefore a direct therapeutic effect by themselves by activating or blocking key cellular functions upon interaction with their cellular targets. Particularly, aptamers have been successfully used as agonists of co-stimulatory receptors, like CD28, OX40 and 4-1BB, in aptamer-mediated cancer immunotherapy [177–179]. Multivalent aptamers which induce receptor multimerization, are often more efficient than monovalent aptamers to trigger downstream signaling [87]. Aptamers can also be used as delivery tools of therapeutic agents [15,180–183]. Internalized receptors carry along loaded aptamers [184]. Aptamers are thus cargoes which deliver therapeutics inside the cytosol of specific targeted cells where therapeutics exert their intracellular actions. Aptamer chimera, composed of an aptamer and a therapeutic nucleic acid, may target cancer cells and deliver anti-cancer nucleic acids, e.g. small interfering RNA, micro RNA, antimicroRNA and small hairpin RNA, for aptamer-mediated gene therapy [185]. Aptamers can also act as carriers for anti-tumor drugs or toxins [186,187]. Therapeutic agents are either non-covalently or covalently conjugated to aptamers. Doxorubicin, a chemotherapeutic agent extensively used in the treatment of various cancers, has often been used as a drug non-covalently conjugated to aptamers containing CG/GC sequences or covalently conjugated to aptamer through a functional linker [87]. Other aptamer-drug or-toxin conjugates include gemcitabine, docetaxel, daunorubicin, cisplatin, gelonin. For aptamer-mediated therapeutics delivery, aptamers have also been associated to nanoparticles [87,188–193]. Such aptamer nanocomplexes can be composed of copolymers, liposomes, metal nanomaterials (like gold nanoparticles, [194]), or virus-like particles.

5. Aptamers in Clinical Trials

Eleven aptamers have entered clinical stages [175,195] for eye disorders (three aptamers), coagulation (four aptamers), inflammation (two aptamers) and cancer (two aptamers). The majority of aptamer targets in clinical trials are extracellular proteins. The advantage linked to an extracellular protein is that the aptamer activity can be reversed by the use of an oligonucleotide antidote. Pegnivacogin is an antithrombotic aptamer that binds and inhibits coagulation factor IXa. The pegnivacogin dose-dependent antithrombotic activity can be reversed with an antidote, anivamersen, a 15-nucleotide long 2′-*O*-methyl RNA [196,197]. Pegnivacogin is a 2′-fluoro-2′-*O*-methyl 31 nucleotide long RNA aptamer, protected from exonuclease degradation by a 3′ inverted deoxythymidine cap. It is branched with a 40 kDa PEG carrier. PEGylation is generally used to increase aptamers molecular weight, prolong their circulating half-life by limiting renal clearance,

enhance their stability and decrease their toxic accumulation in tissues and the volume of distribution of therapeutic molecules [198–200]. Tested in a phase IIb study, in patients with acute coronary syndrome, pegnivacogin administration resulted in allergic reactions after the first dose in three patients of 640. Two of them presented an anaphylactic reaction and one presented an isolated dermal reaction. These observations induced an early termination of the trial [201]. A phase III clinical trial (NCT01848106), enrolling 3232 patients undergoing percutaneous coronary intervention, terminated at an early stage, due to severe allergic reactions reported in 1% of patients receiving pegnivacogin versus <1% of patients treated with bivalirudin [202–204]. However, it was observed that pegnivacogin did not induce inflammation response or histamine release. This aptamer, or its degradation, was therefore not responsible for the observed severe allergic reactions. Patients with allergic reactions had high levels of antibody to PEG, induced by complement activation and trypase release [205]. In 1983 was first reported the induction of antibodies against PEG in animals [206], but induction of PEG immunogenicity became clearer these last years as more PEGylated therapeutics enter clinical trials [207–209]. Currently formulated with a 40 kDa PEG carrier, pegnivacogin is associated with severe allergic reactions [203].

Pegaptanib sodium or Macugen [210] was the first aptamer-based drug approved by the U.S. Food and Drug Administration, in December 2004. Pegaptanib sodium is a 2′-fluoropyrimidine RNA-based aptamer, 28 nucleotides in length that terminates in a pentylamino linker, to which two 20-kiloDalton monomethoxy PEG units are covalently attached. It recognizes the abundant isoform of vascular endothelial growth factor, $VEGF_{165}$. As an inhibitor of $VEGF_{165}$-associated vessel formation, pegaptanib sodium is an anti-angiogenic medicine for the treatment of wet age-related macular degeneration. Pegaptanib sodium has also potential therapeutic effects as an agent for solid cancers characterized by extensive angiogenesis [15].

In oncology, two aptamers have undergone clinical trials. The first one was AS1411 (AGRO100), a DNA quadruplex targeting nucleolin. This multifunctional protein, located in the nucleolus but overexpressed at the membrane of several cancer cells, is implicated in cancer development by interacting with key oncogenes (bcl-2, Rb, p53, Akt-1) and by transferring specific extracellular ligands into the cells. The interaction of AS1411 and nucleolin induces internalization, inhibition of DNA synthesis and induction of apoptosis [127,211–214]. In a phase I study (September 2003 and July 2004), AS1411was tested in advanced cancer. Results showed that 8/16 patients had a stable disease during 2–9 months and one patient presented a complete response after more than 6 months [215]. In another phase I study (NCT00881244, September 2003–April 2009) [216], AS1411 was tested in patients with advanced solid tumors. AS1411 was well-tolerated. It induced a partial and a complete response in twelve patients with metastatic renal-cell carcinoma (RCC) and a stabilization of disease (>2 months) for seven patients. In 2008, Aptamer AS1411 was tested in a phase II study, in monotherapy, in patients with advanced metastatic RCC who had failed treatment with >1prior tyrosine kinase inhibitor (NCT00740441, August 2008–September 2009). AS1411 has been administrated at 40 mg/kg/j for the 4 first days of a 28 days cycle for two cycles. Out of 35 patients, 33 finished the two cycles. One patient presented a partial response. The OOR was only 2.9% (24 months). Twelve (34.3%) patients presented a stabilization of disease (5.5 month) and 21 patients (60%) presented a progression of disease. Adverse effects were observed on 12 grade 1 or 2 patients. This study showed a low level of activity of AS1411 in patients with metastatic RRC. An important and durable response has however been observed without toxicity [217]. AS1411 has also been evaluated in a phase II study combined with cytarabine (chemotherapy) for the treatment of patients with primary refractory or relapsed acute myeloid leukemia (NCT00512083, December 2009–February 2011). Few patients presented a durable remission. But the drug combination was proved to be safe (40 mg/kg/day for 7 days), well tolerated and shows promising signs of activity [218].

NOX-A12 (olaptesed pegol) is in clinical development for the treatment of chronic lymphatic leukemia and multiple myeloma [219–221]. NOX-A12 is a 45 nucleotide long L-stereoisomer RNA aptamer (Spiegelmer®, NOXXON Pharma AG, Berlin, Germany), which is a specific antagonist of CXCL12/SDF-1 (C-X-C motif ligand 12/stromal cell-derived factor 1). This chemokine, via interaction

with the receptors CXCR4 and CXCR7, induces attraction and activation of immune and non-immune cells, migration and adhesion of tumor cells to the protective tissue microenvironment. In tumor cells expressing a high level of CXCR4, the disruption of the CXCR4-CXCL2 interaction induces a diminution of the interactions of cancer cells with the bone marrow environment. This cell mobilization sensitizes cancer cells to therapy. NOX-A12 has been evaluated in two phase I and two phase II clinical studies. In a phase IIa study, in combination with bendamustine and rituximab (chemotherapy) in patients with relapsed/refractory chronic lymphocytic leukemia (CCL) (NCT01486797 march 2012 and January 2016) [222], results showed an effective long-term mobilization of CLL cell and an increased CLL cells circulating in the periphery blood. In term of clinical efficacy, all patients responded to the combination of chemotherapy and NOX-A12. The ORR was 100%. A partial response was achieved for 19/28 patients (68%) and a complete remission for 4/28 patient (14%). Among them, 8 high-risk patients, who had relapsed within 24 months after the first fludarabine/bendamustine treatment or presenting TP53-deletion/mutation, presented a partial or complete response. NOX-A12 was safe and well tolerated. In another independent phase IIa clinical study, NOX-A12 has been evaluated in combination with a proteasome inhibitor, bortezomib, and a corticosteroid, dexamethasone (VD) in previously treated patients with multiple myeloma. This study started in March 2012 and finished in October 2015 (NCT01521533) [223]. A mobilization of myeloma cells was shown in plasma. The OOR was estimated at 68%. Five patients (18%) presented a very good partial response, 2/28 (7%) a complete response and 12/28 (43%) a partial response. These studies showed that aptamer NOX-A12 merits further study in randomized controlled trials.

6. Conclusions

Due to their pleiotropic characteristics and improvements in the SELEX technology, aptamers, which can be selected to virtually any type of targets, are thought to gain rapidly an important place in clinical applications and may replace in many cases animal-derived antibodies. Aptamers as synthetic molecules are believed to save cost and time in R&D and manufacture. The targets of aptamers actually in clinical trials [175] are extracellular proteins (VEGF165, C5, PDGFβ, coagulation factor IXa, A1 domain of von Willebrand factor, thrombin, TFPI, CXCL12, CCL2, hepcidin peptide hormone), except nucleolin which is highly expressed at the surface of several tumor cells. Most of the aptamers in clinical trials were identified by protein-SELEX. Combination of protein-and cell-based selection processes may allow the discovery of highly selective but also conformation-dependent aptamers against tumor cell membrane biomarkers. Other selection processes more difficult to settle than protein-and cell-based SELEX and for which targets cannot be determined before selection, have been described to target a tumor under near-in vivo conditions. Aptamers have been selected on tissue sections [224,225], and very recently by Morph-X-Select (morphology based tissue aptamer selection, a combination of image-directed laser micro-dissection technology with tissue SELEX) on targeted tissue sections for ovarian cancer biomarker discovery [226]. Such selected DNA thio-aptamers have shown specificity to tumor vasculature of human ovarian tissue and human microvascular endothelial cells but not to the tumor stromal cells. Aptamers selected in living animals, through in vivo tissue-specific SELEX, have been shown to localize to hepatic colon cancer metastase [227] or to enter the brain after peripheral delivery [228]. These processes should prove helpful to characterize new tumor cell surface protein biomarkers, post-selection. Exciting new fields for aptamer applications in oncology emerge nowadays including detection of circulating tumor cells or tumor exosomes in biological fluid, and specific delivery of therapeutics inside cells with possibilities of co-targeting multiple oncogenic pathways. New opportunities for aptamers as multipotent tools will be characterized and will provide the pavement for approved clinical applications in the near future.

Acknowledgments: We are grateful to Pierre Fechter for valuable comments of the manuscript. This study was supported by the CNRS-French National Center for Scientific Research, the University of Strasbourg (PEPS-IDEX W15RPE24) and SATT-Conectus. Marie-Cécile Mercier is a doctoral fellow from Hospital of Strasbourg.

Conflicts of Interest: The authors declare no conflict of interest.

References

1. Ellington, A.D.; Szostak, J.W. In vitro selection of RNA molecules that bind specific ligands. *Nature* **1990**, *346*, 818–822. [CrossRef] [PubMed]
2. Robertson, D.L.; Joyce, G.F. Selection in vitro of an RNA enzyme that specifically cleaves single-stranded DNA. *Nature* **1990**, *344*, 467–468. [CrossRef] [PubMed]
3. Tuerk, C.; Gold, L. Systematic evolution of ligands by exponential enrichment: RNA ligands to bacteriophage T4 DNA polymerase. *Science* **1990**, *249*, 505–510. [CrossRef] [PubMed]
4. Ponomarenko, J.V.; Orlova, G.V.; Frolov, A.S.; Gelfand, M.S.; Ponomarenko, M.P. SELEX_DB: A database on in vitro selected oligomers adapted for recognizing natural sites and for analyzing both SNPs and site-directed mutagenesis data. *Nucleic Acids Res.* **2002**, *30*, 195–199. [CrossRef] [PubMed]
5. Aptamer Database Apta-Index™. Available online: http://www.aptagen.com/aptamer-index/aptamer-list.aspx (accessed on 1 June 2017).
6. Cruz-Toledo, J.; McKeague, M.; Zhang, X.; Giamberardino, A.; McConnell, E.; Francis, T.; DeRosa, M.C.; Dumontier, M. Aptamer base: A collaborative knowledge base to describe aptamers and SELEX experiments. *Database* **2012**, *2012*, bas006. [CrossRef] [PubMed]
7. Lao, Y.-H.; Phua, K.K.L.; Leong, K.W. Aptamer nanomedicine for cancer therapeutics: Barriers and potential for translation. *ACS Nano* **2015**, *9*, 2235–2254. [CrossRef] [PubMed]
8. Jacobi, N.; Seeboeck, R.; Hofmann, E.; Eger, A. ErbB family signalling: A paradigm for oncogene addiction and personalized oncology. *Cancers* **2017**, *9*, 33. [CrossRef] [PubMed]
9. Lemech, C.; Arkenau, H.-T. Biomarkers in advanced colorectal cancer: Challenges in translating clinical research into practice. *Cancers* **2011**, *3*, 1844–1860. [CrossRef] [PubMed]
10. Ciriello, G.; Miller, M.L.; Aksoy, B.A.; Senbabaoglu, Y.; Schultz, N.; Sander, C. Emerging landscape of oncogenic signatures across human cancers. *Nat. Genet.* **2013**, *45*, 1127–1133. [CrossRef] [PubMed]
11. Camorani, S.; Crescenzi, E.; Gramanzini, M.; Fedele, M.; Zannetti, A.; Cerchia, L. Aptamer-mediated impairment of EGFR-integrin αvβ3 complex inhibits vasculogenic mimicry and growth of triple-negative breast cancers. *Sci. Rep.* **2017**, *7*, 46659. [CrossRef] [PubMed]
12. Szász, A.M.; Győrffy, B.; Marko-Varga, G. Cancer heterogeneity determined by functional proteomics. *Semin. Cell Dev. Biol.* **2017**, *64*, 132–142. [CrossRef] [PubMed]
13. Ceccarelli, M.; Barthel, F.P.; Malta, T.M.; Sabedot, T.S.; Salama, S.R.; Murray, B.A.; Morozova, O.; Newton, Y.; Radenbaugh, A.; Pagnotta, S.M.; et al. Molecular profiling reveals biologically discrete subsets and pathways of progression in diffuse glioma. *Cell* **2016**, *164*, 550–563. [CrossRef] [PubMed]
14. Monaco, I.; Camorani, S.; Colecchia, D.; LOCATELLI, E.; Calandro, P.; Oudin, A.; Niclou, S.; Arra, C.; Chiariello, M.; Cerchia, L.; et al. Aptamer functionalization of nanosystems for glioblastoma targeting through the blood-brain-barrier. *J. Med. Chem.* **2017**, *60*, 4510–4516. [CrossRef] [PubMed]
15. Zhou, G.; Wilson, G.; Hebbard, L.; Duan, W.; Liddle, C.; George, J.; Qiao, L. Aptamers: A promising chemical antibody for cancer therapy. *Oncotarget* **2016**, *7*, 13446–13463. [PubMed]
16. Xiang, D.; Zheng, C.; Zhou, S.-F.; Qiao, S.; Tran, P.H.-L.; Pu, C.; Li, Y.; Kong, L.; Kouzani, A.Z.; Lin, J.; et al. Superior performance of aptamer in tumor penetration over antibody: Implication of aptamer-based theranostics in solid tumors. *Theranostics* **2015**, *5*, 1083–1097. [CrossRef] [PubMed]
17. Avci-Adali, M.; Paul, A.; Wilhelm, N.; Ziemer, G.; Wendel, H.P. Upgrading SELEX technology by using lambda exonuclease digestion for Single-Stranded DNA generation. *Molecules* **2009**, *15*, 1–11. [CrossRef] [PubMed]
18. Paul, A.; Avci-Adali, M.; Ziemer, G.; Wendel, H.P. Streptavidin-coated magnetic beads for DNA strand separation implicate a multitude of problems during cell-SELEX. *Oligonucleotides* **2009**, *19*, 243–254. [CrossRef] [PubMed]
19. Eulberg, D.; Klussmann, S. Spiegelmers: Biostable aptamers. *ChemBioChem* **2003**, *4*, 979–983. [CrossRef] [PubMed]
20. Padilla, R.; Sousa, R. Efficient synthesis of nucleic acids heavily modified with non-canonical ribose 2′-groups using a mutant T7 RNA polymerase (RNAP). *Nucleic Acids Res.* **1999**, *27*, 1561–1563. [CrossRef] [PubMed]
21. Burmeister, P.E.; Lewis, S.D.; Silva, R.F.; Preiss, J.R.; Horwitz, L.R.; Pendergrast, P.S.; McCauley, T.G.; Kurz, J.C.; Epstein, D.M.; Wilson, C.; et al. Direct in vitro selection of a 2′-*O*-methyl aptamer to VEGF. *Chem. Biol.* **2005**, *12*, 25–33. [CrossRef] [PubMed]

22. Pinheiro, V.B.; Taylor, A.I.; Cozens, C.; Abramov, M.; Renders, M.; Zhang, S.; Chaput, J.C.; Wengel, J.; Peak-Chew, S.-Y.; McLaughlin, S.H.; et al. Synthetic genetic polymers capable of heredity and evolution. *Science* **2012**, *336*, 341–344. [CrossRef] [PubMed]
23. Kuwahara, M.; Obika, S. In vitro selection of BNA (LNA) aptamers. *Artif. DNA PNA XNA* **2013**, *4*, 39–48. [CrossRef] [PubMed]
24. Kasahara, Y.; Irisawa, Y.; Ozaki, H.; Obika, S.; Kuwahara, M. 2′,4′-BNA/LNA aptamers: CE-SELEX using a DNA-based library of full-length 2′-*O*,4′-C-methylene-bridged/linked bicyclic ribonucleotides. *Bioorg. Med. Chem. Lett.* **2013**, *23*, 1288–1292. [CrossRef] [PubMed]
25. Veedu, R.N.; Wengel, J. Locked nucleic acid nucleoside triphosphates and polymerases: On the way towards evolution of LNAaptamers. *Mol. Biosyst.* **2009**, *5*, 787–792. [CrossRef] [PubMed]
26. Shigdar, S.; Macdonald, J.; O'Connor, M.; Wang, T.; Xiang, D.; Al.Shamaileh, H.; Qiao, L.; Wei, M.; Zhou, S.-F.; Zhu, Y.; et al. Aptamers as theranostic agents: Modifications, serum stability and functionalisation. *Sensors* **2013**, *13*, 13624–13637. [CrossRef] [PubMed]
27. Anosova, I.; Kowal, E.A.; Dunn, M.R.; Chaput, J.C.; Van Horn, W.D.; Egli, M. The structural diversity of artificial genetic polymers. *Nucleic Acids Res.* **2016**, *44*, 1007–1021. [CrossRef] [PubMed]
28. Pinheiro, V.B.; Holliger, P. Towards XNA nanotechnology: New materials from synthetic genetic polymers. *Trends Biotechnol.* **2014**, *32*, 321–328. [CrossRef] [PubMed]
29. Gold, L.; Ayers, D.; Bertino, J.; Bock, C.; Bock, A.; Brody, E.N.; Carter, J.; Dalby, A.B.; Eaton, B.E.; Fitzwater, T.; et al. Aptamer-based multiplexed proteomic technology for biomarker discovery. *PLoS ONE* **2010**, *5*, e15004. [CrossRef] [PubMed]
30. Eaton, B.E. The joys of in vitro selection: Chemically dressing oligonucleotides to satiate protein targets. *Curr. Opin. Chem. Biol.* **1997**, *1*, 10–16. [CrossRef]
31. Sun, H.; Zu, Y. A Highlight of recent advances in aptamer technology and its application. *Molecules* **2015**, *20*, 11959–11980. [CrossRef] [PubMed]
32. Andreola, M.-L.; Calmels, C.; Michel, J.; Toulmé, J.-J.; Litvak, S. Towards the selection of phosphorothioate aptamers. *Eur. J. Biochem.* **2000**, *267*, 5032–5040. [CrossRef] [PubMed]
33. Lato, S.M.; Ozerova, N.D.S.; He, K.; Sergueeva, Z.; Shaw, B.R.; Burke, D.H. Boron-containing aptamers to ATP. *Nucleic Acids Res.* **2002**, *30*, 1401–1407. [CrossRef] [PubMed]
34. Keefe, A.D.; Cload, S.T. SELEX with modified nucleotides. *Curr. Opin. Chem. Biol.* **2008**, *12*, 448–456. [CrossRef] [PubMed]
35. Vater, A.; Klussmann, S. Turning mirror-image oligonucleotides into drugs: The evolution of Spiegelmer® therapeutics. *Drug Discov. Today* **2015**, *20*, 147–155. [CrossRef] [PubMed]
36. Farokhzad, O.C.; Cheng, J.; Teply, B.A.; Sherifi, I.; Jon, S.; Kantoff, P.W.; Richie, J.P.; Langer, R. Targeted nanoparticle-aptamer bioconjugates for cancer chemotherapy in vivo. *Proc. Natl. Acad. Sci. USA* **2006**, *103*, 6315–6320. [CrossRef] [PubMed]
37. Lee, I.-H.; An, S.; Yu, M.K.; Kwon, H.-K.; Im, S.-H.; Jon, S. Targeted chemoimmunotherapy using drug-loaded aptamer–dendrimer bioconjugates. *J. Control. Release* **2011**, *155*, 435–441. [CrossRef] [PubMed]
38. Baek, S.E.; Lee, K.H.; Park, Y.S.; Oh, D.-K.; Oh, S.; Kim, K.-S.; Kim, D.-E. RNA aptamer-conjugated liposome as an efficient anticancer drug delivery vehicle targeting cancer cells in vivo. *J. Control. Release* **2014**, *196*, 234–242.
39. Willis, M.C.; Collins, B.; Zhang, T.; Green, L.S.; Sebesta, D.P.; Bell, C.; Kellogg, E.; Gill, S.C.; Magallanez, A.; Knauer, S.; et al. Liposome-anchored vascular endothelial growth factor aptamers. *Bioconjug. Chem.* **1998**, *9*, 573–582. [CrossRef] [PubMed]
40. Farokhzad, O.C.; Jon, S.; Khademhosseini, A.; Tran, T.-N.T.; LaVan, D.A.; Langer, R. Nanoparticle-aptamer bioconjugates. *Cancer Res.* **2004**, *64*, 7668–7672. [CrossRef] [PubMed]
41. Healy, J.M.; Lewis, S.D.; Kurz, M.; Boomer, R.M.; Thompson, K.M.; Wilson, C.; McCauley, T.G. Pharmacokinetics and biodistribution of novel aptamer compositions. *Pharm. Res.* **2004**, *21*, 2234–2246. [CrossRef] [PubMed]
42. Wang, J.; Li, G. Aptamers against cell surface receptors: Selection, modification and application. *Curr. Med. Chem.* **2011**, *18*, 4107–4116. [CrossRef] [PubMed]
43. Dua, P.; Kim, S.; Lee, D. Nucleic acid aptamers targeting cell-surface proteins. *Methods* **2011**, *54*, 215–225. [CrossRef] [PubMed]

44. Cibiel, A.; Dupont, D.M.; Ducongé, F. Methods to identify aptamers against cell surface biomarkers. *Pharmaceuticals* **2011**, *4*, 1216–1235. [CrossRef]
45. Shigdar, S.; Lin, J.; Yu, Y.; Pastuovic, M.; Wei, M.; Duan, W. RNA aptamer against a cancer stem cell marker epithelial cell adhesion molecule. *Cancer Sci.* **2011**, *102*, 991–998. [CrossRef] [PubMed]
46. Song, Y.; Zhu, Z.; An, Y.; Zhang, W.; Zhang, H.; Liu, D.; Yu, C.; Duan, W.; Yang, C.J. Selection of DNA aptamers against epithelial cell adhesion molecule for cancer cell imaging and circulating tumor cell capture. *Anal. Chem.* **2013**, *85*, 4141–4149. [CrossRef] [PubMed]
47. Lee, Y.J.; Han, S.R.; Kim, N.Y.; Lee, S.; Jeong, J.; Lee, S. An RNA aptamer that binds carcinoembryonic antigen inhibits hepatic metastasis of colon cancer cells in mice. *Gastroenterology* **2012**, *143*, 155–165.e8. [CrossRef] [PubMed]
48. Ruckman, J.; Gold, L.; Stephens, A.; Janjic, N. Nucleic acid ligands to integrins. U.S. Patent 6,331,394, 18 December 2001.
49. Mi, J.; Zhang, X.; Giangrande, P.H.; McNamara II, J.O.; Nimjee, S.M.; Sarraf-Yazdi, S.; Sullenger, B.A.; Clary, B.M. Targeted inhibition of αvβ3 integrin with an RNA aptamer impairs endothelial cell growth and survival. *Biochem. Biophys. Res. Commun.* **2005**, *338*, 956–963. [CrossRef] [PubMed]
50. Gong, Q.; Wang, J.; Ahmad, K.M.; Csordas, A.; Zhou, J.; Nie, J.; Stewart, R.; Thomson, J.A.; Rossi, J.J.; Soh, H.T. Selection strategy to generate aptamer pairs that bind to distinct sites on protein targets. *Anal. Chem.* **2012**, *84*, 5365–5371. [CrossRef] [PubMed]
51. Faryammanesh, R.; Lange, T.; Magbanua, E.; Haas, S.; Meyer, C.; Wicklein, D.; Schumacher, U.; Hahn, U. SDA, a DNA aptamer Inhibiting E- and P-Selectin mediated adhesion of cancer and leukemia cells, the first and pivotal step in transendothelial migration during metastasis formation. *PLoS ONE* **2014**, *9*, e93173. [CrossRef] [PubMed]
52. O'Connell, D.; Koenig, A.; Jennings, S.; Hicke, B.; Han, H.L.; Fitzwater, T.; Chang, Y.F.; Varki, N.; Parma, D.; Varki, A. Calcium-dependent oligonucleotide antagonists specific for L-selectin. *Proc. Natl. Acad. Sci. USA* **1996**, *93*, 5883–5887. [CrossRef] [PubMed]
53. Hicke, B.J.; Watson, S.R.; Koenig, A.; Lynott, C.K.; Bargatze, R.F.; Chang, Y.F.; Ringquist, S.; Moon-McDermott, L.; Jennings, S.; Fitzwater, T.; et al. DNA aptamers block L-selectin function in vivo. Inhibition of human lymphocyte trafficking in SCID mice. *J. Clin. Invest.* **1996**, *98*, 2688–2692. [CrossRef] [PubMed]
54. Li, N.; Larson, T.; Nguyen, H.H.; Sokolov, K.V.; Ellington, A.D. Directed evolution of gold nanoparticle delivery to cells. *Chem. Commun. Camb. Engl.* **2010**, *46*, 392–394. [CrossRef] [PubMed]
55. Li, N.; Nguyen, H.H.; Byrom, M.; Ellington, A.D. Inhibition of cell proliferation by an anti-EGFR aptamer. *PLoS ONE* **2011**, *6*, e20299. [CrossRef] [PubMed]
56. Ray, P.; Cheek, M.A.; Sharaf, M.L.; Li, N.; Ellington, A.D.; Sullenger, B.A.; Shaw, B.R.; White, R.R. Aptamer-mediated delivery of chemotherapy to pancreatic cancer cells. *Nucleic Acid Ther.* **2012**, *22*, 295–305. [PubMed]
57. Wang, D.-L.; Song, Y.-L.; Zhu, Z.; Li, X.-L.; Zou, Y.; Yang, H.-T.; Wang, J.-J.; Yao, P.-S.; Pan, R.-J.; Yang, C.J.; et al. Selection of DNA aptamers against epidermal growth factor receptor with high affinity and specificity. *Biochem. Biophys. Res. Commun.* **2014**, *453*, 681–685. [CrossRef] [PubMed]
58. Liu, Y.; Kuan, C.-T.; Mi, J.; Zhang, X.; Clary, B.M.; Bigner, D.D.; Sullenger, B.A. Aptamers selected against the unglycosylated EGFRvIII ectodomain and delivered intracellularly reduce membrane-bound EGFRvIII and induce apoptosis. *Biol. Chem.* **2009**, *390*, 137–144. [CrossRef] [PubMed]
59. Kim, M.Y.; Jeong, S. In Vitro Selection of RNA Aptamer and Specific Targeting of ErbB2 in Breast Cancer Cells. *Nucleic Acid Ther.* **2011**, *21*, 173–178. [CrossRef] [PubMed]
60. Liu, Z.; Duan, J.-H.; Song, Y.-M.; Ma, J.; Wang, F.-D.; Lu, X.; Yang, X.-D. Novel HER2 aptamer selectively delivers cytotoxic drug to HER2-positive breast cancer cells in vitro. *J. Transl. Med.* **2012**, *10*, 148. [CrossRef] [PubMed]
61. Hu, Y.; Duan, J.; Cao, B.; Zhang, L.; Lu, X.; Wang, F.; Yao, F.; Zhu, Z.; Yuan, W.; Wang, C.; et al. Selection of a novel DNA thioaptamer against HER2 structure. *Clin. Transl. Oncol.* **2015**, *17*, 647–656. [CrossRef] [PubMed]
62. Sett, A.; Borthakur, B.B.; Bora, U. Selection of DNA aptamers for extra cellular domain of human epidermal growth factor receptor 2 to detect HER2 positive carcinomas. *Clin. Transl. Oncol.* **2017**, 1–13. [CrossRef] [PubMed]

63. Chen, C.B.; Chernis, G.A.; Hoang, V.Q.; Landgraf, R. Inhibition of heregulin signaling by an aptamer that preferentially binds to the oligomeric form of human epidermal growth factor receptor-3. *Proc. Natl. Acad. Sci. USA* **2003**, *100*, 9226–9231. [CrossRef] [PubMed]
64. Boltz, A.; Piater, B.; Toleikis, L.; Guenther, R.; Kolmar, H.; Hock, B. Bi-specific aptamers mediating tumor cell lysis. *J. Biol. Chem.* **2011**, *286*, 21896–21905. [CrossRef] [PubMed]
65. Piater, B.; Doerner, A.; Guenther, R.; Kolmar, H.; Hock, B. Aptamers binding to c-Met inhibiting tumor cell migration. *PLoS ONE* **2015**, *10*, e0142412. [CrossRef] [PubMed]
66. Lupold, S.E.; Hicke, B.J.; Lin, Y.; Coffey, D.S. Identification and characterization of nuclease-stabilized rna molecules that bind human prostate cancer cells via the prostate-specific membrane antigen. *Cancer Res.* **2002**, *62*, 4029–4033. [PubMed]
67. McNamara, J.O.; Andrechek, E.R.; Wang, Y.; Viles, K.D.; Rempel, R.E.; Gilboa, E.; Sullenger, B.A.; Giangrande, P.H. Cell type–specific delivery of siRNAs with aptamer-siRNA chimeras. *Nat. Biotechnol.* **2006**, *24*, 1005–1015. [CrossRef] [PubMed]
68. Ferreira, C.S.M.; Matthews, C.S.; Missailidis, S. DNA aptamers that bind to MUC1 tumour marker: design and characterization of MUC1-binding single-stranded DNA aptamers. *Tumour Biol.* **2006**, *27*, 289–301. [CrossRef] [PubMed]
69. Ferreira, C.S.M.; Papamichael, K.; Guilbault, G.; Schwarzacher, T.; Gariepy, J.; Missailidis, S. DNA aptamers against the MUC1 tumour marker: Design of aptamer–antibody sandwich ELISA for the early diagnosis of epithelial tumours. *Anal. Bioanal. Chem.* **2008**, *390*, 1039–1050. [CrossRef] [PubMed]
70. Pratico, E.D.; Sullenger, B.A.; Nair, S.K. Identification and characterization of an agonistic aptamer against the T Cell costimulatory receptor, OX40. *Nucleic Acid Ther.* **2013**, *23*, 35–43. [CrossRef] [PubMed]
71. Dollins, C.M.; Nair, S.; Boczkowski, D.; Lee, J.; Layzer, J.M.; Gilboa, E.; Sullenger, B.A. Assembling OX40 Aptamers on a molecular scaffold to create a receptor-activating aptamer. *Chem. Biol.* **2008**, *15*, 675–682. [CrossRef] [PubMed]
72. McNamara, J.O.; Kolonias, D.; Pastor, F.; Mittler, R.S.; Chen, L.; Giangrande, P.H.; Sullenger, B.; Gilboa, E. Multivalent 4-1BB binding aptamers costimulate CD8+ T cells and inhibit tumor growth in mice. *J. Clin. Investig.* **2008**, *118*, 376–386. [CrossRef] [PubMed]
73. Mori, T.; Oguro, A.; Ohtsu, T.; Nakamura, Y. RNA aptamers selected against the receptor activator of NF-κB acquire general affinity to proteins of the tumor necrosis factor receptor family. *Nucleic Acids Res.* **2004**, *32*, 6120–6128. [CrossRef] [PubMed]
74. Pastor, F.; Soldevilla, M.M.; Villanueva, H.; Kolonias, D.; Inoges, S.; de Cerio, A.L.; Kandzia, R.; Klimyuk, V.; Gleba, Y.; Gilboa, E.; et al. CD28 aptamers as powerful immune response modulators. *Mol. Ther. Nucleic Acids* **2013**, *2*, e98. [CrossRef] [PubMed]
75. Santulli-Marotto, S.; Nair, S.K.; Rusconi, C.; Sullenger, B.; Gilboa, E. Multivalent RNA aptamers that inhibit Ctla-4 and enhance tumor immunity. *Cancer Res.* **2003**, *63*, 7483–7489. [PubMed]
76. Zhou, J.; Tiemann, K.; Chomchan, P.; Alluin, J.; Swiderski, P.; Burnett, J.; Zhang, X.; Forman, S.; Chen, R.; Rossi, J. Dual functional BAFF receptor aptamers inhibit ligand-induced proliferation and deliver siRNAs to NHL cells. *Nucleic Acids Res.* **2013**, *41*, 4266–4283. [CrossRef] [PubMed]
77. Roth, F.; Fuente, A.C.D.L.; Vella, J.L.; Zoso, A.; Inverardi, L.; Serafini, P. Aptamer-mediated blockade of IL4Rα triggers apoptosis of MDSCs and limits tumor progression. *Cancer Res.* **2012**, *72*, 1373–1383. [CrossRef] [PubMed]
78. Chauveau, F.; Aissouni, Y.; Hamm, J.; Boutin, H.; Libri, D.; Ducongé, F.; Tavitian, B. Binding of an aptamer to the N-terminal fragment of VCAM-1. *Bioorg. Med. Chem. Lett.* **2007**, *17*, 6119–6122. [CrossRef] [PubMed]
79. Watanabe, T.; Ito, K.; Matsumoto, M.; Seya, T.; Nishikawa, S.; Hasegawa, T.; Fukuda, K. Isolation of RNA aptamers against human Toll-like receptor 3 ectodomain. *Nucleic Acids Symp. Ser.* **2006**, 251–252. [CrossRef] [PubMed]
80. Somasunderam, A.; Thiviyanathan, V.; Tanaka, T.; Li, X.; Neerathilingam, M.; Lokesh, G.L.R.; Mann, A.; Peng, Y.; Ferrari, M.; Klostergaard, J.; et al. Combinatorial selection of DNA thioaptamers targeted towards the HA binding domain of human CD44. *Biochemistry* **2010**, *49*, 9106–9112. [CrossRef] [PubMed]
81. Ababneh, N.; Alshaer, W.; Allozi, O.; Mahafzah, A.; El-Khateeb, M.; Hillaireau, H.; Noiray, M.; Fattal, E.; Ismail, S. In vitro selection of modified RNA aptamers against CD44 cancer stem cell marker. *Nucleic Acid Ther.* **2013**, *23*, 401–407. [CrossRef] [PubMed]

82. White, R.R.; Roy, J.A.; Viles, K.D.; Sullenger, B.A.; Kontos, C.D. A nuclease-resistant RNA aptamer specifically inhibits angiopoietin-1-mediated Tie2 activation and function. *Angiogenesis* **2008**, *11*, 395–401. [CrossRef] [PubMed]
83. White, R.R.; Shan, S.; Rusconi, C.P.; Shetty, G.; Dewhirst, M.W.; Kontos, C.D.; Sullenger, B.A. Inhibition of rat corneal angiogenesis by a nuclease-resistant RNA aptamer specific for angiopoietin-2. *Proc. Natl. Acad. Sci. USA* **2003**, *100*, 5028–5033. [CrossRef] [PubMed]
84. Bates, P.J.; Laber, D.A.; Miller, D.M.; Thomas, S.D.; Trent, J.O. Discovery and development of the g-rich oligonucleotide AS1411 as a novel treatment for cancer. *Exp. Mol. Pathol.* **2009**, *86*, 151–164. [CrossRef] [PubMed]
85. Tam, R.C.; Phan, U.T.; Milovanovic, T.; Pai, B.; Lim, C.; Bard, J.; He, L. Oligonucleotide-mediated inhibition of CD28 expression induces human T-cell hyporesponsiveness and manifests impaired contact hypersensitivity in mice. *J. Immunol.* **1997**, *158*, 200–208. [PubMed]
86. Spencer, D.I.; Missailidis, S.; Denton, G.; Murray, A.; Brady, K.; Matteis, C.I.; Searle, M.S.; Tendler, S.J.; Price, M.R. Structure/activity studies of the anti-MUC1 monoclonal antibody C595 and synthetic MUC1 mucin-core-related peptides and glycopeptides. *Biospectroscopy* **1999**, *5*, 79–91. [CrossRef]
87. Sun, H.; Zhu, X.; Lu, P.Y.; Rosato, R.R.; Tan, W.; Zu, Y. Oligonucleotide aptamers: New tools for targeted cancer therapy. *Mol. Ther. Nucleic Acids* **2014**, *3*, e182. [CrossRef] [PubMed]
88. Blind, M.; Blank, M. Aptamer selection technology and recent advances. *Mol. Ther. Nucleic Acids* **2015**, *4*, e223. [CrossRef] [PubMed]
89. Shangguan, D.; Bing, T.; Zhang, N. Cell-SELEX: Aptamer selection against whole cells. In *Aptamers Selected by Cell-SELEX for Theranostics*; Tan, W., Fang, X., Eds.; Springer: Berlin/Heidelberg, Germany, 2015; pp. 13–33.
90. Mallikaratchy, P. Evolution of complex target SELEX to identify aptamers against mammalian cell-surface antigens. *Molecules* **2017**, *22*, 215. [CrossRef] [PubMed]
91. Mayer, G.; Ahmed, M.-S.L.; Dolf, A.; Endl, E.; Knolle, P.A.; Famulok, M. Fluorescence-activated cell sorting for aptamer SELEX with cell mixtures. *Nat. Protoc.* **2010**, *5*, 1993–2004. [CrossRef] [PubMed]
92. Raddatz, M.-S.L.; Dolf, A.; Endl, E.; Knolle, P.; Famulok, M.; Mayer, G. Enrichment of cell-targeting and population-specific aptamers by fluorescence-activated cell sorting. *Angew. Chem. Int. Ed.* **2008**, *47*, 5190–5193. [CrossRef] [PubMed]
93. Avci-Adali, M.; Metzger, M.; Perle, N.; Ziemer, G.; Wendel, H.P. Pitfalls of cell-systematic evolution of ligands by exponential enrichment (SELEX): Existing dead cells during in vitro selection anticipate the enrichment of specific aptamers. *Oligonucleotides* **2010**, *20*, 317–323. [CrossRef] [PubMed]
94. Wilner, S.E.; Wengerter, B.; Maier, K.; de Lourdes Borba Magalhães, M.; Del Amo, D.S.; Pai, S.; Opazo, F.; Rizzoli, S.O.; Yan, A.; Levy, M. An RNA alternative to human transferrin: a new tool for targeting human cells. *Mol. Ther. Nucleic Acids* **2012**, *1*, e21. [CrossRef] [PubMed]
95. Yan, A.; Levy, M. Cell Internalization SELEX: in vitro selection for molecules that internalize into cells. In *Therapeutic Applications of Ribozymes and Riboswitches*; Lafontaine, D., Dubé, A., Eds.; Methods in Molecular Biology; Humana Press: New York, NY, USA, 2014; pp. 241–265.
96. Gourronc, F.A.; Rockey, W.M.; Thiel, W.H.; Giangrande, P.H.; Klingelhutz, A.J. Identification of RNA aptamers that Internalize into HPV-16 E6/E7 transformed tonsillar epithelial cells. *Virology* **2013**, *446*, 325–333. [CrossRef] [PubMed]
97. Zhou, J.; Bobbin, M.L.; Burnett, J.C.; Rossi, J.J. Current progress of RNA aptamer-based therapeutics. *Front. Genet.* **2012**, *3*, 234. [CrossRef] [PubMed]
98. Thiel, W.H.; Bair, T.; Peek, A.S.; Liu, X.; Dassie, J.; Stockdale, K.R.; Behlke, M.A.; Miller, F.J.; Giangrande, P.H. Rapid identification of cell-specific, internalizing RNA aptamers with bioinformatics analyses of a cell-based aptamer selection. *PLoS ONE* **2012**, *7*, e43836. [CrossRef] [PubMed]
99. Camorani, S.; Esposito, C.L.; Rienzo, A.; Catuogno, S.; Iaboni, M.; Condorelli, G.; de Franciscis, V.; Cerchia, L. Inhibition of receptor signaling and of glioblastoma-derived tumor growth by a novel PDGFRβ aptamer. *Mol. Ther.* **2014**, *22*, 828–841. [CrossRef] [PubMed]
100. Thiel, K.W.; Hernandez, L.I.; Dassie, J.P.; Thiel, W.H.; Liu, X.; Stockdale, K.R.; Rothman, A.M.; Hernandez, F.J.; McNamara, J.O.; Giangrande, P.H. Delivery of chemo-sensitizing siRNAs to HER2^{+}-breast cancer cells using RNA aptamers. *Nucleic Acids Res.* **2012**, *40*, 6319–6337. [CrossRef] [PubMed]

101. Souza, A.G.; Marangoni, K.; Fujimura, P.T.; Alves, P.T.; Silva, M.J.; Bastos, V.A.F.; Goulart, L.R.; Goulart, V.A. 3D cell-SELEX: Development of RNA aptamers as molecular probes for PC-3 tumor cell line. *Exp. Cell Res.* **2016**, *341*, 147–156. [CrossRef] [PubMed]
102. Ohuchi, S.P.; Ohtsu, T.; Nakamura, Y. Selection of RNA aptamers against recombinant transforming growth factor-β type III receptor displayed on cell surface. *Biochimie* **2006**, *88*, 897–904. [CrossRef] [PubMed]
103. Delač, M.; Motaln, H.; Ulrich, H.; Lah, T.T. Aptamer for imaging and therapeutic targeting of brain tumor glioblastoma. *Cytometry A* **2015**, *87*, 806–816. [CrossRef] [PubMed]
104. Wadajkar, A.S.; Dancy, J.G.; Hersh, D.S.; Anastasiadis, P.; Tran, N.L.; Woodworth, G.F.; Winkles, J.A.; Kim, A.J. Tumor-targeted nanotherapeutics: overcoming treatment barriers for glioblastoma. *Wiley Interdiscip. Rev. Nanomed. Nanobiotechnol.* **2016**. [CrossRef] [PubMed]
105. Zumrut, H.E.; Ara, M.N.; Maio, G.E.; Van, N.A.; Batool, S.; Mallikaratchy, P.R. Ligand-guided selection of aptamers against T-cell receptor-cluster of differentiation 3 (TCR-CD3) expressed on Jurkat.E6 cells. *Anal. Biochem.* **2016**, *512*, 1–7. [CrossRef] [PubMed]
106. Zumrut, H.E.; Ara, M.N.; Fraile, M.; Maio, G.; Mallikaratchy, P. Ligand-guided selection of target-specific aptamers: A screening technology for identifying specific aptamers against cell-surface proteins. *Nucleic Acid Ther.* **2016**, *26*, 190–198. [CrossRef] [PubMed]
107. Chang, Y.-C.; Kao, W.-C.; Wang, W.-Y.; Wang, W.-Y.; Yang, R.-B.; Peck, K. Identification and characterization of oligonucleotides that inhibit Toll-like receptor 2-associated immune responses. *FASEB J.* **2009**, *23*, 3078–3088. [CrossRef] [PubMed]
108. Pestourie, C.; Cerchia, L.; Gombert, K.; Aissouni, Y.; Boulay, J.; Franciscis, V.D.; Libri, D.; Tavitian, B.; Ducongé, F. Comparison of different strategies to select aptamers against a transmembrane protein target. *Oligonucleotides* **2006**, *16*, 323–335. [CrossRef] [PubMed]
109. Zhu, G.; Zhang, H.; Jacobson, O.; Wang, Z.; Chen, H.; Yang, X.; Niu, G.; Chen, X. Combinatorial screening of DNA aptamers for molecular imaging of HER2 in cancer. *Bioconjug. Chem.* **2017**, *28*, 1068–1075. [CrossRef] [PubMed]
110. Berg, K.; Lange, T.; Mittelberger, F.; Schumacher, U.; Hahn, U. Selection and characterization of an α6β4 Integrin blocking DNA aptamer. *Mol. Ther. Nucleic Acids* **2016**, *5*, e294. [CrossRef] [PubMed]
111. Soldevilla, M.M.; Villanueva, H.; Casares, N.; Lasarte, J.J.; Bendandi, M.; Inoges, S.; de Cerio, A.L.-D.; Pastor, F. MRP1-CD28 bi-specific oligonucleotide aptamers: Target costimulation to drug-resistant melanoma cancer stem cells. *Oncotarget* **2016**, *7*, 23182–23196. [CrossRef] [PubMed]
112. Takahashi, M.; Sakota, E.; Nakamura, Y. The efficient cell-SELEX strategy, Icell-SELEX, using isogenic cell lines for selection and counter-selection to generate RNA aptamers to cell surface proteins. *Biochimie* **2016**, *131*, 77–84. [CrossRef] [PubMed]
113. Kang, S.K.; Huh, Y.M.; Lee, D. Isolation of RNA aptamers targeting HER-2-overexpressing breast cancer cells using cell-SELEX. *Bull. Korean Chem. Soc.* **2009**, *30*, 1827–1831.
114. Dastjerdi, K.; Tabar, G.H.; Dehghani, H.; Haghparast, A. Generation of an enriched pool of DNA aptamers for an HER2-overexpressing cell line selected by Cell SELEX. *Biotechnol. Appl. Biochem.* **2011**, *58*, 226–230. [CrossRef] [PubMed]
115. Parekh, P.; Kamble, S.; Zhao, N.; Zeng, Z.; Portier, B.P.; Zu, Y. Immunotherapy of CD30-expressing lymphoma using a highly stable ssDNA aptamer. *Biomaterials* **2013**, *34*, 8909–8917. [CrossRef] [PubMed]
116. Mahlknecht, G.; Maron, R.; Mancini, M.; Schechter, B.; Sela, M.; Yarden, Y. Aptamer to ErbB-2/HER2 enhances degradation of the target and inhibits tumorigenic growth. *Proc. Natl. Acad. Sci. USA* **2013**, *110*, 8170–8175. [CrossRef] [PubMed]
117. Tan, Y.; Shi, Y.; Wu, X.; Liang, H.; Gao, Y.; Li, S.; Zhang, X.; Wang, F.; Gao, T. DNA aptamers that target human glioblastoma multiforme cells overexpressing epidermal growth factor receptor variant III in vitro. *Acta Pharmacol. Sin.* **2013**, *34*, 1491–1498. [CrossRef] [PubMed]
118. Wu, X.; Liang, H.; Tan, Y.; Yuan, C.; Li, S.; Li, X.; Li, G.; Shi, Y.; Zhang, X. Cell-SELEX aptamer for highly specific radionuclide molecular imaging of glioblastoma in vivo. *PLoS ONE* **2014**, *9*, e90752. [CrossRef] [PubMed]
119. Huang, Y.Z.; Hernandez, F.J.; Gu, B.; Stockdale, K.R.; Nanapaneni, K.; Scheetz, T.E.; Behlke, M.A.; Peek, A.S.; Bair, T.; Giangrande, P.H.; et al. RNA Aptamer-Based Functional Ligands of the Neurotrophin Receptor, TrkB. *Mol. Pharmacol.* **2012**, *82*, 623–635. [CrossRef] [PubMed]

120. Kim, J.W.; Kim, E.Y.; Kim, S.Y.; Byun, S.K.; Lee, D.; Oh, K.-J.; Kim, W.K.; Han, B.S.; Chi, S.-W.; Lee, S.C.; et al. Identification of DNA aptamers toward epithelial cell adhesion molecule via cell-SELEX. *Mol. Cells* **2014**, *37*, 742–746. [CrossRef] [PubMed]
121. Shigdar, S.; Qiao, L.; Zhou, S.-F.; Xiang, D.; Wang, T.; Li, Y.; Lim, L.Y.; Kong, L.; Li, L.; Duan, W. RNA aptamers targeting cancer stem cell marker CD133. *Cancer Lett.* **2013**, *330*, 84–95. [CrossRef] [PubMed]
122. Chen, M.; Yu, Y.; Jiang, F.; Zhou, J.; Li, Y.; Liang, C.; Dang, L.; Lu, A.; Zhang, G. Development of cell-SELEX technology and its application in cancer diagnosis and therapy. *Int. J. Mol. Sci.* **2016**, *17*, 2079. [CrossRef] [PubMed]
123. Chang, Y.M.; Donovan, M.J.; Tan, W. Using aptamers for cancer biomarker discovery. *J. Nucleic Acids* **2013**, *2013*. [CrossRef] [PubMed]
124. Jin, C.; Qiu, L.; Li, J.; Fu, T.; Zhang, X.; Tan, W. Cancer Biomarker Discovery Using DNA Aptamers. *Analyst* **2016**, *141*, 461–466. [CrossRef] [PubMed]
125. Daniels, D.A.; Chen, H.; Hicke, B.J.; Swiderek, K.M.; Gold, L. A tenascin-C aptamer identified by tumor cell-SELEX: Systematic evolution of ligands by exponential enrichment. *Proc. Natl. Acad. Sci. USA* **2003**, *100*, 15416–15421. [CrossRef] [PubMed]
126. Ireson, C.R.; Kelland, L.R. Discovery and development of anticancer aptamers. *Mol. Cancer Ther.* **2006**, *5*, 2957–2962. [CrossRef] [PubMed]
127. Soundararajan, S.; Chen, W.; Spicer, E.K.; Courtenay-Luck, N.; Fernandes, D.J. The nucleolin targeting aptamer AS1411 destabilizes Bcl-2 messenger RNA in human breast cancer cells. *Cancer Res.* **2008**, *68*, 2358–2365. [CrossRef] [PubMed]
128. Soundararajan, S.; Wang, L.; Sridharan, V.; Chen, W.; Courtenay-Luck, N.; Jones, D.; Spicer, E.K.; Fernandes, D.J. Plasma membrane nucleolin is a receptor for the anticancer aptamer AS1411 in MV4-11 leukemia cells. *Mol. Pharmacol.* **2009**, *76*, 984–991. [CrossRef] [PubMed]
129. Bates, P.J.; Reyes-Reyes, E.M.; Malik, M.T.; Murphy, E.M.; O'Toole, M.G.; Trent, J.O. G-quadruplex oligonucleotide AS1411 as a cancer-targeting agent: Uses and mechanisms. *Biochim. Biophys. Acta* **2017**, *1861*, 1414–1428. [CrossRef] [PubMed]
130. Esposito, C.L.; Passaro, D.; Longobardo, I.; Condorelli, G.; Marotta, P.; Affuso, A.; de Franciscis, V.; Cerchia, L. A neutralizing rna aptamer against egfr causes selective apoptotic cell death. *PLoS ONE* **2011**, *6*, e24071. [CrossRef] [PubMed]
131. Dua, P.; Kang, H.S.; Hong, S.-M.; Tsao, M.-S.; Kim, S.; Lee, D. Alkaline phosphatase ALPPL-2 Is a novel pancreatic carcinoma-associated protein. *Cancer Res.* **2013**, *73*, 1934–1945. [CrossRef] [PubMed]
132. Bing, T.; Shangguan, D.; Wang, Y. Facile discovery of cell-surface protein targets of cancer cell aptamers. *Mol. Cell. Proteom.* **2015**, *14*, 2692–2700. [CrossRef] [PubMed]
133. Lu, M.; Zhou, L.; Zheng, X.; Quan, Y.; Wang, X.; Zhou, X.; Ren, J. A novel molecular marker of breast cancer stem cells identified by cell-SELEX method. *Cancer Biomark.* **2015**, *15*, 163–170. [CrossRef] [PubMed]
134. Sefah, K.; Bae, K.-M.; Phillips, J.A.; Siemann, D.W.; Su, Z.; McClellan, S.; Vieweg, J.; Tan, W. Cell-based selection provides novel molecular probes for cancer stem cells. *Int. J. Cancer J. Int. Cancer* **2013**, *132*, 2578–2588. [CrossRef] [PubMed]
135. Xiao, Z.; Shangguan, D.; Cao, Z.; Fang, X.; Tan, W. Cell-specific internalization study of an aptamer from whole cell selection. *Chem. Weinh. Bergstr. Ger.* **2008**, *14*, 1769–1775. [CrossRef] [PubMed]
136. Iaboni, M.; Fontanella, R.; Rienzo, A.; Capuozzo, M.; Nuzzo, S.; Santamaria, G.; Catuogno, S.; Condorelli, G.; de Franciscis, V.; Esposito, C.L. Targeting insulin receptor with a novel internalizing aptamer. *Mol. Ther. Nucleic Acids* **2016**, *5*, e365. [CrossRef] [PubMed]
137. Cerchia, L.; Esposito, C.L.; Camorani, S.; Rienzo, A.; Stasio, L.; Insabato, L.; Affuso, A.; de Franciscis, V. Targeting axl with an high-affinity inhibitory aptamer. *Mol. Ther.* **2012**, *20*, 2291–2303. [CrossRef] [PubMed]
138. Mallikaratchy, P.; Tang, Z.; Kwame, S.; Meng, L.; Shangguan, D.; Tan, W. Aptamer directly evolved from live cells recognizes membrane bound immunoglobin heavy mu chain in burkitt's lymphoma cells. *Mol. Cell. Proteom.* **2007**, *6*, 2230–2238. [CrossRef] [PubMed]
139. Berezovski, M.V.; Lechmann, M.; Musheev, M.U.; Mak, T.W.; Krylov, S.N. Aptamer-facilitated biomarker discovery (AptaBiD). *J. Am. Chem. Soc.* **2008**, *130*, 9137–9143. [CrossRef] [PubMed]
140. Zamay, G.S.; Kolovskaya, O.S.; Zamay, T.N.; Glazyrin, Y.E.; Krat, A.V.; Zubkova, O.; Spivak, E.; Wehbe, M.; Gargaun, A.; Muharemagic, D.; et al. Aptamers selected to postoperative lung adenocarcinoma detect circulating tumor cells in human blood. *Mol. Ther.* **2015**, *23*, 1486–1496. [CrossRef] [PubMed]

141. Zhang, K.; Tang, L.; Sefah, K.; Zhao, Z.; Zhu, G.; Sun, W.; Goodison, S.; Tan, W. Novel aptamer developed for breast cancer cell internalization. *Chem. Med. Chem.* **2012**, *7*, 79–84. [CrossRef] [PubMed]
142. Sefah, K.; Meng, L.; Lopez-Colon, D.; Jimenez, E.; Liu, C.; Tan, W. DNA aptamers as molecular probes for colorectal cancer study. *PLoS ONE* **2010**, *5*, e14269. [CrossRef] [PubMed]
143. Chen, H.W.; Medley, C.D.; Smith, J.E.; Sefah, K.; Shangguan, D.; Tang, Z.; Meng, L.; Tan, W. Molecular recognition of small cell lung cancer cells using aptamers. *Chem. Med. Chem.* **2008**, *3*, 991–1001. [CrossRef] [PubMed]
144. Kunii, T.; Ogura, S.; Mie, M.; Kobatake, E. Selection of DNA aptamers recognizing small cell lung cancer using living cell-SELEX. *Analyst* **2011**, *136*, 1310–1312. [CrossRef] [PubMed]
145. Zhao, Z.; Xu, L.; Shi, X.; Tan, W.; Fang, X.; Shangguan, D. Recognition of subtype non-small cell lung cancer by DNA aptamers selected from living cells. *Analyst* **2009**, *134*, 1808–1814. [CrossRef] [PubMed]
146. Shangguan, D.; Meng, L.; Cao, Z.C.; Xiao, Z.; Fang, X.; Li, Y.; Cardona, D.; Witek, R.P.; Liu, C.; Tan, W. Identification of liver cancer-specific aptamers using whole live cells. *Anal. Chem.* **2008**, *80*, 721–728. [CrossRef] [PubMed]
147. Shangguan, D.; Li, Y.; Tang, Z.; Cao, Z.C.; Chen, H.W.; Mallikaratchy, P.; Sefah, K.; Yang, C.J.; Tan, W. Aptamers evolved from live cells as effective molecular probes for cancer study. *Proc. Natl. Acad. Sci. USA* **2006**, *103*, 11838–11843. [CrossRef] [PubMed]
148. Sefah, K.; Tang, Z.; Shangguan, D.; Chen, H.; Lopez-Colon, D.; Li, Y.; Parekh, P.; Martin, J.; Meng, L.; Tan, W. Molecular recognition of acute myeloid leukemia using aptamers. *Leukemia* **2009**, *23*, 235–244. [CrossRef] [PubMed]
149. Zhang, X.; Zhang, J.; Ma, Y.; Pei, X.; Liu, Q.; Lu, B.; Jin, L.; Wang, J.; Liu, J. A cell-based single-stranded DNA aptamer specifically targets gastric cancer. *Int. J. Biochem. Cell Biol.* **2014**, *46*, 1–8. [CrossRef] [PubMed]
150. Wu, X.; Zhao, Z.; Bai, H.; Fu, T.; Yang, C.; Hu, X.; Liu, Q.; Champanhac, C.; Teng, I.-T.; Ye, M.; Tan, W. DNA aptamer selected against pancreatic ductal adenocarcinoma for in vivo imaging and clinical tissue recognition. *Theranostics* **2015**, *5*, 985–994. [CrossRef] [PubMed]
151. Rong, Y.; Chen, H.; Zhou, X.-F.; Yin, C.-Q.; Wang, B.-C.; Peng, C.-W.; Liu, S.-P.; Wang, F.-B. Identification of an aptamer through whole cell-SELEX for targeting high metastatic liver cancers. *Oncotarget* **2016**, *7*, 8282–8294. [PubMed]
152. Zueva, E.; Rubio, L.I.; Ducongé, F.; Tavitian, B. Metastasis-focused cell-based SELEX generates aptamers inhibiting cell migration and invasion. *Int. J. Cancer* **2011**, *128*, 797–804. [CrossRef] [PubMed]
153. Kim, Y.; Wu, Q.; Hamerlik, P.; Hitomi, M.; Sloan, A.E.; Barnett, G.H.; Weil, R.J.; Leahy, P.; Hjelmeland, A.B.; Rich, J.N. Aptamer Identification of Brain Tumor Initiating Cells. *Cancer Res.* **2013**, *73*, 4923–4936. [CrossRef] [PubMed]
154. Quang, N.; Miodek, A.; Cibiel, A.; Ducongé, F. Selection of aptamers against whole living cells: From cell-SELEX to identification of biomarkers. In *Synthetic Antibodies*; Tiller, T., Ed.; Methods in Molecular Biology; Springer: New York, NY, USA, 2017; pp. 253–272.
155. Griffin, N.M.; Schnitzer, J.E. Overcoming key technological challenges in using mass spectrometry for mapping cell surfaces in tissues. *Mol. Cell. Proteom.* **2011**, *10*, R110.000935. [CrossRef] [PubMed]
156. Camorani, S.; Crescenzi, E.; Colecchia, D.; Carpentieri, A.; Amoresano, A.; Fedele, M.; Chiariello, M.; Cerchia, L. Aptamer targeting EGFRvIII mutant hampers its constitutive autophosphorylation and affects migration, invasion and proliferation of glioblastoma cells. *Oncotarget* **2015**, *6*, 37570–37587. [PubMed]
157. Cibiel, A.; Nguyen Quang, N.; Gombert, K.; Thézé, B.; Garofalakis, A.; Ducongé, F. From Ugly Duckling to Swan: Unexpected identification from Cell-SELEX of an anti-annexin A2 aptamer targeting tumors. *PLoS ONE* **2014**, *9*, e87002. [CrossRef] [PubMed]
158. Xu, L.; Zhang, Z.; Zhao, Z.; Liu, Q.; Tan, W.; Fang, X. Cellular internalization and cytotoxicity of aptamers selected from lung cancer cell. *Am. J. Biomed. Sci.* **2013**, *5*, 47–58.
159. Nimse, S.B.; Sonawane, M.D.; Song, K.-S.; Kim, T. Biomarker detection technologies and future directions. *Analyst* **2016**, *141*, 740–755. [CrossRef] [PubMed]
160. Jayanthi, V.S.P.K.S.A.; Das, A.B.; Saxena, U. Recent advances in biosensor development for the detection of cancer biomarkers. *Biosens. Bioelectron.* **2017**, *91*, 15–23. [CrossRef] [PubMed]
161. Ozalp, V.C.; Kavruk, M.; Dilek, O.; Tahir, A. Aptamers: Molecular Tools for Medical Diagnosis. *Curr. Top. Med. Chem.* **2015**, *15*, 1125–1137. [CrossRef]

162. Prakash, J.S.; Rajamanickam, K. Aptamers and Their Significant Role in Cancer Therapy and Diagnosis. *Biomedicines* **2015**, *3*, 248–269. [CrossRef] [PubMed]
163. Bukari, B.A.; Citartan, M.; Ch'ng, E.S.; Bilibana, M.P.; Rozhdestvensky, T.; Tang, T.-H. Aptahistochemistry in diagnostic pathology: technical scrutiny and feasibility. *Histochem. Cell Biol.* **2017**, *147*, 545–553. [CrossRef] [PubMed]
164. Sun, H.; Tan, W.; Zu, Y. Aptamers: versatile molecular recognition probes for cancer detection. *Analyst* **2016**, *141*, 403–415. [CrossRef] [PubMed]
165. Dickey, D.D.; Giangrande, P.H. Oligonucleotide Aptamers: a Next-Generation Technology for the Capture and Detection of Circulating Tumor Cells. *Methods* **2016**, *97*, 94–103. [CrossRef] [PubMed]
166. Zamay, A.S.; Zamay, G.S.; Kolovskaya, O.S.; Zamay, T.N.; Berezovski, M.V. Aptamer-Based Methods for Detection of Circulating Tumor Cells and Their Potential for Personalized Diagnostics. *Adv. Exp. Med. Biol.* **2017**, *994*, 67–81. [PubMed]
167. Hong, P.; Li, W.; Li, J. Applications of Aptasensors in Clinical Diagnostics. *Sensors* **2012**, *12*, 1181–1193. [CrossRef] [PubMed]
168. Ravalli, A.; Voccia, D.; Palchetti, I.; Marrazza, G. Electrochemical, Electrochemiluminescence, and Photoelectrochemical Aptamer-Based Nanostructured Sensors for Biomarker Analysis. *Biosensors* **2016**, *6*. [CrossRef] [PubMed]
169. Zhou, Q.; Rahimian, A.; Son, K.; Shin, D.-S.; Patel, T.; Revzin, A. Development of an aptasensor for electrochemical detection of exosomes. *Methods* **2016**, *97*, 88–93. [CrossRef] [PubMed]
170. Jin, C.; Zheng, J.; Li, C.; Qiu, L.; Zhang, X.; Tan, W. Aptamers Selected by Cell-SELEX for Molecular Imaging. *J. Mol. Evol.* **2015**, *81*, 162–171. [CrossRef] [PubMed]
171. Dougherty, C.A.; Cai, W.; Hong, H. Applications of Aptamers in Targeted Imaging: State of the Art. *Curr. Top. Med. Chem.* **2015**, *15*, 1138–1152. [CrossRef] [PubMed]
172. Ku, T.-H.; Zhang, T.; Luo, H.; Yen, T.M.; Chen, P.-W.; Han, Y.; Lo, Y.-H. Nucleic acid aptamers: An emerging tool for biotechnology and biomedical sensing. *Sensors* **2015**, *15*, 16281–16313. [CrossRef] [PubMed]
173. Mankoff, D.A.; Link, J.M.; Linden, H.M.; Sundararajan, L.; Krohn, K.A. Tumor receptor imaging. *J. Nucl. Med.* **2008**, *49*, 149S–163S. [CrossRef] [PubMed]
174. Wiraja, C.; Yeo, D.; Lio, D.; Labanieh, L.; Lu, M.; Zhao, W.; Xu, C. Aptamer technology for tracking cells' status & function. *Mol. Cell. Ther.* **2014**, *2*. [CrossRef]
175. Zhou, J.; Rossi, J. Aptamers as targeted therapeutics: current potential and challenges. *Nat. Rev. Drug Discov.* **2017**, *16*, 181–202. [CrossRef] [PubMed]
176. Xiang, D.; Shigdar, S.; Qiao, G.; Wang, T.; Kouzani, A.Z.; Zhou, S.-F.; Kong, L.; Li, Y.; Pu, C.; Duan, W. Nucleic acid aptamer-guided cancer therapeutics and diagnostics: the next generation of cancer medicine. *Theranostics* **2015**, *5*, 23–42. [CrossRef] [PubMed]
177. Pastor, F. Aptamers: A New Technological Platform in Cancer Immunotherapy. *Pharmaceuticals* **2016**, *9*, 64. [CrossRef] [PubMed]
178. Soldevilla, M.M.; Villanueva, H.; Pastor, F. Aptamers: A Feasible Technology in Cancer Immunotherapy. *J. Immunol. Res.* **2016**, *2016*. [CrossRef] [PubMed]
179. Khedri, M.; Rafatpanah, H.; Abnous, K.; Ramezani, P.; Ramezani, M. Cancer immunotherapy via nucleic acid aptamers. *Int. Immunopharmacol.* **2015**, *29*, 926–936. [CrossRef] [PubMed]
180. Wu, X.; Chen, J.; Wu, M.; Zhao, J.X. Aptamers: Active targeting ligands for cancer diagnosis and therapy. *Theranostics* **2015**, *5*, 322–344. [CrossRef] [PubMed]
181. Lee, J.W.; Kim, H.J.; Heo, K. Therapeutic aptamers: Developmental potential as anticancer drugs. *BMB Rep.* **2015**, *48*, 234–237. [CrossRef] [PubMed]
182. Zhu, H.; Li, J.; Zhang, X.-B.; Ye, M.; Tan, W. Nucleic acid aptamer-mediated drug delivery for targeted cancer therapy. *ChemMedChem* **2015**, *10*, 39–45. [CrossRef] [PubMed]
183. Catuogno, S.; Esposito, C.L.; de Franciscis, V. Aptamer-mediated targeted delivery of therapeutics: An update. *Pharmaceuticals* **2016**, *9*, 69. [CrossRef] [PubMed]
184. Gopinath, S.C.B.; Lakshmipriya, T.; Chen, Y.; Arshad, M.K.M.; Kerishnan, J.P.; Ruslinda, A.R.; Al-Douri, Y.; Voon, C.H.; Hashim, U. Cell-targeting aptamers act as intracellular delivery vehicles. *Appl. Microbiol. Biotechnol.* **2016**, *100*, 6955–6969. [CrossRef] [PubMed]
185. Xiang, D.; Shigdar, S.; Qiao, G.; Zhou, S.-F.; Li, Y.; Wei, M.Q.; Qiao, L.; Al. Shamaileh, H.; Zhu, Y.; Zheng, C.; et al. Aptamer-mediated cancer gene therapy. *Curr. Gene Ther.* **2015**, *15*, 109–119. [CrossRef] [PubMed]

186. Parashar, A. Aptamers in Therapeutics. *J. Clin. Diagn. Res. JCDR* **2016**, *10*, BE01–BE06. [CrossRef] [PubMed]
187. Zhu, G.; Niu, G.; Chen, X. Aptamer–Drug Conjugates. *Bioconjug. Chem.* **2015**, *26*, 2186–2197. [CrossRef] [PubMed]
188. Liu, B.; Zhang, J.; Liao, J.; Liu, J.; Chen, K.; Tong, G.; Yuan, P.; Liu, Z.; Pu, Y.; Liu, H. Aptamer-Functionalized Nanoparticles for Drug Delivery. *J. Biomed. Nanotechnol.* **2014**, *10*, 3189–3203. [CrossRef] [PubMed]
189. Meng, H.-M.; Liu, H.; Kuai, H.; Peng, R.; Mo, L.; Zhang, X.-B. Aptamer-integrated DNA nanostructures for biosensing, bioimaging and cancer therapy. *Chem. Soc. Rev.* **2016**, *45*, 2583–2602. [CrossRef] [PubMed]
190. Benedetto, G.; Vestal, C.G.; Richardson, C. Aptamer-Functionalized Nanoparticles as "Smart Bombs": The Unrealized Potential for Personalized Medicine and Targeted Cancer Treatment. *Target. Oncol.* **2015**, *10*, 467–485. [CrossRef] [PubMed]
191. Zhu, J.; Huang, H.; Dong, S.; Ge, L.; Zhang, Y. Progress in Aptamer-Mediated Drug Delivery Vehicles for Cancer Targeting and Its Implications in Addressing Chemotherapeutic Challenges. *Theranostics* **2014**, *4*, 931–944. [CrossRef] [PubMed]
192. Cansiz, S.; Zhang, L.; Wu, C.; Wu, Y.; Teng, I.-T.; Hou, W.; Wang, Y.; Wan, S.; Cai, R.; Jin, C.; et al. DNA Aptamer Based Nanodrugs: Molecular engineering for efficiency. *Chem. Asian J.* **2015**, *10*, 2084–2094. [CrossRef] [PubMed]
193. Mathew, A.; Maekawa, T.; Sakthikumar, D. Aptamers in Targeted Nanotherapy. *Curr. Top. Med. Chem.* **2015**, *15*, 1102–1114. [CrossRef]
194. Wang, C.-C.; Wu, S.-M.; Li, H.-W.; Chang, H.-T. Biomedical Applications of DNA-Conjugated Gold Nanoparticles. *ChemBioChem* **2016**, *17*, 1052–1062. [CrossRef] [PubMed]
195. Nimjee, S.M.; White, R.R.; Becker, R.C.; Sullenger, B.A. Aptamers as therapeutics. *Annu. Rev. Pharmacol. Toxicol.* **2017**, *57*, 61–79. [CrossRef] [PubMed]
196. Rusconi, C.P.; Scardino, E.; Layzer, J.; Pitoc, G.A.; Ortel, T.L.; Monroe, D.; Sullenger, B.A. RNA aptamers as reversible antagonists of coagulation factor IXa. *Nature* **2002**, *419*, 90–94. [CrossRef] [PubMed]
197. Vavalle, J.P.; Rusconi, C.P.; Zelenkofske, S.; Wargin, W.A.; Ortel, T.L.; Alexander, J.H.; Povsic, T.J.; Becker, R.C. The effect of the REG2 Anticoagulation System on thrombin generation kinetics: a pharmacodynamic and pharmacokinetic first-in-human study. *J. Thromb. Thrombolysis* **2014**, *38*, 275–284. [CrossRef] [PubMed]
198. Woodruff, R.S.; Sullenger, B.A. Modulation of the coagulation cascade using aptamers. *Arterioscler. Thromb. Vasc. Biol.* **2015**, *35*, 2083–2091. [CrossRef] [PubMed]
199. Tan, L.; Neoh, K.G.; Kang, E.-T.; Choe, W.S.; Su, X. PEGylated Anti-MUC1 Aptamer-Doxorubicin Complex for Targeted Drug Delivery to MCF7 Breast Cancer Cells. *Macromol. Biosci.* **2011**, *11*, 1331–1335. [CrossRef] [PubMed]
200. Taghdisi, S.M.; Danesh, N.M.; Emrani, A.S.; Tabrizian, K.; ZandKarimi, M.; Ramezani, M.; Abnous, K. Targeted delivery of Epirubicin to cancer cells by PEGylated A10 aptamer. *J. Drug Target.* **2013**, *21*, 739–744. [CrossRef] [PubMed]
201. Povsic, T.J.; Vavalle, J.P.; Aberle, L.H.; Kasprzak, J.D.; Cohen, M.G.; Mehran, R.; Bode, C.; Buller, C.E.; Montalescot, G.; Cornel, J.H.; et al. A Phase 2, randomized, partially blinded, active-controlled study assessing the efficacy and safety of variable anticoagulation reversal using the REG1 system in patients with acute coronary syndromes: results of the RADAR trial. *Eur. Heart J.* **2013**, *34*, 2481–2489. [CrossRef] [PubMed]
202. Povsic, T.J.; Lawrence, M.G.; Lincoff, A.M.; Mehran, R.; Rusconi, C.P.; Zelenkofske, S.L.; Huang, Z.; Sailstad, J.; Armstrong, P.W.; et al. Pre-existing anti-PEG antibodies are associated with severe immediate allergic reactions to pegnivacogin, a PEGylated aptamer. *J. Allergy Clin. Immunol.* **2016**, *138*, 1712–1715. [CrossRef] [PubMed]
203. Lincoff, A.M.; Mehran, R.; Povsic, T.J.; Zelenkofske, S.L.; Huang, Z.; Armstrong, P.W.; Steg, P.G.; Bode, C.; Cohen, M.G.; Buller, C.; et al. Effect of the REG1 anticoagulation system versus bivalirudin on outcomes after percutaneous coronary intervention (REGULATE-PCI): A randomised clinical trial. *Lancet* **2016**, *387*, 349–356. [CrossRef]
204. Verheugt, F.W.A. An anticoagulant too good to be true for revascularisation. *Lancet* **2016**, *387*, 314–315. [CrossRef]

205. Ganson, N.J.; Povsic, T.J.; Sullenger, B.A.; Alexander, J.H.; Zelenkofske, S.L.; Sailstad, J.M.; Rusconi, C.P.; Hershfield, M.S. Pre-existing anti–polyethylene glycol antibody linked to first-exposure allergic reactions to pegnivacogin, a PEGylated RNA aptamer. *J. Allergy Clin. Immunol.* **2016**, *137*, 1610–1613. [CrossRef] [PubMed]
206. Richter, A.W.; Akerblom, E. Antibodies against polyethylene glycol produced in animals by immunization with monomethoxy polyethylene glycol modified proteins. *Int. Arch. Allergy Appl. Immunol.* **1983**, *70*, 124–131. [CrossRef] [PubMed]
207. Ganson, N.J.; Kelly, S.J.; Scarlett, E.; Sundy, J.S.; Hershfield, M.S. Control of hyperuricemia in subjects with refractory gout, and induction of antibody against poly(ethylene glycol) (PEG), in a phase I trial of subcutaneous PEGylated urate oxidase. *Arthritis Res. Ther.* **2006**, *8*, R12. [CrossRef] [PubMed]
208. Hershfield, M.S.; Ganson, N.J.; Kelly, S.J.; Scarlett, E.L.; Jaggers, D.A.; Sundy, J.S. Induced and pre-existing anti-polyethylene glycol antibody in a trial of every 3-week dosing of pegloticase for refractory gout, including in organ transplant recipients. *Arthritis Res. Ther.* **2014**, *16*, R63. [CrossRef] [PubMed]
209. Armstrong, J.K.; Hempel, G.; Koling, S.; Chan, L.S.; Fisher, T.; Meiselman, H.J.; Garratty, G. Antibody against poly(ethylene glycol) adversely affects PEG-asparaginase therapy in acute lymphoblastic leukemia patients. *Cancer* **2007**, *110*, 103–111. [CrossRef] [PubMed]
210. Ruckman, J.; Green, L.S.; Beeson, J.; Waugh, S.; Gillette, W.L.; Henninger, D.D.; Claesson-Welsh, L.; Janjic, N. 2′-Fluoropyrimidine RNA-based Aptamers to the 165-Amino Acid Form of Vascular Endothelial Growth Factor (VEGF165) Inhibition of Receptor Binding and VEGF-induced Vascular Permeability through Interactions Requiring the Exon 7-encoded Domain. *J. Biol. Chem.* **1998**, *273*, 20556–20567. [CrossRef] [PubMed]
211. Chen, W.; Sridharan, V.; Soundararajan, S.; Otake, Y.; Stuart, R.; Jones, D.; Fernandes, D. Activity and Mechanism of Action of AS1411 in Acute Myeloid Leukemia Cells. *Blood* **2007**, *110*, 1604.
212. Xu, X.; Hamhouyia, F.; Thomas, S.D.; Burke, T.J.; Girvan, A.C.; McGregor, W.G.; Trent, J.O.; Miller, D.M.; Bates, P.J. Inhibition of DNA Replication and Induction of S Phase Cell Cycle Arrest by G-rich Oligonucleotides. *J. Biol. Chem.* **2001**, *276*, 43221–43230. [CrossRef] [PubMed]
213. Abdelmohsen, K.; Gorospe, M. RNA-binding protein nucleolin in disease. *RNA Biol.* **2012**, *9*, 799–808. [CrossRef] [PubMed]
214. Xu, Z.; Joshi, N.; Agarwal, A.; Dahiya, S.; Bittner, P.; Smith, E.; Taylor, S.; Piwnica-Worms, D.; Weber, J.; Leonard, J.R. Knocking down nucleolin expression in gliomas inhibits tumor growth and induces cell cycle arrest. *J. Neurooncol.* **2012**, *108*, 59–67. [CrossRef] [PubMed]
215. Laber, D.A.; Sharma, V.R.; Bhupalam, L.; Taft, B.; Hendler, F.J.; Barnhart, K.M. Update on the first phase I study of AGRO100 in advanced cancer. *J. Clin. Oncol.* **2005**, *23*, 3064. [CrossRef]
216. Laber, D.A.; Taft, B.S.; Kloecker, G.H.; Bates, P.J.; Trent, J.O.; Miller, D.M. Extended phase I study of AS1411 in renal and non-small cell lung cancers. *J. Clin. Oncol.* **2006**, *24*, 13098.
217. Rosenberg, J.E.; Bambury, R.; Drabkin, H.A.; Lara, P.N.; Harzstark, A.L.; Figlin, R.A.; Smith, G.W.; Choueiri, T.; Erlandsson, F.; Laber, D.A. A phase II trial of the nucleolin-targeted DNA aptamer AS1411 in metastatic refractory renal cell carcinoma. *Investig. New Drugs* **2014**, *32*, 178–187. [CrossRef] [PubMed]
218. Stuart, R.K.; Stockerl-Goldstein, K.; Cooper, M.; Devetten, M.; Herzig, R.; Medeiros, B.; Schiller, G.; Wei, A.; Acton, G.; Rizzieri, D. Randomized phase II trial of the nucleolin targeting aptamer AS1411 combined with high-dose cytarabine in relapsed/refractory acute myeloid leukemia (AML). *J. Clin. Oncol.* **2009**, *27*, 15s.
219. Vater, A.; Sahlmann, J.; Kröger, N.; Zöllner, S.; Lioznov, M.; Maasch, C.; Buchner, K.; Vossmeyer, D.; Schwoebel, F.; Purschke, W.G.; et al. Hematopoietic Stem and Progenitor Cell Mobilization in Mice and Humans by a First-in-Class Mirror-Image Oligonucleotide Inhibitor of CXCL12. *Clin. Pharmacol. Ther.* **2013**, *94*, 150–157. [CrossRef] [PubMed]
220. Liu, S.-C.; Alomran, R.; Chernikova, S.B.; Lartey, F.; Stafford, J.; Jang, T.; Merchant, M.; Zboralski, D.; Zöllner, S.; Kruschinski, A.; et al. Blockade of SDF-1 after irradiation inhibits tumor recurrences of autochthonous brain tumors in rats. *Neuro-Oncol.* **2014**, *16*, 21–28. [CrossRef] [PubMed]
221. Hoellenriegel, J.; Zboralski, D.; Maasch, C.; Rosin, N.Y.; Wierda, W.G.; Keating, M.J.; Kruschinski, A.; Burger, J.A. The Spiegelmer NOX-A12, a novel CXCL12 inhibitor, interferes with chronic lymphocytic leukemia cell motility and causes chemosensitization. *Blood* **2014**, *123*, 1032–1039. [CrossRef] [PubMed]

222. Steurer, M.; Montillo, M.; Scarfò, L.; Mauro, F.R.; Andel, J.; Wildner, S.; Trentin, L.; Janssens, A.; Burgstaller, S.; Kruschinski, A.; et al. Results from a Phase IIa Study of the Anti-CXCL12 Spiegelmer Olaptesed Pegol (NOX-A12) in Combination with Bendamustine/Rituximab in Patients with Chronic Lymphocytic Leukemia. *Blood* **2014**, *124*, 1996.
223. Ludwig, H.; Weisel, K.; Petrucci, M.T.; Leleu, X.; Cafro, A.M.; Garderet, L.; Leitgeb, C.; Foa, R.; Greil, R.; Yakoub-Agha, I.; et al. Olaptesed pegol, an anti-CXCL12/SDF-1 Spiegelmer, alone and with bortezomib–dexamethasone in relapsed/refractory multiple myeloma: A Phase IIa Study. *Leukemia* **2017**, *31*, 997–1000. [CrossRef] [PubMed]
224. Li, S.; Xu, H.; Ding, H.; Huang, Y.; Cao, X.; Yang, G.; Li, J.; Xie, Z.; Meng, Y.; Li, X.; Zhao, Q.; Shen, B.; Shao, N. Identification of an aptamer targeting hnRNP A1 by tissue slide-based SELEX. *J. Pathol.* **2009**, *218*, 327–336. [CrossRef] [PubMed]
225. Zhang, J.; Li, S.; Liu, F.; Zhou, L.; Shao, N.; Zhao, X. SELEX aptamer used as a probe to detect circulating tumor cells in peripheral blood of pancreatic cancer patients. *PLoS ONE* **2015**, *10*, e0121920. [CrossRef] [PubMed]
226. Wang, H.; Li, X.; Volk, D.E.; Lokesh, G.L.-R.; Elizondo-Riojas, M.-A.; Li, L.; Nick, A.M.; Sood, A.K.; Rosenblatt, K.P.; Gorenstein, D.G. Morph-X-Select: Morphology-based tissue aptamer selection for ovarian cancer biomarker discovery. *BioTechniques* **2016**, *61*, 249–259. [CrossRef] [PubMed]
227. Mi, J.; Liu, Y.; Rabbani, Z.N.; Yang, Z.; Urban, J.H.; Sullenger, B.A.; Clary, B.M. In vivo selection of tumor-targeting RNA motifs. *Nat. Chem. Biol.* **2010**, *6*, 22–24. [CrossRef] [PubMed]
228. Cheng, C.; Chen, Y.H.; Lennox, K.A.; Behlke, M.A.; Davidson, B.L. In vivo SELEX for Identification of Brain-penetrating Aptamers. *Mol. Ther. Nucleic Acids* **2013**, *2*, e67. [CrossRef] [PubMed]

B. Glioblastomes

Résumé :

Les glioblastomes (GBM) sont les tumeurs cérébrales les plus agressives. La durée moyenne de survie de patients atteints de GBM est de 14,8 mois malgré une thérapie combinant une résection chirurgicale, une radiothérapie et une chimiothérapie (témozolomide).

La caractérisation de sous-populations de GBM passe par l'identification de biomarqueurs moléculaires, pour un diagnostic/pronostic plus efficace et pour guider vers des traitements plus ciblés, souvent combinés.

Les glioblastomes (GBM) sont les tumeurs cérébrales les plus agressives (grade IV selon l'OMS, 'Organisation Mondiale de la Santé'), au pronostic redoutable. L'incidence est de 3,2 cas pour 10000 habitants, avec un taux de survie à 5 ans inférieur à 6% (Ostrom et al., 2016). Les deux caractéristiques histologiques majeures des GBM sont la présence de plages de nécroses entourées de cellules proliférantes réalisant un aspect en pseudo-pallissades, et d'une prolifération vasculaire. La grande majorité (90%) des glioblastomes se développe *de novo* on parle alors de glioblastome primaire. Les GBM secondaires sont issus de gliomes de plus bas grade. La caractérisation de sous-populations de GBM passe par l'identification de biomarqueurs moléculaires, pour guider vers des traitements plus ciblés, plus efficaces. La classification de l'OMS en cours depuis 2007, dont découlait le diagnostic et la prise en charge thérapeutique, était uniquement basée sur des critères histologiques (Louis et al., 2007) et devenait obsolète. En intégrant des données phénotypiques et génotypiques, l'OMS a proposé en 2016 (Louis et al., 2016) la classification des gliomes selon le status IDH ('isocitrate deshydrogenase'), la perte du chromosome 1p/19q, la perte d'ATRX et les mutations de p53 (*Figure 16*).

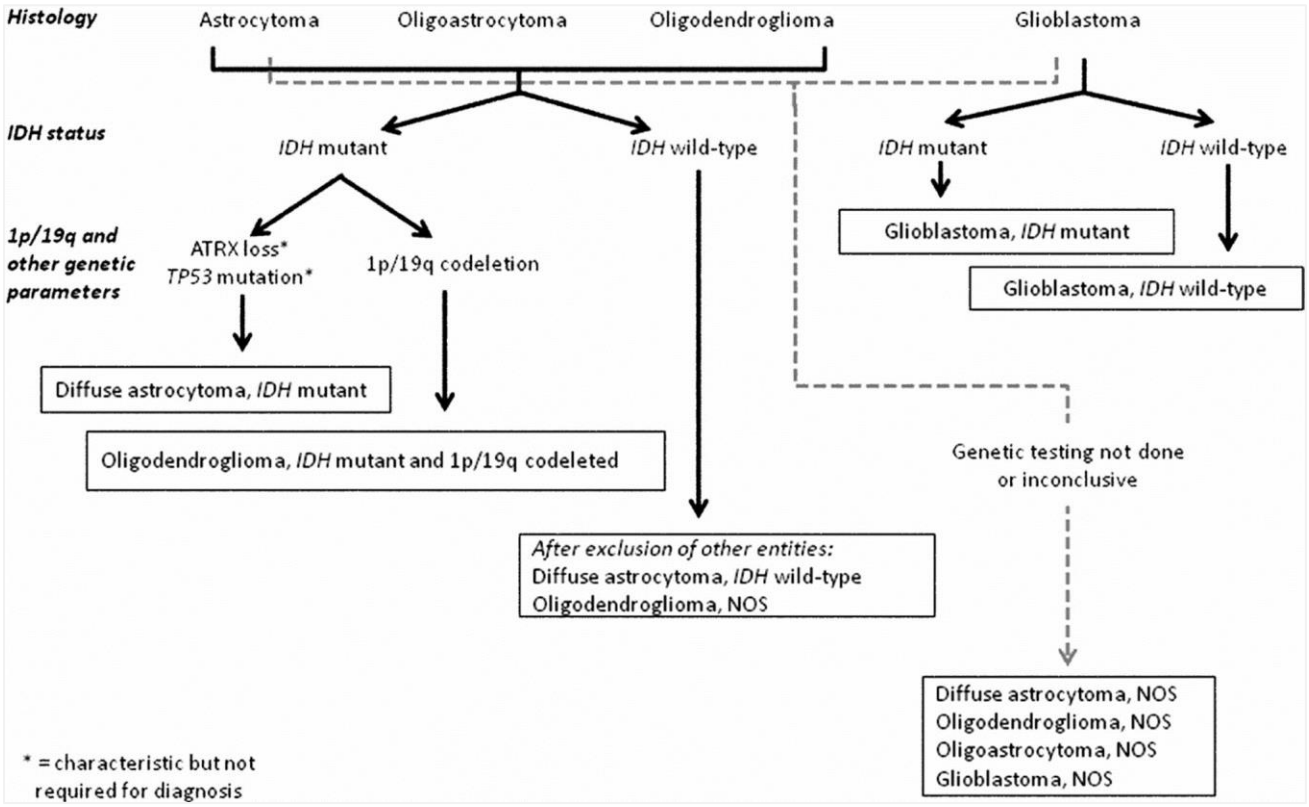

Figure 16. **Classification des gliomes selon des critères histologiques et génétiques** (Louis et al., 2016).

Les GBM sont classés selon leur statut IDH : les GBM IDH WT représentent environ 90% des GBM, les GBM IDH muté environ 10 % des cas et les GBM NOS sont les GBM pour lesquels le statut IDH n'a pas pu être déterminé. La première catégorie concerne majoritairement des glioblastomes primaires. Ces GBM ont également des altérations des gènes EGFR, PTEN, TP53, PGDFRα, NF1 et CDKN2A/2B et des mutations du promoteur TERT (Appin et Bratt., 2015). Les GBM IDH mutés sont principalement des GBM secondaires. L'enzyme IDH mutante produit le D-2-hydroxyglutarate (D-2HG) qui s'accumule dans la cellule tumorale et va notamment profondément modifier l'épigénome tumoral (hyperméthylation de régions spécifiques de l'ADN).

Les GBM se caractérisent donc par une forte hétérogénéité moléculaire (Verhaak et al., 2010 ; Ceccarelli et al., 2016). Selon le profil génétique des GBM, 4 sous-types ont été identifiés en 2010 (Verhaak et al., 2010, mésenchymateux, classique, proneural et neural), réduits à trois sous-types plus récemment (Wang et al., 2017, mésenchymateux, classique, proneural). Le GBM de type mésenchymal, de mauvais pronostic, présente des mutations ou délétions sur les gènes suppresseurs de tumeurs NF1 ('neurofibromatosis type 1') et PTEN ('Phosphatase and TENsin homolog'), induisant leur faible expression. Les marqueurs d'inflammation et de

remodèlement tissulaire (CHI3L1, MET), CD44, les protéines de la famille du TNF (‘tumor necrosis factor’) et NF-kB sont fortement exprimés. Le GBM de type classique est caractérisé par une amplification du chromosome 7 et de l’EGFR, une perte du chromosome 10 et une délétion homozygote de 9p21.3 contenant le gène ciblant CDKN2A (‘cyclin dependent kinase inhibitor 2A’). Ce groupe ne présente aucune altération du gène TP53. Le GBM de type proneural, de meilleur pronostic, est caractérisé par une amplification de PDGFRα et une mutation d’IDH1. Ce sous-type présente un fort taux de mutation TP53 (54%) et de la voie de signalisation PI3K/AKT. Ils expriment aussi fortement des marqueurs d’oligoastrocytes OLIG2 (‘oligodendrocyte transcription factor’) par exemple, ainsi que des gènes impliqués dans le développement proneural tel que DCX (Doublecortin). Les patients jeunes sont plus souvent atteints par ce sous-type, et ont tendance à avoir une survie prolongée. A cette hétérogénéité inter-tumorale, s’ajoute également une hétérogénéité intra-tumorale (Patel et al., 2014 ; Sottoriva et al., 2013).

Le temps moyen de survie de patients atteints de GBM est de 14,8 mois malgré une thérapie suivant le protocole Stupp (Stupp et al., 2005) combinant résection chirurgicale, radio- et chimio-thérapie avec un agent alkylant de l’ADN (témozolomide, TMZ). Les GBM sont infiltrants, ce qui rend la résection chirurgicale totale de la tumeur impossible. Il est difficile de différencier la tumeur du tissu sain environnant. Le faible pronostic de survie est dû à la résistance aux traitements et à la récidive de la tumeur après résection. L’hétérogénéité moléculaire expliquerait en partie l’échec actuel des thérapies ciblées. Aucun protocole n’a pour le moment été validé dans la prise en charge de GBM récurrent. De nombreux essais cliniques ciblent le GBM. Marie-Cécile Mercier, dans la partie de sa thèse (en préparation) intitulée ‘Traitements actuels des glioblastomes’, pour son DES (‘diplôme d’études spécialisées’) Innovation Pharmaceutique et Recherche qui cloturera son internat de pharmacie, a répertorié près de 200 essais cliniques de phase II et plus. Parmi les thérapies ciblées, les plus nombreuses sont celles visant (i) l’EGFR, dont le gène est amplifié ou sur-exprimé dans plus de 50% des GBM (24 essais cliniques) et (ii) le VEGF (31 essais cliniques). Outre l’intérêt diagnostique et pronostique, certains marqueurs peuvent avoir un intérêt prédictif (décisionnel sur le plan thérapeutique), voire constituer une cible moléculaire actionnable par une thérapie spécifique (marqueur theranostique). Les nouvelles données géniques mettent en évidence la nécessité de stratifier les patients selon leur profil moléculaire et d’associer différentes thérapies ciblées.

L’un des challenges actuels est de développer des ligands capables de se lier spécifiquement à leur cible tumorale, sans affecter les cellules saines adjacentes. Les aptamères,

de par leurs proriétés décrites dans la partie A, font partie de ces nouveaux ligands. Plusieurs aptamères ont déjà été sélectionnés contre des cellules de GBM par cell-SELEX (*Tableau 3*).

Aptamer name	Library	Number of variable nucleotides	Number of cycles	Target cell line	Negative selection	Kd value (nM)	Reference
GL43, GL56, GL36, GL35, GL44, GL21	2'F-RNA	45	14 cycles	U87MG GBM cell line	T98G glioma cell line	38-190	Cerchia et al., 2009
Gint4.T	2'F-RNA	45	2 more cycles	U87MG GBM cell line	PDGFRβ gene silenced, U87MG cell line	9.6	Camorani et al., 2014
GTM3, GTM4, GTM5, GTM8, GTM9	ssDNA	30-50	18 cycles	A172 GBM cell line	NO negative selection	61-168	Bayrac et al., 2011
GBM128, GTM131	ssDNA	45	30 cycles	U118 GBM cell line	SVGp12 human astroglial cell line	20-37	Kang et al., 2012
GBI-10	ssDNA	34	21 cycles	U251 GBM cell line	NO negative selection	150	Daniels et al., 2003
TTA1	2'F-RNA	40	11	TN-C expressing U251 GBM cell line	NO negative selection	5	Hicke et al., 2001
A1, A2, A3, A4, A5, A6	ssDNA	50	8 cycles	CD133(+) TIC from human GBM xenografts in mice	Non-TIC from human GBM xenografts in mice	0.12-3.75	Kim et al., 2013
U2, U8	ssDNA	40	11 cycles	U87MG-EGFRvIII, U87MG GBM cells overexpressing EGFRvIII	U87MG WT cell line	3.37-4.35	Wu et al., 2014 ; Zhang et al., 2018
32, 41, 43, 47	ssDNA	30	14 cycles	U87MG-EGFRvIII, U87MG GBM cells overexpressing EGFRvIII	U87MG WT cell line	0.62-37.57	Tan et al., 2013

Tableau 3. **Aptamères ciblant les cellules de glioblastome, sélectionnés par cell-SELEX**. TIC 'tumour initiating cells', GBM 'glioblastome', TN-C 'tenascine-C'. (adapté de Delac et al., 2015 ; Camorani et Cerchia., 2015 ; Hays et al., 2017).

La moitié de ces études a été réalisée sur des cellules de GBM sans cible moléculaire prédéfinie. Pour certains de ces aptamères, la cible a été définie *a posteriori* (par exemple, Axl, récepteur tyrosine kinase pour GL21T). Quant à l'autre moitié, les seules cibles prédéfinies sont une protéine extracellulaire, la tenascine-C et trois protéines de la surface cellulaire : le marqueur CD133 (marqueur de cellules souches de GBM), ainsi que le récepteur PDGFRβ et la forme mutée la plus commune de l'EGFR (EGFRvIII). Un autre aptamère (CL4) ciblant EGFR et EGFRvIII avait été sélectionné par cell-SELEX sur d'autres cellules que des cellules de GBM (sur une lignée cellulaire de carcinome pulmonaire ; Esposito et al., 2011b). L'aptamère AS1411 ciblant la nucléoline fait l'objet d'essais thérapeutiques (voir Table 2 dans la partie A).

Ces aptamères pourraient être utilisés pour marquer les cellules tumorales (applications diagnostiques) ou pour délivrer spécifiquement des agents thérapeutiques (*Figure 17 B & C)*. Le principal obstacle à l'utilisation d'aptamères *in vivo* sur les GBM est le passage de la barrière hémato-encéphalique (BHE), une barrière anatomique qui filtre et contrôle le passage de molécules et cellules dans le cerveau, et inversement. L'aptamère Gint4.T, ciblant le PDGFRβ, conjugué à des nanoparticules, est capable de passer la BHE (Monaco et al., 2017). Une autre

stratégie a été récemment proposée pour passer la BHE également par transcytose (Macdonald et al., 2017). Il s'agit d'un aptamère bifonctionnel, composé de l'aptamère ADN SYL3C, ciblant la molécule d'adhésion EpCAM ('epithelial cell adhesion molecule' ; Song et al., 2013), couplé à l'aptamère ADN GS24 (Chen et al., 2008), ciblant le domaine extracellulaire de la transferrine. La transferrine est surexprimée à la surface de la BHE et EpCAM est un biomarqueur de surface cellulaire surexprimé par de nombreuses tumeurs solides. Le passage de la BHE et le ciblage de la tumeur cérébrale par cet aptamère bispécifique est illustré par la *Figure 17A*.

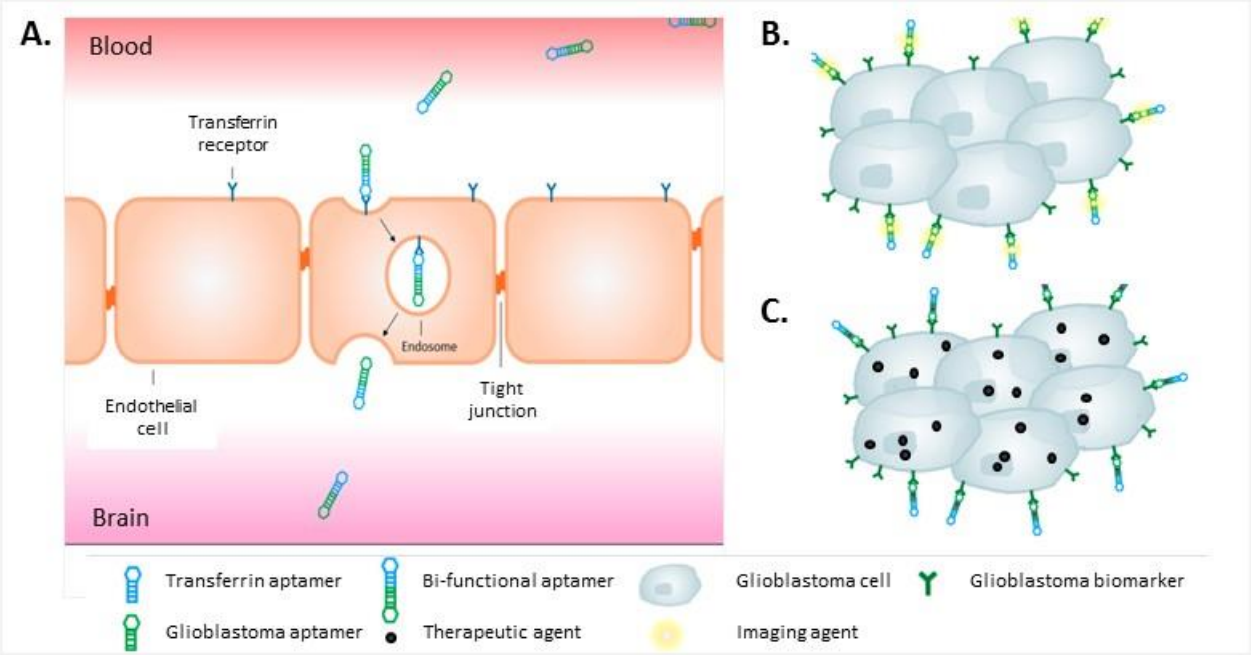

Figure 17. **Illustration du passage de la BHE par un aptamère bi-fonctionnel et ses applications** (Hays et al., 2017). **A.** L'aptamère bifonctionnel est constitué d'un aptamère capable de traverser la BHE, fusionné à un aptamère ciblant les GBM. Une telle construction permettrait la délivrance ciblée d'agents **B.** d'imagerie et **C.** thérapeutiques.

C. Intégrine α5β1

Résumé :

L'intégrine α5β1 est une protéine hétérodimérique transmembranaire, récepteur de la fibronectine.

Elle se positionne comme un marqueur diagnostique, un marqueur pronostique des GBM et d'autres tumeurs solides, et comme une cible thérapeutique lorsqu'elle est sur-exprimée par les cellules d'une tumeur primitive, mais aussi après récidives suite à des thérapies ciblées.

Les ligands spécifiques de α5β1, issus de trois familles de composés (anticorps humanisés, peptides et petites molécules non peptidiques), sont encore peu nombreux.

Les intégrines sont des récepteurs transmembranaires hétéro-dimériques composés des sous-unités α et β (Takada et al., 2007). Chez les vertébrés, on dénombre 18 chaînes α et 8 chaînes β formant 24 intégrines différentes. Leur combinaison (*Figure 18*) détermine la spécificité de l'intégrine au ligand (Hynes, 2002).

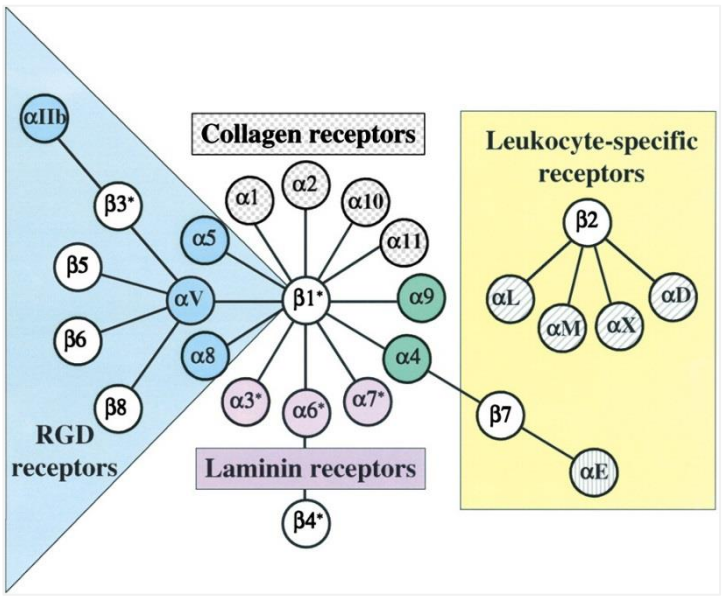

Figure 18. **Schéma représentant la famille des intégrines et leurs ligands** (Hynes et al., 2002). Les 24 combinaisons possibles sont classées en 4 sous-familles : les intégrines récepteurs de la laminine (en violet), les intégrines récepteurs du collagène (en gris), les intégrines reconnaissant des motifs RGD (en bleu) et les intégrines récepteurs spécifiques des leucocytes (en jaune). Les astérisques réfèrent aux intégrines qui peuvent être épissées alternativement.

La liaison intégrine-ligand, par l'activation de voies de signalisation intracellulaire multiples, induit de nombreux processus physiologiques, tels que l'adhérence à la matrice extracellulaire, la prolifération, la régulation de la balance survie/apoptose, la migration, la différentiation cellulaire (Giancotti & Ruoslahti, 1999)… Outre l'action de transmission du signal de l'extérieur de la cellule vers l'intérieur, qualifiée de 'outside-in', les intégrines ont aussi fonction de transmission d'information de l'intérieur vers l'extérieur 'inside-out' (Hynes, 1992). La partie cytoplasmique des intégrines n'a pas de fonction enzymatique propre. La transmission de l'information passe par des changements de conformations permettant ou non la liaison avec différents partenaires extra- ou intra-cellulaires. On parle de conformation active et inactive (*Figure 19*), même si plusieurs modèles et intermédiaires de transition sont décrits (Takagi et al., 2002 ; Arnaout et al., 2005 ; Zhu et al., 2013 ; Su et al., 2016).

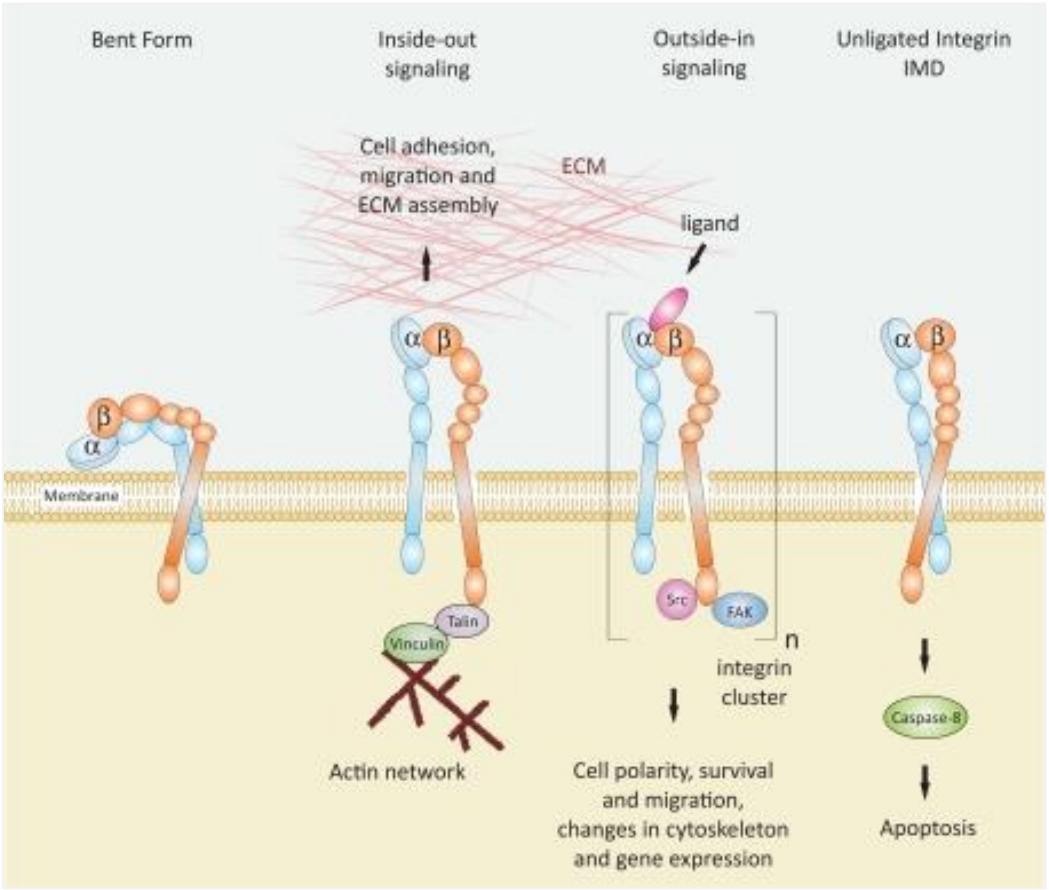

Figure 19. **Représentation schématique des différents états d'activation des intégrines et mécanismes de signalization** (Mas-Moruno et al., 2010). Sous forme repliée, l'intégrine est inactive et ne permet pas de liaison au ligand. Lors de la signalisation 'inside-out', un activateur intracellulaire se lie à la sous-unité β et induit un changement conformationel de l'intégrine permettant ainsi la liaison du ligand de la matrice extracellulaire (MEC). Ce processus permet la régulation de l'adhésion cellulaire, la migration et l'invasion. Lors de la signalisation 'outside-in', le ligand extracellulaire se lie à l'intégrine et induit le 'clustering' des intégrines. Ce signal provoque l'activation de cascades de signalisation au sein de la cellule impliquées dans la polarité, la survie, la migration… Les intégrines à l'état déplié, non liée à un ligand peuvent activer la caspase-8 et induire l'apoptose via un processus appelé IMD ('integrin-mediated death').

Parmi les 24 intégrines hétérodimériques connues, 8 intégrines reconnaissent la séquence RGD (arginine, glycine, acide aspartique). Au laboratoire, nous nous intéressons particulièrement à l'intégrine α5β1, récepteur de la fibronectine. L'intégrine α5β1 se profile comme biomarqueur et cible thérapeutique dans la lutte contre certains cancers, en particulier dans les gliomes.

La dérégulation de l'expression et de la fonction des intégrines est impliquée dans différentes phases de la progression tumorale, telles que la dissémination métastasique, l'angiogenèse tumorale, les phénomènes de résistance aux agents chimiothérapeutiques et à la radiothérapie (Desgrosellier & Cheresh., 2010 ; Bianconi et al., 2016 ; Nieberler et al., 2017). L'intégrine α5β1 est surexprimée dans différentes tumeurs solides (colon, ovaire, sein, poumon, glioblastome, mélanome, oesophage) et dans les cellules endothéliales des néo-vaisseaux tumoraux (Schaffner et al., 2013 ; Kobayashi et al., 2017 ; Xie et al., 2016). Elle participe, à la dissémination, à la progression des tumeurs, à l'angiogenèse tumorale (Bianconi et al., 2016), mais aussi à la formation de métastases (Breuksch et al., 2017 ; Ju et al., 2017 ; Xie et al., 2016 ; Stevens et al., 2017 ; Haber et al., 2015) et à la résistance aux traitements (Unnikrishnan et al., 2017 ; Iwanicki et al., 2016). Une surexpression spécifique de l'intégrine α5β1 a été mise en évidence dans les GBM récurrents après thérapies ciblées au bévacizumab (anticorps anti-VEGF, DeLay et al., 2012), et aux inhibiteurs de la tyrosine kinase de l'EGFR ('Epidermal Growth Factor Receptor') : erlotinib (tumeur du poumon ; Kanda et al., 2013), gefitinib (cancer du poumon non à petites cellules ; Ju et al., 2010). Dans certaines tumeurs (tumeurs des poumons, des ovaires et du sein), la surexpression de l'intégrine α5β1 est associée à un phénotype plus agressif (Adachi et al., 2000 ; Sawada et al., 2008 ; Sawada et al., 2012 ; Nam et al., 2010 ; Iwanicki et al., 2016) et à un mauvais pronostic vital (Adachi et al., 2000).

Des travaux du laboratoire (Cosset et al., 2012 ; Janouskova et al., 2012 ; Ray et al., 2014 ; Maglott et al., 2006) ont montré que l'expression de la sous-unité α5 favorise la prolifération, la migration cellulaire, est associée à un mauvais pronostic vital, et dans des biopsies humaines de tumeurs cérébrales, augmente en fonction du grade tumoral (*Figure 20*). Ces résultats ont été validés sur d'autres cohortes de patients (*Figure 21*) (Freije et al., 2004 ; Phillips et al., 2006). De plus, l'intégrine α5β1 est un facteur de résistance à la chimiothérapie par le témozolomide (TMZ) dans les tumeurs exprimant le suppresseur de tumeur p53 sauvage. L'intégrine α5β1 empêche une activation pro-apoptotique efficace de p53 qui peut être rétablie par des antagonistes de l'intégrine. Cette relation croisée négative intégrine-p53 a été confirmée lors de l'activation de p53 par la nutlin-3a, un agent non génotoxique : l'activation de l'intégrine

α5β1 inhibe p53, et celle de p53 réprime l'expression de l'intégrine α5β1 (Janouskova et al., 2012).

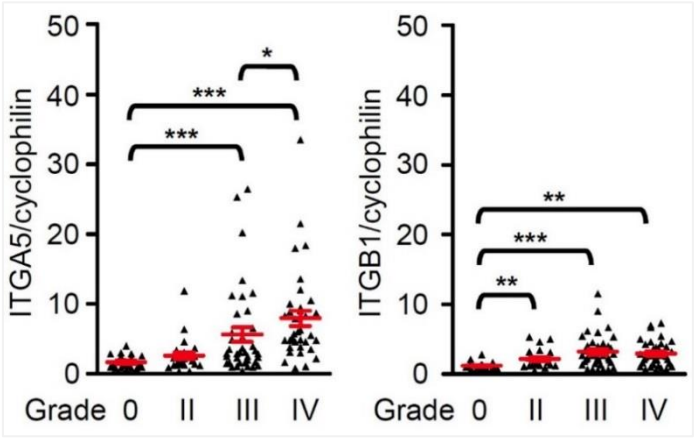

Figure 20. **Taux d'expression des gènes des sous-unités α5** (à gauche) **et β1** (à droite) **en fonction du grade tumoral** (Janouskova et al., 2012). Un taux élevé de la sous unité α5 est associé aux gliomes de haut grade. Le grade IV correspond aux tumeurs cérébrales les plus agressives, les glioblastomes (GBM).

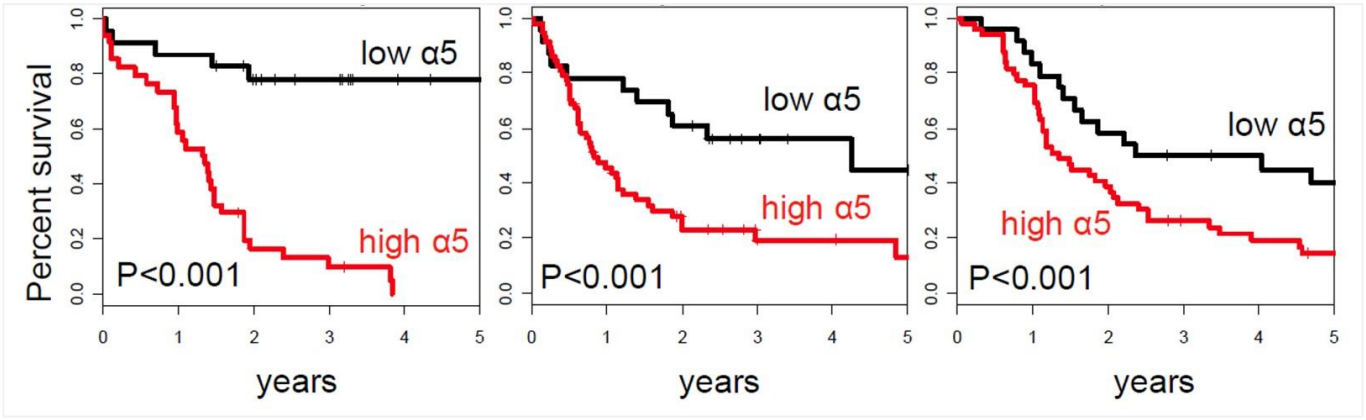

Figure 21. **Courbes de survie des patients atteints de gliomes en fonction de l'expression du gène de la sous-unité α5** (faible expression en noir et forte expression en rouge) (Janouskova et al., 2012). A gauche, au milieu et à droite figurent les études de Janouskova et al., 2012, Freije et al., 2004 et Philips et al., 2006, respectivement. Un taux élevé d'integrine α5 est est un facteur de mauvais pronostic de survie.

L'inhibition seule de l'intégrine ne semble pas être efficace pour activer une voie pro-apoptotique. Les travaux récents du laboratoire ont permis de mieux caractériser les voies de signalisation α5-dépendante et les acteurs de la relation croisée négative entre l'intégrine α5β1 et p53, de caractériser les intervenants moléculaires impliqués dans cette relation (Renner et al., 2016a), de montrer l'association de l'intégrine α5β1 à une mobilisation de la voie β-caténine dans les cellules de GBM (Renner et al., 2016b). La *Figure 22* résume ces travaux. Nous avons également mis en évidence la complexité du rôle de la sous-unité α5 et de la fibronectine dans un modèle de sphéroïdes 3D de GBM (Blandin et al., 2016) : selon la concentration en fibronectine dans l'environnement tumoral, la sous-unité α5 pourra favoriser les interactions entre les cellules et la cohérence de la tumeur (environnement pauvre en fibronectine), ou au

contraire, favoriser les interactions entre les cellules et la MEC à l'origine de l'évasion des cellules (forte concentration en fibronectine).

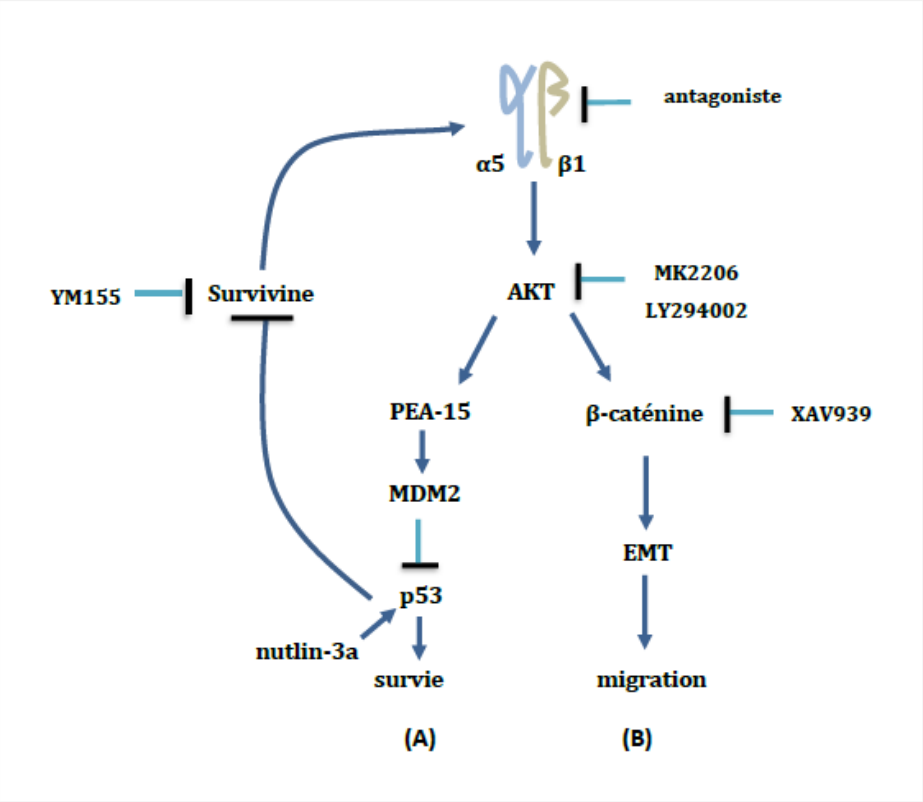

Figure 22. **Le double rôle de l'axe intégrine α5β1/AKT dans les cellules de GBM p53 sauvage. A.** La sur-expression ou l'activation de l'intégrine α5β1 active la protéine kinase AKT. AKT va réprimer p53 par l'activation des protéines anti-apoptotiques PEA-15 et HDM2. La répression du complexe p53/HDM2 par la nutlin-3a va réprimer l'expression de la survivine qui régule positivement l'expression de l'intégrine α5β1. **B.** L'activation d'AKT permet la transactivation de la β-caténine. Cela va induire la migration cellulaire et l'expression de gènes cibles impliqués dans la transition épithélio-mésenchymateuse. (Thèse de Guillaume Renner, 2016).

La caractérisation de ligands spécifiques de l'intégrine α5β1 a pris un essor important ces dernières années faisant suite à la proposition de cette intégrine comme cible thérapeutique bifonctionnelle pour bloquer à la fois l'angiogenèse tumorale et aussi directement les cellules tumorales (Stragies et al., 2007 ; Heckmann et al., 2008). Les antagonistes spécifiques de l'intégrine α5β1 sont issus de trois familles de composés : anticorps, peptides mimant le site synergique et petites molécules non peptidiques.

Anticorps

Le Volociximab (PDL Biopharma/Biogen Idec) est un anticorps chimérique humanisé, inhibiteur de fonction de l'intégrine α5β1, dérivé de l'anticorps murin IIA1, qui avait prouvé son efficacité en préclinique en tant qu'agent anti-tumoral (Sawada et al., 2008). Il inhibe l'angiogenèse *in vitro* et la croissance tumorale *in vivo*. Exploré en clinique dans une dizaine

d'essais, il a notamment été stoppé en phase II chez des patients atteints de cancers ovariens réfractaires à la chimiothérapie ou de cancers du péritoine, par manque d'efficacité (Bell-McGuinn et al., 2011 ; Almokadem et Belani, 2012).

L'anticorps PF-04605412 (Pfizer) a été testé dans un essai clinique de phase I, mais son développement a été stoppé par manque d'effet anti-tumoral aux doses testées, sur des tumeurs solides (Mateo et al., 2014).

L'anticorps OS2966, inhibiteur de β1 a été désigné comme drogue orpheline par la FDA pour le traitement du GBM en août 2014 et pour le cancer des ovaires en janvier 2015 (www. oncosynergy.com).

L'anticorps monoclonal murin P5 (Chungbuk National University), ciblant la sous-unité β1 serait en phase clinicle III pour le traitement d'adénocarcinomes pulmonaires (Kim et al., 2016).

Peptides mimant le site synergique

Le peptide ATN-161 (Attenuon), de 5 acides aminés (*Figure 23*), a été développé à partir de la sequence du site synergique situé sur le domaine FIII9 de la fibronectine. Ce domaine (DRVPHSRN) agit en synergie avec le site RGD pour la liaison de l'intégrine α5β1 à la fibronectine (Leahy et al., 1996 ; Copié et al., 1998). Un essai de phase I est prometteur chez des patients atteints de tumeurs solides résistantes aux traitements conventionnels. ATN-161 est bien toléré et la maladie a été stabilisée pour environ 1/3 des patients (Cianfrocca et al., 2006). Un essai de phase I/II est en cours pour l'étude des effets secondaires et essais de doses d'ATN-161 à utiliser en combinaison avec la carboplatine chez des patients atteints de gliomes récurrents (www.clinicaltrials.gov).

Petites molécules non peptidiques

Le SJ749 (Merck Dupont) est la première molécule non-peptidique décrite comme antagoniste sélectif de l'intégrine α5β1. Il inhibe l'adhésion cellulaire à la fibronectine avec une IC_{50} de 1,8 nM et l'angiogenèse *in vitro* (Kim et al., 2000). Il a également fait l'objet d'études au laboratoire montrant sa capacité à inhiber la prolifération, la clonogénicité et l'invasion de lignées tumorales humaines de glioblastome (Maglott et al., 2006 ; Bartik et al., 2008 ; Martin et al., 2009 ; Martinkova et al., 2010).

D'autres antagonistes sélectifs de l'intégrine α5β1 ont été conçus par l'équipe du Pr Kessler (Munich, Allemagne, Heckmann et al., 2008 ; Rechenmacher et al., 2013). Au laboratoire, il a été montré que la molécule K34c impacte la survie et sensibilise aux agents chimio-thérapeutiques des cellules de gliomes et de cancer colorectal (Cosset et al., 2012 ; Martinkova et al., 2010 ; Janouskova et al., 2013). Nous avons également montré que la migration en cellule isolée des cellules de GBM U87MG est inhibée sélectivement par les antagonistes sélectifs de

l'intégrine α5β1 (K34c et FR248) et non par les antagonistes de l'intégrine αvβ3 (Ray et al., 2014).

La molécule JSM-6427 (Stragies et al., 2007, Jerini Ophthalmic) induit l'apoptose dans les cellules endothéliales *in vitro* et *in vivo* et inhibe fortement la néo-vascularisation dans l'œil. Cette molécule semble être encore en phase clinique I pour le traitement de la dégénerescence maculaire liée à l'âge (NCT00536016).

Les structures des molécules SJ749, JSM6427 et K34c sont représentées Figure 23.

D'autres molécules, telles qu'un pseudo-pentapeptide cyclique mimant la séquence RGD (1a-RGD, Arosio et al., 2008) et un composé non peptidique (GLPG0187, Silginer et al., 2014; Reeves et al., 2015), bloqueurs de l'activité d'intégrines, sont moins sélectifs pour α5β1 que pour d'autres intégrines. Le GLPG0187, un antagoniste d'intégrines à champ large, est en phase clinique I (Cirkel et al., 2016). A l'heure actuelle, les effets biologiques anti-cancéreux de tels antagonistes sont encore peu décrits.

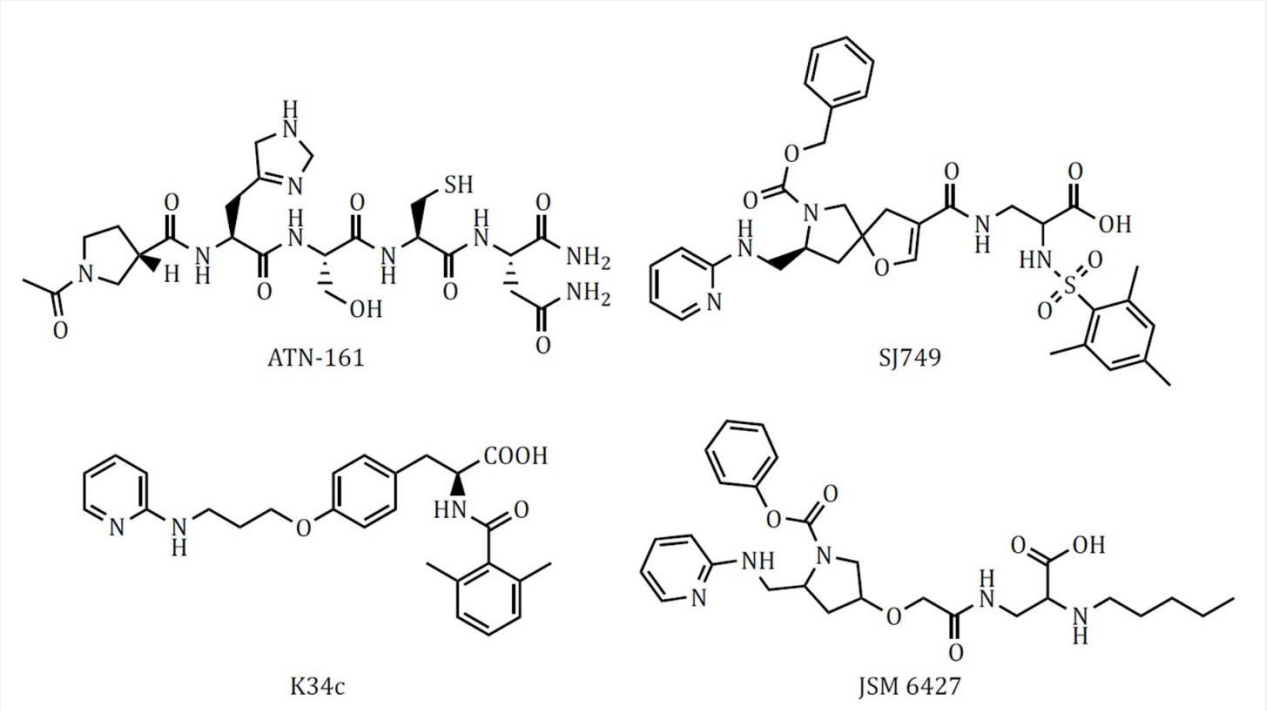

Figure 23. **Structure des ligands synthétiques peptidique** (ATN-161) **ou non** (SJ749, K34c, JSM 6427) **de l'intégrine α5β1** (Thèse d'Anne-Marie Ray, 2013 ; Paolillo et al., 2016).

En vue d'applications cliniques (diagnostic et thérapie), mais aussi pour des applications plus fondamentales telles que le décryptage du fonctionnement des intégrines, les ligands spécifiques de α5β1 restent tout de même peu nombreux.

D. Sélection, identification et caractérisation d'aptamères ciblant des cellules de glioblastome exprimant l'intégrine α5β1

Article 4 (manuscrit en préparation)

Résumé :

A l'issue d'un procédé de SELEX complexe et original, combinant sélection sur cellules surexprimant l'intégrine α5β1 et sur l'intégrine recombinante, nous avons récemment sélectionné un aptamère ARN, nommé H02, en tant que nouveau ligand des cellules de GBM exprimant l'intégrine α5β1.

L'aptamère H02, couplé directement à un fluorophore (cyanine 5) interagit avec les cellules sur-exprimant α5 utilisées pour les étapes de SELEX, et ne se lie pas aux cellules sous-exprimant ou n'exprimant pas α5, utilisées pour les étapes de sélection négative. Des expériences d'aptafluorescence sur un panel de cellules de GBM exprimant différents taux d'intégrine α5 montrent que la liaison de l'aptamère H02 est corrélée à la liaison d'un anticorps anti-α5. De plus, sur des xénogreffes de GBM humains, l'aptamère H02 interagit spécifiquement avec les tissus tumoraux exprimant l'intégrine α5β1.

L'aptamère H02 est un nouveau ligand de cellules et tissus exprimant l'intégrine α5β1. L'aptafluorescence, plus rapide que l'immunofluorescence, pourrait être une alternative intéressante à l'utilisation d'anticorps pour détecter des biomarqueurs cellulaires à la surface de cellules et tissus tumoraux.

Mes projets de recherche actuels visent à explorer les aptamères en tant que nouveaux ligands de l'intégrine α5β1. Les aptamères, par leur capacité à adopter des structures variées et complexes, permettent de fixer des groupements fonctionnels de différentes natures (molécules fluorescentes, biotine, radioéléments, toxines, agents chimiothérapeutiques, siRNA…) et présentent donc un vaste potentiel d'applications biotechnologiques, diagnostiques, thérapeutiques… Les aptamères ciblant l'intégrine α5β1 pourraient servir d'outils moléculaires pour étudier les fonctions cellulaires de α5β1. En recherche translationnelle, ils pourraient servir

d'outils diagnostiques de marquage *ex vivo* de l'expression de l'intégrine dans des tissus tumoraux, et/ou de sondes d'imagerie non invasive pour suivre la progression tumorale, et aussi être utilisés en tant qu'agents thérapeutiques. Seuls ou en association avec d'autres inhibiteurs, ils pourraient servir à cibler les tumeurs exprimant l'intégrine α5β1, en particulier dans le cas des GBM humains.

Une stratégie de sélection originale nous a permis de valider un aptamère, nommé H02, en tant que ligand des cellules de GBM exprimant l'intégrine α5β1. Sélection, identification et caractérisation de cet aptamère sont décrits dans un manuscrit, inséré ci-dessous (Article 4). Ce manuscrit n'a pas encore été soumis pour publication car, en collaboration avec la SATT (Société d'Accélération du Transfert de Technologies) Conectus Alsace, nous étudions la possibilité de valorisation de l'aptamère H02.

Brièvement, nous avons réalisé un SELEX, par hybrid-SELEX, combinant :
- cell-SELEX, ciblant des cellules exprimant l'intégrine α5β1, qui a l'avantage de présenter la cible dans sa conformation native, mais dans un environnement très complexe. La stratégie de sélection utilisée pour le cell-SELEX est originale puisque nous avons utilisé deux lignées cellulaires différentes :
    - une lignée cellulaire de GBM humain (U87MG), dont nous possédons des transfectants stables sous-exprimant la sous-unité α5 pour la contre-sélection (nommés U87MG α5- ; expression d'un shRNA dirigé contre l'ARNm d'α5, Janouskova et al., 2012) et sur-exprimant α5 pour la sélection positive (nommés U87MG α5+ ; transfectés avec le plasmide pcDNA3.1 contenant le gène de la sous-unité α5 humaine, Janouskova et al., 2012)
    - une lignée murine CHO-B2 (Schreiner et al., 1989), transfectée par la sous-unité α5 humaine (CHO-B2 α5+) pour la sélection positive. Les étapes de contre-sélection ont été réalisées sur les cellules CHO-B2 n'exprimant pas la sous-unité α5.
- et SELEX classique, ciblant une protéine recombinante (nommé protein-SELEX), dont la cible a l'avantage d'être pure et bien définie, mais le désavantage de se trouver hors de son environnement membranaire naturel qui peut être important pour sa conformation. Pour les étapes de protein-SELEX, nous avons utilisé comme cible l'intégrine α5β1-Fc. C'est une protéine recombinante (don du Pr M. Humphries, Manchester, GB, Coe et al., 2001), comprenant les parties extracellulaires de α5 (acides aminés 1-951, 180 kDa) et de β1 (acides aminés 1-708, de 140 kDa), couplées au fragment Fc d'anticorps γ1, exprimée par des cellules

myélomateuses murines NS0, et purifiée sur colonne de Protéine A couplée à des billes de sépharose.

La banque de départ (Da Rocha Gomes et al., 2012 ; Dausse et al., 2005) contient 10^{14} séquences différentes. La séquence variable comprend 30 nucléotides. Elle est flanquée de deux régions fixes. Chaque molécule d'ARN compte 68 nucléotides. Dix-huit cycles de sélection/amplification ont été réalisés :

- 15 cycles de Cell-SELEX : 8 cycles sur les cellules U87-MG α5+ (cycles 1-7 et 11) et 7 cycles sur les cellules CHO-B2 α5+ (cycles 12-18). Les cellules ont été cultivées en boîte de culture de 6 puits et utilisées pour les cycles de sélection à 80-90% de confluence.
- 3 cycles de Protein-SELEX (cycles 8-10). Les cycles de sélection sont réalisés sur colonne de protéine-A sépharose chargée avec la protéine recombinante α5β1-Fc.

La stringence a été progressivement augmentée au fur et à mesure des cycles pour augmenter la pression de sélection, par (i) introduction d'étapes de contre-sélection, pour le cell-SELEX sur cellules U87MG α5- et CHO-B2, et pour le protein-SELEX sur billes de sépharose-Protéine A non chargées ou chargées avec un anticorps non-spécifique (Cetuximab, anticorps anti-EGFR, γ1), (ii) augmentation du temps de contact de contre-sélection, (iii) diminution du temps de contact de sélection, (iv) augmentation du nombre d'étapes de lavages, (v) addition d'ARNt compétiteur à partir du cycle 14.

A l'issue des 18 cycles de SELEX, 82 séquences ont été clonées et séquencées. Parmi elles, nous avons sélectionné 5 aptamères. Nous avons utilisé plusieurs techniques pour identifier les meilleurs aptamères ciblant α5β1. Ce sont les techniques de microscopie confocale (plateforme d'imagerie QUEST, Faculté de Pharmacie, UMR 7021 & IGBMC, Illkirch) et de cytométrie de flux (FACS Calibur, BD Biosciences, équipe Biovectorologie, UMR 7199, Illkirch) qui nous ont permis de valider, parmi ces 5 candidats, l'aptamère H02, spécifique de l'intégrine α5β1 sur les cellules utilisées pour la sélection.

L'aptamère H02 est capable de différencier plusieurs lignées cellulaires de GBM (U87MG α5+, U87MG α5- utilisées pour le cell-SELEX et LN319, LN229, SF763, LN18, LN443, LNZ308, U373, T98G) par leur niveau d'expression d'intégrine α5β1. L'aptamère H02 a également été testé en histochimie sur des xénogreffes de GBM humains. Ce type d'expérience

très récente, nommé aptahistochimie, est similaire à l'immunohistochimie, mais l'aptamère remplace anticorps primaires et secondaires (Bukari et al., 2017). L'aptahistochimie est plus rapide que l'immunohistochimie. L'aptamère H02, directement couplé à la cyanine-5, interagit spécifiquement avec les tissus tumoraux exprimant l'intégrine α5β1.

L'aptamère H02 est donc un ligand d'intérêt diagnostique, efficace en aptacyto- et en aptahisto-chimie pour révéler la présence de l'intégrine α5β1 sur cellules et tissus tumoraux. En outre, l'aptamère H02 est probablement internalisé à 37°C via l'internalisation de l'intégrine α5β1. Les propriétés d'internalisation d'un aptamère peuvent s'avérer extrêmement intéressantes en thérapie. En effet, un aptamère couplé à un ligand (agent cytotoxique, nanoparticule, siRNA…), peut permettre de diriger et délivrer spécifiquement ce ligand à la cellule ciblée par l'aptamère. L'internalisation des aptamères est décrite dans la partie 'Perspectives'.

Article 4 (manuscrit en préparation)

Cruz Da Silva E[#], Fechter P[#], Buhr L, Fenat M, Mercier MC, Noulet F, Etienne-Seloum N, Guenot D, Lehmann M, Vauchelles R, Martin S, Lelong-Rebel I, Ray AM, Seguin C, Pinel S, Dontenwill M, Choulier L.*. Identification and characterization of RNA aptamers targeting cells expressing integrin α5β1 as probes for cyto- and histo-fluorescence. ([#]co-first authors, *corresponding author).

Identification and characterization of RNA aptamers targeting cells expressing integrin α5β1 as probes for cyto- and histo-fluorescence

Cruz Da Silva E.[1*], Fechter P.[2*], Buhr L.[1], Fenat M.[1], Mercier M.-C.[1], Noulet F.[1], Etienne-Seloum N.[1], Guenot D.[3], Lehmann M.[1], Vauchelles R.[1], Martin S.[1], Lelong-Rebel I.[1], Ray A.-M.[1], Seguin C.[4], Pinel S.[5], Dontenwill M.[1] & Choulier L.[1#]

[1]CNRS, UMR 7021, Laboratoire de Bioimagerie et Pathologies, Tumoral Signaling and Therapeutic Targets, Université de Strasbourg, Faculté de Pharmacie, 67401 Illkirch, France
[2]CNRS, UMR 7242, Biotechnologie et Signalisation Cellulaire, 67400 Illkirch-Graffenstaden, France and Université de Strasbourg, Institut de Recherche de l'Ecole de Biotechnologie de Strasbourg, 67400 Illkirch-Graffenstaden, France.
[3]EA 3430, Progression tumorale et micro-environnement, Approches translationnelles et épidémiologie, Université de Strasbourg, 67000 Strasbourg, France.
[4]CNRS, UMR 7199, Laboratoire de Conception et Application de Molécules Bioactives, Université de Strasbourg, Faculté de Pharmacie, 67401 Illkirch, France
[5]CNRS UMR 7039, Centre de Recherche en Automatique de Nancy, Université de Lorraine, 54505 Vandoeuvre-lès-Nancy, France
*co-first authors
[#]correspondence: laurence.choulier@unistra.fr; Tel.: +33-36885-4197; Fax: +33-36885-4313

ABSTRACT

Nucleic acid aptamers are often referred as chemical antibodies. As they possess several advantages like their smaller size, temperature stability, ease of chemical modifications, lack of immunogenicity/toxicity and lower cost of production, aptamers are promising tools for clinical applications. Aptamers against cell-surface protein biomarkers are of particular interest for cancer diagnosis and targeted therapy. In this study, we identified and characterized RNA aptamers targeting cells expressing integrin α5β1. This αβ heterodimeric cell-surface receptor is implicated in tumor angiogenesis and solid tumor aggressiveness. In glioblastoma, integrin α5β1 expression is associated with an aggressive phenotype and a decrease in patient survival. We used a complex hybrid SELEX strategy combining protein-SELEX cycles on the recombinant α5β1 protein, surrounded by cell-SELEX cycles, themselves realized using two different cell lines. We identified aptamer H02, able to differentiate, in cyto- and histo-fluorescence assays, glioblastoma cell lines and tissues from patient-derived tumor xenografts according to their α5 expression levels. Aptamer H02 is therefore an interesting tool for glioblastoma tumor characterization.

1. INTRODUCTION

Glioblastoma multiform (GBM), the highest grade glioma tumor (grade IV), is the most aggressive and the most common malignant form of astrocytoma. Standard therapy consists of surgical resection to the extent that is safely feasible, followed by radiotherapy and concomitant chemotherapy with temozolomide (Stupp protocol, [1]). Despite these therapies, the median survival rate is less than 15 months [2]. Histological features that characterize GBM are the presence of necrosis and abnormal growth of blood vessels around the tumor. Defining molecular profiles aims at developing molecularly guided approaches for the treatment of patients. The 2016 World Health Organization (WHO) classification scheme [3] integrated phenotypic and genotypic parameters for central nervous system tumor classification. GBM are divided into isocitrate dehydrogenase (IDH) 1-wild type (about 90 % of cases; corresponds to the most frequently primary or de novo GBM) and IDH-mutant GBM (about 10 % of cases, corresponds to secondary GBM). Some of the GBM biomarkers that have been and are being discovered [4] are cell surface protein biomarkers [5–8]. Expression of cell-surface protein is often remodeled in cancers. Genetic and epigenetic features altered in cancer [8] include modification of copy number (under- or over-expression), truncations, mutations and post-translational modifications. These modified proteins are major clinical targets for diagnosis and therapies considering their accessibility for pharmacological compounds.

Tumor-specific tools such as aptamers can be used as recognition ligands to discriminate a tumor cell from another cell or as carriers to deliver therapeutic payloads to targeted tumor cells [9,10]. Aptamers are single-strand DNA or RNA molecules that constitute an alternative class of molecules emerging as cancer-specific therapeutic and diagnostic tools [9,10]. They are selected through a process known as SELEX (selective evolution of ligands by exponential enrichment)[11,12]. Aptamers, from the Latin aptāre (to fit) and from the Ancient Greek meros (part) are often referred as chemical antibodies [13]. They bind to their specific targets with high affinity and specificity. Aptamers possess numerous advantages over antibodies, like smaller size, temperature stability, self-refolding, lack of immunogenicity and toxicity, more efficient penetration into biological compartments, chemical synthesis with high batch fidelity, option to site-specific and flexible introduction of linkers, reporters, functional groups, siRNA, nanoparticles, drugs… Aptamers have been identified towards a wide variety of targets, the most common ones remaining proteins. *We recently reviewed aptamers to more than thirty different tumor cell-surface protein biomarkers* [14]*, a few of them being* heterodimeric receptors, such as tyrosine kinase receptors and cell-adhesion molecules. The selection of aptamers to cell-surface proteins still remains a complex process.

Among cell-surface biomarkers, integrins are heterodimeric cell-surface receptors for cell migration, differentiation and survival [15], composed of α and β subunits and which deregulation leads to cancer progression and therapy resistance [16]. In mammals, twenty-four distinct integrins are formed by the combination of 18 α and 8 β subunits. Specific heterodimers preferentially bind to distinct extracellular matrix proteins. Integrin α5β1, the fibronectin receptor, belongs to the RGD-binding integrin family. Overexpressed on tumor neovessels and on solid tumor cells, integrin α5β1 is implicated in tumor angiogenesis and solid tumor aggressiveness. We and others have shown that α5β1 integrin is a pertinent therapeutic target for GBM [17] through its active role in tumor proliferation, migration, invasion, metastasis and resistance to chemotherapy [18–22]. At the mRNA level, high α5β1 integrin expression is associated with more aggressive tumors in patients with glioma [18]. At the protein level, to date, only a few *in situ* analysis on GBM tumor section were described [23,24]. Relationship between protein expression and patient survival requires rapid and accurate tools for diagnostics. Moreover, new therapeutics are needed to target α5β1 overexpressed in GBM tumor cells.

In our study, aptamers to integrin α5β1-expressing cells were selected by an original and complex hybrid-SELEX process. This SELEX combines three rounds of protein-SELEX surrounded by fifteen rounds of cell-SELEX on two different cell lines, the human U87MG GBM cell line and the CHO-B2 cell line from Chinese hamster ovary, overexpressing integrin α5. Counter selection steps

were realized on isogenic cell lines under-expressing α5 for U87MG or that do not express α5 for CHO-B2. We identified and characterized an aptamer named H02. Directly coupled to the cyanine 5 fluorophore, aptamer H02 was able to discriminate between ten GBM cell lines expressing high and low levels of integrin α5. We also demonstrated that aptamer H02 is very efficient in apta-fluorescence assays to characterize GBM tumor tissues from patient-derived tumor xenografts expressing high levels of α5 from GBM tumor tissues expressing low levels of α5.

2. RESULTS

2.1. Selection of RNA aptamers by a SELEX strategy combining cell-SELEX on two cell lines and protein-SELEX

To guide selection towards α5β1, we used an original hybrid-SELEX strategy that alternates protein- and cell-SELEX. Our strategy is divided in three steps symbolized by three circles in Figure 1A, using two different cell lines (Figure 1B) and a recombinant α5β1 protein (Figure 1C). The first seven rounds of cell-SELEX were realized on GBM U87MG cells overexpressing the α5 subunit (U87MG α5+) [18]. An RNA library comprising 10^{14} different molecules was incubated with U87MG α5+ cells plated in a cell culture dish. Counter-selection was introduced during rounds 4-6 using isogenic U87MG cells modified to under-express the α5 subunit (U87MG α5-) [18]. The next three rounds of selection were performed by a protein-based SELEX process (rounds 8-10) on the protein A-purified form of integrin α5β1. The recombinant protein α5(E_{951}) β1(D_{708})-Fc (α5β1-Fc) is composed of human α5 and β1 ectodomains, fused to Fcγ1 knobs mutated into their CH3 domains so as to increase the likelihood of heterodimerization between α5 and β1 chains [25]. Negative- and counter- selection steps preceding positive selection steps were realized on protein A-sepharose beads (rounds 8-10) and on an antibody presenting the same γ1 isotype than the Fc fused to α5β1 ectodomains (rounds 9-10). Finally, cell-SELEX rounds were implemented on two different cell lines: on U87MG cells (round 11, as for rounds 1-7) and CHO-B2 cells (rounds 12-18). CHO-B2 cells, which does not naturally express α5 [26], were used for counter selection. For positive selection, CHO-B2 cells were manipulated to generate positive α5 cells by overexpressing human ITGA5. Within the course of the SELEX process, the stringency was progressively increased, by decreasing and increasing incubation time for positive- and counter-selection, respectively, by introducing competitor yeast tRNAs and increasing the number of washes (Table S1). The enrichment of RNA pools during selection was followed by flow cytometry. The RNA pool at round 18 was cloned. Among eighty two sequenced molecules, five aptamers, named H02, H03, G10, B03 and G11, were selected for further characterization.

2.2. Post-SELEX characterization of aptamers

Aptamer H02 was the most frequently represented over all sequences (6 times out of 82 sequences, 7.3%). Aptamers H03, G10 and G11 represented 3.7% of all sequenced molecules, and aptamers B03 1.2%. The predicted secondary structures of the five aptamers H02, G11, H03, G10 and B03 are shown in Figure 2. Fixed regions (represented in dark red on figure 2) were designed to display partial complementarity and pre-organize aptamers in hairpin structures [27]. Secondary structure prediction of aptamers H02, G11 and B03 are highly similar and very different from those of G10 and H03. The bottom parts of aptamers H02, G11 and B03 adopt a mismatched double-stranded structure conducted by the 5' and 3' fixed regions. A long 9-10 nucleotide CG-rich double-stranded structure interrupted by mismatches (H02 and B03) and by an internal loop (G11) constitutes the core of the random region. The 10 and 7 nucleotide long apical loop for H02 and B03 is purine-rich. The apical loop of G11 is short (3 nucleotide long).

Identification of α5β1-binding aptamers was realized using confocal fluorescence microscopy by incubating cyanine-5 (Cy5) labeled aptamers with the cells used for the cell-SELEX process (Figure 3). None of the five aptamers binds to U87MG α5- and CHO-B2 cells used for counter selection steps. At 4°C (Figure 3A & 3B), only aptamer H02 binds to U87MG α5+ and CHO-B2 α5+ cells used for positive selection steps. We next checked whether these aptamers were able to bind to U87MG cells at 37°C, the temperature used for the cell-SELEX process (Figure 4). H02,

G11, B03, G10 and B03 did not bind to U87MG α5- cells (Figure S1). On U87MG α5+ cells, we observed a strong binding not only of aptamer H02, but also to a lesser extent of aptamer G11 (Figure 4). Due to its binding to U87MG α5+ cells at 4°C and at 37°C, further studies were focused on aptamer H02.

2.3. Stability, specificity, affinity, localization of aptamer H02

As aptamer H02 is a non-modified RNA molecule, we tested its stability in the presence of cells at 4°C and 37°C in the buffer used for selection. Results (Figure S2) confirmed that incubation on cells for 30 minutes, which corresponds to the maximum contact time of RNAs with cells during selection and different assays on cells, does not induce aptamer H02 degradation.

The specificity of aptamer H02 for α5 overexpressing cells was confirmed by flow cytometry (Figure 5A). Albeit no shift in fluorescence was detected for CHO-B2 cells after incubation with the two Cy5-labeled H02 and B03 aptamers, a shift was detected for CHO-B2 α5+ cells with aptamer H02 but not with aptamer B03.

The equilibrium affinity parameter K_D of the interaction between aptamer H02 and U87MG α5+ cells was determined using flow cytometry (Figure 5B). Binding events associated with the fluorescence signal of different concentrations of aptamer, ranging from 0.15 to 5 μM, to a constant number of cells were measured. A K_D of 277.8 ± 51.8 nM was determined.

The localization of aptamer H02 on the GBM U87MG α5+ cells was analyzed by confocal microscopy at 4°C and 37°C. Cells were incubated with the Cy5-labeled aptamer H02 and with the anti- α5 IIA1 antibody, followed by incubation of a secondary antibody labeled with Alexa 546. Spots of co-localization were detected between Alexa-546 and Cy5 which reflect spatial proximity between the α5 subunit and the aptamer H02, at 4°C and to a lesser extent at 37°C (Figure 5C). Aptamer H02 detects α5β1 mostly at membrane at 4°C and punctuate spots in the cytoplasm suggest internalized molecules inside cells at 37°C. A weaker co-localization was observed with anti-β1 antibody and aptamer H02 (Figure 4). The β1 subunit associates with different α subunits to form receptor complexes whereas the α5 subunit associates only with the β1 subunit to form the fibronectin receptor. Aptamer H02 seem to be directed to the α5 subunit of integrin α5β1.

2.4. Cyto- and histo-fluorescence with aptamer H02

Aptamers molecules have the potential to revolutionize the field of diagnostics for the detection of cell-specific biomarkers [28]. We evaluated the capacity of aptamer H02 to be a new tool for the characterization of GBM α5 expressing cells and tissues. We first characterized the ability of aptamer H02 to distinguish between ten human GBM cell lines expressing different levels of the α5 subunit (Figure 6A). Among those are encompassed the U87MG α5+ and U87MG α5- used for cell-SELEX, and the eight GBM cell lines LN319, LN229, SF763, LN18, LNZ308, U373, T98G, LN443. For aptacytochemical assays, confluent adherent cells were cultured in monolayers on sterile glass slides. Cells were stained with the Cy5-labeled aptamer H02 at 4°C for 30 minutes. After fixation of cells with paraformaldehyde, a double-staining procedure by immunofluorescence was realized on the same cells using an anti-α5 primary antibody and a secondary antibody labelled with Alexa 546. Quantification of apta- and immuno-stainings of the different cell lines is shown in Figure 6B. A correlation coefficient of 0.76 has been determined between apta- and immuno-fluorescence. Integrin α5β1 in GBM cell lines can therefore be characterized in cytofluorescence with the Cy5-labeled aptamer H02.

Histochemical assays were performed on two patient-derived GBM xenografts, TC22 and TC7. These tissue sections, embedded on paraffin, were first deparaffinized and subjected to antigen unmasking protocol. Analysis were performed on the 2 tissue sections to quantify the level of integrin α5 in both tumor and to compare immuno- and apta-histochemistry assays. Immunohistochemical assays show that TC7 tumor presents a higher integrin α5 expression level than TC22 tumor (Figure 6C and 6D, top panels). Aptahistochemical assays were realized with the Cy5 labeled aptamers H02 and G11 (Figure 6C and 6D, bottom panels). With aptamer H02, the fluorescence intensity is 4 fold higher on TC7 than on TC22. In the conditions used for these histochemical experiments, the signal/noise ratio was better with aptamer H02 than with than

with antibody. Aptamer G11 was also able to discriminate between both tissue sections, but to a much lesser extent than aptamer H02 (difference of 1.6 fold).

Aptamer H02 is therefore an interesting promising new tool to differentiate cells according to their α5 subunit expression levels, whether it be in cyto- and in histo-fluorescence experiments.

3. DISCUSSION

As differential expression of cell-surface proteins often occurs in tumor cells, and considering their accessibility to extracellular ligands, these proteins provide potential biomarkers in oncology for diagnosis, prognosis and therapy. The identification of molecular probes specific for cell-surface protein biomarkers is of great importance [14]. Due to their high affinity and specificity towards their targets, aptamers are attractive alternative promising tools to antibodies for clinical applications. In this study, through a complex and highly stringent SELEX strategy, we showed that it was possible to select an RNA aptamer specific to a pre-identified heterodimeric cell-surface protein embedded in its natural environment. Aptamer H02 was able to differentiate between high and low expression of the α5β1 integrin on cells and tissues. This aptamer is suitable for tumor characterization.

Two main processes have been developed to select aptamers specific for pre-determined cell-surface proteins, namely protein- and cell-based SELEX [14]. In protein-based SELEX, a purified protein is used as target, usually full-length or truncated (generally recombinant ectodomains). The major issues of protein-based SELEX process are that purification of membrane proteins is not easy and that purified proteins may not adopt the same conformational state than in their endogenous cellular environment. Some aptamers identified through protein-based SELEX failed to recognize their target when embedded in whole living cells [29,30]. In cell-based SELEX, targets are cell-surface proteins in their cellular environment. This process is much more complex than protein-based SELEX. Modification of cell lines are often required to guide the selection towards the desired target, like over- and/or under-expression of the protein target for positive- and/or counter-selections, respectively. Cell-SELEX employs generally cells genetically modified to overexpress a defined cell-surface target for positive selection and mock cells for counter selection or mock cells for positive selection and isogenic cells under-expressing the cell-surface target for counter selection [14]. Cancer cell lines have been used for cell-based SELEX process [10,31], both for therapy and diagnosis purposes.

Only three integrins (β2, αvβ3 and α6β4) have been used so far as pre-identified targets for SELEX processes. Blind et al [32] selected, by protein SELEX, RNA aptamers targeting a 46-mer peptide corresponding to the complete cytoplasmic domain of the β2 subunit of integrin αLβ2. Cells infected with vaccinia viruses encoding β2-specific aptamers, enabled high-level cytoplasmic expression of RNA aptamers. Intracellular integrin-binding aptamers reduced inducible cell adhesion to the intercellular adhesion molecules-1 (ICAM-1). To target integrin αvβ3, two different protein-based SELEX processes and a cell-based SELEX were used to identify *2'-fluoropyrimidine* RNA aptamers. The *2'-fluoropyrimidine* modification confers increased nuclease resistance to RNA molecules. Aptamer Apt-αvβ3, selected on αvβ3 purified by immunoaffinity chromatography, was able to bind αvβ3 integrin expressed on the surface of live cells and to impair endothelial cell growth and survival [33,34]. *In order to select for aptamers specific to homodimer αv and β3, Gong et al* [35]*, developed a strategy called MAI-SELEX (MAI for multivalent aptamer isolation). Two distinct selection stages were employed, the first being a classical affinity selection on the purified full-length* αvβ3 *integrin. The second, for specificity, leads selection to* β3 *as integrin* α*IIb* β3 *served as a protein decoy. Two aptamers, specific for* αv *and* β3 *were identified with affinities in the low nanomolar range.* Takahashi et al [36] applied a process that they called Icell-SELEX (isogenic cell-SELEX) to identify RNA aptamers targeting integrins αv (ITGAV) in which isogenic HEK293 cell lines were manipulated for counter-selection by microRNA-mediated silencing and for positive selection by overexpression of target proteins. Integrin α6β4 has recently been the target of a hybrid-SELEX [37,38], a combination of protein- and cell-based SELEX processes, for which five rounds of cell-SELEX on PC-3 cells were followed by 7 rounds of protein-

based SELEX on a recombinant α6β4 protein [39]. In this last study, despite the introduction of counter-selection on PC-3 β4 integrin (ITGB4) knockdown cells to deplete ssDNA aptamers specific for cell surface markers other than the β4 subunit, the cell-SELEX process alone was not sufficient to prevent enrichment of non-target specific aptamers. Affinities of aptamers identified by cell-SELEX for their integrin targets were in the hundreds nM range [14].

To allow the discovery of highly selective but also conformation-dependent aptamers and to guide the selection towards integrin α5β1, the complex SELEX strategy that we adopted presents two originalities compared to other SELEX strategies towards cell-surface biomarkers. In our study, a hybrid SELEX, combining successive rounds of cell-SELEX, protein-SELEX and then again cell-SELEX, was realized. Usually, in hybrid-SELEX, the first rounds of selection are realized by cell-SELEX, and then rounds of selection are realized on the same version of the target in its purified form by protein-based SELEX [37,39]. A reverse hybrid-SELEX combines first protein-SELEX followed by cell-SELEX [38,40,41]. Consequently, our strategy combines hybrid-SELEX and reverse hybrid-SELEX (Figure 1). The second originality is that two different cell lines were used, compared to one in previous studies. These two cell lines were the human GBM U87MG and the CHO-B2 cell lines. Both cell lines were genetically transformed to express high levels of the human α5 subunit for positive selection rounds. These two cell lines do not express the same level of the α5 subunit (Figure 1). The first rounds of selection were realized on the U87MG α5+ cells to guide the selection towards cells highly expressing the α5-subunit. The last rounds of cell-SELEX were realized on CHO-B2 α5+ cells, a cell line expressing α5 levels similar to the α5 expression of the wild type GBM cell line U373 to guide the selection to a more natural expression and probably a more natural conformation and environment of the target. For counter selection rounds, the ideal cell line was CHO-B2 as it does not express at all the α5 subunit. U87MG α5- were stably transfected to repress the human α5 gene by transfecting a pSM2 plasmid coding for a shRNA targeting the α5 mRNA [18]. Despite the fact that U87MG α5- cells were not fully depleted in α5, we showed that the differential expression level of α5 between U87MG α5+ and U87MG α5- was high enough to permit a differential binding pattern of aptamer H02 (Figure 3B). The key to this successful complex SELEX lies in the use of alternative rounds of cell- and protein- SELEX rounds, the use of at least two different cell lines to remove unspecific binding and in the high differential expression of target expressed on cells used for positive selection compared to cells used for counter selection.

Aptamer H02 was selected after eighteen rounds of a stringent SELEX process. This aptamer was the most represented sequence, has a highly stable hairpin predicted secondary structure and is not degraded in contact with cells in the condition used for experiments. Aptamer H02 was identified as a specific binder of α5 expressing cells whether it was on cells used for positive selections or on other GBM cells in aptacytochemistry assays. A K_D value of 277.8 ± 51.8 nM was determined, for the interaction between aptamer H02 and U87MG α5+ cells. This affinity value is in the same order of magnitude than the 100-400 nM that have been determined for aptamers characterized towards other integrins by cell-SELEX or hybrid-SELEX [36,39].

Histological detection of specific biomarkers is almost indispensable for diagnosis confirmation of malignancy. Immunohistochemistry is a cheap, easy method for detection of tumor biomarkers. Aptahistochemistry is a new notion, still rarely described, for which aptamers, as a new class of probes, are used instead of antibodies. In our study, we used aptamer H02 end-labeled with a single cyanine 5 fluorescent dye. Aptamer H02 was able to specifically interact with α5 overexpressing tumor tissues from patient derived xenografts (Figure 6C & 6D) as it efficiently differentiate TC7 (tissue with high α5 expression) from TC22 (tissue with low α5 expression). Aptamer H02 is an effective molecular probe for labeling histological tissue sections and detection of the α5β1 biomarker on tumor cells. Aptamer probes may become powerful tools for pathologists to characterize tumor tissues as protocols are simple to implement and can be applied not only to paraffin-embedded cancer tissue, but also to frozen and formalin-fixed tumoral tissues [42–44]. A recent review describes the technicalities of the current applications of aptahistochemistry [45]. Aptafluorescence reduces the cost, time and cross-reactivity concerns compared to immunofluorescence approaches based on primary and then secondary antibodies.

Conjugation of dye on aptamers is easy and reduces the risks of disrupting the aptamer structure, compared with antibodies generally labeled with multiple tag. Compared with an antibody, aptamer smaller size (10-fold reduction in size) allows for a better penetration in tissues [46,47], particularly in applications for which epitope accessibility is reduced, such as in fixed tissues. A further advantage of aptamers is that the target of interest is not limited to molecules which produce an immune response in the host animal, as for antibodies [28]. Chemical synthesis of aptamers virtually eliminates the issue of batch-to-batch variation.

4. CONCLUSION

In conclusion, we characterized a new, original and powerful aptamer tool to detect GBM tumoral cells and tissues expressing high levels of α5β1 integrin. These detections might be extended for use in other cancers where α5β1 has proven to be a therapeutic target, such as colon, ovarian, breast, lung tumors and melanoma [17]. If internalized, this aptamer might open roads for α5β1-specific therapeutic payloads delivery. Endocytosis may be crucial for targeting and increasing the therapeutic efficacy of GBM drugs. Linked to a cytotoxic agent, an aptamer to integrin α5β1 could serve as a carrier for targeted therapeutic delivery. Such aptamers were very recently called "charomers" [48]. If charomers reach the cytosol, they would become very powerful carriers to deliver therapeutics inside targeted cells.

5. MATERIALS AND METHODS

Materials

The ssDNA library was synthetized and purified by Eurogentec (Seraing, Belgium). All RNA aptamers and chemicals were purchased from IBA and Sigma-Aldrich (Hamburg, Germany), respectively, unless otherwise stated. Sequences of all primers, library, and aptamers described in this study are described in Table S2.

Cell culture and transfection

Cell culture medium and reagents were from Lonza (Basel, Switzerland) or Gibco (Thermo Fisher Scientific, Waltham, MA USA). U87MG cells were from ATCC; U373MG and T98G cells were from ECACC (European Collection of Authenticated Cell Cultures, Sigma). LN319, LN229, LN443, LN18 and LNZ308 cells were kindly provided by Pr. Monika Hegi (Lausanne, Switzerland), SF763 by Frédéric André (Marseille, France), CHO-B2 by Wolfram Ruf (La Jolla, USA). All GMB cells were routinely cultured in Eagle's minimum essential medium (EMEM), 10% heat-inactivated fœtal bovine serum (FBS), 2 mM glutamine. For U373MG and T98G, 1% non-essential amino acids and 1mM sodium pyruvate were added to the medium. For CHO-B2 cells, EMEM was substituted for Dulbecco's Modified Eagle Medium (DMEM, high glucose). U87MG cells were stably transfected respectively to overexpress (U87MG α5+) and to repress (U87MG α5-) the human α5 gene, as previously described [18]. CHO-B2 cells lack the α5 subunit. They were stably transfected by a pcDNA3.1 plasmid, provided by Dr. Ruoshlati, La Jolla, USA, to overexpress the human α5 integrin gene fused to the green fluorescent protein (GFP) by using jetPRIMETM (Polyplus-transfection) according to the manufacturer's instructions and named CHO-B2 α5+ cells.

Expression and purification of α5β1-Fc

The recombinant soluble human $\alpha5(E_{951})\beta1(D_{708})$-Fc (α5β1-Fc) integrin (a gift from Martin Humphries, Manchester, UK) was produced from NSO culture supernatant and purified via the Fc domain on protein A-sepharose, as previously described [25]. The purity of the protein was verified by Coomassie staining of SDS-polyacrylamide gel.

SELEX strategy

The RNA library was obtained by transcription from a starting ssDNA library (Eurogentec), containing 30 random nucleotides (N30), flanked by primer annealing sites: 5'-GTGTGACCGACCGTGGTGC-N30-GCAGTGAAGGCTGGTAACC-3. Two primers P3' (5'-GTGTGACCGACCGTGGTGC-3') and P5' (5'-TAATACGACTCACTATAGGTTACCAGCCTTCACTGC-3')

containing the T7 transcription promoter (underlined), were used for PCR amplification, as described [27]. Synthesis of the RNA library and transcription, followed by DNAse I (Roche) treatment have already been described [49]. The RNA pool was gel purified by denaturing (7 M urea) gel electrophoresis on a 8% polyacrylamide gel. The band corresponding to the RNA was visualized by UV shadowing, cut out for overnight extraction (500 mM NH_4OAc, 1 mM EDTA, 20 % phenol) at 4°C. The RNAs were then purified by phenol/chloroform extraction and ethanol precipitation. Prior to each round, the RNA pool was heated at 80°C for 2 minutes, immediately cooled-down on ice for 5 minutes, and then placed at room temperature for 10 minutes in order to allow the formation of the optimal conformation, in selection buffer composed of 1mM $MgCl_2$, 0.5 mM $CaCl_2$ in phosphate-buffered saline (PBS), pH 7.4. For cell-SELEX, adherent cells at confluency were washed 3 times in PBS and 3 times in selection buffer before incubation with the starting RNA library (1 nmole) at 37°C for 30 minutes under slow agitation (75 rpm). Cells were then washed once for 5 minutes and detached with a cell scraper. Binding RNA molecules were detached from cells by heating at 95°C for 2 minutes. Eluted RNA pools were extracted by phenol/chloroform and ethanol precipitated. They were then amplified by reverse-transcription prior amplification [49]. The dsDNA pool was then transcribed as described above. For next rounds of selection, number of washes were modified compared to the first round as described in Table S1. From the fourth round to the sixth, the RNA pool was first incubated with cells used for counter selection and unbound sequences were then incubated with cells used for positive selection (Figure 1). A protein-based SELEX process was applied during rounds 8-10. The recombinant α5β1-Fc integrin was coupled to protein A-sepharose 4B conjugate (Invitrogen), ahead washed 3 times with selection buffer. We employed a negative selection step in which the RNA pools were pre-incubated with protein A-sepharose beads alone prior to the positive selection. Unbound sequences were incubated under agitation on α5β1-Fc-loaded beads for 20 minutes. Eluted RNA was recovered, reverse transcribed, PCR amplified and transcribed back into RNA for the subsequent round as described above. For rounds 9 and 10, a counter selection was also realized on negative control IgG (cetuximab, Merck Serono). Beginning with round 11, another cell-SELEX process was realized as described above. Cells for counter- and positive-selections and SELEX conditions are described in Figure 1 and Table S1. Since the 14th round of selection, competitor yeast tRNA was added (Table S1). At the end of SELEX, sequences of the 18th pools were cloned with TOPO-TA cloning kit (Invitrogen Life Technologies) before sequencing. The sequences have been compared by MultAlin [50]. Prediction of secondary structure were obtained by the mfold software [51].

Stability assay

RNA aptamers at 5 μM in selection buffer were incubated on adherent cells at 4°C and 37°C for 0, 15, 30 and 45 minutes. Control samples were realized with aptamers which were not in contact with cells. Samples were loaded on a denaturing (7 M urea) 12% polyacrylamide gel and revealed using a Stains all solution (Sigma-Aldrich).

Flow cytometry

Flow cytometry was performed with individual aptamers directly coupled to Cy5 at their 3'-end. For the comparison of the binding profile of different aptamers binding to cells, aptamers were used at a final concentration of 500 nM. For the determination of equilibrium binding affinities, aptamer H02 was used at concentrations ranging from 0.15 to 5 μM. After detachment with EDTA 0.2M, cells were incubated for 30 minutes with Cy5-labeled aptamers. Controls were realized by incubating cells with a 1/100 dilution of an anti-α5 antibody (mouse anti-human CD49e, IIA1 antibody, BD Chemigen) for 30 minutes, followed by a 30 minutes incubation with the Alexa 647-conjugated affine pure goat anti-mouse IgG (Jackson Immonoresearch) at 10 μg/ml. After washing, cells were analyzed using a FACS Calibur flow cytometer (Becton Dickinson), and the mean fluorescence intensity was measured using Flowing software 2.5.1. For K_D determination, experiments were repeated three times and data were evaluated using GraphPad PRISM (version 5.04).

Western blot
Cells were lysed (1% Triton-X100, NaF 100 mmol/L, NaPPi 10 mmol/L, Na_3VO_4 1mmol/L in PBS, supplemented with Complete anti-protease cocktail; Roche) and 10 µg of protein was separated by SDS-PAGE (BioRad) and transferred to PVDF membranes (Amersham). Blots were probed with antibodies to α5 integrin (H104, Santa Cruz Biotechnology) and to GAPDH (Millipore). HRP-coupled secondary antibodies were from Promega. Proteins were visualized with enhanced chemiluminescence using the LAS4000 imager and densitometry analysis was performed using the ImageJ Software (GE Healthcare). GAPDH was used as housekeeping protein to serve as the loading control for cell lysate samples. Analysis were performed on three independent experiments.

Fluorescent-based cytochemical assays on human GBM cell lines
The adherent GBM cell lines (U87MG α5+, U87MG α5-, LN319, LN229, LN443, SF763, LN18, LNZ308, U373 and T98G) were plated on sterile glass slides one night at 37°C in culture medium, washed three times and then saturated for 1h at RT in selection buffer containing 2% BSA. For aptacytochemical assays, Cy5-labeled aptamer H02 was denatured at 95°C for 3 minutes, incubated on ice for 5 minutes and then on cells in selection buffer for 30 minutes on ice, at 5 µM. Cells were then washed in selection buffer, fixed for 8 min in 4% PFA, permeabilized for 2 min with 0.2% triton, and washed again. Sequentially, immunocytochemistry was realized with anti-α5 antibody (mouse anti-human CD49e, IIA1 antibody, BD Chemigen) 1/200 or with anti-β1 antibody (mouse anti-human CD29 antibody, clone TS2/16, Biolegend) 1/500, for 1h at RT followed by a secondary goat anti-mouse antibody coupled to Alexa 546 (Life Technology) at a 2 µg/ml final concentration. Immuno- and apta-stainings were followed by Hoechst staining for 1h at room temperature to visualize nucleus. Washing steps are realized before mounting using the fluorescent mounting medium (S3023, DAKO).

Fluorescent-based histochemical assays on patient-derived xenograft
Two patient-derived heterotopic xenograft (PDX) were selected for *in vivo* analysis [52]. TC7 and TC22 GBM-PDX presented high and low levels of α5 integrins, respectively. PDX mouse models were established using tissues surgically removed from patients as previously described [53,54]. Integrin α5 was apta- and immuno-stained using formalin-fixed, paraffin-embedded xenografts mounted on glass slides. Sections were deparaffinized, rehydrated and subjected to antigen unmasking protocol. Briefly, sections were boiled at 100°C for 10 min in the Target Retrieval Solution, pH 9 (S2367, DAKO), cooled down to room temperature for 20-40 min, rinsed in H_2O. For aptafluorescence, slides were rinsed for 5 min in selection buffer, dried and then incubated in blocking buffer (2% BSA in selection buffer) for 1h at room temperature, rinsed in H_2O and then in selection buffer, and dried. RNA molecules were denatured at 95°C for 3 minutes, incubated on ice for 5 minutes before dilution in selection buffer to a 1 µM final concentration. Aptamers were incubated on tumor sections for 1h at RT in a humid chamber, washed in selection buffer, dried, fixed in 4% PFA, and then washed thrice in PBS. For immunofluorescence, slides were rinsed for 5 min in PBS-T (0.1% Tween-20 in PBS), dried and then incubated in blocking buffer BB-I (5% goat serum in PBS-T) for 1h at RT in a humid chamber. Overnight incubation with the anti-integrin α5 mAb 1928 (6B8516, Millipore) 1/200 in BB-I was followed by a 5 min wash in PBS-T and by an incubation step with a 1/100 dilution of the goat anti-rabbit secondary antibody coupled to Alexa Fluor 647 (A21245, Life technologies). Immuno- and apta-stainings were followed by DAPI (10 µg/ml) staining for 30 min at room temperature to visualize cellular nuclei. The stained samples were then washed in PBS and coverslips were mounted onto tissue sections using the fluorescent mounting medium (S3023, DAKO).

Confocal imaging
Images were acquired using a confocal microscope (LEICA TCS SPE II, 63× magnification oil-immersion).

Mean fluorescence intensity was acquired using the ImageJ software. Statistical analysis of data are represented as mean ± SEM. Statistical analyses were realized with GraphPad PRISM version 5.04.

ACKNOWLEDGEMENTS

We thank Martin Humphries (Manchester, UK) for the gift of NS0 cells expressing α5β1-Fc integrin. This work was supported by a contract from the SATT Conectus Alsace (number I14-057), by a grant from the PEPS-IDEX program of the Université de Strasbourg (number W15RPE24), and by the INTEGLIO program of the Cancéropôle Grand-Est.

REFERENCES

1. Stupp, R.; Mason, W. P.; van den Bent, M. J.; Weller, M.; Fisher, B.; Taphoorn, M. J. B.; Belanger, K.; Brandes, A. A.; Marosi, C.; Bogdahn, U.; Curschmann, J.; Janzer, R. C.; Ludwin, S. K.; Gorlia, T.; Allgeier, A.; Lacombe, D.; Cairncross, J. G.; Eisenhauer, E.; Mirimanoff, R. O. Radiotherapy plus Concomitant and Adjuvant Temozolomide for Glioblastoma. *N. Engl. J. Med.* **2005**, *352*, 987–996.
2. Woodworth, G. F.; Dunn, G. P.; Nance, E. A.; Hanes, J.; Brem, H. Emerging insights into barriers to effective brain tumor therapeutics. *Front. Oncol.* **2014**, *4*, 126.
3. Louis, D. N.; Perry, A.; Reifenberger, G.; Deimling, A. von; Figarella-Branger, D.; Cavenee, W. K.; Ohgaki, H.; Wiestler, O. D.; Kleihues, P.; Ellison, D. W. The 2016 World Health Organization Classification of Tumors of the Central Nervous System: a summary. *Acta Neuropathol. (Berl.)* **2016**, *131*, 803–820.
4. Hung, A. L.; Garzon-Muvdi, T.; Lim, M. Biomarkers and Immunotherapeutic Targets in Glioblastoma. *World Neurosurg.* **2017**, *102*, 494–506.
5. Cloughesy, T. F.; Cavenee, W. K.; Mischel, P. S. Glioblastoma: from molecular pathology to targeted treatment. *Annu. Rev. Pathol.* **2014**, *9*, 1–25.
6. Wadajkar, A. S.; Dancy, J. G.; Hersh, D. S.; Anastasiadis, P.; Tran, N. L.; Woodworth, G. F.; Winkles, J. A.; Kim, A. J. Tumor-targeted nanotherapeutics: overcoming treatment barriers for glioblastoma. *Wiley Interdiscip. Rev. Nanomed. Nanobiotechnol.* **2016**, 9(4).
7. Jacobi, N.; Seeboeck, R.; Hofmann, E.; Eger, A. ErbB Family Signalling: A Paradigm for Oncogene Addiction and Personalized Oncology. *Cancers* **2017**, *9*, 33.
8. Ciriello, G.; Miller, M. L.; Aksoy, B. A.; Senbabaoglu, Y.; Schultz, N.; Sander, C. Emerging landscape of oncogenic signatures across human cancers. *Nat. Genet.* **2013**, *45*, 1127–1133.
9. Yoon, S.; Rossi, J. J. Emerging cancer-specific therapeutic aptamers. *Curr. Opin. Oncol.* **2017**, *29*, 366–374.
10. Chen, M.; Yu, Y.; Jiang, F.; Zhou, J.; Li, Y.; Liang, C.; Dang, L.; Lu, A.; Zhang, G. Development of Cell-SELEX Technology and Its Application in Cancer Diagnosis and Therapy. *Int. J. Mol. Sci.* **2016**, *17*, 2079.
11. Ellington, A. D.; Szostak, J. W. In vitro selection of RNA molecules that bind specific ligands. *Nature* **1990**, *346*, 818–822.
12. Tuerk, C.; Gold, L. Systematic evolution of ligands by exponential enrichment: RNA ligands to bacteriophage T4 DNA polymerase. *Science* **1990**, *249*, 505–510.
13. Zhou, G.; Wilson, G.; Hebbard, L.; Duan, W.; Liddle, C.; George, J.; Qiao, L. Aptamers: A promising chemical antibody for cancer therapy. *Oncotarget* **2016**, *7*, 13446–13463.
14. Mercier, M.-C.; Dontenwill, M.; Choulier, L. Selection of Nucleic Acid Aptamers Targeting Tumor Cell-Surface Protein Biomarkers. *Cancers* **2017**, *9*.
15. Hynes, R. O. Integrins: Bidirectional, Allosteric Signaling Machines. *Cell* **2002**, *110*, 673–687.
16. Desgrosellier, J. S.; Cheresh, D. A. Integrins in cancer: biological implications and therapeutic opportunities. *Nat. Rev. Cancer* **2010**, *10*, 9–22.
17. Schaffner, F.; Ray, A. M.; Dontenwill, M. Integrin α5β1, the Fibronectin Receptor, as a Pertinent Therapeutic Target in Solid Tumors. *Cancers* **2013**, *5*, 27–47.
18. Janouskova, H.; Maglott, A.; Leger, D. Y.; Bossert, C.; Noulet, F.; Guerin, E.; Guenot, D.; Pinel, S.; Chastagner, P.; Plenat, F.; Entz-Werle, N.; Lehmann-Che, J.; Godet, J.; Martin, S.; Teisinger, J.; Dontenwill, M. Integrin α5β1 plays a critical role in resistance to temozolomide by interfering with the p53 pathway in high-grade glioma. *Cancer Res.* **2012**, *72*, 3463–3470.
19. Maglott, A.; Bartik, P.; Cosgun, S.; Klotz, P.; Rondé, P.; Fuhrmann, G.; Takeda, K.; Martin, S.; Dontenwill, M. The Small α5β1 Integrin Antagonist, SJ749, Reduces Proliferation and Clonogenicity of Human Astrocytoma Cells. *Cancer Res.* **2006**, *66*, 6002–6007.
20. Martin, S.; Cosset, E. C.; Terrand, J.; Maglott, A.; Takeda, K.; Dontenwill, M. Caveolin-1 regulates glioblastoma aggressiveness through the control of α5β1 integrin expression and modulates glioblastoma responsiveness to SJ749, an α5β1 integrin antagonist. *Biochim. Biophys. Acta BBA - Mol. Cell Res.* **2009**, *1793*, 354–367.

21. Freije, W. A.; Castro-Vargas, F. E.; Fang, Z.; Horvath, S.; Cloughesy, T.; Liau, L. M.; Mischel, P. S.; Nelson, S. F. Gene Expression Profiling of Gliomas Strongly Predicts Survival. *Cancer Res.* **2004**, *64*, 6503–6510.
22. Phillips, H. S.; Kharbanda, S.; Chen, R.; Forrest, W. F.; Soriano, R. H.; Wu, T. D.; Misra, A.; Nigro, J. M.; Colman, H.; Soroceanu, L.; Williams, P. M.; Modrusan, Z.; Feuerstein, B. G.; Aldape, K. Molecular subclasses of high-grade glioma predict prognosis, delineate a pattern of disease progression, and resemble stages in neurogenesis. *Cancer Cell* **2006**, *9*, 157–173.
23. Riemenschneider, M. J.; Mueller, W.; Betensky, R. A.; Mohapatra, G.; Louis, D. N. In Situ Analysis of Integrin and Growth Factor Receptor Signaling Pathways in Human Glioblastomas Suggests Overlapping Relationships with Focal Adhesion Kinase Activation. *Am. J. Pathol.* **2005**, *167*, 1379–1387.
24. Cosset, E. C.; Godet, J.; Entz-Werlé, N.; Guérin, E.; Guenot, D.; Froelich, S.; Bonnet, D.; Pinel, S.; Plenat, F.; Chastagner, P.; Dontenwill, M.; Martin, S. Involvement of the TGFβ pathway in the regulation of α5 β1 integrins by caveolin-1 in human glioblastoma. *Int. J. Cancer* **2012**, *131*, 601–611.
25. Coe, A. P.; Askari, J. A.; Kline, A. D.; Robinson, M. K.; Kirby, H.; Stephens, P. E.; Humphries, M. J. Generation of a minimal alpha5beta1 integrin-Fc fragment. *J. Biol. Chem.* **2001**, *276*, 35854–35866.
26. Schreiner, C. L.; Bauer, J. S.; Danilov, Y. N.; Hussein, S.; Sczekan, M. M.; Juliano, R. L. Isolation and characterization of Chinese hamster ovary cell variants deficient in the expression of fibronectin receptor. *J. Cell Biol.* **1989**, *109*, 3157–3167.
27. Da Rocha Gomes, S.; Miguel, J.; Azéma, L.; Eimer, S.; Ries, C.; Dausse, E.; Loiseau, H.; Allard, M.; Toulmé, J.-J. (99m)Tc-MAG3-aptamer for imaging human tumors associated with high level of matrix metalloprotease-9. *Bioconjug. Chem.* **2012**, *23*, 2192–2200.
28. Bauer, M.; Macdonald, J.; Henri, J.; Duan, W.; Shigdar, S. The Application of Aptamers for Immunohistochemistry. *Nucleic Acid Ther.* **2016**, *26*, 120–126.
29. Liu, Y.; Kuan, C.-T.; Mi, J.; Zhang, X.; Clary, B. M.; Bigner, D. D.; Sullenger, B. A. Aptamers selected against the unglycosylated EGFRvIII ectodomain and delivered intracellularly reduce membrane-bound EGFRvIII and induce apoptosis. *Biol. Chem.* **2009**, *390*.
30. Chauveau, F.; Aissouni, Y.; Hamm, J.; Boutin, H.; Libri, D.; Ducongé, F.; Tavitian, B. Binding of an aptamer to the N-terminal fragment of VCAM-1. *Bioorg. Med. Chem. Lett.* **2007**, *17*, 6119–6122.
31. Ohuchi, S. Cell-SELEX Technology. *BioResearch Open Access* **2012**, *1*, 265–272.
32. Blind, M.; Kolanus, W.; Famulok, M. Cytoplasmic RNA modulators of an inside-out signal-transduction cascade. *Proc. Natl. Acad. Sci. U. S. A.* **1999**, *96*, 3606–3610.
33. Mi, J.; Zhang, X.; Giangrande, P. H.; McNamara II, J. O.; Nimjee, S. M.; Sarraf-Yazdi, S.; Sullenger, B. A.; Clary, B. M. Targeted inhibition of αvβ3 integrin with an RNA aptamer impairs endothelial cell growth and survival. *Biochem. Biophys. Res. Commun.* **2005**, *338*, 956–963.
34. Ruckman, J.; Gold, L.; Stephens, A.; Janjic, N. Nucleic acid ligands to integrins. U.S. Patent 6,331,394, 18 December 2001
35. Gong, Q.; Wang, J.; Ahmad, K. M.; Csordas, A.; Zhou, J.; Nie, J.; Stewart, R.; Thomson, J. A.; Rossi, J. J.; Soh, H. T. Selection Strategy to Generate Aptamer Pairs that Bind to Distinct Sites on Protein Targets. *Anal. Chem.* **2012**, *84*, 5365–5371.
36. Takahashi, M.; Sakota, E.; Nakamura, Y. The efficient cell-SELEX strategy, Icell-SELEX, using isogenic cell lines for selection and counter-selection to generate RNA aptamers to cell surface proteins. *Biochimie* **2016**, *131*, 77–84.
37. Pestourie, C.; Cerchia, L.; Gombert, K.; Aissouni, Y.; Boulay, J.; Franciscis, V. D.; Libri, D.; Tavitian, B.; Ducongé, F. Comparison of Different Strategies to Select Aptamers Against a Transmembrane Protein Target. *Oligonucleotides* **2006**, *16*, 323–335.
38. Zhu, G.; Zhang, H.; Jacobson, O.; Wang, Z.; Chen, H.; Yang, X.; Niu, G.; Chen, X. Combinatorial Screening of DNA Aptamers for Molecular Imaging of HER2 in Cancer. *Bioconjug. Chem.* **2017**, *28*, 1068–1075.

39. Berg, K.; Lange, T.; Mittelberger, F.; Schumacher, U.; Hahn, U. Selection and Characterization of an α6β4 Integrin blocking DNA Aptamer. *Mol. Ther. Nucleic Acids* **2016**, *5*, e294.
40. Wilner, S. E.; Wengerter, B.; Maier, K.; de Lourdes Borba Magalhães, M.; Del Amo, D. S.; Pai, S.; Opazo, F.; Rizzoli, S. O.; Yan, A.; Levy, M. An RNA Alternative to Human Transferrin: A New Tool for Targeting Human Cells. *Mol. Ther. Nucleic Acids* **2012**, *1*, e21.
41. Boltz, A.; Piater, B.; Toleikis, L.; Guenther, R.; Kolmar, H.; Hock, B. Bi-specific Aptamers Mediating Tumor Cell Lysis. *J. Biol. Chem.* **2011**, *286*, 21896–21905.
42. Zamay, G. S.; Ivanchenko, T. I.; Zamay, T. N.; Grigorieva, V. L.; Glazyrin, Y. E.; Kolovskaya, O. S.; Garanzha, I. V.; Barinov, A. A.; Krat, A. V.; Mironov, G. G.; Gargaun, A.; Veprintsev, D. V.; Bekuzarov, S. S.; Kirichenko, A. K.; Zukov, R. A.; Petrova, M. M.; Modestov, A. A.; Berezovski, M. V.; Zamay, A. S. DNA Aptamers for the Characterization of Histological Structure of Lung Adenocarcinoma. *Mol. Ther. Nucleic Acids* **2017**, *6*, 150–162.
43. Pu, Y.; Liu, Z.; Lu, Y.; Yuan, P.; Liu, J.; Yu, B.; Wang, G.; Yang, C. J.; Liu, H.; Tan, W. Using DNA Aptamer Probe for Immunostaining of Cancer Frozen Tissues. *Anal. Chem.* **2015**, *87*, 1919–1924.
44. Zeng, Z.; Zhang, P.; Zhao, N.; Sheehan, A. M.; Tung, C.-H.; Chang, C.-C.; Zu, Y. Using oligonucleotide aptamer probes for immunostaining of formalin-fixed and paraffin-embedded tissues. *Mod. Pathol. Off. J. U. S. Can. Acad. Pathol. Inc* **2010**, *23*, 1553–1558.
45. Bukari, B. A.; Citartan, M.; Ch'ng, E. S.; Bilibana, M. P.; Rozhdestvensky, T.; Tang, T.-H. Aptahistochemistry in diagnostic pathology: technical scrutiny and feasibility. *Histochem. Cell Biol.* **2017**, *147*, 545–553.
46. Xiang, D.; Zheng, C.; Zhou, S.-F.; Qiao, S.; Tran, P. H.-L.; Pu, C.; Li, Y.; Kong, L.; Kouzani, A. Z.; Lin, J.; Liu, K.; Li, L.; Shigdar, S.; Duan, W. Superior Performance of Aptamer in Tumor Penetration over Antibody: Implication of Aptamer-Based Theranostics in Solid Tumors. *Theranostics* **2015**, *5*, 1083–1097.
47. Sun, H.; Tan, W.; Zu, Y. Aptamers: versatile molecular recognition probes for cancer detection. *The Analyst* **2016**, *141*, 403–415.
48. Hahn, U. Charomers-Interleukin-6 Receptor Specific Aptamers for Cellular Internalization and Targeted Drug Delivery. *Int. J. Mol. Sci.* **2017**, *18*.
49. Dausse, E.; Cazenave, C.; Rayner, B.; Toulmé, J.-J. In vitro selection procedures for identifying DNA and RNA aptamers targeted to nucleic acids and proteins. *Methods Mol. Biol. Clifton NJ* **2005**, *288*, 391–410.
50. Corpet, F. Multiple sequence alignment with hierarchical clustering. *Nucleic Acids Res.* **1988**, *16*, 10881–10890.
51. Zuker, M. Mfold web server for nucleic acid folding and hybridization prediction. *Nucleic Acids Res.* **2003**, *31*, 3406–3415.
52. Blandin, A.-F.; Noulet, F.; Renner, G.; Mercier, M.-C.; Choulier, L.; Vauchelles, R.; Ronde, P.; Carreiras, F.; Etienne-Selloum, N.; Vereb, G.; Lelong-Rebel, I.; Martin, S.; Dontenwill, M.; Lehmann, M. Glioma cell dispersion is driven by α5 integrin-mediated cell–matrix and cell–cell interactions. *Cancer Lett.* **2016**, *376*, 328–338.
53. Leuraud, P.; Taillandier, L.; Medioni, J.; Aguirre-Cruz, L.; Crinière, E.; Marie, Y.; Kujas, M.; Golmard, J.-L.; Duprez, A.; Delattre, J.-Y.; Sanson, M.; Poupon, M.-F. Distinct Responses of Xenografted Gliomas to Different Alkylating Agents Are Related to Histology and Genetic Alterations. *Cancer Res.* **2004**, *64*, 4648–4653.
54. Pinel, S.; Mriouah, J.; Vandamme, M.; Chateau, A.; Plénat, F.; Guérin, E.; Taillandier, L.; Bernier-Chastagner, V.; Merlin, J.-L.; Chastagner, P. Synergistic antitumor effect between gefitinib and fractionated irradiation in anaplastic oligodendrogliomas cannot be predicted by the Egfr signaling activity. *PloS One* **2013**, *8*, e68333.

FIGURE LEGENDS

Figure 1. SELEX strategy. **A.** Scheme of cell- and protein-based SELEX strategy used for aptamer selection. Briefly, one round of SELEX involves first a selection step: the nucleic acid library is incubated with a target (positive selection), which can be preceded by a counter selection to remove non-specific nucleic acid molecules. During the partitioning step, bound and unbound fractions are separated. The bound fraction is amplified to obtain an enriched pool for next round of selection. First, cell-SELEX processes were realized (rounds 1-7), followed by protein-SELEX (round 8-10) and then by cell-SELEX (rounds 11-18). The combination of cell- and protein-based SELEX is called hybrid-SELEX. At the end of the selection, nucleic acid molecules were cloned and sequenced. Individual sequences are aptamers. **B.** Description of cells used for counter- and positive-selections (rounds 1-7 and 11-18). On the right, western blots show the level of expression of α5 in the different cell lines used for the SELEX strategy. **C.** Description of proteins used for counter- and positive-selections (rounds 8-10). Counter-selection was also performed on protein-A sepharose beads alone in rounds 8-10. Below is shown a denaturing SDS polyacrylamide gel loaded with the protein A-purified recombinant α5β1-Fc protein and Coomassie blue stained.

Figure 2. Predicted secondary structure of aptamers H02, G11, H03, G10 and B03. Structures were predicted using the mfold web server [51]. Nucleotides 1−19 and 50−68 correspond to fixed flanks of the candidate sequences. They are shown in dark red. ΔG values are noted above structures.

Figure 3. Monitoring of the binding of five Cy5-labeled aptamers H02, G11, H03, G10 and B03 on CHO-B2 and U87MG cell lines, at 4°C, using confocal microscopy. Nuclei, counterstained with Hoechst are represented in royal blue. Aptamers, coupled to Cy5, are represented in white. **A.** Binding on CHO-B2 (left panel) and on CHO-B2 α5+ (right panel). **B.** Binding on U87MG α5- (left panel) and U87MG α5+ (right panel).

Figure 4. Monitoring of the binding of five Cy5-labeled aptamers H02, G11, H03, G10 and B03 on U87MG α5+ cells, at 37°C, using confocal microscopy. In the upper line section, in white, are represented anti-β1 antibody (Ab) and aptamer (Apt) labeling. In the lower line section, the merge figures in colors, show nucleus (in royal blue), anti-β1 antibody (in green) and aptamer (in red) labeling.
Antibody TS2/16 was used for β1 subunit labeling. Aptamers were labeled with Cy5. Nuclei were counterstained with Hoechst (royal blue).

Figure 5. A. Comparison of the binding profiles of aptamers H02 (left) and B03 (right) on CHO-B2 cells (grey lines) and CHO-B2 α5+ cells (black lines). Profiles without aptamer labeling is shown to the right. **B.** Determination of the equilibrium affinity parameter K_D for the interaction between U87MG α5+ cells and aptamers H02. Cy5-aptamer H02 at concentrations ranging from 0.15 to 5 μM was incubated with a constant amount of cells and analyzed by flow cytometry. **C.** Confocal microscopy analysis with aptamer H02 and the anti-α5 antibody IIA1 on U87MG α5+ cells at 4°C and 37°C. Aptamer is labeled with Cy5 (red). Incubation of antibody IIA1 was followed by incubation with a secondary antibody labeled with Alexa-546 (green). Nucleus are stained with Hoechst (blue). Arrows show zones of co-localization.

Figure 6. Aptafluorescence on GBM cells (**A & B**) and tissues (**C & D**). **A.** Western blot analysis. One representative western blot with the GBM cell lines (U87MG α5+, U87MG α5-, LN319, LN229, SF763, LN18, LNZ308, U373, LN443 and T98G) used in this study is represented at the top panel. Histograms, at the bottom, show the quantification of α5 integrin expression normalized to GAPDH levels (mean ± SEM of 3 independent experiments). GAPDH was used as a loading control. **B**. Immuno-quantification versus apta-quantification of fluorescence experiments on ten GBM cell lines. Immuno-quantification was realized with an anti- α5 antibody, followed with a secondary

antibody coupled to Alexa 647. Aptafluorescence was realized with Cy5-labeled aptamer H02. Quantifications were realized on at least 5 images / cell line. The correlation coefficient is 0.76 with P value < 0.0001. **C.** Immuno- (top panel) and apta-fluorescence (bottom panel) on patient-derived tumor xenografts TC7 and TC22 presenting high and low levels of α5 integrins, respectively. In immunofluorescence, detection of α5 (in red) was realized with antibody followed by a secondary antibody coupled to Alexa 647. In aptafluorescence, detection of α5 (in red) was realized with Cy5-labeled aptamers H02 and G11. DAPI staining is shown in blue. One representative image per condition is shown. **D**. Quantification of immino- (top panel) and apta- (bottom panel) fluorescence. Histograms show quantifications of 10-26 different images per condition. Statistical analyses were done with the Student's t-test with **** $p < 0.0001$ and **$p<0.003$.

FIGURES

Figure 1

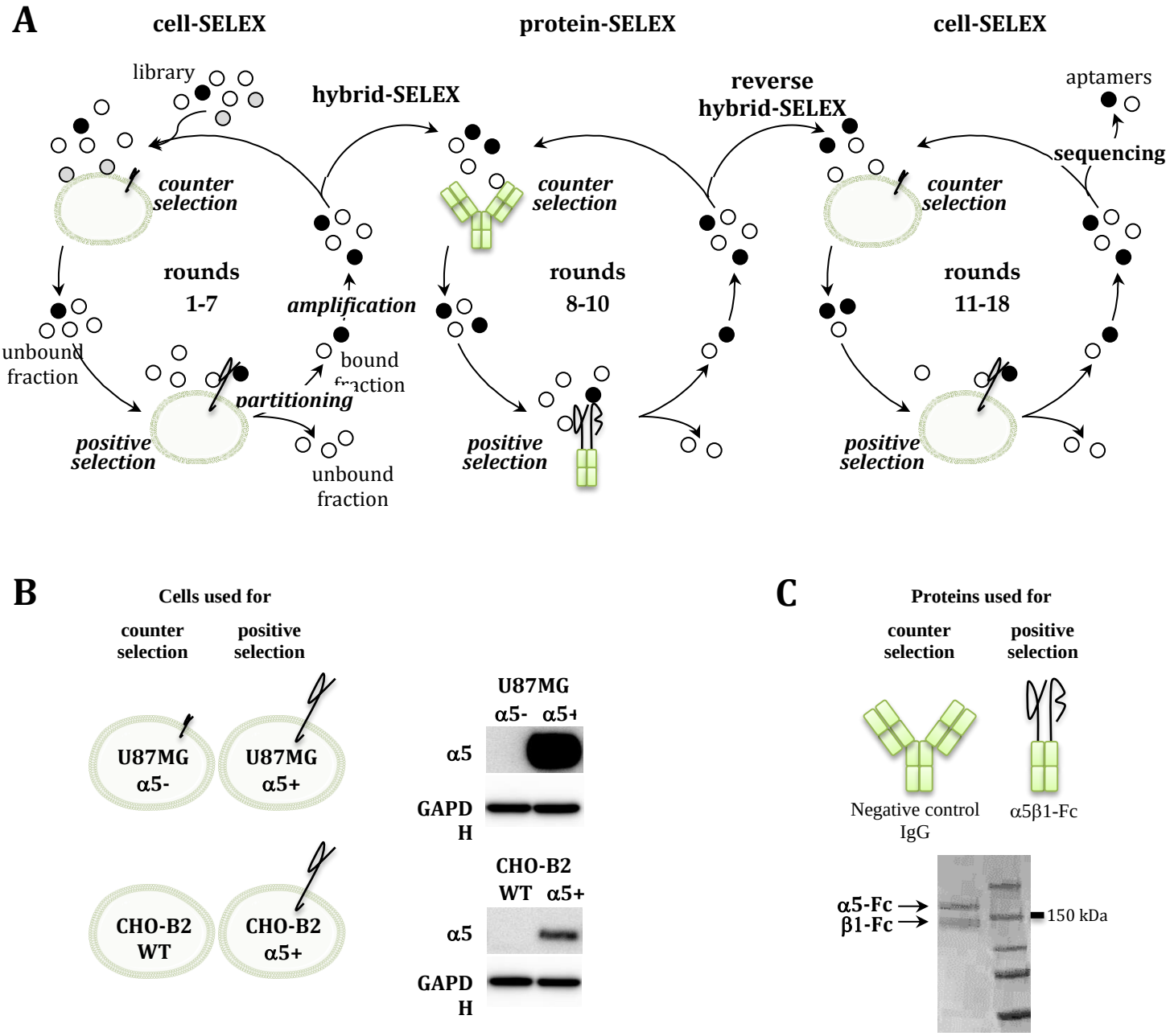

Figure 2

Remarque : L'aptamère H02 est actuellement en cours d'étude à la SATT Conectus en vue d'une éventuelle prématuration. Sa séquence est partiellement masquée dans ce manuscrit.

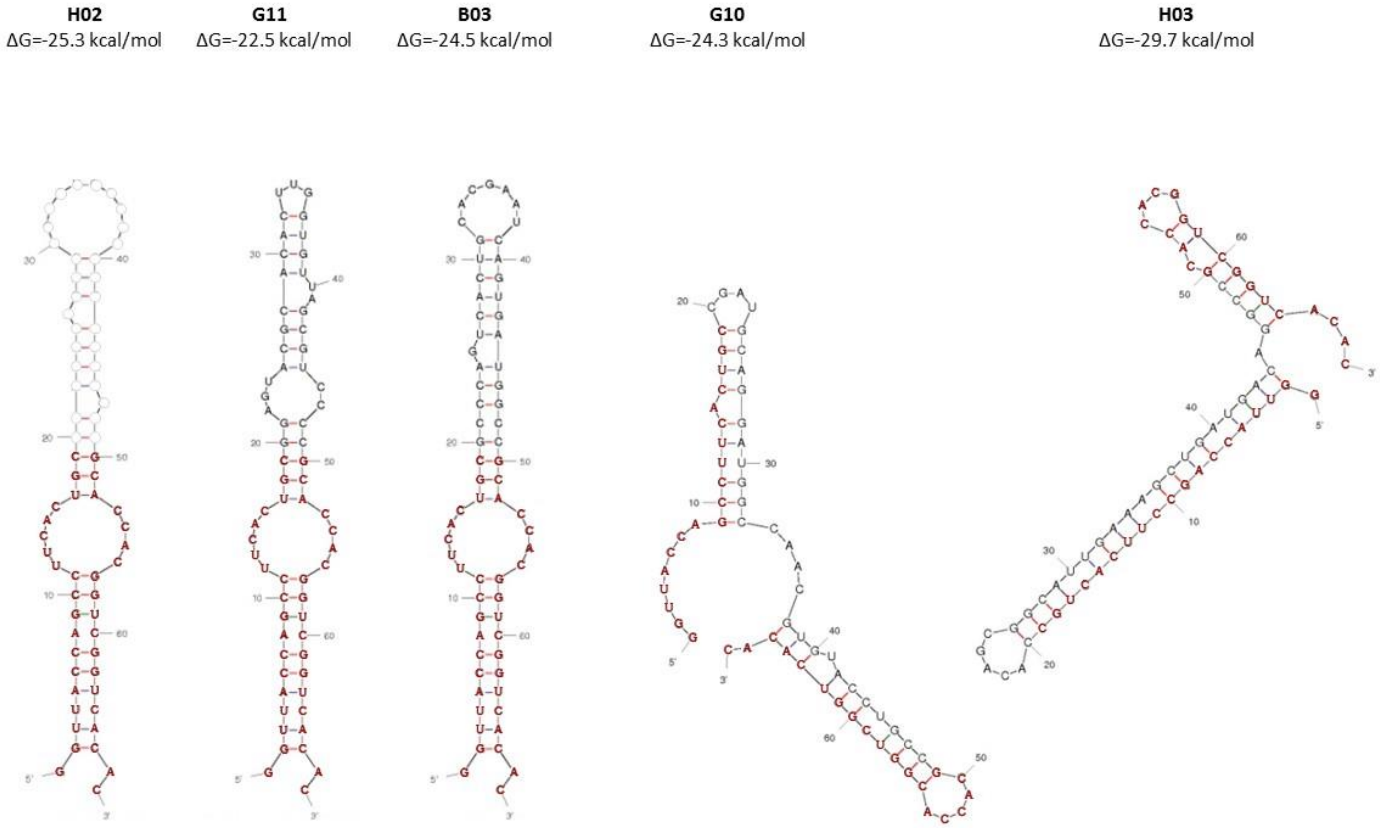

Figure 3

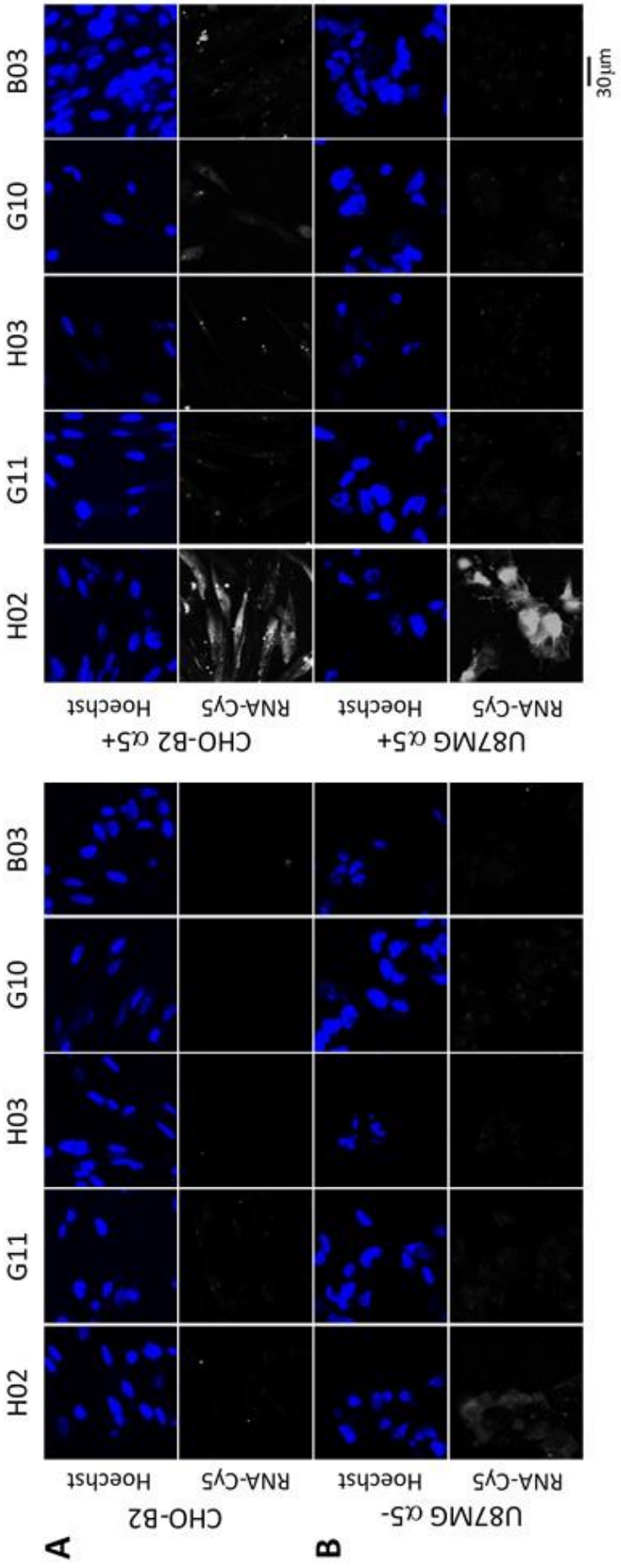
A
CHO-B2
RNA-Cy5
Hoechst
B
U87MG α5-
RNA-Cy5
Hoechst
CHO-B2 α5+
RNA-Cy5
Hoechst
U87MG α5+
RNA-Cy5
Hoechst
H02
G11
H03
G10
B03
30µm

Figure 4

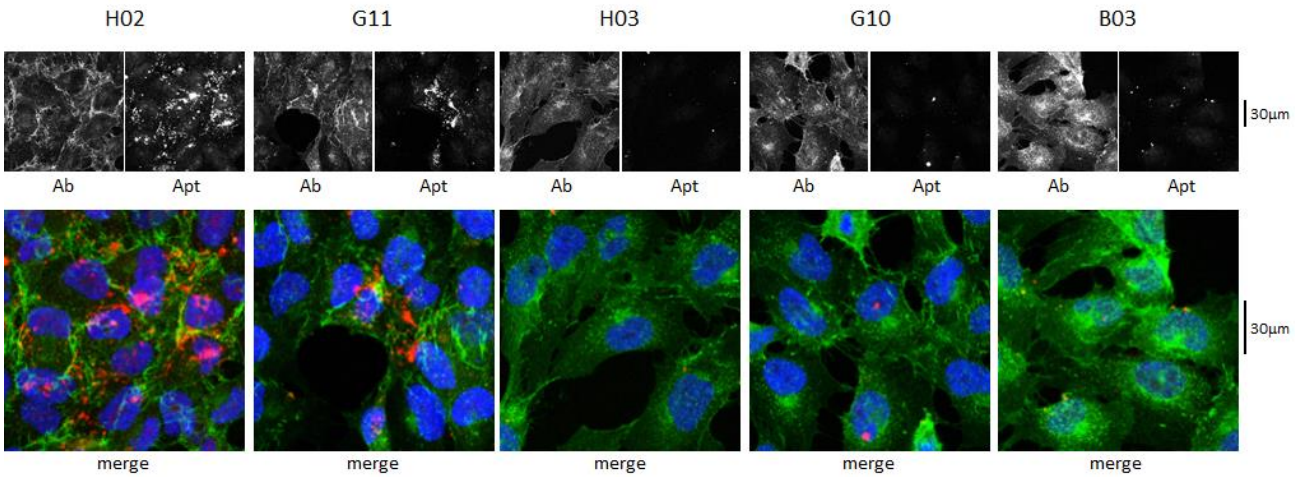
H02
G11
H03
G10
B03
30μm
Ab
Apt
Ab
Apt
Ab
Apt
Ab
Apt
Ab
Apt
30μm
merge
merge
merge
merge
merge

Figure 5

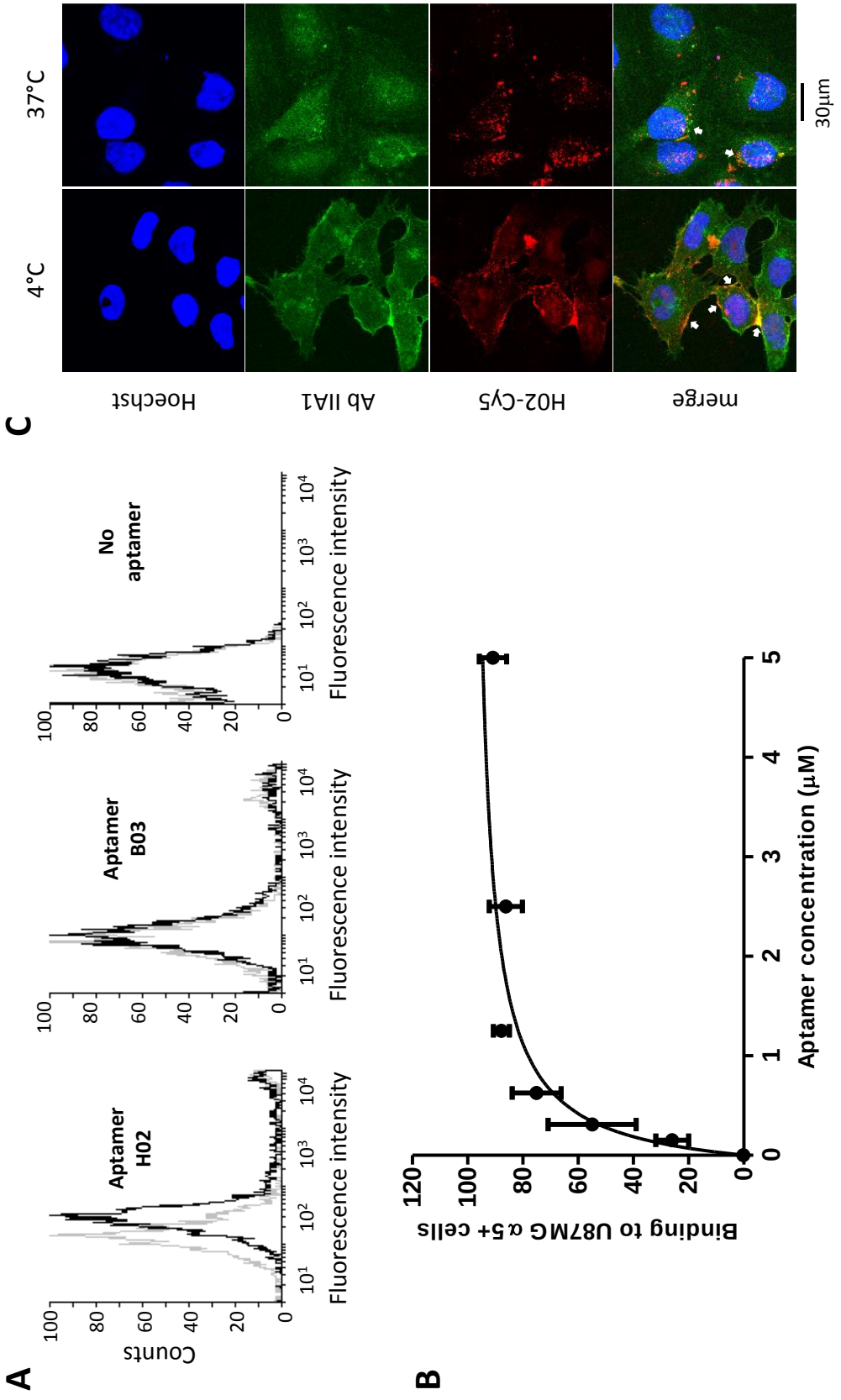
A
Counts
Aptamer H02
Aptamer B03
No aptamer
Fluorescence intensity
B
Binding to U87MG α5+ cells
Aptamer concentration (μM)
C
Hoechst
Ab IIA1
H02-Cy5
merge
4°C
37°C
30μm

Figure 6

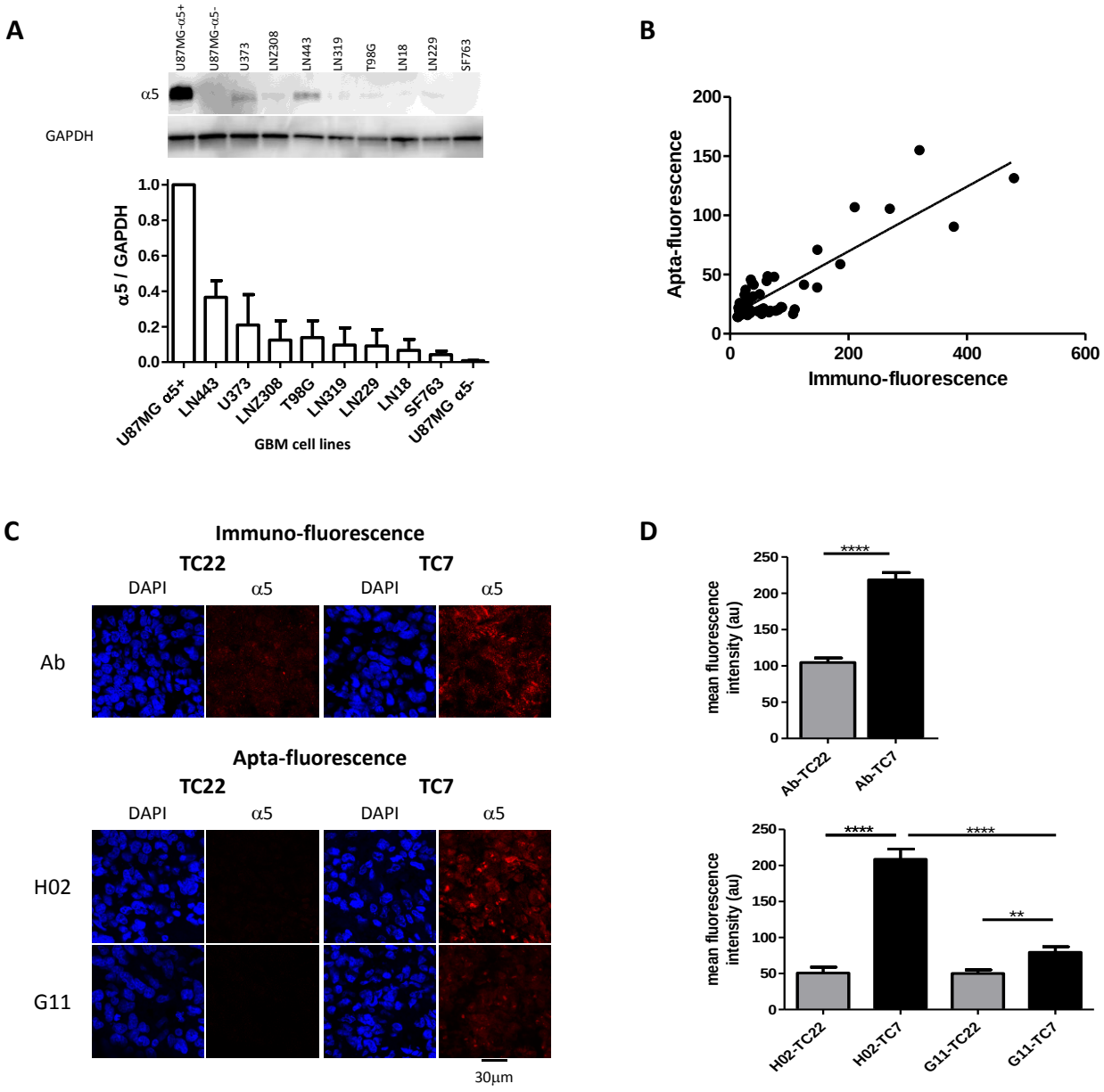
A
U87MG-α5+
U87MG-α5-
U373
LNZ308
LN443
LN319
T98G
LN18
LN229
SF763
α5
GAPDH
α5 / GAPDH
GBM cell lines
B
Apta-fluorescence
Immuno-fluorescence
C
Immuno-fluorescence
TC22
TC7
DAPI
α5
Ab
Apta-fluorescence
H02
G11
30µm
D
mean fluorescence intensity (au)
Ab-TC22
Ab-TC7
H02-TC22
H02-TC7
G11-TC22
G11-TC7

SUPPLEMENTARY DATA

Table S1. Selection conditions in SELEX process.

Rounds	Yeast tRNA (mg/ml)	Nb of washes (2-5 min/wash)	Counter-selection incubation time	Positive-selection incubation time
		cell-SELEX		
1	/	1	/	30 min
2	/	1	/	30 min
3	/	4	/	20 min
4	/	4	15 min	20 min
5	/	4	20 min	15 min
6	/	7	25 min	10 min
7	/	7	/	20 min
		protein-SELEX		
8	/	3	15 min[a]	20 min
9	/	3	15 min[b]	20 min
10	/	6	20 min[b]	20 min
		cell-SELEX		
11	/	9	/	25 min
12	/	6	13 min	30 min
13	/	8	3 min x 6 wells[c]	30 min
14	1	8	3 min x 6 wells[c]	30 min
15	1	8	3 min x 6 wells[c]	25 min
16	1	8	3 min x 6 wells[c]	17 min
17	1	10	3 min x 6 wells[c]	15 min
18	1	10	25 min	10 min

[a]Incubation on protein A-sepharose

[b]Incubation on protein A-sepharose, followed by incubation on Cetuximab

[c]The RNA pool was incubated for 3 minutes on 6 successive adherent cells containing wells

Table S2. Sequences of all primers, library, and aptamers described in this study. Fixed sequences of library and aptamers are written in dark red.

Name	Sequence
Primer P3'	5'-GTGTGACCGACCGTGGTGC-3'
Primer P5'	5'-TAATACGACTCACTATAGGTTACCAGCCTTCACTGC-3'
RNA library	5'-GGUUACCAGCCUUCACUGC-N_{30}-GCACCACGGUCGGUCACAC-3'
Aptamer H02	5'- GGUUACCAGCCUUCACUGC[redacted]GCACCACGGUCGGUCACAC-3'
Aptamer G11	5'- GGUUACCAGCCUUCACUGCGGAGUACGCACACUUGGUGUUAGCGUCCCCGCACCACGGUCGGUCACAC-3'
Aptamer H03	5'- GGUUACCAGCCUUCACUGCCACAGCGGCAUUGAAAGCUGAUGACAGGCCGCACCACGGUCGGUCACAC-3'
Aptamer B03	5'-GGUUACCAGCCUUCACUGCGCCCAGUCACUGCACGAAUCAGUGAUGGCCGCACCACGGUCGGUCACAC-3'
Aptamer G10	5'- GGUUACCAGCCUUCACUGCCGAUGCAGGAUGGCCAACGUGUACCUGCCGCACCACGGUCGGUCACAC-3'

Remarque : L'aptamère H02 est actuellement en cours d'étude à la SATT Conectus en vue d'une éventuelle prématuration. Sa séquence est partiellement masquée dans ce manuscrit.

Figure S1

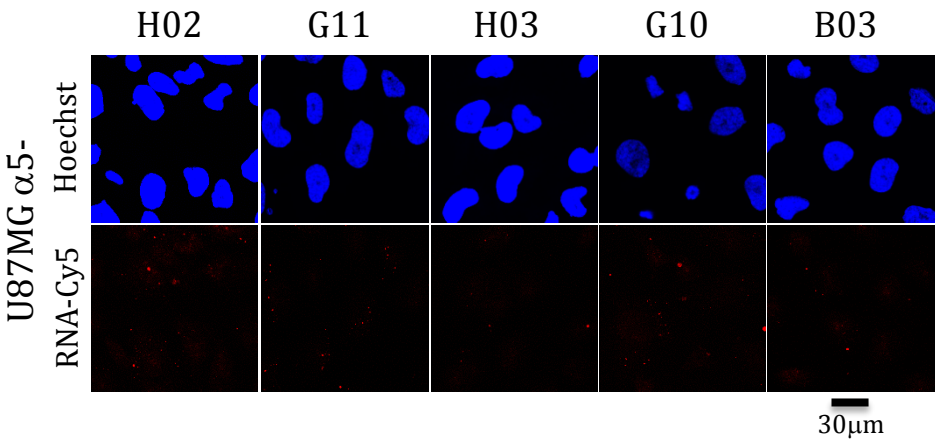

Figure S1. Monitoring of the binding of five Cy5-labeled aptamers H02, G11, H03, G10 and B03 on U87MG α5- cell, at 37°C, using confocal microscopy. Nuclei are colored in royal blue (upper line) and aptamers in red (lower line).

Figure S2

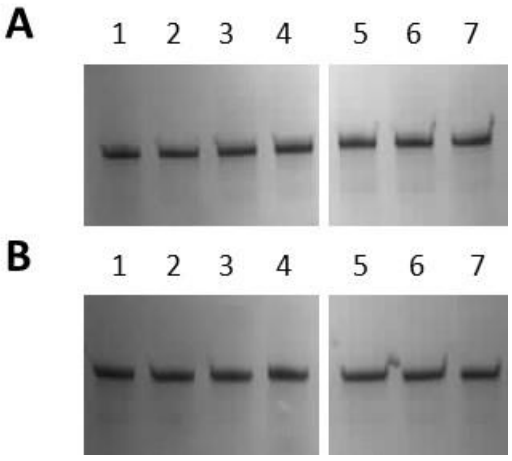

Figure S2. Stability of RNA aptamers during incubation with cells. Aptamer at 5 μM at **A.** 4°C and **B.** 37°C was incubated without cells (lanes 2-4) or with U87MG α5+ cells (lanes 5-7). Lane 1 corresponds to RNA at the beginning of the experiment (time 0). Incubation time: 15 min (Lanes 2 and 5), 30 min (lanes 3 and 6) and 45 min (lanes 4 and 7).

E. PERSPECTIVES

Les intégrines ont rarement été les cibles d'un SELEX. Outre le fait que les intégrines soient des protéines membranaires, elles sont hétéro-dimériques, ce qui complexifie la sélection d'aptamères. Seules trois intégrines cibles de SELEX ont été répertoriées dans la littérature à ce jour :

- β2 : Blind et al. (1999) ont sélectionné par protein-SELEX, des aptamères ARN contre un peptide de 46 mers correspondant au domaine cytoplasmique de la sous-unité β2 de l'intégrine αLβ2. L'aptamère, exprimé en grande quantité dans le cytoplasme de cellules infectées par le virus de la vaccine codant pour la sous-unité β2, induit une diminution d'adhésion cellulaire.
- αvβ3 a été la cible de deux protein-SELEX et d'un cell-SELEX. Un aptamère ARN, nommé Apt-αvβ3, ciblant l'intégrine αvβ3, sélectionné par un SELEX sur l'intégrine recombinante (Mi et al., 2005), se lie à la surface de cellules HUVECs et affecte la réponse cellulaire (diminution de la prolifération cellulaire, inhibition de l'adhésion, augmentation de l'apoptose par inhibition de la signalisation via FAK phosphorylée). Gong et al., (2012) ont sélectionné des aptamères ARN-2'fluoro par une technique nommée MAI-SELEX ('multivalent aptamer isolation-SELEX') permettant de séparer les aptamères ciblant αv de ceux ciblant β3. Takahashi et al (2016) ont utilisé une technique qu'ils ont nommée Icell-SELEX ('isogenic cell-SELEX') pour identifier des aptamères ARN sur des cellules HEK293 manipulées pour la contre-sélection et pour la selection positive par sous-expression et sur-expression respectivement de la sous-unité αv.
- α6β4, récepteur de la laminine, a été la cible d'un hybrid-SELEX (Berg et al., 2016). Cinq cycles de sélection ont été réalisés sur des cellules tumorales de prostate PC-3 (avec des étapes de contre sélection à partir du cycle 3, sur des cellules PC-3 déplétées en β4), complétés par 7 cycles sur la protéine recombinante. Les étapes de cell-SELEX seules n'ont pas été suffisantes pour enrichir les pools d'ARNs en candidats spécifiques. L'aptamère ADN simple brin sélectionné, IDA, a une affinité de 137 ± 22 nM pour les cellules PC-3, inhibe l'interaction α6β4-laminine et est internalisé dans ces cellules à 37°C.

Nous avons ciblé l'intégrine α5β1 et montré que des aptamères ARN ciblant des cellules exprimant l'intégrine, α5β1, ont été obtenus par un SELEX complexe alternant cell- et protein-SELEX.

Les perspectives de ce travail sont résumées sur le schéma suivant :

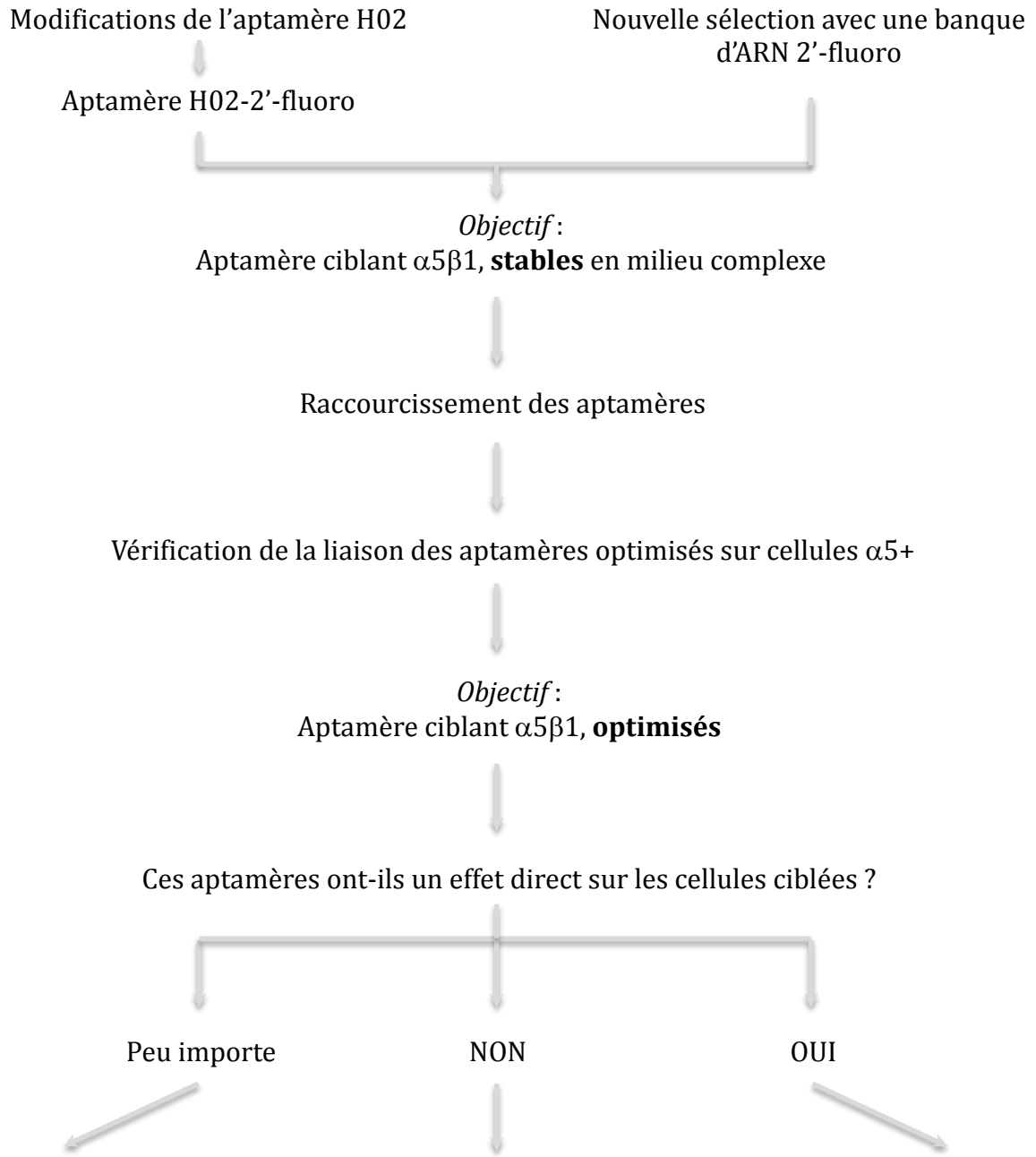
Modifications de l'aptamère H02
Nouvelle sélection avec une banque d'ARN 2'-fluoro
Aptamère H02-2'-fluoro
Objectif :
Aptamère ciblant α5β1, **stables** en milieu complexe
Raccourcissement des aptamères
Vérification de la liaison des aptamères optimisés sur cellules α5+
Objectif :
Aptamère ciblant α5β1, **optimisés**
Ces aptamères ont-ils un effet direct sur les cellules ciblées ?
Peu importe
NON
OUI
Intérêt diagnostique :
Aptamère =
Agent diagnostique
In vitro : Détection de cellules α5+ en histo-fluorescence
In vivo : Imagerie moléculaire
Intérêt thérapeutique:
Aptamère =
molécule d'adressage
Internalisation d'aptamères dans les cellules ciblées (cApt)
Intérêt thérapeutique:
Aptamère =
agent thérapeutique
Seul ou en association avec des agents chimiothérapeutiques

Aptamères ciblant l'intégrine α5β1, stables en milieu complexe

L'aptamère H02 a un fort potentiel en histochimie pour discriminer les tumeurs exprimant fortement l'intégrine des tumeurs l'exprimant peu. Cependant, l'aptamère H02 est un aptamère ARN non modifié. Bien que nous ayons vérifié que l'aptamère ne se dégrade pas au contact des cellules en une heure, il est évident que des ARNs non-modifiés ne pourront pas être utilisés pour des expériences cellulaires plus longues et encore moins en diagnostic ou thérapie. L'aptamère H02 serait très peu stable en milieu complexe et devrait faire l'objet de précautions lors de sa manipulation.

Pour des applications thérapeutiques, les aptamères ciblant l'intégrine α5β1 doivent être résistants en milieu complexe. Nous proposons deux stratégies parallèles :

Modification de l'aptamère H02 en 2'-fluoro

La première consiste à modifier l'aptamère H02 pour le rendre résistant à l'hydrolyse alcaline et à l'action des ribonucléases. Plusieurs types de modifications post-SELEX sont possibles. La *Figure 9* (Chapître A consacré aux aptamères) montre tous les sites possibles de modification de l'ARN. Les modifications internes des cytosines et uridines ont l'effet bénéfique le plus important pour stabiliser un ARN dans un sérum. Le remplacement du groupement 2'-hydroxyl des ribopyrimidines avec des groupements 2'-amino, 2'-fluoro ou 2'-O-méthyl augmente la stabilité dans le sérum des molécules d'ARN. Un aptamère d'ARN naturel a un temps de demi-vie dans le sérum estimé à 10 sec. Ce temps de demi-vie est augmenté à 170 h et 90 h, si les pyrimidines sont substitutées en 2'-amino et 2'-fluoro, respectivement (Wilson 2007).

Les aptamères substitués en 2'-fluoro ont été décrits comme ayant une meilleure affinité pour leurs cibles protéiques que les aptamères subtitués en 2'-amino (Wilson 2007). Pour stabiliser l'aptamère H02, nous commencerons par modifier ses pyrimidines en 2'-fluoro (*Figure 24*).

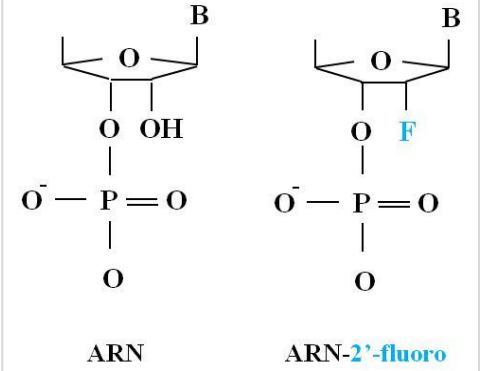

Figure 24. **ARN non modifié et ARN-2'-fluoro (2'F)**

Nouvelle sélection d'aptamères ARN-2'F ciblant α5β1 par cell-SELEX

Pour augmenter nos chances de trouver des aptamères anti-α5β1 de bonne affinité et sélectivité pour l'intégrine α5β1, nous avons commencé un nouveau SELEX. Il s'agit d'un cell-SELEX réalisé, sur cellules CHO-B2 α5+, les étapes de sélection négative étant réalisées sur les cellules CHO-B2. Les modifications en 2'-fluoro (2'F) et 2'-amino sont deux modifications augmentant la stabilité des ARN qui peuvent être introduites lors des étapes de SELEX. La T7 ARN polymérase naturelle peut catalyser

la synthèse de transcrits modifiés en 2'-fluoro et 2'-amino, mais avec un rendement faible. Ce rendement est significativement augmenté par l'utilisation d'une T7 ARN polymérase mutée en $Y_{639}F$ (Padilla et Sousa., 1999). La banque de départ et les pools d'ARN utilisés pour ce nouveau SELEX sont modifiés en 2'-fluoro. Les aptamères identifiés à l'issue du SELEX seront donc déjà résistants en milieu complexe, rendant ainsi obsolète certaines modifications post-SELEX. En effet, le changement complet de structure *a posteriori* d'un aptamère sélectionné sous forme ARN et même ADN conduit généralement à une diminution, voire à une perte des propriétés pour lesquelles il a été sélectionné, notamment des propriétés de liaison à sa cible.

Actuellement, 11 cycles de sélection ont déjà été réalisés (*Tableau 4*).

	Negative selection	Positive selection				
Cycles	CHOB2	CHOB2 a5+	Addition of BSA	Addition of tRNA	Temperature of selection	Number of washes - [NaCl]
1	30 ' - P100	30 ' - P100	No	No	4°C	1x5' - 136mM
2	30 ' - P100	30 ' - P100	Yes	No	4°C	1x5' - 136mM
3	30 ' - P100	30 ' - P100	Yes	No	4°C	4x5' - 136mM
4	30 ' - P100	30 ' - P100	Yes	Yes	4°C	4x5' - 136mM
5	30 ' - P60	30 ' - P60	Yes	Yes	4°C	4x5' - 136mM
6	30 ' - P100	30 ' - P60	Yes	Yes	4°C	4x5' - 200mM
7	30 ' - P100	30 ' - P60	Yes	Yes	4°C	7x5' - 250mM
8	30 ' - P100	15 ' - P60	Yes	Yes	4°C	7x5' - 250mM
9	30 ' - P100	10 ' - P60	Yes	Yes	4°C	7x5' - 250mM
10	15 ' - P100	30 ' - P60	Yes	Yes	37°C	3x5' - 500mM
11	15 ' - P100	30 ' - P60	Yes	Yes	37°C	7x5' - 500mM

Tableau 4. **Conditions expérimentales des cycles du cell-SELEX 2'-fluoro**. En vert sont indiqués les changements intervenus d'un cycle à l'autre.

La banque ADN simple-brin de départ est la même que celle utilisée pour le SELEX précédent, les primers également. Les étapes de RT, PCR, transcription sont similaires à celles décrites par Da Rocha Gomes et al. (2012). La quantité d'ARN-2'F mise en contact avec les cellules est constante (1 nmole). Le tampon de sélection est le tampon PBS ('phosphate buffered saline'), supplémenté avec 2 mM de $MgCl_2$. Au cours des cycles de sélection, la stringence est augmentée en ajoutant au tampon de sélection de la BSA ('bovine serum albumine', 1 mg/ml) et/ou de l'ARNt compétiteur (10 fois plus que d'ARN 2'-fluoro), en augmentant le nombre de lavages et la concentration saline du tampon de lavage, en diminuant la taille des boîtes de culture dans lesquelles est réalisée la sélection (P100 ou P60). La température de sélection a également changé au cours des cycles. Ce changement est expliqué dans le paragraphe consacré à l'internalisation des aptamères. L'analyse des séquences en fin de SELEX sera probablement réalisée par NGS ('next generation sequencing'). Puis, l'identification des

aptamères 2'-fluoro sera réalisée comme cela a déjà été décrit précédemment pour l'aptamère H02 (chapître D).

Optimisation des aptamères

A court terme, les aptamères (H02, H02-2'-fluoro ou les nouveaux aptamères qui seront sélectionnés à l'issue du cell-SELEX en utilisant une banque d'ARN 2'-fluoro) ciblant l'intégrine α5β1 seront optimisés dans l'objectif de déterminer leur séquence minimale d'interaction par raccourcissement progressif des extrémités 3' et 5'. Etant donné que la conformation et donc la fonction de liaison des oligonucléotides est extrêmement dépendante de la taille et de la nature chimique de l'acide nucléique, nous vérifierons que les modifications n'auront que peu altéré la capacité de liaison des aptamères. Nous caractériserons notamment l'interaction entre les aptamères et les cellules U87MG α5+, CHO-B2 α5+. Nous pourrons avoir accès aux cinétiques d'association et de dissociation d'aptamères fluorescents sur les cellules adhérentes, vivantes, grâce à un appareil de mesure d'interactions moléculaires nommé LigandTracer® (Ridgeview instruments, Uppsala, Suède, Björke & Andersson. 2006a, 2006b ; Renaud et al., 2016), développé par Karl Andersson un collaborateur de longue date, et récemment acquis par l'UMR 7199 (Laboratoire de Conception et Application de Molécules Bioactives, Illkirch). Les données cinétiques à l'équilibre seront comparées à celles obtenues par des techniques plus classiques de gel-retard (collaboration Pierre Fechter, UMR7242, équipe Membrane bactérienne et transport', Illkirch).

Caractérisations fonctionnelles des aptamères sur cellules tumorales in vitro

L'effet direct des aptamères ciblant α5β1 sera mesuré sur cellules par des tests fonctionnels *in vitro*. L'expertise pour l'évaluation des caractéristiques de ligands d'intégrines est largement disponible au sein de notre équipe et des plateformes PCBIS (Pascal Villa, IREBS UMS 3286, Illkirch) et de criblage à haut débit HTSF (Laurent Brino, IGBMC, Illkirch). Les tests, qui ont déjà fait leur preuve pour évaluer les effets fonctionnels d'antagonistes et d'anticorps bloquants de l'intégrine α5β1, seront utilisés pour caractériser les effets fonctionnels potentiels des aptamères *in vitro*, sur cellules tumorales. Il s'agit de tests : (i) d'adhérence cellulaire sur fibronectine/vitronectine/collagène (pour vérifier la spécificité de l'aptamère), (ii) de potentiel invasif (migration sur cellules isolées et migration collective, d'invasion en chambre de Boyden, 'blessure/cicatrisation'), (iii) de croissance de cellules (prolifération/clonogénicité), et (iv) de sensibilisation à la chimiothérapie, mesure de l'apoptose. Ainsi, nous vérifierons l'impact des aptamères sur les cellules.

Diagnostic

Le GBM est la tumeur cérébrale la plus fréquente. Or les approches thérapeutiques actuelles ne permettent que trop peu d'augmenter l'espérance de vie des patients. Le développement de nouvelles approches diagnostiques et thérapeutiques est nécessaire. Des aptamères spécifiques de GBM ont été développés. Ils restent encore peu nombreux mais devraient gagner en importance dans les prochaines années, pour le diagnostic *ex vivo*, mais aussi en imagerie biomédicale et thérapie (Delac et al., 2015). Ils sont répertoriés dans le *Tableau 3* (chapître B).

Diagnostic : détection de l'intégrine α5β1 en histochimie

L'aptahistochimie émerge depuis peu en tant que nouveau concept pour le diagnostic et/ou le pronostic en cancérologie (Bauer et al., 2016 ; Bukari et al., 2017 ; Simmons et al., 2012 ; Sun et al., 2016). C'est une méthode d'histochimie basée sur une détection par des aptamères, molécules comparables aux anticorps en terme d'affinité et de sélectivité pour leurs cibles, mais possèdant des avantages par rapport à leur alter ego protéique : ils sont stables, synthétisés chimiquement, et surtout facilement modifiables. Pour le diagnostic par histochimie, généralement un fluorophore est directement couplé à l'aptamère, souvent à l'une de ses extrémités terminales. L'aptamère fluorescent reconnaît ainsi sa cible en une seule étape. L'aptahistochimie est donc plus rapide que l'immunohistochimie et permet d'éviter les réactions croisées dues aux anticorps secondaires. Dans un futur proche, il n'est pas illusoire d'utiliser des aptamères en routine en tant qu'outils diagnostiques *ex vivo*.

Testé de manière préliminaire en aptahistochimie sur des coupes de deux xénogreffes de GBM humains, l'aptamère H02 couplé à un fluorophore se révèle intéressant pour caractériser les tissus tumoraux de GBM exprimant l'intégrine α5β1 (chapître D). L'aptahistochimie est très prometteuse mais n'en est encore à ses prémices. Notre objectif vise à l'étudier à plus grande échelle sur plusieurs cohortes de patients ce qui n'a encore jamais été réalisé. La détection de l'intégrine α5β1 sur 96 coupes paraffinées de GBM, issues de la tumorothèque du CHU d'Amiens (collaboration avec Pr. Bruno Chauffert), a d'ores et déjà été réalisée en immunohistochimie au laboratoire. Les résultats montrent une hétérogénéité inter- et intra-tumorale (publication en cours d'écriture). Nous testerons par aptafluorescence une trentaine de ces coupes exprimant des niveaux variables de l'intégrine. Cette cohorte nous servira à comparer apta- et immuno-histochimie. Nous utiliserons une autre cohorte, issue de la tumorothèque du CHU de Strasbourg, pour comparer des tumeurs conditionnées en paraffine et des tumeurs congelées provenant d'un même patient. Nous vérifierons ainsi si le conditionnement de la tumeur pourrait avoir une influence sur la technique de l'aptahistochimie. La sélection des coupes

se fera d'après les données qui ont déjà été publiées par notre équipe, sur le niveau d'expression des ARNm de l'intégrine α5 (Cosset et al., 2012).

Les aptamères H02, H02-2'F et/ou les aptamères qui seront identifiés par le nouveau cell-SELEX devraient permettre de différencier les tumeurs présentant des niveaux variables d'expression en intégrine (hétérogénéité inter-tumorale), et pourraient également permettre de détecter l'hétérogénéité intratumorale au sein d'une même tumeur. Ce projet a fait l'objet d'une demande de financement au Cancéropôle Est (projet Emergence, soumis fin mars 2018). Les expériences d'apta-histochimie seront également réalisées sur des coupes de xénogreffes de lignées cellulaires d'autres tumeurs (VADS, gliomes pédiatriques).

Diagnostic *in vivo* : imagerie moléculaire

Les techniques d'imagerie pour le diagnostic se développent sans cesse. Les études utilisant les aptamères comme sondes d'imagerie sont nombreuses (par exemple : Varmira et al., 2014 ; Hicke et al., 2006 ; Da Rocha Gomes et al., 2010, 2012 ; Martinez et al., 2014 ; Sun et al., 2016 ; Kryza et al., 2016). En ce qui concerne les GBM, elles ont été répertoriées en 2015 (Delac et al., 2015).

A plus long terme, si les aptamères ciblant α5β1 se révèlent être des ligands performants pour marquer l'intégrine *in vivo*, couplés à des sondes fluorescentes ou radioactives, ils pourraient servir d'agents d'imagerie non invasive par exemple pour visualiser les bords d'une tumeur cérébrale, *in vivo*, pour effectuer un suivi de la progression tumorale lors d'expériences d'imagerie préclinique *in vivo* chez la souris dans les modèles de xénogreffes orthotopiques de tumeurs, en collaboration avec David Brasse (plateforme d'imagerie de l'IPHC, Strasbourg). Si ce modèle de suivi d'évolution de tumeurs s'avérait concluant, il pourrait être utilisé à l'avenir pour tester *in vivo* sur modèle murin, le potentiel anti-tumoral de nouvelles molécules dans le traitement des GBM.

Internalisation d'aptamères dans les cellules ciblées

Même dépourvus d'effets directs (de type agonistes ou antagonistes) sur les cellules ciblées, les aptamères possèdent un fort potentiel thérapeutique *in vivo*, comme molécules d'adressage lorsqu'ils ciblent un récepteur cellulaire et sont associés à une molécule active dont ils assurent la vectorisation vers sa cible (*Figure 25*).

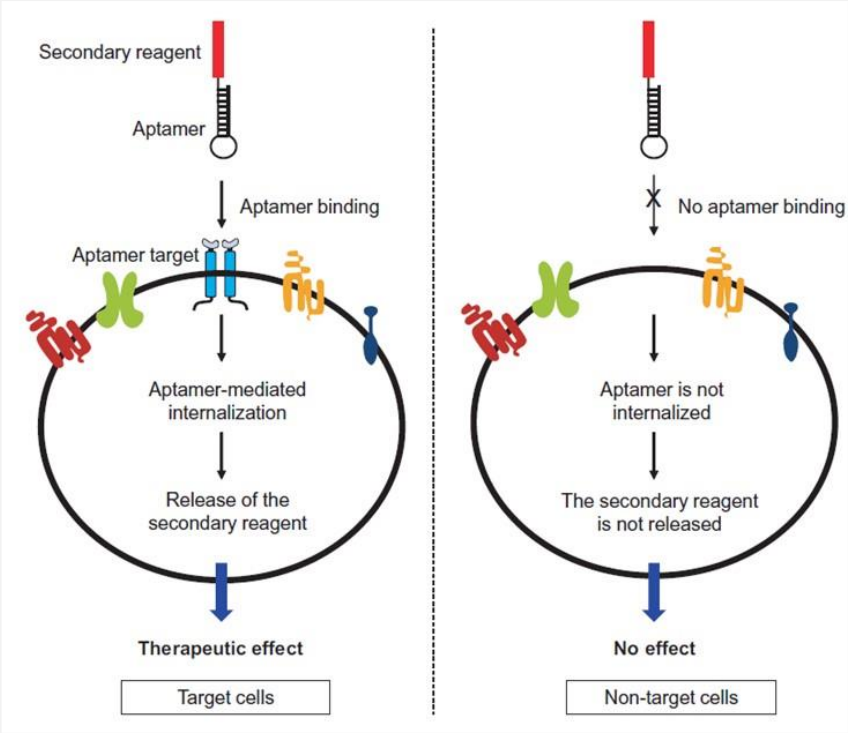

Figure 25. **Délivrance ciblée d'agents thérapeutiques par des aptamères** (Esposito et al., 2014). Les aptamères peuvent être utilisés pour délivrer un agent thérapeutique (ici nommé 'secondary reagent') spécifiquement aux cellules ciblées qui expriment la cible de l'aptamère à leur surface (à gauche). Seules les cellules qui expriment cette cible seront exposées à l'agent, alors que les cellules qui ne l'expriment pas ne seront pas affectées (à droite).

Les aptamères sont une alternative aux anticorps en tant que molécules d'adressage en oncologie (Xiang et al., 2015a). Les aptamères ciblant un récepteur membranaire peuvent être internalisés, et s'ils sont couplés à un agent thérapeutique, ils peuvent servir de véhicule pour délivrer l'agent thérapeutique à l'intérieur des cellules ciblées (Gopinath et al., 2016). Les aptamères internalisés peuvent ainsi délivrer des agents cytotoxiques, des siRNA, des nanoparticules… au sein des cellules qu'ils ciblent spécifiquement. Ces aptamères ont récemment été nommés 'charomères' par Uhlrich Hahn (Hahn, 2017) en référence à Charon, passeur de la mythologie grecque qui transportait les morts en barque vers l'enfer. Aucun charomère n'est encore en développement clinique.

Quel est le cheminement intra-cellulaire des aptamères ? Cette question se pose depuis peu pour les aptamères (Tawiah et al., 2017). Pour atteindre le cytosol, le tandem aptamère-agent doit s'échapper des endosomes. Or, cette étape clé est peu documentée.

Pour étudier le trafic intracellulaire des aptamères, nous utiliserons les aptamères ciblant l'intégrine α5β1 décrits dans ce manuscrit et/ou ceux en cours de sélection. Les mécanismes de l'endocytose et du recyclage des intégrines sont décrits (Paul et al. 2015 ; de Franceschi et al., 2015).

Les intégrines sont des récepteurs de choix pour étudier l'endocytose, le passage vers le cytosol et plus généralement le devenir des aptamères à l'intérieur des cellules ciblées.

Nous proposons les pistes décrites ci-dessous pour essayer de comprendre le trafic intracellulaire des complexes aptamères-récepteurs et la délivrance des aptamères dans le cytosol. Ce projet visant à caractériser le trafic intracellulaire des complexes aptamères-récepteurs et la délivrance des aptamères dans le cytosol, devrait permettre, à terme, d'améliorer le développement d'aptamères thérapeutiques.

Sélection d'aptamères cytosoliques (cApt)

Un procédé de cell-SELEX particulier, réalisé à 37°C, nommé 'cell-SELEX internalisant' permet de ne récupérer que les aptamères internalisés. Les séquences qui ne se lient pas et celles qui ne sont pas internalisées sont exclues par lavages à forte stringence et/ou par l'addition de nucléases (Thiel et al., 2012 ; Wilner et al., 2012 ; Magalhães et al., 2012). Toutefois, toutes les séquences internalisées n'atteignent pas le cytosol des cellules ciblées. L'efficacité de passage des aptamères des endosomes vers le cytosol a été estimée inférieure à 0,01 % (Tawiah et al., 2017). La plupart des aptamères internalisés restent emprisonnés à l'intérieur des compartiments intracellulaires, puis sont dégradés ou sont recyclés à la membrane externe (*Figure 26*).

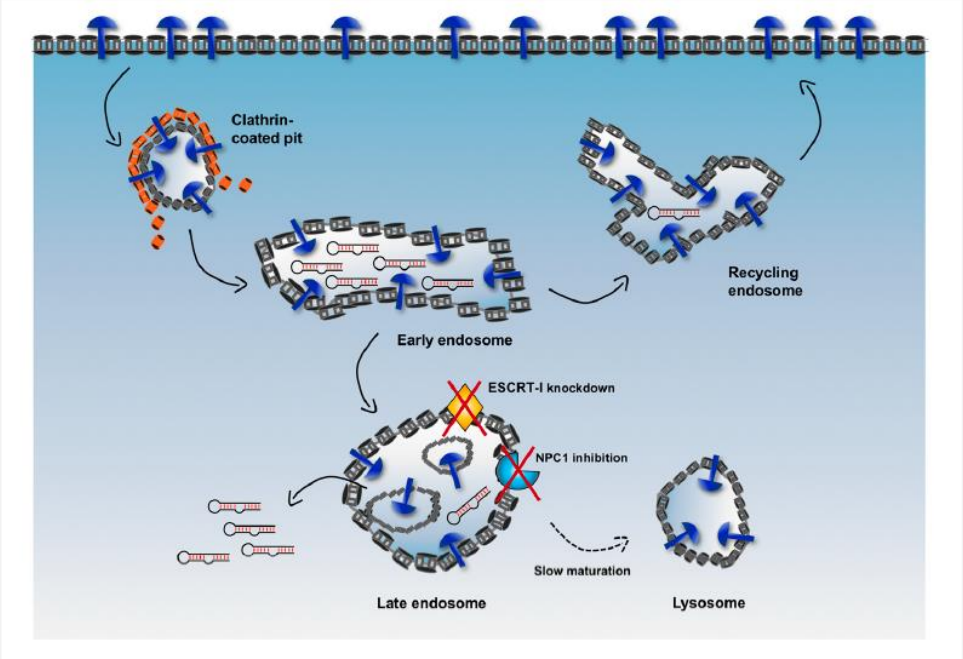

Figure 26. **Illustration du trafic présumé des aptamères internalisés** (Tawiah et al., 2017). Les aptamères entrent dans la cellule par endocytose médié par les clathrines ou par les cavéolines, puis sont transportés aux endosomes. Dans ce compartiment, les aptamères pourraient se dissocier du récepteur qu'ils ciblent. Certains récepteurs peuvent être recyclés à la surface cellulaire, d'autres sont dirigés vers le lysosome pour dégradation. Les aptamères internalisés pourraient suivre les mêmes voies. Certaines stratégies visent à retarder la maturation des endosomes (par ciblage de protéines associées aux endosomes telles que ESCRT-I et NPC1) et donc à augmenter le temps de résidence des molécules internalisées, ce qui permettrait d'augmenter le pourcentage d'aptamères s'échappant des endosomes.

Notre objectif est de développer une méthode SELEX innovante pour identifier des aptamères ayant la double capacité d'interagir spécifiquement avec les récepteurs ciblés et d'accéder au cytosol. Ces aptamères seront nommés cApt pour 'cytosolic aptamers'.

Sur l'intégrine α5β1, les premiers cycles de cell-SELEX ont déjà été réalisés. Il s'agit du cell-SELEX sur cellules CHO-B2 α5+ décrit ci-dessus dans le paragraphe sur la sélection d'aptamères substitués en 2'-fluoro (*Tableau 4*). Onze cycles de sélection ont été réalisés à 4°C. A cette température, les aptamères ne sont pas internalisés, puisque dans un premier temps, nous souhaitions diriger la sélection vers l'intégrine α5β1, cible extracellulaire. Dans un deuxième temps (actuellement), nous réalisons des cycles classiques de cell-SELEX internalisant, à 37°C, avec des lavages de plus en plus nombreux à forte concentration saline pour exclure les aptamères non internalisés. L'originalité de notre sélection vient dans un troisième temps : les pools d'ARNs enrichis à l'issue des étapes de cell-SELEX internalisant, seront couplés à des sondes ratiométriques fluorescentes sensibles au pH. Ces sondes émettront un signal différent en fonction de la localisation intracellulaire des aptamères car le pH varie dans les compartiments cellulaires (pH 7,4 dans le cytosol ; pH 5,9-6 dans les endosomes précoces ; pH 5-6 dans les endosomes tardifs ; pH 4-5 dans les lysosomes ; pH 6,4-6,5 dans les endosomes de recyclage). Ces sondes seront spécialement crées pour ce projet par Mayeul Collot (UMR 7021, équipe Nanochimie et nanoimagerie, Illkirch), sur la base des sondes commerciales SNARF. Mais ces dernières ne sont pas assez brillantes et n'ont pas les longueurs d'ondes d'excitation et d'émission adaptées à notre projet. En pratique, les nouvelles sondes fluorescentes seront covalemment couplées à une séquence ADN de 15-mers, qui elle-même s'appariera à une séquence ajoutée aux acides nucléiques du pool d'ARN 2'-fluoro. Lors des étapes de sélection, les cellules qui émettront un signal correspondant à la présence d'aptamères dans le cytosol, seront séparées par cytométrie en flux, et la fraction cytosolique sera récupérée pour amplification. Ce nouveau pool sera utilisé pour le cycle de sélection suivant.

A l'issue de ce nouveau procédé de SELEX, nous espérons identifier plusieurs cApt spécifiques de l'intégrine α5β1, localisés dans le cytosol après internalisation.

Propriétés physico-chimiques des interactions aptamères-récepteurs

Pour entrer dans le cytosol, les aptamères doivent s'échapper des endosomes avant d'entrer dans les lysosomes. La délivrance des aptamères au cytosol doit être influencée par la force d'interaction du complexe aptamère-récepteur, force qui varie probablement avec le pH, facteur qui, lui-même varie dans les différents compartiments cellulaires. De plus, la charge de certains acides aminés, tels l'acide aspartique, l'histidine… et la protonation des nucléotides, dépendent du pH. Les interactions moléculaires aptamères-récepteurs seront dont caractérisées dans différents pH mimant les

compartiments sub-cellulaires, par différentes méthodes, telles que EMSA (ElectroMobility Shift Assay), empreintes chimiques ou enzymatiques (pour déterminer les nucléotides impliqués dans l'interaction), en collaboration avec Pierre Fechter (UMR 7242, équipe Membrane bactérienne et transport', Illkirch). Ces études devraient aider à comprendre si et comment les deux molécules se dissocient dans des conditions données permettant le transfert des aptamères des endosomes au cytosol.

C'est également avec Pierre Fechter que nous rechercherons les aptatopes de certains des cApt par des techniques de 'cross-linking' entre protéine et aptamères-biotinylés, suivies de digestions protéiques, récupération des aptamères liés aux fragments protéiques sur colonne de streptavidine, et détermination des séquences peptidiques par spectrométrie de masse.

Suivi du trafic intracellulaire des aptamères

Des études d'imagerie à haute résolution (Plateforme QUEST, IGBMC & Faculté de Pharmacie UMR 7021, Illkirch) seront réalisées pour suivre le trafic intracellulaire des aptamères. Pour localiser les aptamères marqués, nous utiliserons deux sondes fluorescentes brillantes développées dans l'UMR : l'une sensible au pH, décrite ci-dessus ; l'autre nommée 7AF (Zamotaiev et al., 2014), sensible à l'environnement (Andrey Klymchenko, URM 7021, équipe Nanochimie et nanoimagerie, Illkirch). Des marqueurs spécifiques des compartiments cellulaires seront également utilisés pour marquer les endosomes (précoces : Rab5 or EEA1 ; tardifs : Rab25 ou CD63 ; de recyclage : Rab4 ou Rab11), les lysosomes (Lamp1 ou LysoTracker®). En collaboration avec Sylvie Friant (UMR 7156, équipe Trafic membranaire et signalisation lipidique, Strasbourg), nous utiliserons différentes drogues bloquant le trafic à des sites cellulaires spécifiques. Nous quantifierons les aptamères présents dans le cytosol par RT-qPCR.

Ces études devraient permettre de déterminer les sites d'échappement sub-cellulaire des aptamères et de quantifier les aptamères présents dans le cytosol.

Associations thérapeutiques

Si les aptamères ont un effet direct sur leurs cibles par activation/inhibition de différentes voies de signalisation, ils pourraient être utilisés en tant qu'agents thérapeutiques en oncologie, seuls ou en association avec des agents chimothérapeutiques (TMZ, nutlin-3a) dans des expériences précliniques *in vitro* (lignées cellulaires tumorales) et *in vivo* (modèles de xénogreffes de tumeurs de patients dans la souris Nude), en collaboration avec Sophie Pinel (UMR 7039, Vandoeuvre-les-Nancy) dans l'objectif de proposer l'utilisation de thérapies ciblées sur des sous-populations de patients (Janouskova et al., 2012 ; Renner et al., 2016a).

Les aptamères peuvent également être utilisés comme véhicule pour délivrer spécifiquement un agent thérapeutique à une cellule ciblée (voir ci-dessus). Couplés à des siRNA, nanoparticules ou à d'autres agents thérapeutiques, ils peuvent délivrer ces agents à l'intérieur des cellules qu'ils ciblent spécifiquement via leur récepteur membranaire. Pour un exemple récent : Alshaer et al. (2018) ont construit un nanocomposé capable de cibler les cellules souches cancéreuses de cancers du sein. Ont été associés au sein de ce nanocomposé à base de lipides, en surface des aptamères pour la reconnaissance moléculaire du CD44, et à l'intérieur des siRNA pour supprimer l'expression de gènes. L'affinité de l'aptamère pour le récepteur est améliorée quand il est présenté à la surface des nanocomposés par rapport à l'aptamère seul. L'internalisation des nanocomposés est plus importante par les cellules exprimant le récepteur CD44 par rapport à celle des cellules ne l'exprimant pas.

Au laboratoire, des travaux récents ont permis de caractériser les intervenants moléculaires impliqués dans la relation croisée négative entre intégrine α5β1 et p53. Deux protéines anti-apoptotiques ont été caractérisées, dont la survivine (Renner et al., 2016a). Les siRNA sont particulièrement utiles pour atteindre des cibles intracellulaires, telles que la survivine. Liu et al. (2016) ont montré sur des cellules de cancer de la prostate (PCa) l'utilisation d'une molécule chimère constituée de deux aptamères ciblant le PMSA ('prostate specific membrane antigen') reliés par deux siRNA ciblant EGFR et survivine. *In vivo*, les difficultés liées au ciblage des cellules tumorales puis à la délivrance du siRNA (Whitehead et al., 2009) pourront être surmontées par l'utilisation d'une molécule chimère constituée d'un aptamère ciblant l'intégrine α5β1 (pour le ciblage et l'internalisation) et du siRNA survivine, ou d'une nanoconstruction (en collaboration avec Delphine Felder, IPCMS, Strasbourg et avec Guy Zuber, équipe Intervention chémobiologique, UMR 7242). Nous comparerons l'effet des différentes constructions à ceux des ARN seuls, par différentes techniques (microscopie confocale, western blot, RTqPCR…). Nous pouvons également envisager de coupler directement les aptamères, molécules synthétiques et facilement fonctionnalisables, à un agent thérapeutique pour l'administration d'agents cytotoxiques spécifiquement délivrés aux cellules ciblées.

Conclusion

Les aptamères sont en développement dans les domaines analytique, diagnostique et thérapeutique. En oncologie, les aptamères semblent offrir des possibilités infinies pour le diagnostic, la bio-détection, la bio-imagerie, l'administration de médicaments et la thérapie.

Les glioblastomes (GBM) sont les tumeurs cérébrales les plus agressives. Le développement de nouvelles approches diagnostiques et thérapeutiques est nécessaire. L'intégrine α5β1 est une protéine transmembranaire, biomarqueur des GBM et d'autres tumeurs solides. Ses ligands actuels sont peu nombreux.

Nous avons récemment sélectionné un nouveau ligand de cette intégrine, un aptamère nommé H02. Nous proposons le développement de cet aptamère et/ou de nouveaux aptamères en cours de sélection :

- en tant qu'outil diagnostique de marquage ex vivo *de l'expression des récepteurs dans des tissus tumoraux, et à plus long terme de sondes d'imagerie non invasive pour suivre la progression tumorale.*

- et en tant qu'agent thérapeutique. Seuls ou en association avec d'autres inhibiteurs/agents cytotoxiques/siRNA…, les aptamères pourraient servir à cibler les tumeurs exprimant fortement des biomarqueurs protéiques cellulaires, en particulier dans le cas des GBM humains.

Références bibliographiques

Adachi M, Taki T, Higashiyama M, Kohno N, Inufusa H, Miyake M. (2000). Significance of integrin alpha5 gene expression as a prognostic factor in node-negative non-small cell lung cancer. Clin Cancer Res. 6(1), 96-101.

Almokadem S, Belani CP. (2012). Volociximab in cancer. Expert. Opin. Biol. Ther. 12(2), 251-7.

Altroff H, Choulier L, Mardon HJ. (2003). Synergistic activity of the ninth FIII domain of fibronectin depends on its structural stability. J. Biol. Chem. 278, 491-497.

Altschuh D, Björkelund, H, Strandgård J, Choulier, Malmqvist M, Andersson K. (2012). Deciphering complex protein interaction kinetics using Interaction Map. Biochem Biophys Res Commun. 428, 74-9.

Alshaer W, Hillaireau H, Vergnaud J, Mura S, Deloménie C, Sauvage F, Ismail S, Fattal E. (2018). Aptamer-guided siRNA-loaded nanomedicines for systemic gene silencing in CD-44 expressing murine triple-negative breast cancer model. J. Control Release 271, 98-106.

Andersson K, Choulier L, Hämäläinen M, Van Regenmortel MHV, Altschuh D, Malmqvist M. (2001). Predicting the kinetics of peptide-antibody interactions using a multivariate experimental "design" of sequence and chemical space. J. Mol. Recognit. 14, 62-71.

Appin CL, Brat DJ. (2015). Biomarker-driven diagnosis of diffuse gliomas. Mol. Aspects Med. 45, 87–96.

Arnaout MA, Mahalingam B, Xiong JP. (2005). Integrin structure, allostery, and bidirectional signaling. Annu Rev Cell Dev Biol. 21, 381-410.

Arosio D, Belvisi L, Colombo L, Colombo M, Invernizzi D, Manzoni L, Potenza D, Serra M, Castorina M, Pisano C, Scolastico C. (2008). A potent integrin antagonist from a small library of cyclic RGD pentapeptide mimics including benzyl-substituted azabicycloalkane amino acids. ChemMedChem. 3(10), 1589-603.

Bartik P, Maglott A, Entlicher G, Vestweber D, Takeda K, Martin S, Dontenwill M. (2008). Detection of a hypersialylated beta1 integrin endogenously expressed in the human astrocytoma cell line A172. Int J Oncol. 32(5), 1021-31.

Bass BL, Cech TR. (1984). Specific interaction between the self-splicing RNA of Tetrahymena and its guanosine substrate: implications for biological catalysis by RNA. Nature. 308(5962), 820-6.

Bauer M, Macdonald J, Henri J, Duan W,Shigdar S. (2016). The Application of Aptamers for Immunohistochemistry. Nucl. Acid Ther. 26(3), 120-6.

Bayrac AT, Sefah K, Parekh P, Bayrac C, Gulbakan B, Oktem HA, Tan W. (2011). In vitro Selection of DNA Aptamers to Glioblastoma Multiforme. ACS Chem Neurosci. 2(3), 175-81.

Bell-McGuinn KM, Matthews CM, Ho SN, Barve M, Gilbert L, Penson RT, Lengyel E, Palaparthy R, Gilder K, Vassos A et al. (2011). A phase II, single-arm study of the anti-alpha5beta1 integrin antibody volociximab as monotherapy in patients with platinum-resistant advanced epithelial ovarian or primary peritoneal cancer. Gynecol. Oncol 121(2), 273-9.

Berg K, Lange T, Mittelberger F, Schumacher U, Hahn U. (2016). Selection and Characterization of an α6β4 Integrin blocking DNA Aptamer. Mol Ther Nucleic Acids. 5:e294.

Bianconi D, Unseld M, Prager GW. (2016). Integrins in the spotlight of cancer. Int. J. Mol. Sci. 17, 2037.

Björke H, Andersson K. (2006a). Measuring the affinity of a radioligand with its receptor using a rotating cell dish with in situ reference area. Appl Radiat Isot. 64(1), 32-37

Bjorke H, Andersson K. (2006b). Automated, high-resolution cellular retention and uptake studies in vitro. Appl Radiat Isot. 64(8), 901-905.

Blandin AF, Noulet F, Renner G, Mercier MC, Choulier L, Vauchelles R, Rondé P, Carreiras F, Etienne-Selloum N, Vereb G, Lelong-Rebel I, Martin S, Dontenwill M, Lehmann M. (2016). Glioma cell dispersion is driven by α5 integrin-mediated cell-matrix and cell-cell interactions. Cancer Lett. 376(2), 328-38.

Blank M, Weinschenk T, Priemer M, Schluesener H. (2001). Systematic evolution of a DNA aptamer binding to rat brain tumor microvessels. Selective targeting of endothelial regulatory protein pigpen. J Biol Chem. 276(19), 16464-8.

Blind M, Kolanus W, Famulok M. (1999). Cytoplasmic RNA modulators of an inside-out signal-transduction cascade. Proc. Natl. Acad. Sci. U. S. A. 96, 3606-10.

Breuksch I, Prosinger F, Baehr F, Engelhardt FP, Bauer HK, Thüroff JW, Heimes AS, Hasenburg A, Prawitt D, Brenner W. (2017). Integrin α5 triggers the metastatic potential in renal cell carcinoma. Oncotarget. 8(64), 107530-42.

Bukari BA, Citartan M, Ch'ng ES, Bilibana MP, Rozhdestvensky T, Tang T-H. (2017). Aptahistochemistry in diagnostic pathology: technical scrutiny and feasibility. Histochem. Cell Biol. 147, 545-53.

Camorani S, Esposito CL, Rienzo A, Catuogno S, Iaboni M, Condorelli G, de Franciscis V, Cerchia L. (2014). Inhibition of receptor signaling and of glioblastoma-derived tumor growth by a novel PDGFRβ aptamer. Mol Ther. 22(4), 828-41.

Camorani S, Cerchia L. (2015). Oligonucleotide aptamers for glioma targeting: an update. Cent Nerv Syst Agents Med Chem. 15(2), 126-37.

Ceccarelli M, Barthel FP, Malta TM, Sabedot TS, Salama SR, Murray BA, Morozova O, Newton Y, Radenbaugh A, Pagnotta SM, Anjum S, Wang J, Manyam G, Zoppoli P, Ling S, Rao AA, Grifford M, Cherniack AD, Zhang H, Poisson L, Carlotti CG Jr, Tirapelli DP, Rao A, Mikkelsen T, Lau CC, Yung WK, Rabadan R, Huse J, Brat DJ, Lehman NL, Barnholtz-Sloan JS, Zheng S, Hess K, Rao G, Meyerson M, Beroukhim R, Cooper L, Akbani R, Wrensch M, Haussler D, Aldape KD, Laird PW, Gutmann DH; TCGA Research Network, Noushmehr H, Iavarone A, Verhaak RG. (2016). Molecular Profiling Reveals Biologically Discrete Subsets and Pathways of Progression in Diffuse Glioma. Cell. 164(3), 550-63.

Cerchia L, Esposito CL, Jacobs AH, Tavitian B, de Franciscis V. (2009). Differential SELEX in human glioma cell lines. PLoS One. 4(11), e7971.

Charbonnier S, Nominé Y, Ramirez J, Luck K, Chapelle A, Stote RH, Travé G, Kieffer B, Atkinson RA. (2011). The structural and dynamic response of MAGI-1 PDZ1 with noncanonical domain boundaries to the binding of human papillomavirus E6. J. Mol. Biol. 406, 745-63.

Chatellier J, Van Regenmortel MH, Vernet T, Altschuh D. (1996a). Functional mapping of conserved residues located at the VL and VH domain interface of a Fab. J Mol Biol. 264(1), 1-6.

Chatellier J, Rauffer-Bruyère N, Van Regenmortel MH, Altschuh D, Weiss E. (1996b). Comparative interaction kinetics of two recombinant Fabs and of the corresponding antibodies directed to the coat protein of tobacco mosaic virus. J Mol Recognit. 9(1), 39-51.

Chen C-hB., Dellamaggiore KR, Ouellette CP, Sedano CD, Lizadjohry M, Chernis GA, Gonzales M, Baltasar FE, Fan AL, Myerowitz R, Neufeld EF. (2008). Aptamer-based endocytosis of a lysosomal enzyme. Proc. Natl. Acad. Sci. U. S. A. 105, 15908-13.

Choulier L, Rauffer-Bruyère N, Ben Khalifa M, Martin F, Vernet T Altschuh D. (1999). Kinetic analysis of the effect on Fab binding of identical substitutions in a peptide and its parent protein. Biochemistry 38, 3530-3537.

Choulier L, Lafont V, Hugo N, Altschuh D. (2000). Covariance analysis of protein families: the case of the variable domains of antibodies. Proteins 41, 475-484.

Choulier L, Laune D, Orfanoudakis G, Wlad H, Janson JC, Granier C, Altschuh D. (2001). Delineation of a linear epitope by multiple peptide synthesis and phage display. J. Immunol. Methods 249, 253-264.

Choulier L, Orfanoudakis G, Robinson P, Laune D, Ben Khalifa M, Granier C, Weiss E, Altschuh D. (2002a). Comparative properties of two peptide-antibody interactions, as deduced from epitope delineation. J. Immunol. Methods 259, 77-86.

Choulier L, Andersson K, Hämäläinen M, Van Regenmortel MHV, Malmqvist M, Altschuh D. (2002b). QSAR studies applied to the prediction of antigen-antibody interaction kinetics as measured by BIACORE. Protein Eng. 15, 373-382.

Choulier L, Altschuh D, Zeder-Lutz G, Van Regenmortel MHV. (2005). Biosensor characterization of structure-function relationships in viral proteins. Methods in Microbiology. 34, 213-238.

Choulier L, Schvadchak VV, Naidoo A, Klymchenko AS, Mély Y, Altschuh D. (2010). A peptide-based fluorescent ratiometric sensor for quantitative detection of proteins. Anal. Biochem. 401, 188-195.

Choulier L, Enander K. (2010). Environmentally Sensitive Fluorescent Sensors Based on Synthetic Peptides. Sensors 10, 3126-3144.

Choulier L, Nominé Y, Zeder-Lutz G, Charbonnier S, Didier B, Jung ML, Altschuh D. (2013). Chemical library screening using a SPR-based inhibition in solution assay: simulations and experimental validation. Anal. Chem. 85, 8787-95.

Cianfrocca ME, Kimmel KA, Gallo J, Cardoso T, Brown MM, Hudes G, Lewis N, Weiner L, Lam GN, Brown SC, Shaw DE, Mazar AP, Cohen RB. (2006). Phase 1 trial of the antiangiogenic peptide ATN-161 (Ac-PHSCN-NH(2)), a beta integrin antagonist, in patients with solid tumours. Br. J. Cancer. 94(11), 1621-6.

Cibiel A, Quang NN, Gombert K, Thézé B, Garofalakis A, Ducongé F. (2014). From ugly duckling to swan: unexpected identification from cell-SELEX of an anti-Annexin A2 aptamer targeting tumors. PLoS One. 9(1), e87002.

Cirkel GA, Kerklaan BM, Vanhoutte F, Van der Aa A, Lorenzon G, Namour F, Pujuguet P, Darquenne S, de Vos FY, Snijders TJ, Voest EE, Schellens JH, Lolkema MP. (2016). A dose escalating phase I study of GLPG0187, a broad spectrum integrin receptor antagonist, in adult patients with progressive high-grade glioma and other advanced solid malignancies. Invest New Drugs. 34(2), 184-92.

Coe AP1, Askari JA, Kline AD, Robinson MK, Kirby H, Stephens PE, Humphries MJ. (2001). Generation of a minimal alpha5beta1 integrin-Fc fragment. J Biol Chem. 276(38), 35854-66.

Copié V, Tomita Y, Akiyama SK, Aota S, Yamada KM, Venable RM, Pastor RW, Krueger S, Torchia DA. (1998). Solution structure and dynamics of linked cell attachment modules of mouse fibronectin containing the RGD and synergy regions: comparison with the human fibronectin crystal structure. J Mol Biol. 277(3), 663-82.

Cosset EC, Godet J, Entz-Werlé N, Guérin E, Guenot D, Froelich S, Bonnet D, Pinel S, Plenat F, Chastagner P, Dontenwill M, Martin S. (2012). Involvement of the TGFβ pathway in the regulation of α5 β1 integrins by caveolin-1 in human glioblastoma. Int J Cancer. 131(3), 601-11.

Daniels DA1, Chen H, Hicke BJ, Swiderek KM, Gold L. (2003). A tenascin-C aptamer identified by tumor cell SELEX: systematic evolution of ligands by exponential enrichment. Proc Natl Acad Sci U S A. 100(26), 15416-21.

Darmostuk M, Rimpelova S, Gbelcova H, Ruml T. (2015). Current approaches in SELEX: An update to aptamer selection technology. Biotechnol Adv. 33(6 Pt 2), 1141-61.

Da Rocha Gomes S, Azéma L, Allard M, Toulmé JJ. (2010). Aptamers as imaging agents. Expert Opin Med Diagn. 4(6), 511-8.

Da Rocha Gomes S, Miguel J, Azema L, Eimer S, Ries C, Dausse E, Loiseau H, Allard M, Toulmé JJ. (2012) (99 m)Tc-MAG3-aptamer for imaging human tumors associated with high level of matrix metalloprotease-9. Bioconjug Chem 23, 2192–200

Dausse E, Cazenave C, Rayner B, Toulmé JJ. (2005). In vitro selection procedures for identifying DNA and RNA aptamers targeted to nucleic acids and proteins. Methods Mol Biol. 288, 391-410.

Dausse E, Barré A, Aimé A, Groppi A, Rico A, Ainali C, Salgado G, Palau W, Daguerre E, Nikolski M, Toulmé JJ, Di Primo C. (2016). Aptamer selection by direct microfluidic recovery and surface plasmon resonance evaluation. Biosens Bioelectron. 80, 418-25.

De Franceschi N, Hamidi H, Alanko J, Sahgal P, Ivaska J. (2015). Integrin traffic - the update. J Cell Sci. 128(5), 839-52.

Dejaegere A, Choulier L, Lafont V, De Genst E, Altschuh D. (2005). Variations in antigen-antibody association kinetics as a function of pH and salt concentration: a QSAR and molecular modeling study. Biochemistry 44, 14409-14418.

Delač M, Motaln H, Ulrich H, Lah TT. (2015). Aptamer for imaging and therapeutic targeting of brain tumor glioblastoma. Cytometry A. 87(9), 806-16.

DeLay M, Jahangiri A, Carbonell WS, Hu YL, Tsao S, Tom MW, Paquette J, Tokuyasu TA, Aghi MK. (2012). Microarray analysis verifies two distinct phenotypes of glioblastomas resistant to antiangiogenic therapy. Clin Cancer Res. 18(10), 2930-42.

Delibegovic M, Mody N. (2009). Protein tyrosine phosphatase 1B (PTP1B) in obesity and type 2 diabetes. Acta Med. Sal. 38(1), 2-7.

Desgrosellier JS, Cheresh DA. (2010). Integrins in cancer: biological implications and therapeutic opportunities. Nat Rev Cancer. 10(1), 9-22.

Dua P, Kim S, Lee DK. (2011). Nucleic acid aptamers targeting cell-surface proteins. Methods. 54(2), 215-25.

Duval M, Korepanov A, Fuchsbauer O, Fechter P, Haller A, Fabbretti A, Choulier L, Micura R, Klaholz B, Romby P, Springer M, Marzi S. (2013). Escherichia coli ribosomal protein S1 unfolds structured mRNAs onto the ribosome for active translation initiation. Plos. Biol. 11, e1001731.

Elchebly M, Cheng A, Tremblay ML. (2000). Modulation of insulin signaling by protein tyrosine phosphatases. J Mol Med (Berl). 78(9), 473-82.

Ellington AD, Szostak JW. (1990). In vitro selection of RNA molecules that bind specific ligands. Nature. 346(6287), 818-22.

Enander K, Choulier L, Linnéa-Olsson A, Yushchenko DA, Kanmert D, Klymchenko AS, Demchenko AP, Mély Y, Altschuh, D. (2008). A peptide-based, ratiometric biosensor construct for direct fluorescence detection of a protein analyte. Bioconjug. Chem. 19, 1864-70

Esposito CL, Catuogno S, de Franciscis V, Cerchia L. (2011a). New insight into clinical development of nucleic acid aptamers. Discov Med. 11(61), 487-96.

Esposito CL, Passaro D, Longobardo I, Condorelli G, Marotta P, et al. (2011b). A neutralizing RNA aptamer against EGFR causes selective apoptotic cell death. PLoS ONE 6(9): e24071.

Esposito CL, Catuogno S, de Franciscis V. (2014). Aptamer-mediated selective delivery of short RNA therapeutics in cancer cells. J RNAi Gene Silencing. 10, 500-6.

Fournane S, Charbonnier S, Chapelle A, Kieffer B, Orfanoudakis G, Travé G, Masson M, Nominé Y. (2011). Surface plasmon resonance analysis of the binding of high-risk mucosal HPV E6 oncoproteins to the PDZ1 domain of the tight junction protein MAGI-1. J Mol Recognit. 24(4), 511-23.

Freije WA, Castro-Vargas FE, Fang Z, Horvath S, Cloughesy T, Liau LM, Mischel PS, Nelson SF. (2004). Gene expression profiling of gliomas strongly predicts survival. Cancer Res. 64(18), 6503-10.

Fry, MY, Clemons Jr WM. (2018). Complexity in targeting membrane proteins. Science 26, 359(6374), 390-1.

Ganson NJ, Povsic TJ, Sullenger BA, Alexander JH, Zelenkofske SL, Sailstad JM, Rusconi CP, Hershfield MS (2016). Pre-existing anti–polyethylene glycol antibody linked to first-exposure allergic reactions to pegnivacogin, a PEGylated RNA aptamer. J. Allergy Clin. Immunol. 137, 1610–1613.

García MA, Martín-Santamaría S, de Pascual-Teresa B, Ramos A, Julián M, Martínez A. (2006). Adrenomedullin: a new and promising target for drug discovery. Expert Opin Ther Targets. 10(2), 303-17.

Giancotti FG, Ruoslahti E. (1999). Integrin signaling. Science. 285(5430), 1028-32.

Gijs M, Aerts A, Impens N, Baatout S, Luxen A. (2015). Aptamers as radiopharmaceuticals for nuclear imaging and therapy. Nucl Med Biol. 43(4), 253-71.

Gilbert W. (1986). Origin of life: The RNA world. Nature 319, 618.

Giovane C, Trave G, Briones A, Lutz Y, Wasylyk B, Weiss E. (1999). Targetting of the N-terminal domain of the human papillomavirus type 16 E6 oncoprotein with monomeric ScFvs blocks the E6-mediated degradation of cellular p53. J Mol Recognit. 12(2), 141-52.

Gold L, Ayers D, Bertino J, Bock C, Bock A, Brody EN, Carter J, Dalby AB, Eaton BE, Fitzwater T, Flather D, Forbes A, Foreman T, Fowler C, Gawande B, Goss M, Gunn M, Gupta S, Halladay D, Heil J, Heilig J, Hicke B, Husar G, Janjic N, Jarvis T, Jennings S, Katilius E, Keeney TR, Kim N, Koch TH, Kraemer S, Kroiss L, Le N, Levine D, Lindsey W, Lollo B, Mayfield W, Mehan M, Mehler R, Nelson SK, Nelson M, Nieuwlandt D, Nikrad M, Ochsner U, Ostroff RM, Otis M, Parker T, Pietrasiewicz S, Resnicow DI, Rohloff J, Sanders G, Sattin S, Schneider D, Singer B, Stanton M, Sterkel A, Stewart A, Stratford S, Vaught JD, Vrkljan M, Walker JJ, Watrobka M, Waugh S, Weiss A, Wilcox SK, Wolfson A, Wolk SK, Zhang C, Zichi D. (2010). Aptamer-based multiplexed proteomic technology for biomarker discovery. PLoS One. 5(12), e15004.

Gong K, Wang J, Ahmad KM, Csordas AT, Zhou J, Nie J, Stewart R, Thomson JA, Rossi JJ, Soh HT. (2012). Selection strategy to generate aptamer pairs that bind to distinct sites on protein targets. Anal. Chem. 84, 5365-71.

Gopinath SC, Lakshmipriya T, Chen Y, Arshad MK, Kerishnan JP, Ruslinda AR, Al-Douri Y, Voon CH, Hashim U. (2016). Cell-targeting aptamers act as intracellular delivery vehicles. Appl Microbiol Biotechnol. 100(16), 6955-69.

Haber T, Jöckel E, Roos FC, Junker K, Prawitt D, Hampel C, Thüroff JW, Brenner W. (2015). Bone Metastasis in Renal Cell Carcinoma is Preprogrammed in the Primary Tumor and Caused by AKT and Integrin α5 Signaling. J Urol. 194(2), 539-46.

Hahn U. (2017). Charomers-Interleukin-6 Receptor Specific Aptamers for Cellular Internalization and Targeted Drug Delivery. Int. J. Mol. Sci. 18(12), pii: E2641

Hamers-Casterman C, Atarhouch T, Muyldermans S, Robinson G, Hamers C, Songa EB, Bendahman N, Hamers R. (1993). Naturally occurring antibodies devoid of light chains. Nature. 363(6428), 446-8.

Hammani K, Gobert A, Hleibieh K, Choulier L, Small I, Giegé P. (2011) An Arabidopsis dual-localized pentatricopeptide repeat protein interacts with nuclear proteins involved in gene expression regulation. Plant Cell. 23, 730-40.

Hansch C, Fujita T. (1964). p-s-p Analysis. A method for the correlation of biological activity and chemical structure. J. Am. Chem. Soc. 86, 1616-26.

Hays, EM, Duan W, Shigdar S. (2017). Aptamers and glioblastoma: their potential use for imaging and therapeutic applications. Int. J. Mol. Sci. 257, 2576.

Heckmann D, Meyer A, Laufer B, Zahn G, Stragies R, Kessler H. (2008). Rational design of highly active and selective ligands for the alpha5beta1 integrin receptor. Chembiochem. 9(9), 1397-407.

Hellinga HW, Marvin JS. (1998). Protein engineering and the development of generic biosensors. Trends Biotechnol. 16(4), 183-9.

Hicke BJ, Marion C, Chang YF, Gould T, Lynott CK, Parma D, Schmidt PG, Warren S. (2001). Tenascin-C aptamers are generated using tumor cells and purified protein. J Biol Chem. 276(52), 48644-54.

Hicke BJ, Stephens AW, Gould T, Chang YF, Lynott CK, Heil J, Borkowski S, Hilger CS, Cook G, Warren S, Schmidt PG. (2006). Tumor targeting by an aptamer. J Nucl Med. 47(4), 668-78.

Hori S-I, Herrera A, Rossi JJ, Zhou J. (2018). Current advances in aptamers for cancer diagnosis and therapy. Cancers. 10, 9.

Horning DP, Joyce GF. (2016). Amplification of RNA by an RNA polymerase ribozyme. Proc Natl Acad Sci U S A. 113(35), 9786-91.

Huber W. (2005). A new strategy for improved secondary screening and lead optimization using high-resolution SPR characterization of compound–target interactions. J Mol Recognit 18, 273–81.

Hynes RO. (1992). Integrins: versatility, modulation, and signaling in cell adhesion. Cell. 69(1), 11-25.

Hynes RO. (2002). Integrins: bidirectional, allosteric signaling machines. Cell 110(6), 673-87.

Iwanicki MP, Chen HY, Iavarone C, Zervantonakis IK, Muranen T, Novak M, Ince TA, Drapkin R, Brugge JS. (2016). Mutant p53 regulates ovarian cancer transformed phenotypes through autocrine matrix deposition. JCI Insight. 1(10). pii: e86829.

Janouskova H, Maglott A, Leger DY, Bossert C, Noulet F, Guerin E, Guenot D, Pinel S, Chastagner P, Plenat F, Entz-Werle N, Lehmann-Che J, Godet J, Martin S, Teisinger J, Dontenwill M. (2012). Integrin α5β1 plays a critical role in resistance to temozolomide by interfering with the p53 pathway in high-grade glioma. Cancer Res. 72(14), 3463-70.

Janouskova H, Ray AM, Noulet F, Lelong-Rebel I, Choulier L, Schaffner F, Lehmann M, Martin S, Teisinger J, Dontenwill M. (2013). Activation of p53 pathway by Nutlin-3a inhibits the expression of the therapeutic target α5 integrin in colon cancer cells. Cancer Lett. 336, 307-18.

Jayanesa SD. (1999). Aptamers: an emerging class of molecules that rival antibodies in diagnostics. Clin. Chem. 45(9), 1628-50.

Jayanti VSPKSA, Das AB, Saxena U. (2017). Recent advances in biosensor development for the detection of cancer biomarkers. Biosens. Bioelectron. 91, 15-23

Jenison RD, Gill SC, Pardi A, Polisky B. (1994). High-resolution molecular discrimination by RNA. Science. 263(5152), 1425-9.

Jovanovic J, Takagi J, Choulier L, Abrescia NGA, Stuart DI, Van der Merwe PA, Mardon HJ, Handford PA. (2007). Avb6 is a novel receptor for human fibrillin-1: comparative studies of molecular determinants underlying integrin-RGD affinity and specificity. J. Biol. Chem. 282, 6743-51.

Ju L, Zhou C, Li W, Yan L. (2010). Integrin beta1 over-expression associates with resistance to tyrosine kinase inhibitor gefitinib in non-small cell lung cancer. J Cell Biochem. 111(6), 1565-74.

Ju JA, Godet I, Ye IC, Byun J, Jayatilaka H, Lee SJ, Xiang L, Samanta D, Lee MH, Wu PH, Wirtz D, Semenza GL, Gilkes DM. (2017). Hypoxia Selectively Enhances Integrin α5β1 Receptor Expression in Breast Cancer to Promote Metastasis. Mol Cancer Res. 15(6), 723-34.

Julián M, Cacho M, García MA, Martín-Santamaría S, de Pascual-Teresa B, Ramos A, Martínez A, Cuttitta F. (2005). Adrenomedullin: a new target for the design of small molecule modulators with promising pharmacological activities. Eur J Med Chem. 40(8), 737-50.

Kanda R, Kawahara A, Watari K, Murakami Y, Sonoda K, Maeda M, Fujita H, Kage M, Uramoto H, Costa C, Kuwano M, Ono M. (2013). Erlotinib resistance in lung cancer cells mediated by integrin β1/Src/Akt-driven bypass signaling. Cancer Res. 73(20), 6243-53.

Kang D, Wang J, Zhang W, Song Y, Li X, Zou Y, Zhu M, Zhu Z, Chen F, Yang CJ. (2012). Selection of DNA aptamers against glioblastoma cells with high affinity and specificity. PLoS One. 7(10), e42731.

Khalifa M, Weidenhaupt M, Choulier L, Chatellier J, Rauffer-Bruyère N, Altschuh D, Vernet T. (2000). Effects on interaction kinetics of mutations at the VH-VL interface of Fabs depend on the structural context. J. Mol. Recognit. 13, 127-139.

Khalifa M, Choulier L, Hortat-Jacob H, Altschuh D, Vernet T. (2001). BIACORE® data processing: an evaluation of the global fitting procedure. Anal. Biochem. 293, 194-203.

Kim S, Bell K, Mousa SA, Varner JA. (2000). Regulation of angiogenesis in vivo by ligation of integrin alpha5beta1 with the central cell-binding domain of fibronectin. Am J Pathol. 156(4), 1345-62.

Kim Y, Wu Q, Hamerlik P, Hitomi M, Sloan AE, Barnett GH, Weil RJ, Leahy P, Hjelmeland AB, Rich JN. (2013). Aptamer identification of brain tumor-initiating cells. Cancer Res. 73(15), 4923-36.

Kim MY, Cho WD, Hong KP, Choi da B, Hong JW, Kim S, Moon YR, Son SM, Lee OJ, Lee HC et al. (2016). Novel monoclonal antibody against beta 1 integrin enhances cisplatin efficacy in human lung adenocarcinoma cells. J Biomed Res 30(3), 217-24.

Kiyono T, Hiraiwa A, Fujita M, Hayashi Y, Akiyama T, Ishibashi M. (1997).Binding of high-risk human papillomavirus E6 oncoproteins to the human homologue of the Drosophila discs large tumor suppressor protein. Proc Natl Acad Sci U S A. 94(21), 11612-6.

Kobayashi M, Sawada K, Kimura T. (2017). Potential of Integrin Inhibitors for Treating Ovarian Cancer: A Literature Review. Cancers (Basel) 9(7). pii: E83.

Kryza D, Debordeaux F, Azéma L, Hassan A, Paurelle O, Schulz J, Savona-Baron C, Charignon E, Bonazza P, Taleb J, Fernandez P, Janier M, Toulmé JJ. (2016) Ex vivo and in vivo imaging and biodistribution of aptamers targeting the human matrix metalloprotease-9 in melanomas. PLoS ONE 11(2), e0149387.

Leahy DJ, Aukhil I, Erickson HP. (1996). 2.0 A crystal structure of a four-domain segment of human fibronectin encompassing the RGD loop and synergy region. Cell. 84(1), 155-64.

Lee SS, Knott V, Jovanovic J, Harlos K, Grimes JM, Choulier L, Mardon HJ, Stuart DI, Handford PA. (2004). Structure of the integrin binding fragment from fibrillin-1 gives new insights into microfibril organization. Structure. 12, 717-729.

Lincoff AM, Mehran R, Povsic TJ, Zelenkofske SL, Huang Z, Armstrong PW, Steg PG, Bode C, Cohen MG, Buller C, et al. (2016). Effect of the REG1 anticoagulation system versus bivalirudin on outcomes after percutaneous coronary intervention (REGULATE-PCI): A randomised clinical trial. Lancet 387, 349-56.

Liu HY, Yu X, Liu H, Wu D, She JX. (2016). Co-targeting EGFR and survivin with a bivalent aptamer-dual siRNA chimera effectively suppresses prostate cancer. Sci Rep. 6, 30346.

Lodish H, Berk A, Matsudaira P, Kaiser, Krieger, Scott, Zipursky, Darnell J. (2005). Biologie moléculaire de la cellule. De boeck, 3ème édition.

Löfas S, Choulier L, Zeder-Lutz G, Baltzinger M, Altschuh D. (2011) Surface plasmon resonance. RSC Biomolecular Sciences. 22, 136-55.

Louis DN, Ohgaki H, Wiestler OD, Cavenee WK, Burger PC, Jouvet A, Scheithauer BW, Kleihues P. (2007). The 2007 WHO classifcation of tumours of the central nervous system. Acta Neuropathol (2007) 114:97–109

Louis DN, Perry A, Reifenberger G, Deimling A von, Figarella-Branger D, Cavenee WK, Ohgaki H, Wiestler OD, Kleihues P, Ellison DW. (2016). The 2016 World Health Organization Classification of Tumors of the Central Nervous System: a summary. Acta Neuropathol. (Berl.) 131, 803-20.

Lundqvist T. (2005). The devil is still in the details: driving early drug discovery forward with biophysical experimental methods. Curr Opin Drug Discov Dev 8, 513-9.

Macdonald J, Henri J, Goodman L, Xiang D, Duan W, Shigdar S. (2017). Development of a bifunctional aptamer targeting the transferrin receptor and epithelial cell adhesion molecule (EpCAM) for the Treatment of Brain Cancer Metastases. ACS Chem. Neurosci. 8, 777-84

Magalhães MLB, Byrom M, Yan A, Kelly L, Li N, Furtado R, Palliser D, Ellington AD, Levy M. (2012). A general RNA motif for cellular transfection. Mol. Ther. 20, 616–24.

Maglott A, Bartik P, Cosgun S, Klotz P, Rondé P, Fuhrmann G, Takeda K, Martin S, Dontenwill M. (2006). The small alpha5beta1 integrin antagonist, SJ749, reduces proliferation and clonogenicity of human astrocytoma cells. Cancer Res. 66(12), 6002-7.

Martin S, Cosset EC, Terrand J, Maglott A, Takeda K, Dontenwill M. (2009). Caveolin-1 regulates glioblastoma aggressiveness through the control of alpha(5)beta(1) integrin expression and modulates glioblastoma responsiveness to SJ749, an alpha(5)beta(1) integrin antagonist. Biochim Biophys Acta. 1793(2), 354-67.

Martínez A, Julián M, Bregonzio C, Notari L, Moody TW, Cuttitta F. (2004). Identification of vasoactive nonpeptidic positive and negative modulators of adrenomedullin using a neutralizing antibody-based screening strategy. Endocrinology. 145(8), 3858-65.

Martínez O, Bellard E, Golzio M, Mechiche-Alami S, Rols MP, Teissié J, Ecochard V, Paquereau L. (2014). Direct validation of aptamers as powerful tools to image solid tumor. Nucleic Acid Ther. 24(3), 217-25.

Martinkova E, Maglott A, Leger DY, Bonnet D, Stiborova M, Takeda K, Martin S, Dontenwill M. (2010). alpha5beta1 integrin antagonists reduce chemotherapy-induced premature senescence and facilitate apoptosis in human glioblastoma cells. Int J Cancer. 127(5), 1240-8.

Mas-Moruno C, Rechenmacher F, Kessler H. (2010). Cilengitide: the first anti-angiogenic small molecule drug candidate. Design, synthesis and clinical evaluation. Anticancer Agents Med Chem. 10(10): 753-68.

Mateo J, Berlin J, de Bono JS, Cohen RB, Keedy V, Mugundu G, Zhang L, Abbattista A, Davis C, Gallo Stampino C, Borghaei H. (2014). A first-in-human study of the anti-α5β1 integrin monoclonal antibody PF-04605412 administered intravenously to patients with advanced solid tumors. Cancer Chemother Pharmacol. 74(5):1039-46

Maurel. (2005). Quand les ARN peuplaient le monde. Les dossiers de la recherche 19, 30-33.

Mercier M-C. Classification des gliomes et traitements actuels des glioblastomes. Manuscrit en préparation pour soumission au DES IPR Strasbourg.

Mercier M-C, Dontenwill M, Choulier, L. (2017). Selection of nucleic acid aptamers targeting tumor cell-surface protein biomarkers. *Cancers*. **21**(9), pii: E69.

Mi J, Zhang X, Giangrande PH, McNamara JO 2nd, Nimjee SM, Sarraf-Yazdi S, Sullenger BA, Clary BM. (2005). Targeted inhibition of alphavbeta3 integrin with an RNA aptamer impairs endothelial cell growth and survival. Biochem Biophys Res Commun. 338(2), 956-63.

Monaco I, Camorani S, Colecchia D, Locatelli E, Calandro P, Oudin A, Niclou S, Arra C, Chiariello M, Cerchia L, Franchini MC. (2017). Aptamer functionalization of nanosystems for Glioblastoma targeting through the Blood-Brain-Barrier. J. Med. Chem. 60(10), 4510-6.

Musumeci D, Platella C, Riccardi C, Moccia F, Montesarchio D. (2017). Fluorescence sensing using DNA aptamers in cancer research and clinical diagnostics. Cancers 9, 174.

Nam JM, Onodera Y, Bissell MJ, Park CC. (2010). Breast cancer cells in three-dimensional culture display an enhanced radioresponse after coordinate targeting of integrin alpha5beta1 and fibronectin. Cancer Res. 70(13), 5238-48.

Ng EW, Shima DT, Calias P, Cunningham ET Jr, Guyer DR, Adamis AP. (2006). Pegaptanib, a targeted anti-VEGF aptamer for ocular vascular disease. Nat Rev Drug Discov. 5(2), 123-32.

Ngubane NA, Gresh L, Pym A, Rubin EJ, Khati M. (2014). Selection of RNA aptamers against the M. tuberculosis EsxG protein using surface plasmon resonance-based SELEX. Biochem Biophys Res Commun. 449(1), 114-9.

Ni X, Castanares M, Mukherjee A, Lupold SE. (2011). Nucleic acid aptamers: clinical applications and promising new horizons. Curr Med Chem. 18(27), 4206-14.

Ni S, Yao H, Wang L, Lu J, Jiang F, Lu A, Zhang G. (2017). Chemical modifications of nucleic acid aptamers for therapeutic purposes. Int. J. Mol. Sci. 18, 1683.

Nieberler M, Reuning U, Reichart F, Notni J, Wester HJ, Schwaiger M, Weinmüller M, Räder A, Steiger K, Kessler H. (2017). Exploring the role of RGD-recognizing integrins in cancer. Cancers 9(9). pii: E116.

Nimjee SM, White RR, Becker RC, Sullenger, BA. (2017). Aptamers as therapeutics. Annu. Rev. Pharmacol. Toxicol. 57, 61-79.

Nominé Y, Choulier L, Travé G, Vernet T, Altschuh, D. (2015). Antibody Binding Selectivity: Alternative Sets of Antigen Residues Entail High-Affinity Recognition. PLoS One. 10(12):e0143374.

O'Malley RP, Mariano TM, Siekierka J, Mathews MB. (1986). A mechanism for the control of protein synthesis by adenovirus VA RNAI. Cell. 44(3), 391-400.
10.

Ostrom QT, Gittleman H, Xu J, Kromer C, Wolinsky Y, Kruchko C, Barnholtz-Sloan JS. (2016). Cbtrus statistical report: Primary brain and other central nervous system tumors diagnosed in the united states in 2009–2013. Neuro Oncol. 18, v1–v75.

Padilla R, Sousa R. (1999). Efficient synthesis of nucleic acids heavily modified with non-canonical ribose 2′-groups using a mutant T7 RNA polymerase (RNAP). Nucleic Acids Res. 27, 1561-3

Paolillo M, Serra M, Schinelli S. (2016). Integrins in glioblastoma: Still an attractive target? Pharmacol Res. 113(Pt A), 55-61.

Patel AP, Tirosh I, Trombetta JJ, Shalek AK, Gillespie SM, Wakimoto H, Cahill DP, Nahed BV, Curry WT, Martuza RL, Louis DN, Rozenblatt-Rosen O, Suvà ML, Regev A, Bernstein BE. (2014). Single-cell RNA-seq highlights intratumoral heterogeneity in primary glioblastoma. Science. 344(6190), 1396-401.

Paul NR, Jacquemet G, Caswell PT. (2015). Endocytic Trafficking of Integrins in Cell Migration. Curr Biol. 25(22), R1092-105.

Phillips HS, Kharbanda S, Chen R, Forrest WF, Soriano RH, Wu TD, Misra A, Nigro JM, Colman H, Soroceanu L, Williams PM, Modrusan Z, Feuerstein BG, Aldape K. (2006). Molecular subclasses of high-grade glioma predict prognosis, delineate a pattern of disease progression, and resemble stages in neurogenesis. Cancer Cell. 9(3), 157-73.

Pinheiro VB, Holliger P. (2014). Towards XNA nanotechnology: new materials from synthetic genetic polymers. Trends Biotechnol. 32(6), 321-8.

Povsic TJ, Lawrence MG, Lincoff AM, Mehran R, Rusconi CP, Zelenkofske SL, Huang Z, Sailstad J, Armstrong PW, et al. (2016). Pre-existing anti-PEG antibodies are associated with severe immediate allergic reactions to pegnivacogin, a PEGylated aptamer. J. Allergy Clin. Immunol. 138, 1712–1715.

Ray AM (2013). Conception et caractérisation d'antagonistes allostériques de l'intégrine α5β1 pour le traitement des glioblastomes. Thèse de l'Université de Strasbourg.

Ray AM, Schaffner F, Janouskova H, Noulet F, Rognan D, Lelong-Rebel I, Choulier L, Blandin AF, Lehmann M, Martin S, Neubauer S, Rechenmacher F, Kessler H, Dontenwill, M. (2014). Single cell tracking assay reveals an opposite effect of selective small non-peptidic α5β1 or αvβ3/β5 integrin antagonists in U87MG glioma cells. Biochim Biophys Acta. 1840, 2978-87.

Rechenmacher F, Neubauer S, Polleux J, Mas-Moruno C, De Simone M, Ada Cavalcanti-Adam E, Spatz JP, Fässler R, Kessler H. (2013). Functionalizing αvβ3- or α5β1-selective integrin antagonists for surface coating: a method to discriminate integrin subtypes in vitro. Angew. Chem. Int. Ed., 52, 1572-75.

Reeves KJ1, Hurrell JE, Cecchini M, van der Pluijm G, Down JM, Eaton CL, Hamdy F, Clement-Lacroix P, Brown NJ. (2015). Prostate cancer cells home to bone using a novel in vivo model: modulation by the integrin antagonist GLPG0187. Int J Cancer. 136(7), 1731-40.

Renaud JP, Chung CW, Danielson UH, Egner U, Hennig M, Hubbard RE, Nar H. (2016). Biophysics in drug discovery: impact, challenges and opportunities. Nat Rev Drug Discov. 15(10), 679-98.

Renner G (2016). Caractérisation de l'axe intégrine α5β1/protéine p53 dans les glioblastomes humains. Application à une thérapie ciblée anti-tumorale. Thèse de l'Université de Strasbourg.

Renner G, Janouskova H, Noulet F, Koenig V, Guerin E, Bär S, Nuesch J, Rechenmacher F, Neubauer S, Kessler H, Blandin AF, Choulier L, Etienne-Selloum N, Lehmann M, Lelong-Rebel I, Martin S, Dontenwill M. (2016a). Integrin α5β1 and p53 convergent pathways in the control of anti-apoptotic proteins PEA-15 and survivin in high-grade glioma. Cell Death Differ. 23(4), 640-53.

Renner G, Noulet F, Mercier MC, Choulier L, Etienne-Selloum N, Gies JP, Lehmann M, Lelong-Rebel I, Martin S, Dontenwill, M. (2016b). Expression/activation of α5β1 integrin is linked to the β-catenin signaling pathway to drive migration in glioma cells. Oncotarget 7(38), 62194-207.

Robertson DL1, Joyce GF. (1990). Selection in vitro of an RNA enzyme that specifically cleaves single-stranded DNA. Nature. 344(6265), 467-8.

Roldós V, Martín-Santamaría S, Julián M, Martínez A, Choulier L, Altschuh D, de Pascual-Teresa B, Ramos A. (2008). Small Molecule Negative Modulators of Adrenomedullin: Design, Synthesis, and 3D-QSAR Study. Chem. Med. Chem. 3, 1345-55.

Rusconi CP, Roberts JD, Pitoc GA, Nimjee SM, White RR, Quick G Jr, Scardino E, Fay WP, Sullenger BA. (2004). Antidote-mediated control of an anticoagulant aptamer in vivo. Nat Biotechnol. 22(11), 1423-8. Epub 2004 Oct 17.

Sawada K, Mitra AK, Radjabi AR, Bhaskar V, Kistner EO, Tretiakova M, Jagadeeswaran S, Montag A, Becker A, Kenny HA, Peter ME, Ramakrishnan V, Yamada SD, Lengyel E. (2008). Loss of E-cadherin promotes ovarian cancer metastasis via alpha 5-integrin, which is a therapeutic target. Cancer Res. 68(7), 2329-39.

Sawada K, Ohyagi-Hara C, Kimura T, Morishige K. (2012). Integrin inhibitors as a therapeutic agent for ovarian cancer. J Oncol. 2012, 915140.

Schaffner F, Ray AM, Dontenwill M. (2013). Integrin α5β1, the Fibronectin Receptor, as a Pertinent Therapeutic Target in Solid Tumors. Cancers (Basel). 5(1), 27-47.

Schreiner CL, Bauer JS, Danilov YN, Hussein S, Sczekan MM, Juliano RL. (1989). Isolation and characterization of Chinese hamster ovary cell variants deficient in the expression of fibronectin receptor. J Cell Biol. 109(6 Pt 1), 3157-67.

Schwalbach G, Sibler AP, Choulier L, Deryckère F, Weiss, E. (2000). Production of fluorescent single-chain antibody fragments in Escherichia coli. Protein Expr. Purif. 18, 121-132.

Sibler AP, Baltzinger M, Choulier L, Desplancq D, Altschuh D. (2008). SPR identification of mild elution conditions for affinity purification of E6 oncoprotein, using a multivariate experimental design. J. Mol. Recognit. 21, 46-54.

Silginer M, Weller M, Ziegler U, Roth P. (2014). Integrin inhibition promotes atypical anoikis in glioma cells. Cell Death Dis. 5, e1012.

Simmons SC, McKenzie EA, Harris LK, Aplin JD, Brenchley PE, Velasco-Garcia MN, Missailidis S. (2012). Development of novel single-stranded nucleic acid aptamers against the pro-angiogenic and metastatic enzyme heparanase (HPSE1). PLoS One. 7(6), e37938.

Song Y, Zhu Z, An Y, Zhang W, Zhang H, Liu D, Yu C, Duan W, Yang CJ. (2013). Selection of DNA aptamers against epithelial cell adhesion molecule for cancer cell imaging and circulating tumor cell capture. Anal. Chem. 85, 4141-9.

Sottoriva A, Spiteri I, Piccirillo SG, Touloumis A, Collins VP, Marioni JC, Curtis C, Watts C, Tavaré S. (2013). Intratumor heterogeneity in human glioblastoma reflects cancer evolutionary dynamics. Proc Natl Acad Sci U S A. 110(10), 4009-14.

Stevens LE, Cheung WKC, Adua SJ, Arnal-Estapé A, Zhao M, Liu Z, Brewer K, Herbst RS, Nguyen DX. (2017). Extracellular Matrix Receptor Expression in Subtypes of Lung Adenocarcinoma Potentiates Outgrowth of Micrometastases. Cancer Res. 77(8):1905-17.

Stragies R, Osterkamp F, Zischinsky G, Vossmeyer D, Kalkhof H, Reimer U, Zahn G. (2007). Design and synthesis of a new class of selective integrin alpha5beta1 antagonists. J Med Chem. 50(16), 3786-94.

Stupp R, Mason WP, van den Bent M J, Weller M, Fisher B, Taphoorn MJB, Belanger K, Brandes AA, Marosi C, Bogdahn U, Curschmann J, Janzer RC, Ludwin SK, Gorlia T, Allgeier A, Lacombe D, Cairncross JG, Eisenhauer E, Mirimanoff

RO. (2005). Radiotherapy plus Concomitant and Adjuvant Temozolomide for Glioblastoma. N. Engl. J. Med. 352, 987–96.

Su Y, Xia W, Li J, Walz T, Humphries MJ, Vestweber D, Cabañas C, Lu C, Springer TA. (2016). Relating conformation to function in integrin α5β1. Proc Natl Acad Sci U S A. 113(27), E3872-81.

Sullenger BA, Gallardo HF, Ungers GE, Gilboa E. (1990). Overexpression of TAR sequences renders cells resistant to human immunodeficiency virus replication. Cell. 63(3), 601-8.

Sun H, Zhu X, Lu PY, Rosato RR, Tan W, Zu Y. (2014). Oligonucleotide aptamers: new tools for targeted cancer therapy. Mol Ther Nucleic Acids. 3, e182.

Sun H, Tan W, Zu Y. (2016). Aptamers: versatile molecular recognition probes for cancer detection. Analyst. 141(2), 403-15.

Sundaram P, Kurniawan H, Byrne ME, Wower J. (2013). Therapeutic RNA aptamers in clinical trials. Eur J Pharm Sci. 48(1-2), 259-71.

Takada Y, Ye X, Simon S. (2007). The integrins. Genome Biol 8(5), 215.

Takagi J, Petre BM, Walz T, Springer TA. (2002). Global conformational rearrangements in integrin extracellular domains in outside-in and inside-out signaling. Cell. 110(5), 599-11.

Takahashi M, Sakota E, Nakamura Y. (2016). The efficient cell-SELEX strategy, Icell-SELEX, using isogenic cell lines for selection and counter-selection to generate RNA aptamers to cell surface proteins. Biochimie 131, 77-84.

Tan Y, Shi YS, Wu XD, Liang HY, Gao YB, Li SJ, Zhang XM, Wang F, Gao TM. (2013). DNA aptamers that target human glioblastoma multiforme cells overexpressing epidermal growth factor receptor variant III in vitro. Acta Pharmacol Sin. 34(12), 1491-8.

Tawiah KD, Porciani D, Burke DH. (2017). Toward the Selection of Cell Targeting Aptamers with Extended Biological Functionalities to Facilitate Endosomal Escape of Cargoes. Biomedicines. 5(3), pii: E51.

Thiel KW, Hernandez LI, Dassie JP, Thiel WH, Liu X, Stockdale KR, Rothman AM, Hernandez FJ, McNamara JO, Giangrande PH. (2012). Delivery of chemo-sensitizing siRNAs to HER2+-breast cancer cells using RNA aptamers. Nucleic Acids Res. 40, 6319-37.

Tuerk C, Gold L. (1990). Systematic evolution of ligands by exponential enrichment: RNA ligands to bacteriophage T4 DNA polymerase. Science. 249(4968), 505-10.

Unnikrishnan A, Papaemmanuil E, Beck D, Deshpande NP, Verma A, Kumari A, Woll PS, Richards LA, Knezevic K, Chandrakanthan V, Thoms JAI, Tursky ML, Huang Y, Ali Z, Olivier J, Galbraith S, Kulasekararaj AG, Tobiasson M, Karimi M, Pellagatti A, Wilson SR, Lindeman R, Young B, Ramakrishna R, Arthur C, Stark R, Crispin P, Curnow J, Warburton P, Roncolato F, Boultwood J, Lynch K, Jacobsen SEW, Mufti GJ, Hellstrom-Lindberg E, Wilkins MR, MacKenzie KL, Wong JWH, Campbell PJ, Pimanda JE. (2017). Integrative Genomics Identifies the Molecular Basis of Resistance to Azacitidine Therapy in Myelodysplastic Syndromes. Cell Rep. 20(3), 572-85.

Van Regenmortel MHV, Choulier L. (2001). Recognition of peptides by antibodies and investigations of affinity measurements using biosensor technology. Combinatorial Chemistry & High Throughput Screening 4, 385-395.

Varmira K, Hosseinimehr SJ, Noaparast Z, Abedi SM. (2014). An improved radiolabelled RNA aptamer molecule for HER2 imaging in cancers. J Drug Target. 22(2), 116-22.

Vavalle JP , Cohen MG. (2012). The REG1 anticoagulation system: a novel actively controlled factor IX inhibitor using RNA aptamer technology for treatment of acute coronary syndrome. Future Cardiol. 8(3), 371-82.

Verhaak RG, Hoadley KA, Purdom E, Wang V, Qi Y, Wilkerson MD, Miller CR, Ding L, Golub T, Mesirov JP, Alexe G, Lawrence M, O'Kelly M, Tamayo P, Weir BA, Gabriel S, Winckler W, Gupta S, Jakkula L, Feiler HS, Hodgson JG, James CD, Sarkaria JN, Brennan C, Kahn A, Spellman PT, Wilson RK, Speed TP, Gray JW, Meyerson M, Getz G, Perou CM,

Hayes DN; Cancer Genome Atlas Research Network. (2010). Integrated genomic analysis identifies clinically relevant subtypes of glioblastoma characterized by abnormalities in PDGFRA, IDH1, EGFR, and NF1. Cancer Cell. 17(1), 98-110.

Verheugt FWA. (2016). An anticoagulant too good to be true for revascularisation. Lancet 387, 314-15.

Vernet T, Choulier L, Nominé Y, Bellard L, Baltzinger M, Travé G, Altschuh, D. (2015). Spot peptide arrays and SPR measurements: throughput and quantification in antibody selectivity studies J. Mol. Recognit. 28(10), 635-44.

Wang DL, Song YL, Zhu Z, Li XL, Zou Y, Yang HT, Wang JJ, Yao PS, Pan RJ, Yang CJ, Kang DZ. (2014). Selection of DNA aptamers against epidermal growth factor receptor with high affinity and specificity. Biochem Biophys Res Commun. 453(4), 681-5.

Wang Q, Hu B, Hu X, Kim H, Squatrito M, Scarpace L, deCarvalho AC, Lyu S, Li P, Li Y, Barthel F, Cho HJ, Lin Y-H, Satani N, Martinez-Ledesma E, Zheng S, Chang E, Sauvé C-EG, Olar A, Lan ZD, Finocchiaro G, Phillips JJ, Berger MS, Gabrusiewicz KR, Wang G, Eskilsson E, Hu J, Mikkelsen T, DePinho RA, Muller F, Heimberger AB, Sulman EP, Nam DH, Verhaak RGW. (2017). Tumor Evolution of Glioma-Intrinsic Gene Expression Subtypes Associates with Immunological Changes in the Microenvironment. Cancer Cell 32, 42–56.

Weidenhaupt M, Khalifa MB, Hugo N, Choulier L, Altschuh D, Vernet T. (2002). Functional mapping of conserved, surface-exposed charges of antibody variable domains. J. Mol. Recognit. 15, 94-103.

Whitehead KA, Langer R, Anderson DG. (2009). Knocking down barriers: advances in siRNA delivery. Nat. Rev. Drug Discov. 8, 129-38.

Wilner SE, Wengerter B, Maier K, de Lourdes Borba Magalhães M, Del Amo DS, Pai S, Opazo F, Rizzoli SO, Yan A, Levy M. (2012). An RNA alternative to human transferrin: A new tool for targeting human cells. Mol. Ther. Nucleic Acids 1, e21.

Wilson C. (2007). Aptamer opportunities and challenges. In Antisense drug technology. Principles, strategies, and applications. Second edition. CRC Press. Taylor & Francis Group.

Wu X, Liang H, Tan Y, Yuan C, Li S, Li X, Li G, Shi Y, Zhang X. (2014). Cell-SELEX aptamer for highly specific radionuclide molecular imaging of glioblastoma in vivo. PLoS One. 9(6), e90752.

Xiang D, Zheng C, Zhou SF, Qiao S, Tran PH, Pu C, Li Y, Kong L, Kouzani AZ, Lin J, Liu K, Li L, Shigdar S, Duan W. (2015a). Superior Performance of Aptamer in Tumor Penetration over Antibody: Implication of Aptamer-Based Theranostics in Solid Tumors. Theranostics. 5(10), 1083-97.

Xiang D, Shigdar S, Qiao G, Wang T, Kouzani AZ, Zhou SF, Kong L, Li Y, Pu C, Duan W. (2015b). Nucleic acid aptamer-guided cancer therapeutics and diagnostics: the next generation of cancer medicine. Theranostics. 5(1), 23-42.

Xie JJ, Guo JC, Wu ZY, Xu XE, Wu JY, Chen B, Ran LQ, Liao LD, Li EM, Xu LY. (2016). Integrin α5 promotes tumor progression and is an independent unfavorable prognostic factor in esophageal squamous cell carcinoma. Hum Pathol. 48, 69-75.

Yildirim MA, Goh KI, Cusick ME, Barabási AL, Vidal M. (2007). Drug-target network. Nat Biotechnol. 25(10), 1119-26.

Zamotaiev OM, Postupalenko VY, Shvadchak VV, Pivovarenko VG, Klymchenko AS, Mély Y. (2014). Monitoring penetratin interactions with lipid membranes and cell internalization using a new hydration-sensitive fluorescent probe. Org Biomol Chem. 12(36):7036-44.

Zeder-Lutz G, Choulier L, Besse M, Cousido-Siah A, Figueras FXR, Didier B, Jung ML, Podjarny A, Altschuh D. (2012). Validation of SPR screening of a diverse chemical library for the discovery of protein tyrosine phosphatase 1b binders. Anal. Biochem. 421, 417-427.

Zhang S, Zhang Z-Y. (2007). PTP1B as a drug target: recent developments in PTP1B inhibitor discovery. Drug Discov. Today 12(9-10), 373-81.

Zhang X, Peng L, Liang Z, Kou Z, Chen Y, Shi G, Li X, Liang Y, Wang F, Shi Y. (2018). Effects of aptamer to U87-EGFRvIII cells on the proliferation, radiosensitivity, and radiotherapy of glioblastoma cells. Mol. Ther. Nucleic acids. 10, 438-49.

Zhou J, Rossi J. (2017). Aptamers as targeted therapeutics: current potential and challenges. Nat. Rev. Drug Discov. 16(3), 181-202.

Zhou G, Wilson G, Hebbard L, Duan W, Liddle C, George J, Qiao L. (2016). Aptamers: A promising chemical antibody for cancer therapy. Oncotarget. 7(12), 13446-63.

Zhu J, Zhu J, Springer TA. (2013). Complete integrin headpiece opening in eight steps. J Cell Biol. 201(7), 1053-68.

Zudaire E, Martinez A Cuttitta F. (2003). Adrenomedullin and cancer. Regul. Pept. 112(1-3), 175-83

ANNEXE

Travaux développés avant 2008

Caractérisation biophysique d'interactions moléculaires

Dans cette partie, sont brièvement décrits les projets que j'ai développés avant 2008, selon deux axes thématiques :

A. Détection et modulation d'interactions moléculaires antigène-anticorps
B. Quantification d'interactions moléculaires complexes

A. Détection et modulation d'interactions moléculaires antigène-anticorps

L'objectif général est d'améliorer la compréhension et la prédiction des propriétés de reconnaissance moléculaire.

A1. Précision et évaluation des mesures cinétiques SPR (résonance des plasmons de surface)

L'équipe 'Biocapteurs' a acquis une bonne expérience de la maîtrise de la technologie des biocapteurs SPR par des interactions, notamment de Marc Van Regenmortel (alors directeur de l'UPR 9021, Strasbourg), avec le département de recherche et développements de la société Biacore, avant même que les appareils de la gamme Biacore soient commercialisés. Parmi les revues issues de cette équipe, nous avons notament décrit la technologie SPR et ses applications dans le cadre des interactions peptide-anticorps (Van Regenmortel et Choulier, 2001) et protéines virales-anticorps (Choulier et al., 2005).

En collaboration avec T. Vernet (Institut de Biologie Structurale, Grenoble), nous avons comparé les performances de deux logiciels d'évaluation des données SPR pour le traitement par intégration numérique de

données expérimentales complexes (Khalifa et al., 2001). Ces développements nous ont permis, entre autres, d'établir des effets faibles mais significatifs sur le k_{off} suite à des remplacements conservateurs d'acides aminés à l'interface VH/VL (Khalifa et al., 2000**)** ou de changements de charges à la surface (Weidenhaupt et al., 2002) d'anticorps recombinants. Les interactions protéine-protéine n'obéissent que rarement à des modèles simples 1 :1 (Langmuir). *In vivo*, elles sont souvent régies par des modèles complexes faisant intervenir des dimérisations, de multiples acteurs, des changements de conformation… Avec l'un de nos collaborateurs, Karl Andersson (Ridgeview Instruments AB, Uppsala, Suède), nous avons validé un nouveau logiciel d'analyses d'interactions complexes, nommé 'Interaction map' (IM), basé sur des cartes moléculaires reflétant les caractéristiques et la complexité des interactions, à partir de données SPR d'interactions déjà bien caractérisées au sein de l'équipe 'Biocapteur' (décrites ci-dessous). Un système d'interaction hétérogène complexe a été créé artificiellement en injectant un fragment d'anticorps (Fab 57P) sur des surfaces SPR immobilisées avec différents ratio de deux peptides dont, séparément, les K_D diffèrent d'un facteur 14. Nous avons montré que le logiciel IM permet de retrouver les paramètres cinétiques des interactions indépendantes, quel que soit le ratio des deux peptides immobilisés (Altschuh et al., 2012).

A2. Relation structure-activité de reconnaissance

Antigènes peptidiques et protéiques

L'effet fonctionnel de 5 mutations identiques a été comparé dans 2 contextes différents : un antigène peptidique (correspondant à la région 134-151 de la protéine de coque du virus de la mosaïque du tabac : VMTP) et un antigène protéique (VMTP) (Choulier et et al., 1999). Les cinétiques d'interaction ont été déterminées entre ces mutants et un fragment d'anticorps (Fab 57P, dirigé contre la VMTP).

Les affinités à l'équilibre (K_A) et l'effet des mutations sur les K_A sont similaires pour les interactions Fab-peptide et Fab-protéine. Cependant, les paramètres cinétiques des interactions Fab-peptide sont 5 à 10 fois plus élevés que ceux des interactions Fab-protéine, suggérant des processus de liaison différents pour les deux formes antigéniques. Ces travaux ont montré l'importance d'une analyse quantitative des affinités à l'équilibre, mais aussi des cinétiques de liaison, pour la conception de molécules synthétiques mimant les propriétés de liaison de molécules naturelles.

Caractérisation épitopique par synthèse multiple de peptides sur membrane SPOT et sélection de peptides à la surface de bactériophages ('phage display')

L'objectif principal de ces travaux était d'identifier les résidus de l'antigène peptidique dont la substitution influence les cinétiques d'interaction, sans pour autant abolir la liaison, afin de choisir des positions à substituer pour les analyses QSAR (ci-dessous). Cette étude a été menée en parallèle sur les systèmes Fab 57P et scFv 1F4 ('single chain fragment variable'). Le scFv 1F4 est dirigé contre la protéine E6 du papillomavirus humain

de type 16 (HPV 16) intervenant dans le cancer du col de l'utérus (Giovane et al., 1999). Sa production a également été décrite (Schwalbach et al., 2000).

Les résidus qui influencent la liaison dans les systèmes VMTP (Choulier et al., 2001) et E6 (Choulier et al., 2002a) ont été caractérisés par la technique SPOT (i.e. synthèse multiple de peptides sur membrane et immunorévélation ; collaboration avec Claude Granier, Montpellier), par 'phage display' (collaboration avec Georges Orfanoudakis et Etienne Weiss, ESBS, Strasbourg), et par SPR. La définition de l'épitope fonctionnel diffère nettement pour ces deux systèmes. L'épitope de la VMTP comprend quatre résidus (N_{140}, R_{141}, S_{143} et F_{144}) indispensables à la liaison du Fab 57P. Trois résidus (S_{142}, E_{145} et S_{146}) de part et d'autre de ces derniers influencent l'affinité d'interaction. Ils ont été sélectionnés pour l'analyse QSAR. L'épitope de E6 ne peut être délimité avec précision : aucun résidu n'est indispensable à l'interaction et plusieurs séquences sont compatibles avec la liaison du scFv 1F4.

Compréhension et prédiction des facteurs influençant les interactions moléculaires

L'optimisation de l'affinité des interactions moléculaires est d'un grand intérêt thérapeutique et biotechnologique. La méthodologie QSAR ('Quantitative Structure-Activity Relationship') offre une alternative intermédiaire entre la sélection à partir de banques de molécules et la conception totalement rationnelle de nouveaux ligands. Une analyse QSAR permet d'établir des relations mathématiques entre les propriétés physico chimiques (appelées facteurs) de molécules et l'activité biologique (Hansch et Fujita, 1964). Elle consiste à traduire toute ou partie de la structure d'une molécule en un ensemble de descripteurs numériques et à établir des relations quantitatives entre les variations de ces descripteurs et les variations de propriétés biologiques des molécules. Les relations établies permettent d'identifier les facteurs qui influencent l'activité, et de prédire des variations d'activité en fonction de variations de facteurs, puis de les vérifier.

En collaboration avec Magnus Malmqvist et Karl Andersson de la société Biacore AB (Uppsala), nous avons montré la faisabilité de l'approche QSAR appliquée à la prédiction des paramètres cinétiques des interactions moléculaires (Andersson et al., 2001 ; Choulier et al., 2002b). Nous avons également étudié les relations existant entre 3 facteurs environnementaux (force ionique, pH et température) sur les paramètres cinétiques d'interaction mesurés par SPR entre le fragment d'anticorps de chameau (VHH, Hamers-Casterman et al., 1993) et le lysozyme (Dejaegere et al., 2005) et sur le système d'interaction entre un peptide correspondant à la séquence N-terminale de la protéine E6 du virus à papillome humain de type 16 (Giovane et al., 1999) et le scFv 1F4 (Sibler et al., 2008, *Figure 27*). Pour le modèle scFv 1F4-peptide, les modèles mathématiques nous ont permis de prédire les facteurs expérimentaux permettant une dissociation rapide des complexes : pH<5 ou pH ≥10 à température élevée.

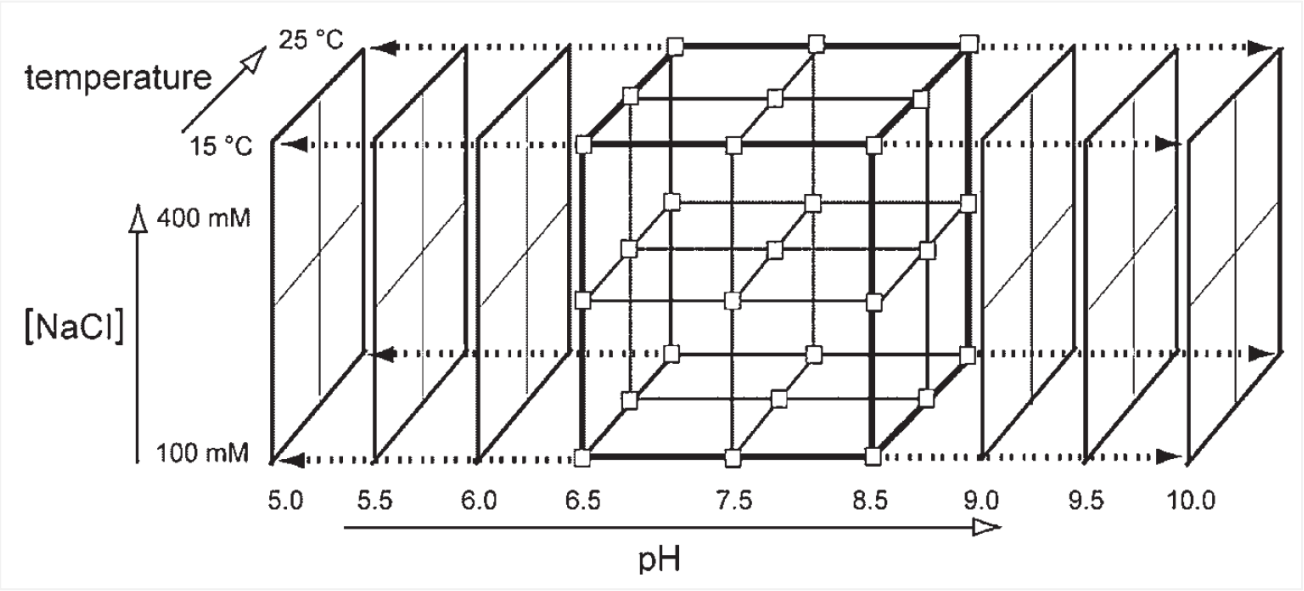

Figure 27. **Design du QSAR.** Différentes températures et conditions salines ont été analysées pour chaque valeur de pH comprises entre 5 et 10 avec des paliers de 0,5 (pH 7 et 8 exclus).

A3. Sélectivité

Une meilleure compréhension de la spécificité requiert l'identification des déterminants de liaison sur un des partenaires de l'interaction en fonction des motifs structuraux présents sur l'autre partenaire. Nous avons combiné des approches d'analyse permutationnelle et de SPR pour établir des relations structure/affinité/sélectivité sur le modèle d'interaction entre le scFv 1F4 (anti-protéine E6 de HPV_{16}) et des peptides mimant l'extrémité N-terminale de l'oncoprotéine E6, déjà bien caractérisé au laboratoire. La nature peptidique de l'antigène a permis une analyse étendue de la relation entre séquence et capacité de liaison par synthèse chimique sur plaques (X-scan). L'analyse permutationnelle a été réalisée sur l'ensemble des 10 acides aminés du peptide mimant l'extréminé N-terminale de E6. L'analyse de l'interaction entre le scFv 1F4 fluorescent et plus de 3000 peptides différents synthétisés par la technologie PEPperCHIP (PEPperPRINT GmbH, Heidelberg, Allemagne) a permis de déterminer les résidus peptidiques essentiels à l'interaction, les inter-dépendances entre résidus, mais surtout de définir des épitopes alternatifs de liaison, qui n'auraient pas été décelés par des analyses plus conventionnelles telles qu'Ala-scan ou X-scan (Vernet et al., 2015 ; Nominé et al., 2015).

A4. Recherche de positions co-variantes dans des alignements de séquences multiples

Notre objectif a été d'identifier les positions de la région charpente des anticorps susceptibles de jouer un rôle structural et/ou fonctionnel, malgré leur variabilité. La stratégie choisie est de chercher des positions co-variantes dans des alignements de séquences d'anticorps murins et humains (Choulier et al., 2000). Cette étude a permis de mettre en évidence l'existence de co-variants dans les séquences d'anticorps étudiées, suggérant que différents anticorps utilisent des arrangements structuraux alternatifs et mutuellement exclusifs, compatibles avec leurs fonctions.

B. Quantification d'interactions moléculaires complexes

B1. Interactions acides nucléiques-protéines

Par SPR, l'identification après récupération d'un ligand spécifique d'une cible immobilisée sur une surface *sensor* est difficile lorsque des mélanges de molécules sont injectés, en raison des faibles quantités de matériel élué. La possibilité d'amplifier par PCR les oligonucléotides retenus sur une cible puis récupérés, permettait d'envisager l'adaptation de la technique SELEX au criblage de grandes banques oligoribonucléotidiques par SPR (BIA-SELEXion).

En 2003, mon projet de post-doctorat à l'Université Victor Ségalen de Bordeaux s'inscrivait dans le contexte d'un projet européen sur les biocapteurs dont l'objectif était la mise au point d'un test quantitatif pour l'identification de glutène. Mon projet concernait plus particulièrement la sélection *in vitro* d'oligoribonucléotides contre des peptides toxiques de glutène (marqueurs de la maladie coeliaque humaine), par la technique SELEX ('Systematic Evolution of Ligand by Exponential Enrichment'). Cette technique permet le criblage de grandes banques d'acides nucléiques (comprenant jusqu'à 10^{15} séquences différentes synthétisées de façon aléatoire) contre des cibles diverses (qui peuvent ou non être des molécules liant naturellement des acides nucléiques). La méthode SELEX consiste à réaliser des cycles successifs de sélection et d'amplification permettant d'enrichir la population en candidats possédant les propriétés requises. Clonage et séquençage permettent d'identifier les ligands oligonucléotidiques (appelés aptamères) ayant de fortes affinités pour leurs cibles. Cette technique est décrite dans la partie 'Projets de recherche actuels' de ce manuscrit. Les étapes de sélection ont été réalisées par SPR. Les peptides toxiques de glutène étaient immobilisés sur une surface *sensor*. La banque d'ARNs modifiés était injectée dans un tampon de sélection de composition aussi proche que possible du tampon qui serait utilisé pour extraire le glutène de la nourriture.

Cette stratégie de sélection originale a nécessité plusieurs mises au point des conditions (i) de transcription des ARN modifiés, (ii) de RT/PCR pour amplifier les ARN 2'F sélectionnés, (iii) de stabilité de la banque et des peptides toxiques dans le tampon de sélection, (iv) de criblage par SPR. A l'issue des 7 tours de sélection/amplification réalisés durant la période de mon post-doctorat, l'évolution de la population ARN n'était pas encore détectable par SPR. Toutefois, la banque semblait avoir évolué par rapport à la banque initiale (détecté par digestion enzymatique). A mon départ, ce projet a ensuite été poursuivi, en réalisant un SELEX 'classique' (sans SPR). Aucun aptamère anti-gliadine n'a toutefois été sélectionné dans l'unité de Jean-Jacques Toulmé. A cette époque, nous ne savions pas quelles étaient les causes de ces échecs, ces causes pouvant être de nature biologique et pas forcément technique. Donc, à l'IREBS, à partir de 2004, j'avais initié une nouvelle stratégie de SELEX, par SPR. Nous avions décidé d'utiliser une protéine stable et bien caractérisée par SPR pour mettre au point cette méthode de BIA-SELEXion. Il s'agissait de la protéine de coque du virus de la mosaïque du tabac (VMTP). Cette protéine était disponible au laboratoire sous forme recombinante (Chatellier et al., 1996a, 1996b). Après plusieurs cycles de sélection/amplification, SPR et séquençage ont montré que la

banque n'avait toujours pas évolué. Avant d'éventuellement poursuivre ces expériences, nous avions décidé de nous familiariser aux mesures cinétiques d'interactions entre acides nucléiques et protéines par SPR, en utilisant plusieurs modèles. Depuis, deux études relatent un processus de sélection d'aptamères par SPR sur deux cibles : ARN structuré (Dausse et al., 2016) et la protéine EsxG de *Mycobacterium tuberculosis* (Ngubane et al., 2014).

Philippe Giégé et son équipe (UPR2357, IBMP, Strasbourg) travaillent sur les protéines PPR ('pentatricopeptide repeat proteins'). Ces protéines sont abondantes dans les plantes. Leur fonction est reliée principalement à la biogenèse des organelles. L'équipe de Philippe Giégé s'intéresse à l'analyse fonctionnelle de protéines PPR et à leur mode d'action, par différentes approches : génétiques, biochimiques, et de biologie moléculaire et structurale. Ils ont identifié l'une de ces protéines d'*Arabidopsis thaliana*, appelée PNM1 ('PPR protein localized to the nucleus and mitochondria 1'). Plusieurs études suggéraient une interaction entre les protéines PPR et l'ARN. Il fallait vérifier cette hypothèse pour la protéine PNM1. Nous avons donc testé l'interaction entre PNM1 et différents ARN par SPR. PNM1 a été immobilisée sur une surface *sensor*. Des ARN de taille et séquence variables ont été utilisés en tant que ligands potentiels. Des liaisons de forte affinité ont été observées avec les extraits d'ARN mitochondriaux totaux d'*Arabidopsis*. La dissociation de ces complexes est lente, suggérant que l'interaction de PNM1-ARN est stable et non transitoire. Nous avons également observé des interactions entre PNM1 et des ARNm, des ARNr 26S et 18S. Quant aux ARNt et ARNr 5S, ils ne se lient pas à la protéine. Quand des oligonucléotides représentant des poly A, C, G et U ont été utilisés, PNM1 n'était capable que de se lier aux poly G, mais avec une forte affinité. Ces résultats ont permis de valider la liaison PNM1-ARN (Hammani et al., 2011).

Une autre étude a porté sur l'initiation de la traduction d'*E. coli*, et notamment sur le décryptage du mécanisme d'action de la protéine ribosomale S1 sur les ARN messagers naturels, en collaboration avec l'équipe de Pascale Romby (UPR 9002, IBMC, Strasbourg), qui s'intéresse aux ARN messagers et aux ARN régulateurs bactériens. Plusieurs ARNm bactériens sont structurés dans les régions non traduites qui modulent l'accessibilité de l'ARNm à la sous-unité ribosomale 30S. La conformation des ARNm est directement impliquée dans ce processus de régulation. Certaines étapes de l'initiation de la traduction étaient déjà connues. Mais n'étaient pas connus, ni la façon dont le ribosome 'déstructure' l'ARNm pour promouvoir l'initiation de la traduction, ni les facteurs ribosomaux impliqués. Cette étude a montré que ce sont les 3 premiers domaines de la protéine ribosomale S1 qui lui confèrent une activité ARN chaperone essentielle à la liaison et au 'dépliage' des ARNm structurés, permettant ainsi le positionnement correct du codon d'initiation. Mais la protéine S1 n'est pas nécessaire au dépliement de tous les ARNm (Duval et al., 2013).

B2. Interactions intégrines-protéines de la matrice extra-cellulaire

Lors de mon stage post-doctoral à l'Université d'Oxford, j'ai étudié des interactions moléculaires, sur protéines membranaires, hétérodimériques purifiées (intégrines α5β1, αvβ3 et αvβ6) et deux protéines de la matrice extra-cellulaire (fibronectine et fibrilline). Ce travail a été réalisé au sein d'un réseau de cinq laboratoires de l'Université d'Oxford : I. Campbell, P. Handford, Y. Jones, H. Mardon et D. Stuart.

Interaction intégrine-fibronectine

Le module FIII (*Figure 28a*) est responsable de la plupart des propriétés adhésives de la fibronectine. La séquence RGD, généralement critique pour la reconnaissance des intégrines, est présente sur une boucle flexible protubérante du domaine FIII10, domaine qui, isolé, est capable d'interagir avec certaines intégrines. Concernant l'intégrine α5β1, le domaine FIII9 agit en synergie avec le domaine adjacent FIII10, pour promouvoir l'adhésion cellulaire, via le site synergique ('synergy site', séquence DRVPHSRN, Leahy et al., 1996 ; Copié et al., 1998 ; *Figure 28a*). Nous avons étudié les propriétés fonctionnelles et structurales d'une série de mutants de FIII9-10 possédant diverses substitutions par alanine dans le site synergique de FIII9, en combinaison ou non avec une autre substitution (L_{1408}P). La mutation L_{1408}P de la paire FIII9-10 confère une augmentation de stabilité du domaine FIII9 tout en maintenant intacte la boucle synergique. Les mutations du site synergique de FIII9 provoquent une réduction importante (i) de l'adhésion de fibroblastes, (ii) de l'affinité de α5β1 pour FIII9-10 (déterminée par ELISA et SPR), et (iii) de la stabilité du domaine FIII9 (dénaturation chimique). Néanmoins, ces effets peuvent être contrecarrés par l'introduction de la mutation L_{1408}P (Altroff et al., 2003) ou du domaine FIII8, et ainsi retrouver les propriétés de la molécule sauvage FIII9-10. Des études cinétiques similaires réalisées avec l'intégrine αvβ3 montrent que quelque soit la molécule étudiée, ses paramètres cinétiques sont les mêmes que ceux obtenus avec le domaine FIII10 seul (non publié).

Interaction intégrine-fibrilline

Le module TB4 ('Transforming growth factor β-Binding protein') de la fibrilline (*Figure 28b*) est le seul module possédant une séquence RGD, susceptible d'interagir avec les intégrines. La structure cristallographique du triple domaine cbEGF22-TB4-cbEGF23 de la fibrilline humaine a été résolue (Lee et al., 2004). Nous avons montré que l'intégrine α5β1 n'interagit pas avec le triple domaine recombinant cbEGF22-TB4-cbEGF23, au contraire de αvβ6 et αvβ3. Le domaine cbEGF22 pourrait posséder des propriétés fonctionnelles dans la liaison de l'intégrine αvβ3. En effet, la suppression de ce domaine dans la molécule TB4-cbEGF23 provoque une dissociation deux fois plus rapide de αvβ3, mais également une réduction d'adhésion cellulaire (Jovanovic et al., 2007).

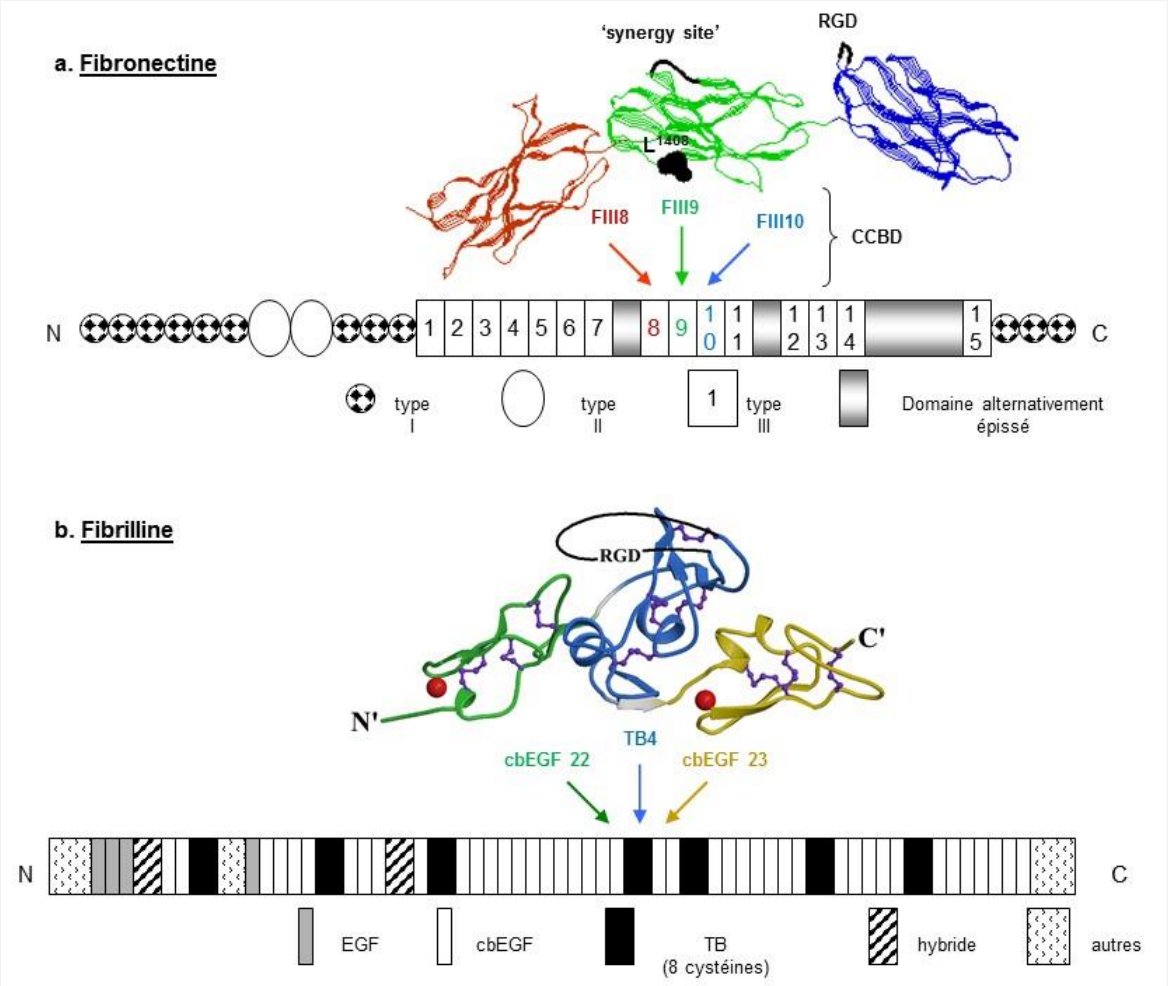

Figure 28.

a. Organisation modulaire de la fibronectine humaine et structure de FIII8-10. Sur la structure figurent les localisations du résidu L1408, et des boucles synergique et RGD.

b. Organisation modulaire de la fibrilline humaine et structure de cbEGF22-TB4-cbEGF23. Sur la structure, les atomes de Ca^{2+} sont représentés par des cercles rouges. La structure de la boucle contenant le site RGD n'est pas définie.